Spring 2018

EXPERIMENTS AND ANALYSIS OF ALUMINUM TUBE HYDROFORMING

Adam Ryan Kaplan
University of New Hampshire, Durham

EXPERIMENTS AND ANALYSIS OF ALUMINUM TUBE HYDROFORMING

BY

ADAM R. KAPLAN

B.S. MECHANICAL ENGINEERING, 2010

THESIS

Submitted to the University of New Hampshire
in Partial Fulfillment of
the Requirements for the Degree of

Master of Science
in
Mechanical Engineering

May, 2018

This thesis has been examined and approved in partial fulfillment of the requirements for the degree of Master of Science in Mechanical Engineering by:

Thesis Director, Assoc. Professor Yannis Korkolis, Dept. of Mechanical Engineering

Professor Brad Kinsey, Dept. of Mechanical Engineering

Professor Todd Gross, Dept. of Mechanical Engineering

On March 16, 2018

Original approval signatures are on file with the University of New Hampshire Graduate School.

TABLE OF CONTENTS

ACKNOWLEDGMENTS

Dedicated with love to my grandmother Marion Kaplan.

I want to express sincere appreciation to University of New Hampshire professors Yannis Korkolis, Brad Kinsey, and Todd Gross for their assistance in the preparation of this manuscript. Yannis's vision and expertise were a huge contribution towards this manuscript and my own education. My parents, April and Ben, have always supported me and emphasized the importance of my academic pursuits. Without all the support and motivation from my grandmother, Marion; my sisters, Ashley and Bre; and whole extended family, this would not have been possible. They continued to follow the progress of this thesis even after I had finished my coursework. In addition, I would like to thank to Graham Cullen, with whom I spent much of my graduate school experience working. His experience with machining, fabrication, and hydraulics was vital to the development of the laboratory tube hydroforming machine. I must additionally thank all the graduate members of the mechanics, materials, & manufacturing research group for their valuable support and friendship during my time at the University of New Hampshire.

LIST OF FIGURES

LIST OF TABLES

ABSTRACT

EXPERIMENTS AND ANALYSIS OF ALUMINUM TUBE HYDROFORMING

by Adam R. Kaplan

University of New Hampshire, May, 2018

This is a thesis on the development of an experimental table-top sized tube hydroforming machine at the University of New Hampshire. This thesis documents the design of the machine and the exploration of the forming envelope of the device via finite element modeling of the forming process. Several experiments on Al-6061-T4 tubes were used to evaluate the plastic behavior and strain limits of the tube in the axial and circumferential (hoop) directions. Two of these material tests, the uniaxial tension test and the ring hoop tension tests, were simulated with finite element models to refine the Al-6061-T4 plasticity curve, including the extrapolation of the hardening curve beyond the point of ultimate tensile stress. 2D and 3D finite element models of the hydroforming process were also used to evaluate potential tube materials, outer diameters, and wall-thickness for future experiments and research efforts.

CHAPTER 1

THE TUBE HYDROFORMING PROCESS

1.1 Introduction to the Process

Tube hydroforming is a manufacturing process that utilizes pressure from a working fluid to form tubular blanks into complex geometries. First, a tubular specimen is placed inside a forming die of the desired geometry. The ends of the tube are sealed and the working fluid fills the internal cavity of the tube. As more incompressible fluid is introduced, the pressure increases and the tube deforms elastically. The tube material reaches the elastic limit of the material and begins yielding. The tube continues to deform as the material enters the plastic region. Most ductile metals exhibit strain-hardening of the tube material, which allows the material to withstand even higher stresses as the deformations become significant. As a result, the tube continues expanding and the pressure continues to rise. To completely fill the forming die, the volume must continue to increase; however, the pressure response becomes dependent on both the die geometry to be formed as well as the geometry of the tube and the behavior of the tube material. Figure 1.1 illustrates the basic concept of the tube hydroforming process with a simple die geometry.

Hydroforming has seen a surge of commercial applications since the 1980's, and tube hydroforming has been especially widespread throughout the automotive manufacturing industry. For production runs in commercial applications, the typical cycle

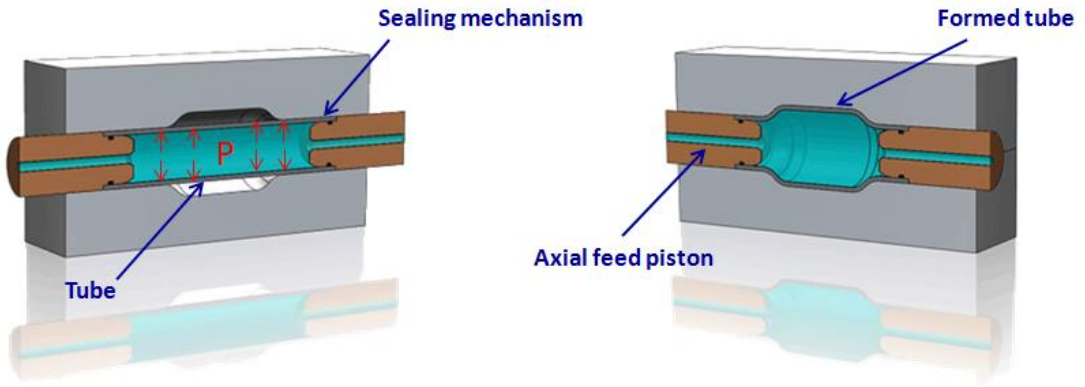

Figure 1.1: Illustration of the tube hydroforming process with axial feeding (modified from http://www.muraropresse.com).

time for a hydroformed part is between 10 to 30 seconds. A typical manufacturing press would include an automated process to place the tube between two opposing die halves, which are then closed on the tube and may subsequently perform some pre-forming. Next the tube ends are rapidly sealed and fluid is pumped into the tube until the part is formed. Sometimes, the ends of the tube are also fed towards the center, as depicted in Figure 1.1. The seals retract and the part is removed as the fluid drains. Although slower than stamping cycle times for individual parts, the hydroforming process offers many advantages that may lead to improved part quality and comparable cycle times for finished parts and assemblies. These advantages include decreasing the number of parts in an assembly, reduced manufacturing and finishing operations, and reduced tooling wear [1]. Instead of high frictional forces on the die and tooling, fluid is used to form the part and the frictional forces on the die are reduced to small amounts of material stretching as the tube fills the cavity. Hydroformed parts can be made from a single, continuous tube, which reduces post-forming operations, such as welding multiple stamped parts together, and increases rigidity and strength of the part. Hydroformed parts typically have increased thickness uniformity, better strength-to-weight ratios, and smoother surface finished when compared to stamped

or cast alternatives.

Today, there are countless examples of hydroformed parts. Hydroforming is used for many automotive parts, such as frame rails, tubular door members, intake manifolds and exhausts, hollow camshafts, rear axle components, and roll bars. Many tubular products, such as bicycle frames, musical instruments, pipe fittings, and specialty parts for the aerospace industry, are also produced by hydroforming. Softer, ductile materials such as brass, copper, magnesium, and variants of aluminum have seen widespread use with hydroforming [2].

The hydroforming process allows tubes to be formed into unique profiles with a varying cross-section along the axial length of the formed part. This allows the strength and rigidity of the part to be tailored locally to accommodate the in-service loading. Figure 1.2 depicts some possible cross-sections that have been formed using the hydroforming process. Additional structural rigidity is achieved over a similar part created from multiple stamped components welded together. The tube wall is formed into the desired cross-section as a continuous, fully boxed section. Fully boxed sections produced from tubes are stronger than C, U, or I section shapes used in extrusions. The inflation of the tube causes the resulting cross-section of the part to expand (increasing the section modulus) while simultaneously work-hardening the material, greatly improving the overall rigidity from the stock tubular specimen. As a result, less material and weight can be used to produce a part of equivalent stiffness - a benefit that is highly desired by the commercial transportation industry.

The modern automotive industry has embraced tube hydroforming in an effort to

decrease vehicle weight and improve part stiffness and performance [3]. There are numerous examples of manifolds, hollow camshafts, and rear axle components throughout the various manufacturers. The technology has found widespread use for vehicle spaceframes/unibodies and lightweight performance parts such as magnesium engine cradles, roll bars, door reinforcement members, and aluminum frame rails on vehicles such as the Corvette Z06 (see Figure 1.3). The Corvette's hydroformed aluminum frame is 33% lighter than its steel predecessor for the same stiffness [4]. The Z06 has also updated its performance V8 engine with a hydroformed exhaust manifold. Similarly, BMW's 3-series convertible has adopted a hydroformed A-pillar and windshield header, increasing the strength of the roof by 70%, while reducing the number of parts by 44% [5]. BMW also uses several different hydroformed parts to produce the rear axle subframe for the 3-series and 5-series automobiles. High performance vehicles like the Porsche Boxster, shown in Figure 1.4, are using hydroformed tubes for roll bars [6].

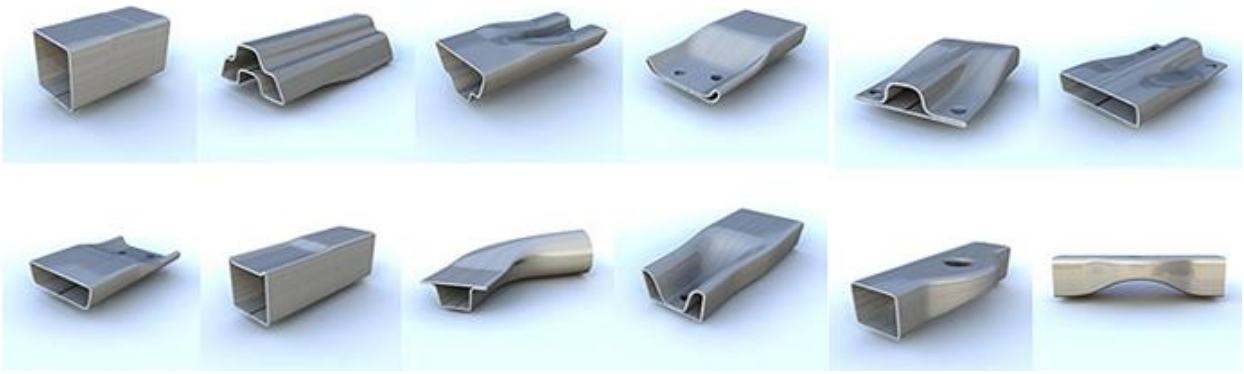

Figure 1.2: Examples of formed cross-sections, which vary along the length of the formed part (http://www.excellatechnologies.com/)

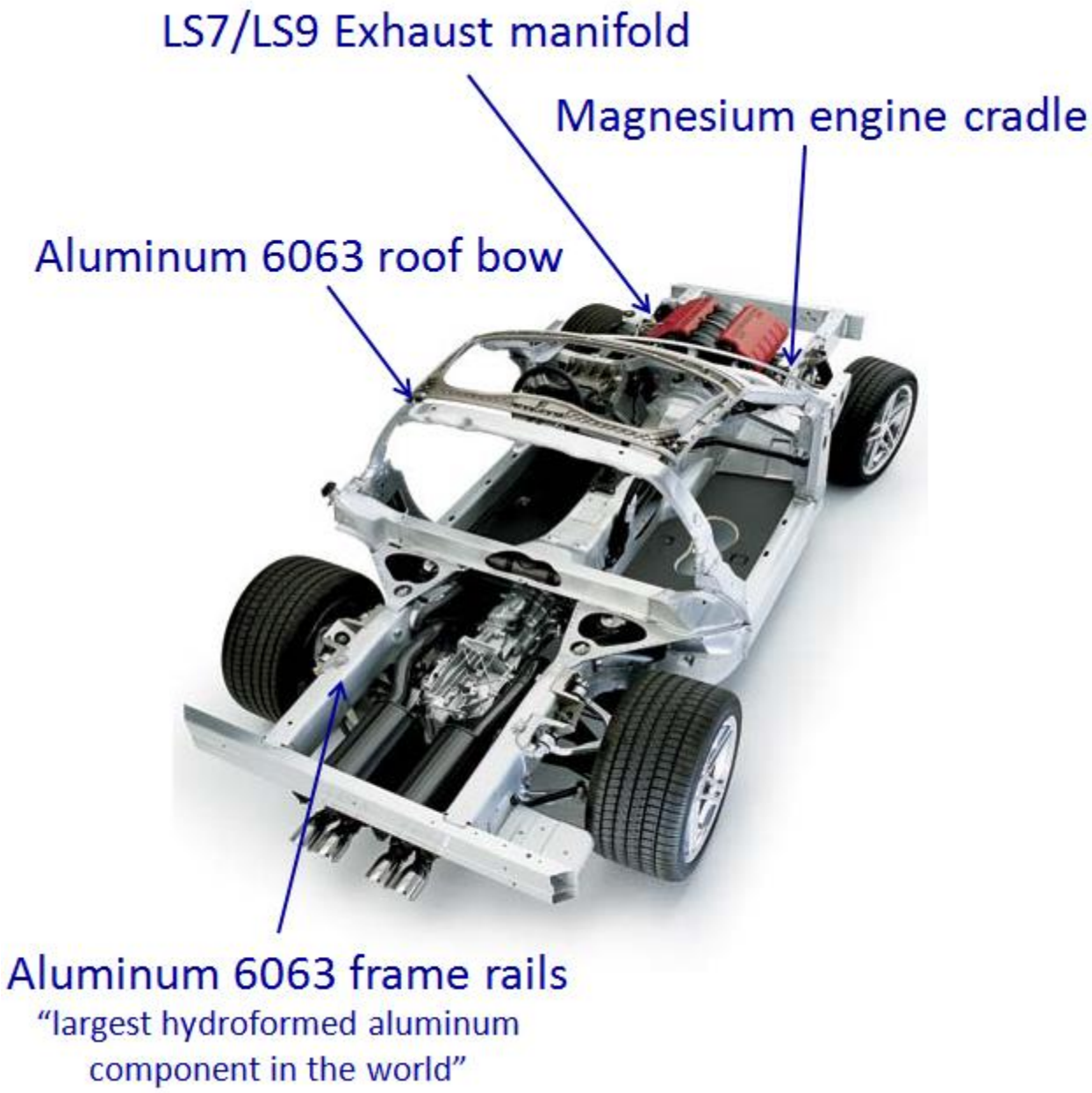

Figure 1.3: Examples of hydroformed components in the Chevrolet Corvette Z06 (modified from http://www.gm.com/).

Figure 1.4: An example of how hydroformed componentrs are being used in the transportation industry. This particular 2-piece roll bar is from a convertible Porsche Boxster (http://www.schulergroup.com/, http://www.autospeed.com/).

1.2 History of Tube Hydroforming

Although contemporary tube hydroforming has been widely adopted by industry, the tube hydroforming process has seen limited use since the introduction of the first tube hydroforming patents at the turn of the 20th century. Fluid pressure was used in the United States in 1900's to create complex and hollow parts - specifically mentioned are "serpentine" shaped boiler tubes [2, 7-8]), and bent brass tubes for wind instruments such as trumpets and trombones (Foster, 1917). These early processes used molten low temperature metals such as lead or tin alloys as the working fluid to pressurize the tube, and also featured mechanisms for sealing the ends of the tubes. Previously, the creation of complex tube geometries such as specialized boiler heating tubes required casting and hand-finishing. The combination of pre-forming the tube by closing the die cavity and the subsequent internal pressure to form the tube against the cavity walls made the manufacturing of these parts possible from straight steel tubes. In fact, the tube hydroforming process resulted in improved dimensions, smoothness, and quality of the parts. Internal smoothness was likely an advantage to these types of applications. The first patent for these boiler tubes was filed by Kennedy Park in 1903 [8] - his blue prints are shown in Figure 1.5.

A later patent filed by John G. Liddell in 1922 [9] described a hydroforming machine for forming thin metal tubes into a female die, which was closed around the tube using a hand-wheel [9]. An internal member slides through the tube to be formed to the sealing mechanism on the other side. This member has an internal passage that pressurized the section of the tube with oil in the die cavity and is sealed using an O-ring recess filled with suitable packing (see Figure 1.6).

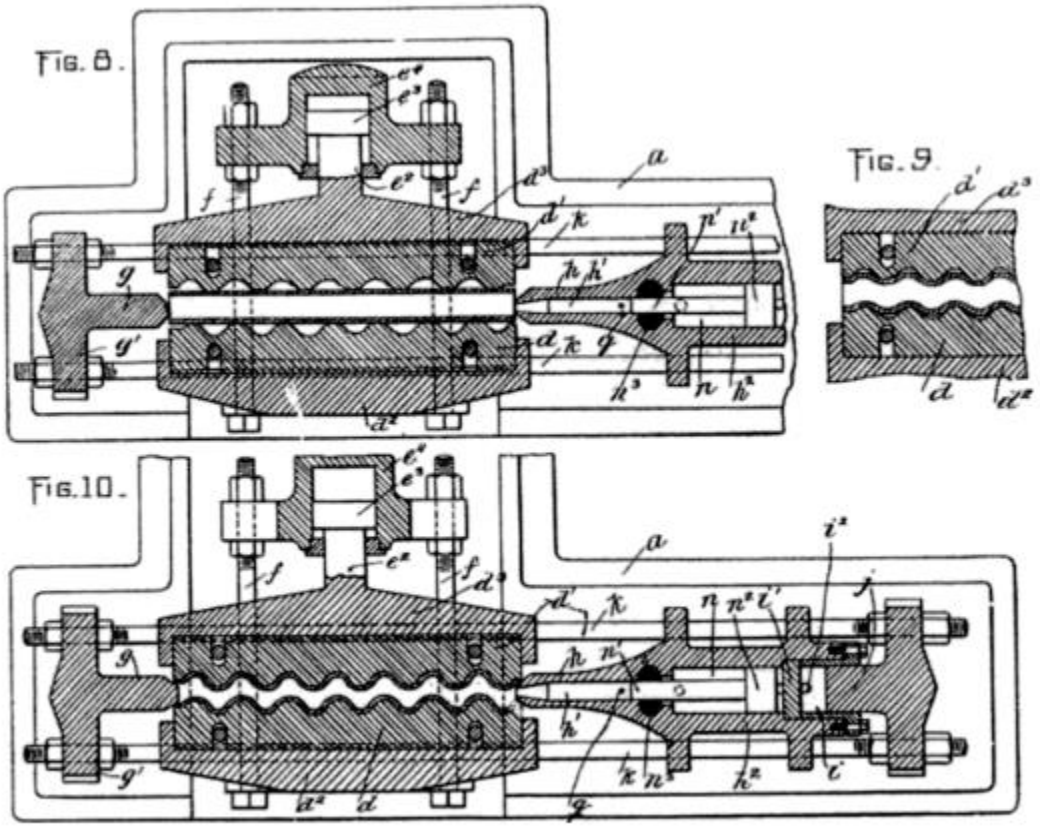

Figure 1.5: Patent drawings of one of the first tube hydroforming devices to make boiler tubes (Park, 1903 [8]).

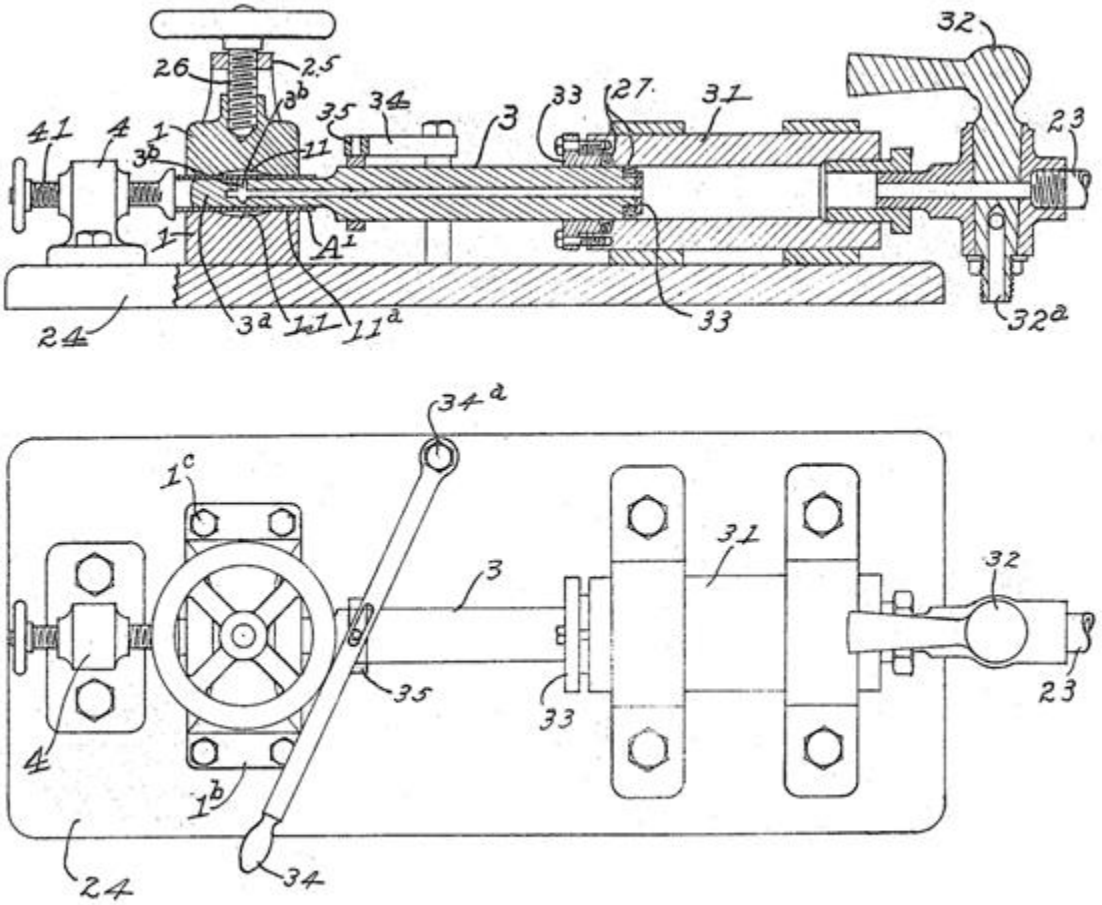

Patent 1,448,457– "Method and Apparatus for Die Shaping Metal"

Figure 1.6: Patent drawings for an early tube hydroforming machine with sealing mechanism (Liddell, 1922 [9]).

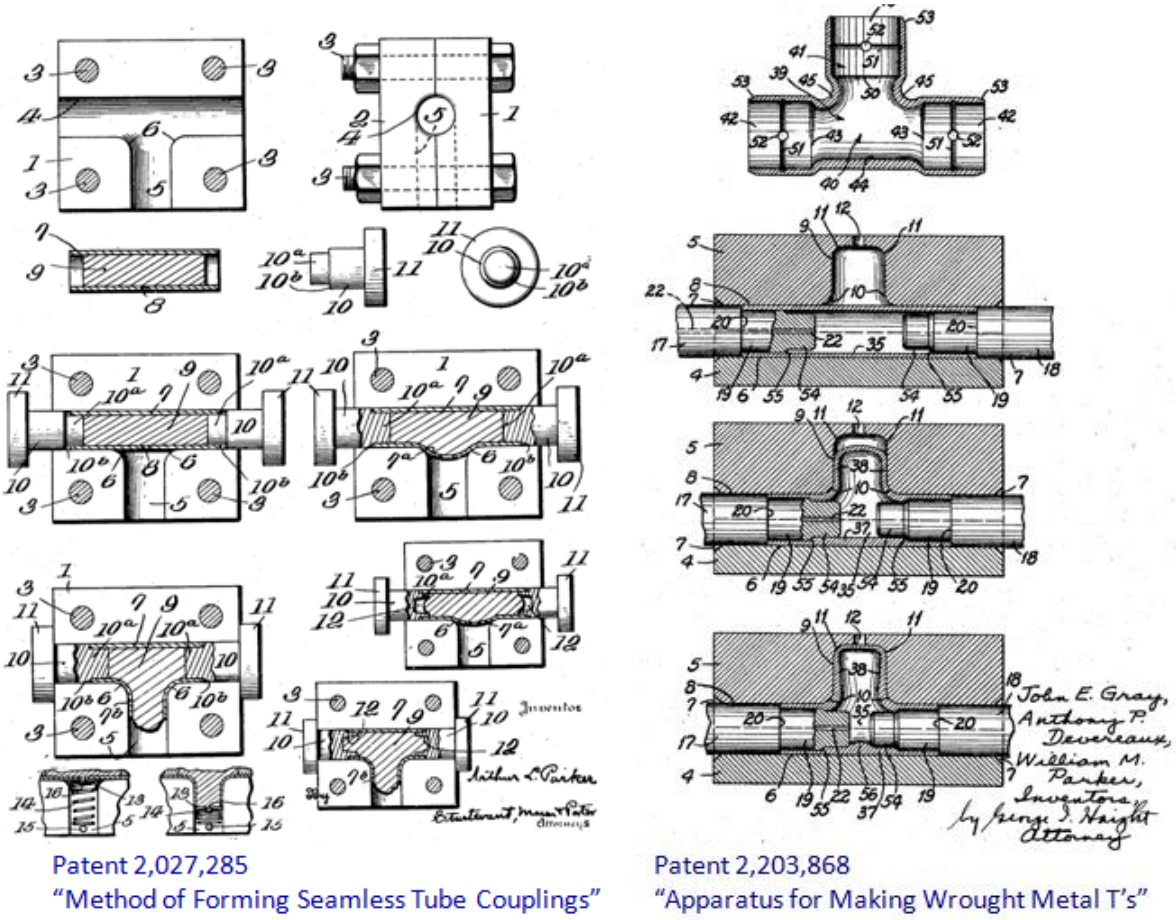

Figure 1.7: Patent drawings for hydroforming machines that create branched T's from tubes (Parker, 1936 [10]; Gray, 1940 [11]).

In 1932, one of the first patents emerged from Arthur Davies detailing the use of aluminum tubes being used to form the base structure for artificial limbs (1932, Davies, [2]). In 1933, an important patent filed by Arthur R. L. Parker illustrated a hydroforming device to manufacture seamless branched members from steel tubing (Parker, 1936, [10]). This patent is important because in order to achieve such large shape deformations, the ends of the tubes needed to be fed axially into the forming zone. Axial feeding is now a common

process variant that greatly enhances the formability of tubes. A similar patent was given to Gray E. Grant in 1940 for "An apparatus for making wrought metal T's" (Gray, 1940, [11]). This manufacturing process was quickly adopted as a practical industrial application for branched profiles, and continues to be used today for many plumbing fittings, fixtures, and faucets, and remained the dominant application of commercial hydroforming through the 1970's. Both of their devices can be seen in Figure 1.7.

While the tube hydroforming process was emerging in industrial applications, the research community was also embracing tube hydroforming as both a method of material testing, fracture mechanics modeling, and understanding combined stress state deformation modes. The objective of this initial research was to understand and predict failure behavior and forming limits for ductile materials. New manufacturing applications for sheet metal and thin walled tubes required accurate prediction of "safe" forming zones.

After the 1940's, a number of metal forming investigations began to focus on thin and thick walled cylinders. Research by Davis is one of the first papers cited to combine axial tension with internal pressure in his forming experiments [1, 12]. The use of axial force at the tube ends is an important variation of the tube hydroforming process, where the tube ends can either be axially compressed and fed into the deformation zone, or can be under tension to limit excessive local deformations (particularly wrinkling). In Davis's experiments, axial tension was used to investigate plasticity mechanics of medium carbon steel tubes. The axial tension creates additional longitudinal stress in the tube wall, which can be varied along with the internal pressure to create different biaxial states of stress. This state of stress allowed for testing material yield limits in a biaxial deformation mode. At the time,

this technique was used to identify the yield surface (failure locus for distortion energy theorem) for different loading modes. Axial tension also found applications in low-pressure tube forming applications such as rotary bending by preventing wrinkling of the inner bend radius wall. For use in practical hydroforming, where the material enters the plastic region, this technique was later used to track the evolution of the yield surface as it is modified by the plastic strain, an effect known as kinematic hardening, or work hardening. Such research required sophisticated experiments and equipment.

For a period of time, hydroforming was primarily a manufacturing process with limited applications. The technology saw progressive improvements in areas of high pressure hydraulics, control systems, and flow and pressure measurements, which enabled later research applications in 1978 by Sauer et al. In these forming experiments [13], nine tubes were internally pressurized and axially compressed in order to expand the tube plastically. The relatively uniform expansion eventually led to asymmetric bulging, localization, and finally failure via rupture or buckling. It was found that different geometries and expansion diameters could be achieved using specific loading ratios of axial and internal pressure. From these types of experiments, an envelope of the forming process can be identified in order to improve manufacturing processes and applications. The authors attempted to quantify this envelope by developing a mathematical model to determine the failure limit in terms of strain, but found poor correlation between their simplified model and the actual experiments.

In the last three decades, tube hydroforming has seen increasing applications as automotive manufacturers strive to decrease vehicle weight and fuel consumption while

maintaining crashworthiness and strength. This is driving research for hydroforming materials, high pressure hydraulics, simulation, and process engineering. The advent of mature finite element codes that can not only accurately model the plastic behavior of materials but can also utilize custom yield functions and failure models have enhanced the modeling of the working envelope of the hydroforming process, especially for materials with complex constitutive behavior. Research into lightweight aluminum alloys for manufacturing has been a well-studied region of material science. It has been shown by Hosford, Hill, Barlat, and others that aluminum alloys cannot be accurately modeled by the quadratic von Mises yield function, and that they are particularly sensitive to deformation induced anisotropy [7, 14-16]. Tubular specimens, due to their manufacturing process, have inherent differences in axial and circumferential pre-strain histories. The result is that these materials require more complex models. Non-quadratic yield functions include Hosford's 1979 anisotropic yield function [15], Karafillis and Boyce's 1993 anisotropic yield function [16], and Barlat's 2003 anisotropic yield function [17].

The content of this thesis in particular follows the work of Y.P. Korkolis and S. Kyriakides from 2000-2009, who published several papers on aluminum tube hydroforming [18-22]. The work points out that aluminum is well suited to the automotive industry as an alternative to steel parts, but that development of practical applications is widely limited by our understanding of aluminum forming behavior. Designing an aluminum equivalent of a steel part is more difficult due to the reduced ductility, anisotropic behavior, and highly sensitive plasticity models - all of which determine the evolution of the yield surface under plastic strain. The experiments in 2009 [19] focused on forming 2.36 inches (60 mm) OD x 0.080 inches (2 mm) thick Aluminum 6260-T4 tubes, which is comparatively ductile for

aluminum and also features significant work hardening. The uniaxial testing of this material showed strains at the ultimate tensile strength of the material to be 19.5% in the axial direction and 11% in the hoop direction. The axial direction was tested using uniaxial tension specimens which failed after localized necking and fracture. The hoop direction was tested by pressurizing the tubes, and the failure was abrupt. The differences in the material response, as shown in Figure 1.8, are believed to be caused by the geometry of the specimens in circumferential loading, which leads to different forms of instabilities, localizations, and failure modes. Tubular specimens were also loaded in shear using torsion loading, and the material response exhibited a greater work hardening rate and higher yield stress than the other modes of deformation, indicating the need for a complex anisotropic material model.

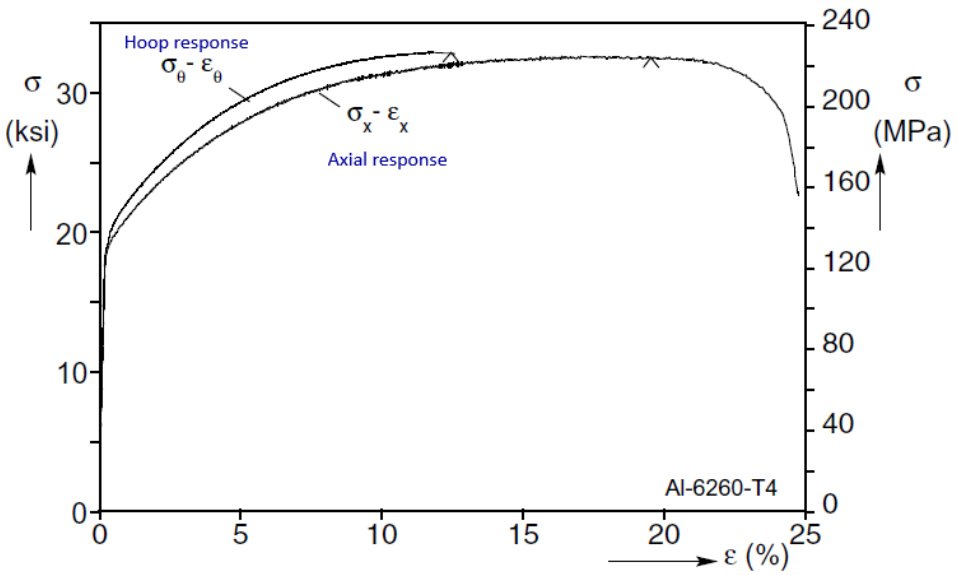

Figure 1.8: Example of different material response for Al-6062-T4 tubes tested by Korkolis, Kyriakides at University of Texas at Austin [18].

The hydroforming machine used in later Korkolis and Kyriakides experiments utilized

axial feeding with two opposed 150 kips (667.2 kN) cylinders and 20,000 psi (1,380 bar) internal pressurization system. The die featured 2.400 inches x 2.400 inches (60.96mm x 60.96 mm) cross-section with 0.500 inches (12.7 mm) corner radii. The die length was 24 inches (609.6 mm) including a 3 inches (76.2 mm) transition zone on either end. The initial hydroforming experiments included a variety of loading paths which resulted in successful part formation and also some rupturing by bursting, but the phenomenon proved difficult to model accurately in finite element simulation using classical plasticity models such as the von-Mises, Tresca, or Karafillis and Boyce's plasticity models [18].

As a result, the study further investigated the role of bursting as a dominant failure mode for hydroforming aluminum, and attempted to improve the constitutive models for use in the finite element simulations. The aluminum tubes in the experiments had thickness variations that led to predictable failure zones in free-expansion experiments, where the tube was loaded without a die to limit forming. This experimental setup is valuable for exploring the yield and failure surfaces of material under different combinations of axial and circumferential stress. The engineering stresses in axial and circumferential stresses can be expressed in terms of the mid-thickness tube radius and wall thickness as follows:

$$\sigma_x = \frac{F}{2\pi R t} + \frac{PR}{2t} \quad \textit{and} \quad \sigma_\theta = \frac{PR}{t} \qquad (1.1)$$

By prescribing nine different constant ratios of engineering stress paths, the authors were able to plot the contours of plastic work (see Figure 1.9 and Figure 1.10). Note that the contours evolve non-linearly, indicating a complex yield surface. Essentially, the free-expansion test was utilized as a form of biaxial testing. This data was later used to calibrate

the different anisotropic yield functions.

A second set of experiments focused on the role of a non-linear stress path. In three tests, the tube was loaded by axial tension and internal pressure in order to maintain three different stress biaxiality ratios until failure. Cleverly, the researchers then performed two other loading paths. One path pressurized the tube to the same level as the biaxial experiment, and subsequently increased the tension until failure. The other path first tensioned the tube and then increased pressure until failure. Tests using these paths were conducted to match the three constant stress ratio tests for comparison, however the results showed very different ultimate strains depending on the loading path [17]. These two modes represented the extremes that a given region of tube material might experience in a commercial hydroforming application, allowing the researchers to investigate how the loading path affects formability and the process envelope. The experiments demonstrate that the failure strains achieved are dependent on the strain path.

Utilizing FEA, the authors calibrated and applied the three anisotropic yield functions to simulate the tests, and found that Barlat's anisotropic model was slightly better at modeling the evolution of the plastic work contours in the former set of experiments and strain paths of the latter set of experiments than Hosford or Karafillis/Boyce models.

Figure 1.9: Burst failure in Al-6062-T6 obtained in free expansion experiments with different ratios of pressure and axial force, tested by Korkolis, Kyriakides [18].

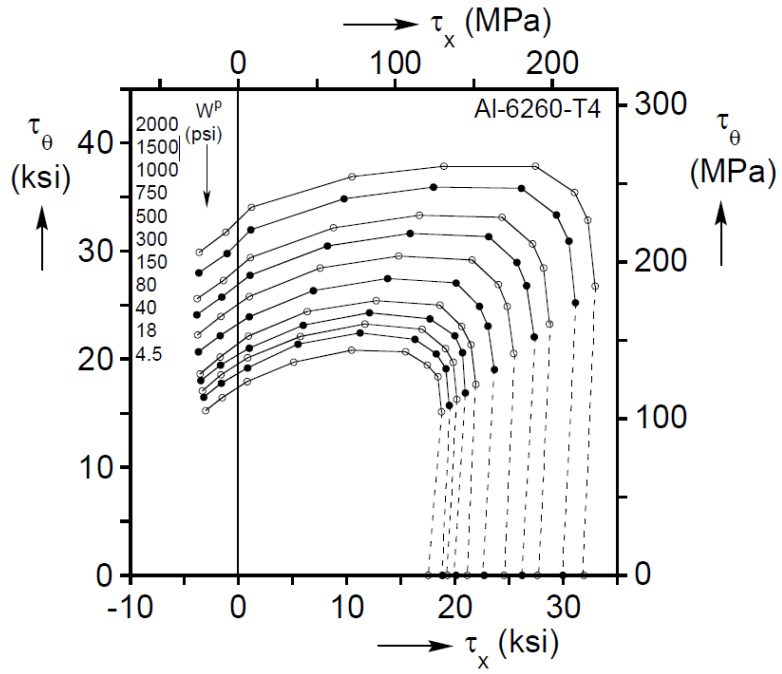

Figure 1.10: Illustration of evolving contours of plastic work from nine Al-6062-T6 constant ratio loading paths, tested by Korkolis, Kyriakides [18].

1.3 Capabilities and Process Variants:

Although still emerging technology, several process variants have emerged from hydroforming research over the past two decades. These include multi-operation processes, such as hydropiercing, pre-forming, and low-pressure hydroforming, where additional manufacturing operations are performed simultaneously with the pressurization of the tube. These variations are designed to decrease the number of manufacturing operations and reduce the total manufacturing time [1, 2].

Low-pressure hydroforming is a variation of hydroforming that uses small internal pressures to stabilize the tube wall. The low-pressure prevents the tube walls from wrinkling during bending and crushing operations. To make a final part that has bends such as an exhaust system, the tubes can be pre-bent into shapes that fit into a hydroforming die. The dies themselves can accomplish this pre-bending process to some degree when they are closed on the tube. Low pressure hydroforming is often used during these pre-bending and preforming operations. The low pressure process is often followed by a final, high-pressure hydroforming procedure.

Hydropiercing is term for removing a billet of material from a tube during the hydroforming process. The internal pressure stabilizes the tube wall as the punch is moved into the tube. As the material shears at the edges of the punch, the punch itself occupies the hole, minimizing leaking fluid and allowing some forming to continue. Figure 1.11 shows a commercial automotive frame as it undergoes different stages of preforming, low-pressure forming, and hydropiercing.

Other process variants are designed to increase the formability of the part by delaying

the bursting or splitting of the tube wall during the pressurization process. Once the tube material has failed, the internal pressure can no longer be maintained and forming cannot continue. In order to prevent the localized thinning that precedes tube material failure, several forming techniques have been developed. These variants include promising technologies such as warm tube hydroforming, pulsed-pressure tube hydroforming, and hydroforming with axial feeding. Some examples are shown in Figure 1.12.

Figure 1.11: Examples of a tubular blank, pre-forming by tube bending, low-pressure hydroforming by crushing the pressurized tube in the die, and finally, high pressure hydroforming and hydropiercing to create the formed part (http://www.schulergroup.com).

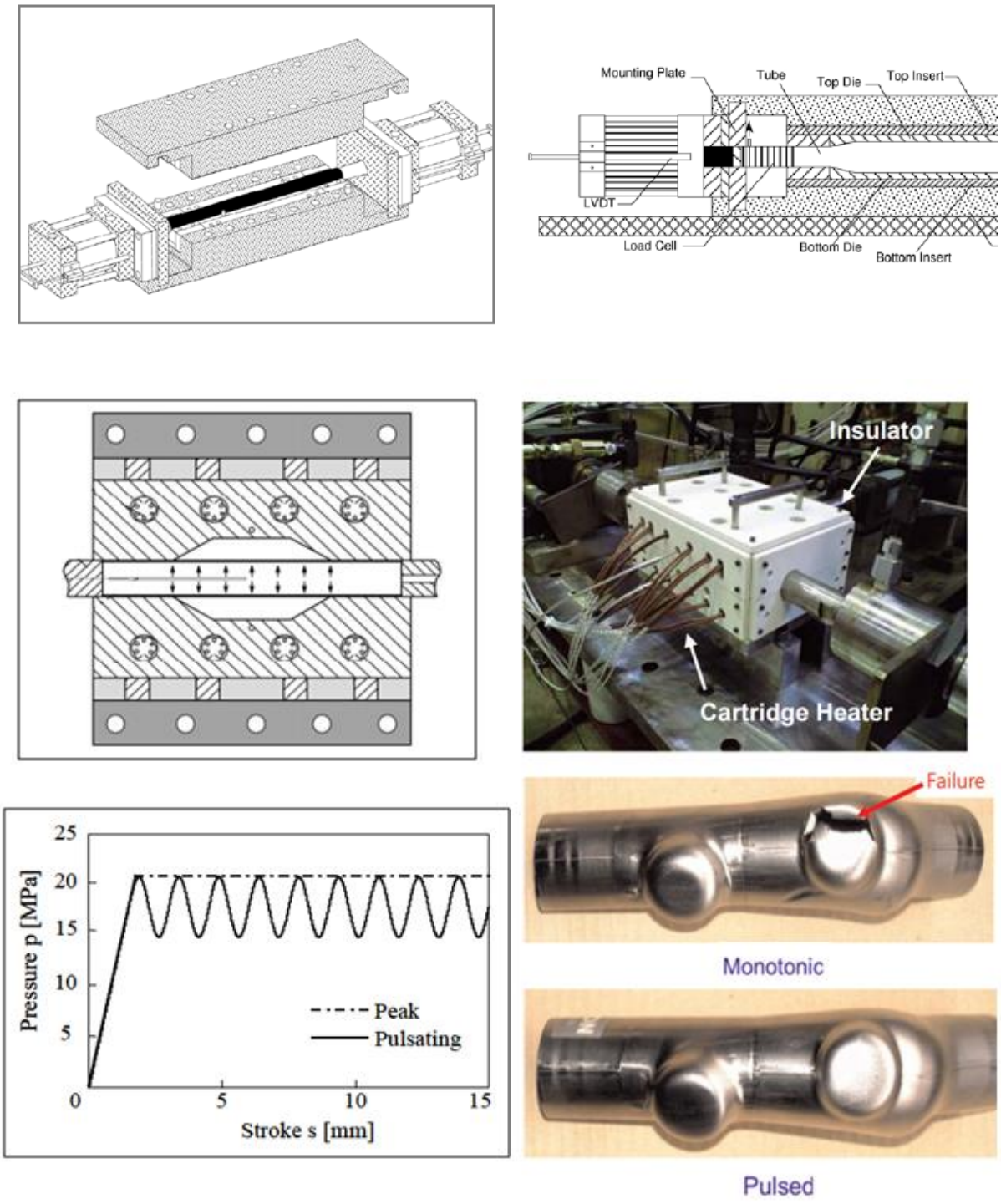

Figure 1.12: Examples of axial feeding of tube ends using hydraulic cylinders (top, Korkolis [7]), warm tube hydroforming using an induction heating system (middle, Manabe [23]), and pulsed tube hydroforming (bottom, Mori [24]).

Warm tube hydroforming covers a variety of processes that use elevated temperatures in order to leverage thermal properties of the tubes, often time aluminum or magnesium alloys [23, 40]. The tubes themselves can be heated before forming, but they can also be heated by the internal fluid or the forming dies themselves. In Figure 1.12, the die is heated to 250°C to successfully form an AZ31 magnesium alloy tube into a T-shape joint.

Axial feeding is a very common method in commercial applications. The ends of the tubes are hydraulically moved inward, feeding more material into the freely deforming region of the tube and increasing the axial loading. The feed can be controlled to delay thinning and allow further expansion of the tube without failure. By controlling the internal pressure and the axial loading independently, different loading paths can be explored and exploited to increase the formability of the tube [7, 40].

Using combinations of the above process variants, very complex parts can be formed through pre-bending, multiple pressure stages, and movements of counterpunches. In many of these processes, plastic wrinkling of the tube wall is a concern that must be addressed and mitigated [40]. Pulsed tube hydroforming is a recent development that oscillates the pressure in a controlled manner to improve part formation. Pulsed-pressure tube hydroforming experiments by Mori et al. [24] have shown that the repeated loading and unloading of the material allowed features to be formed successfully when they could not be formed with monotonic pressurization. The process also alleviated wrinkling and improved the surface quality of the parts.

1.4 Purpose of Study

Across the United States and the world, the manufacturing industry is facing greater demand for final products at lower cost, higher volumes, and with decreased lead time. As tube hydroforming expands within the manufacturing industry, the adaptation of the process to a specific product requires careful planning. In order to reduce the development cost, a fundamental understanding of tube formability and tube failure is required. There are many different ways to establish the formability limits of tubes. The most expensive is full-scale prototyping, where an entire hydroforming system is developed to test new dies and components. This trial and error approach is inefficient and sometimes ineffective for commercial industries, therefore standard material experiments, simplified mechanics models, and numerical simulations are often used to produce a hydroforming system that will be effective and efficient in the manufacturing plant's assembly line.

Process engineers frequently turn to numerical simulation to aid in the design of the hydroforming dies, lubrication, pressurization process, axial feeding and other process parameters. Prediction and prevention of failure during the forming process is extremely important, and numerical simulations provide the most accurate and useful estimates. In order to obtain accurate simulations, the pressurization process, material model, and surface interactions must all be correctly understood and modeled. The tube hydroforming machine developed at the University of New Hampshire allows the process parameters to be investigated alongside numerical simulations. Chapter 2 presents the development of a small, tabletop-sized machine capable of forming tubes along an 8 inch die span. The small scale of the device allows for it to be easily reconfigured for different experiments, while simultaneously minimizing the hardware costs. The numerical simulations will be

developed to accurately characterize the tube hydroforming process, as well as provide insight for improving formability and predicting failure.

The tube hydroforming machine will be used to evaluate the formability of Aluminum 6061 T4 tubes. These tubes are pictured in Figure 1.13, and were provided to the University from Ford Motor Company. The goal of the initial forming experiments will be to establish a baseline of successfully formed tubes (Figure 1.14), the tube material expansion limits, and the required fluid pressures and volumes. Aluminum is seeing increased use in hydroforming applications due to its high strength-to-weight ratio. Unlike steel, however, aluminum alloys (such as Al-6061-T6) tend to have low ductility, and therefore are difficult to hydroform. The less common Al-6061-T4 is specifically chosen for hydroforming in industry due to its enhanced ductility over other more common aluminum alloys.

The hydraulics and forming dies are expensive; therefore the cost of process development can be significantly reduced if the formable limit of the tube can be established beforehand. The tube hydroforming machine allows experiments on Aluminum tubes to be conducted and correlated back to numerical simulations. This allows us to better understand the behavior of anisotropic aluminum tubes for the general hydroforming process. Numerical models that predicting failure and tube-bursting are very valuable tools for improving the tube hydroforming process.

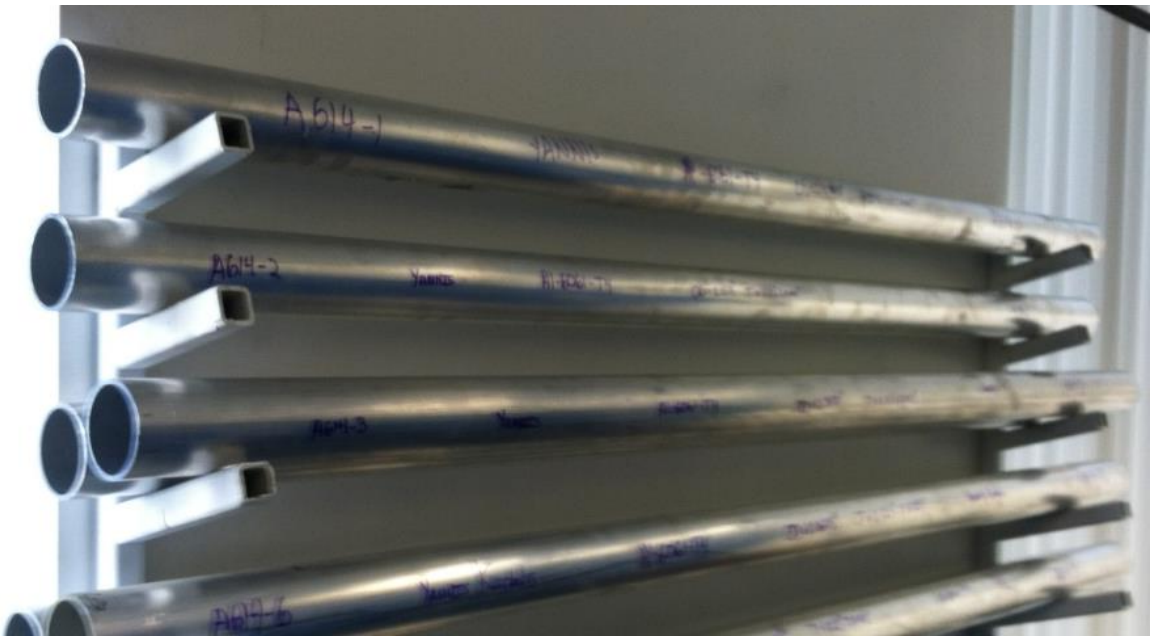

Figure 1.13: Stock Al-6061-T4 tubes for hydroforming at UNH.

Figure 1.14: Hydroformed Al-6061-T4 tubes from the table-top hydroforming machine at UNH.

In Chapter 3, the stock tube materials are tested experimentally to characterize their behavior. The tube material's post-yield plastic behavior is the most important factor in determining the formability of the tube. The material behavior is determined by the material alloy, grade, temper or heat-treatment, and manufacturing process. The type of tube is important for when selecting a candidate for hydroforming. Tubes can be manufactured in a variety of processes, but typically are either extruded from solid stock or electrical resistance welded from material sheets. Extrusions can be uniform (seamless) or have seams where the material is joined (cold welded). Seamless extrusions typically have poor wall uniformity due to their manufacturing process. Electrical resistance welding (ERW) and cold-welded extrusions produce a welded seam, which is typically slightly weaker material but also slightly thicker due to the weld. These tubes are sometimes cold-worked by being drawn over mandrel to achieve better wall uniformity and concentricity, as well as obtain the final dimensions of the tubes. The Al-6061-T4 tubes from Ford have cold-welded seams from an extrusion process using a spider die. There are three equal spaced welds along the axial length of the tube. The presence of the weld region will be identified using metallography and the material characterized in addition to the material in the non-welded region.

To characterize the Al-6061-T4 tube material, they will be tested using small specimens cut from the stock tubes. The tube material will be evaluated in both the axial and circumferential directions. To evaluate the axial direction of the tube, ASTM standard tensile specimens will be cut from both the welded and non-welded regions of the tubes, and loaded until failure by fracture. To evaluate the circumferential direction of the tube, a unique test known as the ring hoop tension test will be used. Additionally, short tubular

specimens will be expanded or flared using a 60° conical punch until failure of the tube wall by fracture. For both material directions, the specimens will be tested at the University of New Hampshire on the MTS 370 Landmark and/or the Instron 1350 servo-hydraulic machine in order to obtain the stress-strain material curves.

Finally, Chapter 4 focuses on the numerical simulations which utilize the material data obtained from the material tests for the stock tube and welded seams in order to model the forming process. The geometry of the laboratory tube hydroforming machine's seals and forming dies (Figure 1.15) will be used to develop a usable constitutive model for calculation forming pressures, volume requirements, etc.

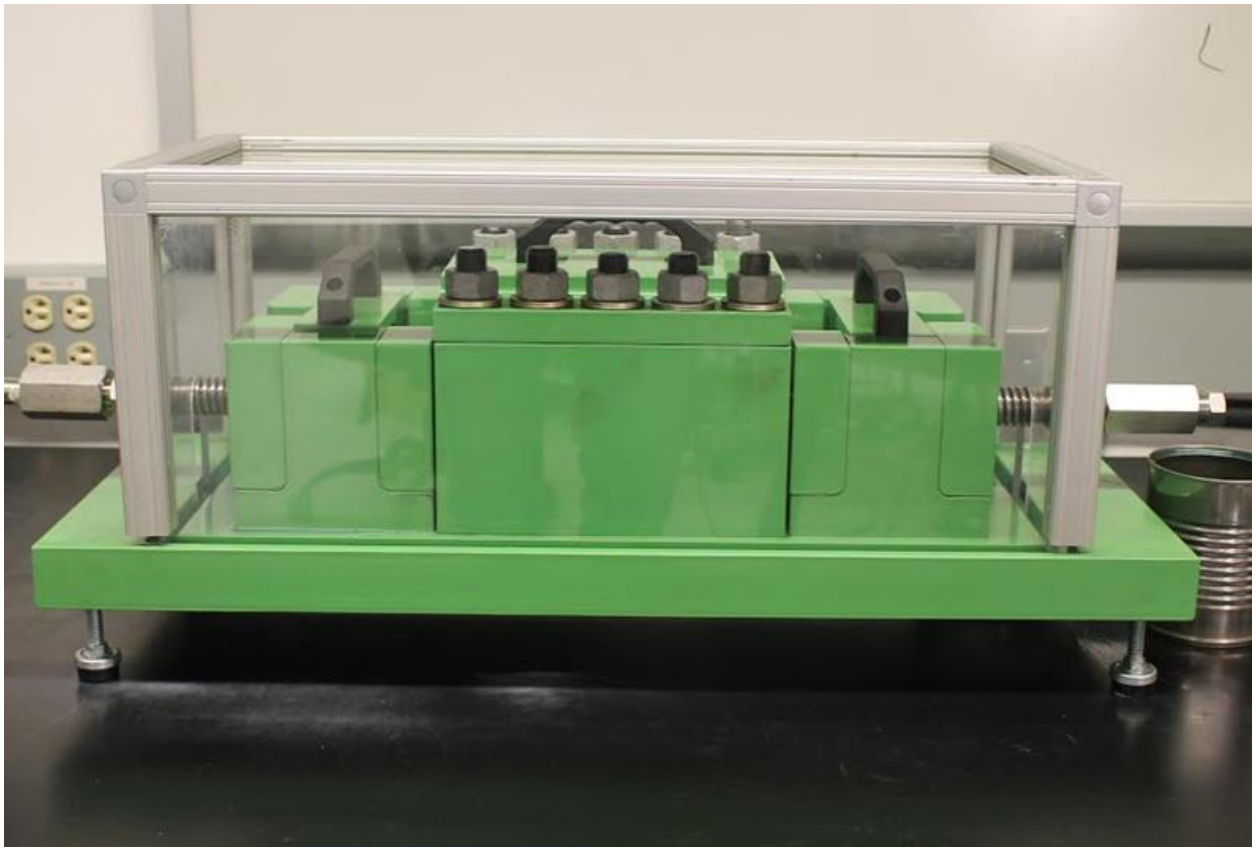

Figure 1.15: The laboratory tube hydroforming machine at UNH.

CHAPTER 2

THE UNH TUBE HYDROFORMING MACHINE

2.1 Design Overview

The laboratory tube hydroforming machine was developed at the University of New Hampshire from the Fall of 2009 to the Fall of 2011. The machine is for laboratory research and is deliberately designed to be reasonably sized for portable use within the Mechanics, Materials and Manufacturing group at the University's Kingsbury Hall facility. The machine is also deliberately designed to be easily reconfigurable for different experiments, die geometries, tube sizes, and process variants. The tube hydroforming machine accomodates tubes from 1 inch to 2.5 inch outer diameter, and 14 inches in length with an 8 inch formed span. The machine is currently setup for tubes of 2.25 inch outer diameter. The full design drawings are available in Appendix A.

The forming dies in Figure 2.1 are removable from the upper and lower halves of the device. This allows the machine to utilize interchangeable dies of different width geometries and corner radii for parametric forming studies. The dies are machined from A2 tool steel and have been heat-treated to a strength of 225 ksi (~1550 MPa). The hydroforming machine is designed for typical forming pressures up to 10,000 psi (690 bar) using a closed loop system consisting of a fluid reservoir and pressure intensifier. Alternatively, it can be used with an independent pressure source, such as an Enerpac hand pump. The machine is designed to accommodate many typically hydroformed materials, including aluminum, brass, copper, or even high grade steel; therefore the machine has been designed to withstand working pressures as high as 20,000 psi (1379 bar). The actual operation at

10,000 psi (690 bar) provides a minimum safety factor of 2.0 for all device components. The tubular blank to be hydroformed is often referred to as the workpiece. Since the tube will often be formed until failure, it is extremely important that the high pressures must be contained safely by the device, and the device able to withstand said pressures without relying on the tubular specimen to contain the load.

The ends of the workpiece are sealed to prevent the pressurized fluid from leaking using the assembly show in Figure 2.2. The cylindrical part is known as the exterior seal housing, and is tapered inside, which allows it to form a snug interference fit with the tube. The taper also aids in accommodating any eccentricity in the tube wall. Pressurization of the cavity helps to press the tube further into the taper. The exterior seal housing has a threaded exterior that is screwed into the square seal housing. This allows for the new exterior seal housing for different tube diameters to be interchanged. Also, since the external seals can be unthreaded, the back of the formed tube can be accessed in order to remove the workpiece from the machine if it becomes seized in the taper after forming.

Inside each external seal assembly is another sealing mechanism, known as the internal seal. The seal screw has a 0.25 inch (6.35 mm) diameter inlet through which fluid is pumped into the tube. The screw is designed to be tightened from the outside using the 1 inch hex head, which compresses a 40 Shore urethane block against the interior of the workpiece, as seen in Figure 2.3. This action provides sealing of the hydraulic fluid at the beginning of a hydroforming experiment. In addition, as the experiment progresses and the internal pressure is further increased, the urethane block is further compressed against the interior of the specimen, thus causing the seal to self-tighten.

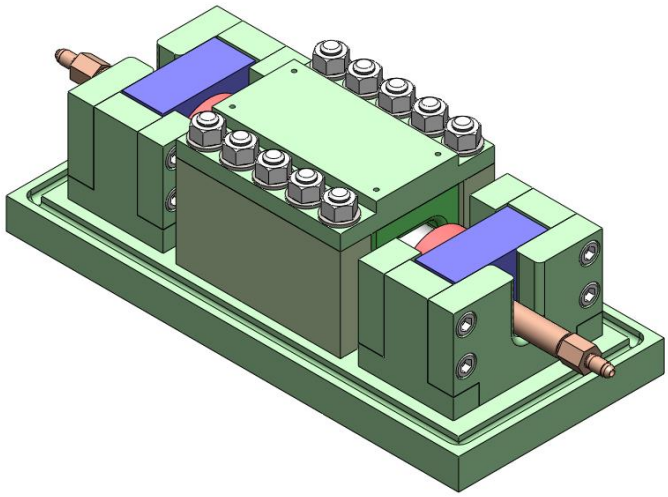

(a)

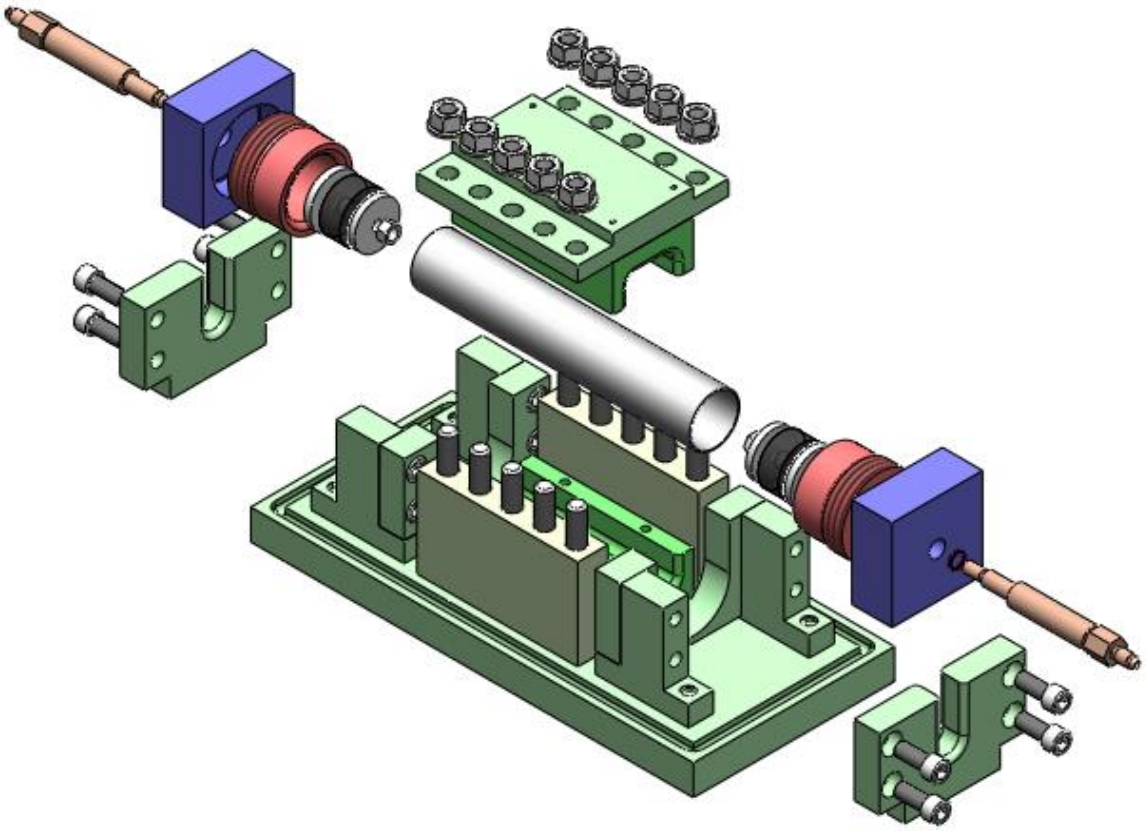

(b)

Figure 2.1: Overview of the UNH Tube Hydroforming machine

(a) collapsed and (b) exploded isometric views.

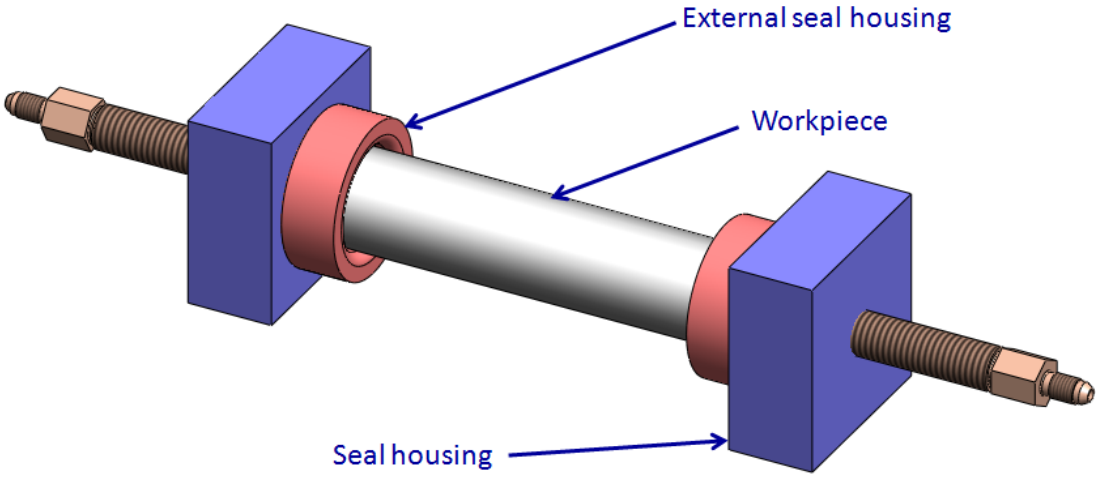

Figure 2.2: A tubular blank workpiece with the seal assembly on either side.

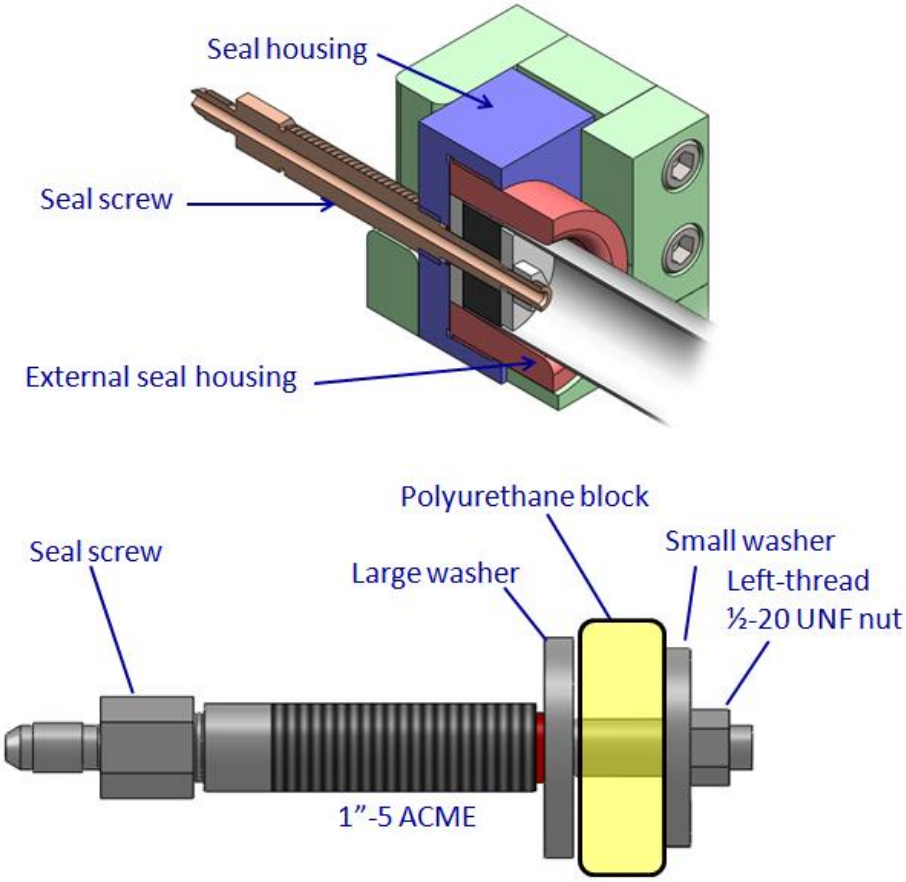

Figure 2.3: Internal sealing mechanism.

The end-block housing assemblies hold the seal housing assemblies and prevent them from rotating or moving axially by transferring the pressure on the seals to the base plate. This assembly is designed so that the sealing assembly and tubular blank can be dropped into the end-blocks for ease of placing, removing and changing specimens, as illustrated in Figure 2.5. Each end-block is assembled out of four components, which allows the end-block back plate to be removed in case the tube seizes inside the taper of the seal after forming. Removing the back plate after forming also alleviates any swaging of the seal housings from the axial forces induced during a test. This plate is secured to the end-block T-components with four bolts. The T-components are secured to the base plate using two shear pins and four preloaded bolts, which resist the shear force and bending moments respectively. The bolts are preloaded to prevent separation due to the elastic stretching of the bolts during full load. The preload creates a frictional force between the bottom of the T-component and the base plate, which reduces the shear load on the shear pin. The base plate has rubber leveling feet which rest on a table.

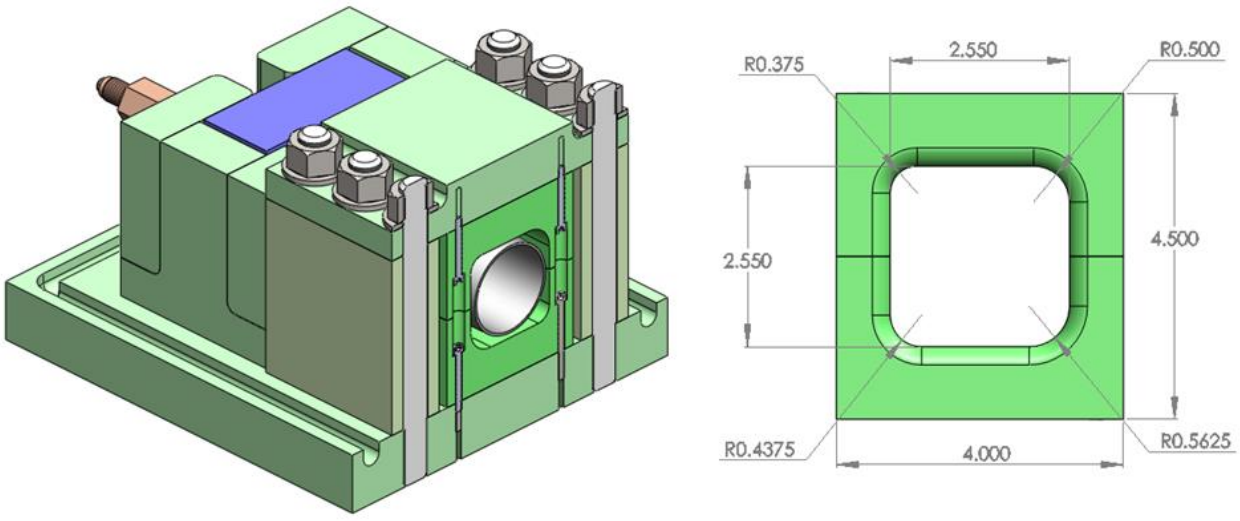

Figure 2.4: Die geometry of the initial configuration.

For the machine's initial configuration, two U-channel shaped die halves will be used to form a square cross section with rounded corners. Each corner radius is unique in order to evaluate the degree of corner filling before failure. The die halves are bolted to the top plate and base plate respectively using four socket head cap screws each, as shown in Figure 2.6. Figure 2.4 shows the machine assembly cross-section. The top die features more common radii of 0.375 inches (9.5 mm) and 0.500 inches (12.7 mm). The bottom die features less common radii of 0.4375 inches (11.1 mm) and 0.5625 inches (14.3 mm). The span of the die is 2.500 inches (63.5 mm), and the die length is 8 inches (203.2 mm). To prevent the dies from separating during full pressurization, the top plate and base plate are clamped together using ten preloaded threaded studs. Aluminum sidewalls are placed between the top plate and base plate to prevent bending of the top plate during preloading. Aluminum was specifically chosen here because it helps preload the forming dies to prevent separation during operation at maximum pressure. The preload calculation will be detailed later in this chapter.

During the detailed design, numerical simulations of critical components under high loads were performed using finite element analysis within PTC Pro/Mechanica and DTS SolidWorks. The results of these simulations have been compared to the stress magnitudes and contours expected from simplified beam analysis. The design was also analyzed to verify that the thickness of the die walls, upper and lower plating, end-blocks, and end-cap seal housings was adequate to withstand an internal pressurization of 20,000 psi (1379 bar). The stresses on the critical components determine the required strength, which in turn determines the material and heat-treatments necessary for that component. These analyses will be described next.

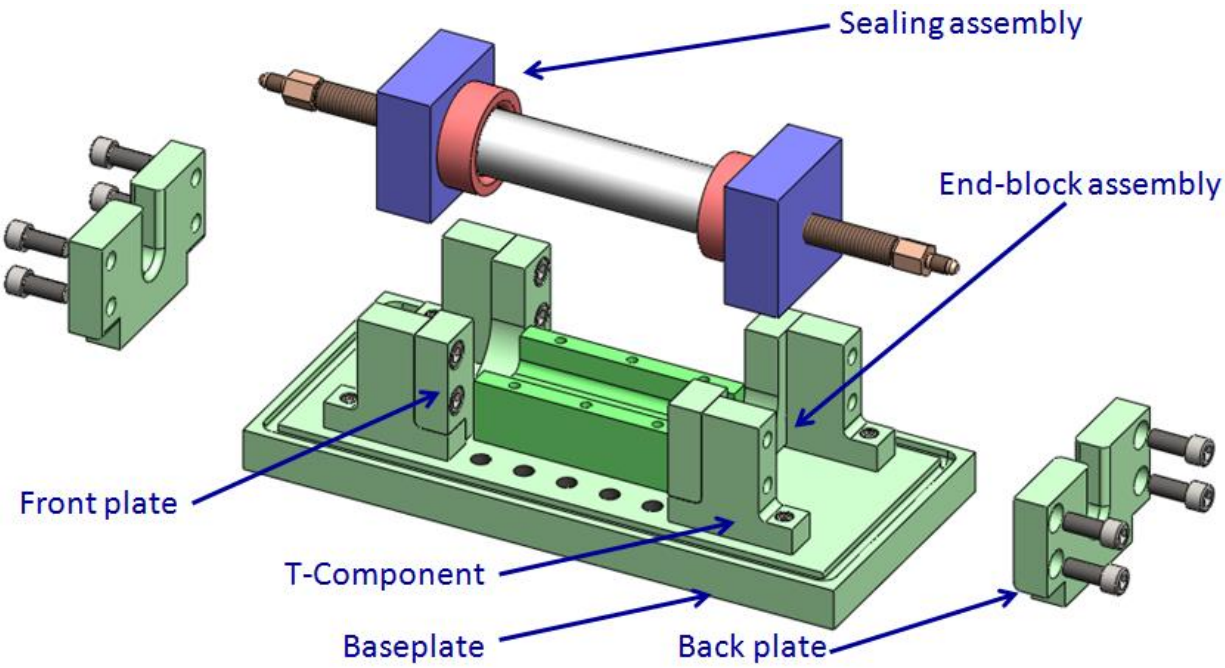

Figure 2.5: End-block assembly to hold seals.

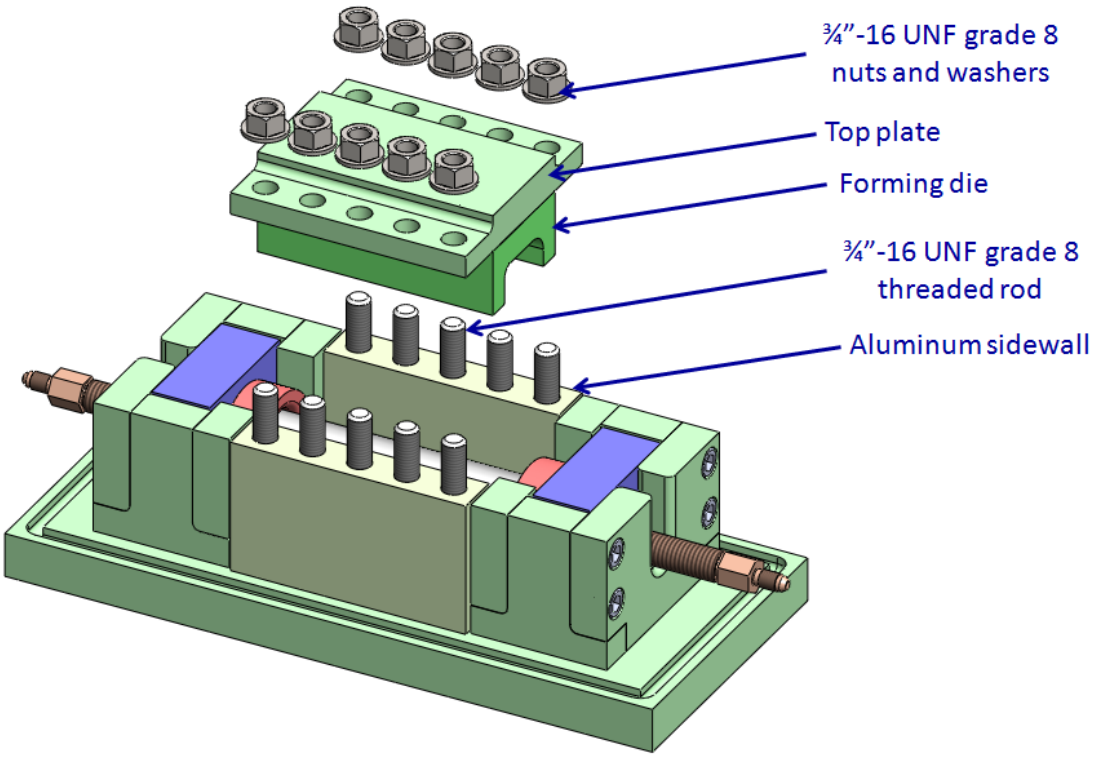

Figure 2.6: Removal of top plate and upper forming die.

2.2 Detailed Component Design

When the tube is fully pressurized, the machine is subjected to the full forces of the internal pressure and must be designed to safely withstand these loads (see Figure 2.7). In order to begin the static analysis of the device, the interaction of the internal pressure on the hydroforming dies must be determined. The internal pressure of the formed tube creates reaction forces on the hydroforming dies and external seals in the horizontal and vertical directions. Since the ends of the tubes are closed, the machine is also subjected to a reaction force in the axial direction. This axial force is transferred to the base plate by the end-block assembly.

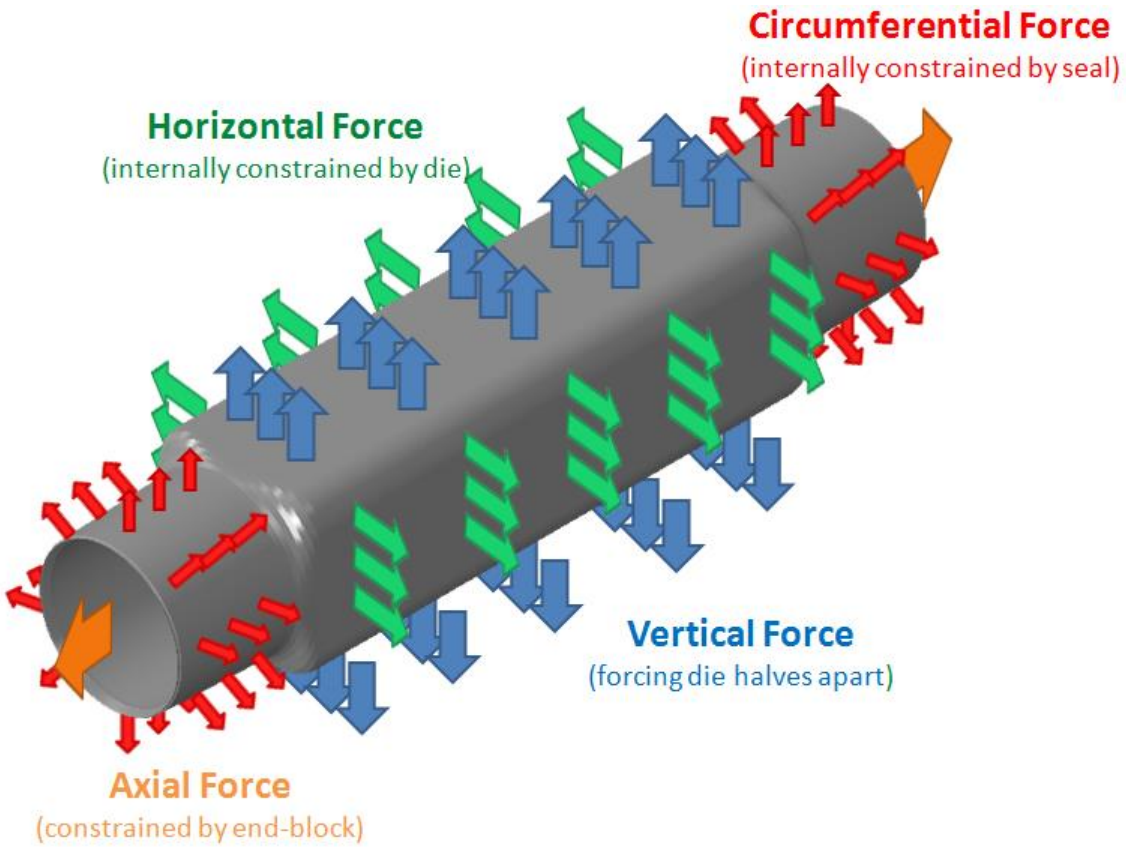

Figure 2.7: Loading of the machine dies due to formed part at full pressurization.

By taking advantage of the geometry of the die, some of the pressure can be constrained within the dies themselves. The machine uses two die halves. Each die half can internally withstand the horizontal force generated from the formed tube at full pressure. The strength of the die design has been verified using linearly elastic FEA code from PTC Pro/Engineer (see Figure 2.8). The model uses a distributed load on the interior die surface of 20,000 psi (1379 bar) to simulate the pressure of the formed tube. Symmetry boundary conditions were implemented for a quarter model of the die half. The minimum corner radius was found to be 0.325 inches (8.25 mm) for the A-2 Tool steel material used for the forming dies. Therefore, future dies could theoretically support a smaller radius than the current 0.375 inch (9.53 mm) radius on the upper die.

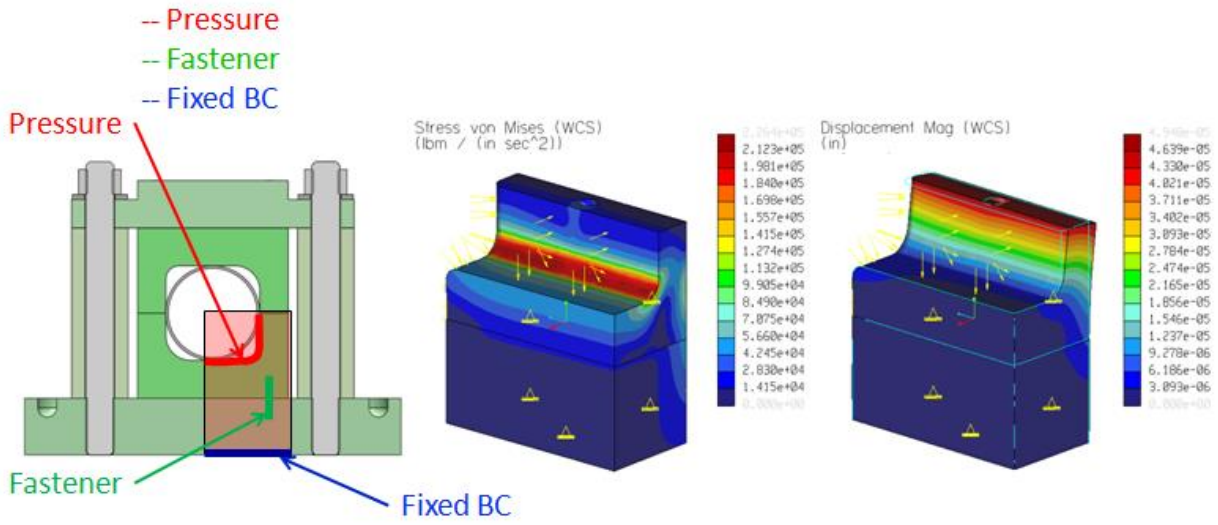

Figure 2.8: FEA of the forming die corner radius was performed using Pro/Engineer. The minimum corner radius for the die was found to be 0.325 inches for A-2 tool steel (σ_{yield}=225 ksi). The quarter model of the lower die shows a maximum stress of 212 ksi.

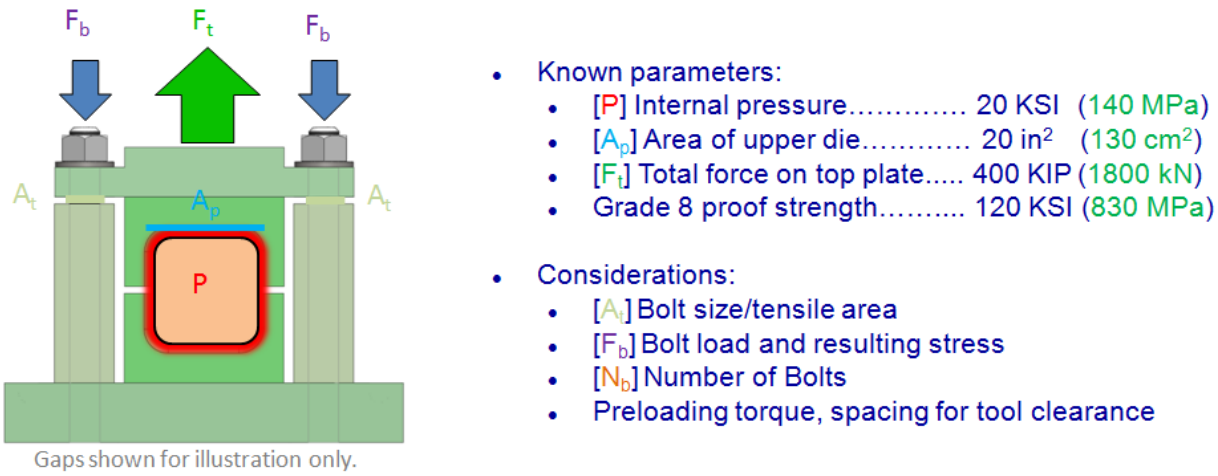

Figure 2.9: Equilibrium state of vertical reaction and bolt loads.

The vertical reaction force is transferred from the upper die to the top plate, and from the lower die to the base plate, as seen in Figure 2.9. The upper die is secured to the top plate, which is made of 4140 steel, using #10-32 socket head cap screws. The base plate is significantly thicker than the other plates of the machine, and therefore is made of 1018 steel for considerations of cost and machinability.

It is very important that the dies remained closed during the tube hydroforming process. Using the vertical area of the die, 20 in^2 (~130 cm^2), and the internal pressure of 20,000 psi (~1400 bar), the net vertical force can be found to be 400 kips (~1800 kN). To resist the vertical reaction force, the plates are held together with ten grade 8, 3/4"-16 UNF threaded studs custom-made from heat treated 4140 steel. The factor of safety against the bolt proof strength is 1.21, based on the full 20,000 psi (1379 bar).

In order to prevent separation of the hydroforming dies at the maximum working pressure of the machine, the ten grade 8, 3/4"-16 UNF studs (see Figure 2.6) must be

preloaded to 361 lbf-ft. This compresses the hydroforming dies so that they will not separate due to the elastic stretching of the preloaded studs. The support walls are made of aluminum 6061-T6 instead of steel in order to aid in the compression of dies during preloading. The steel dies, aluminum sidewalls, and steel bolts form a clamped joint that can be analyzed by finding the effective joint stiffness. A comparison of two different sidewall materials and the effect on separation and preload are shown in Figure 2.10. The analysis of the clamped joint can be found in Appendix B and covers many configurations. The preload must be selected so the joint does not open due to elastic strains on the bolts during pressurization; however, the preload must not exceed the bolts proof strength. These two competing criteria lead to the conclusion that a softer, aluminum sidewall allows a lower preload to be used than a steel sidewall.

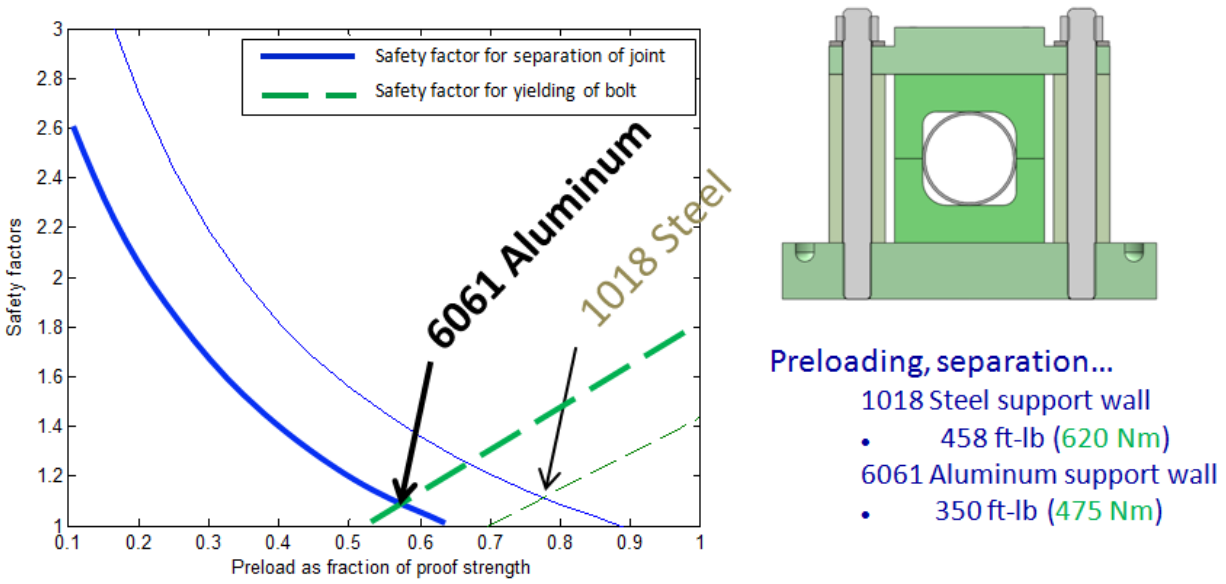

Figure 2.10: The effect of sidewall material on the required preload to prevent separation of the dies within the bolted joint. A safety factor of 1.15 was found for a preload that is 56% of the bolt's proof strength when the machine is at the 20,000 PSI load. The equivalent torque to produce this preload is 361 lbf-ft.

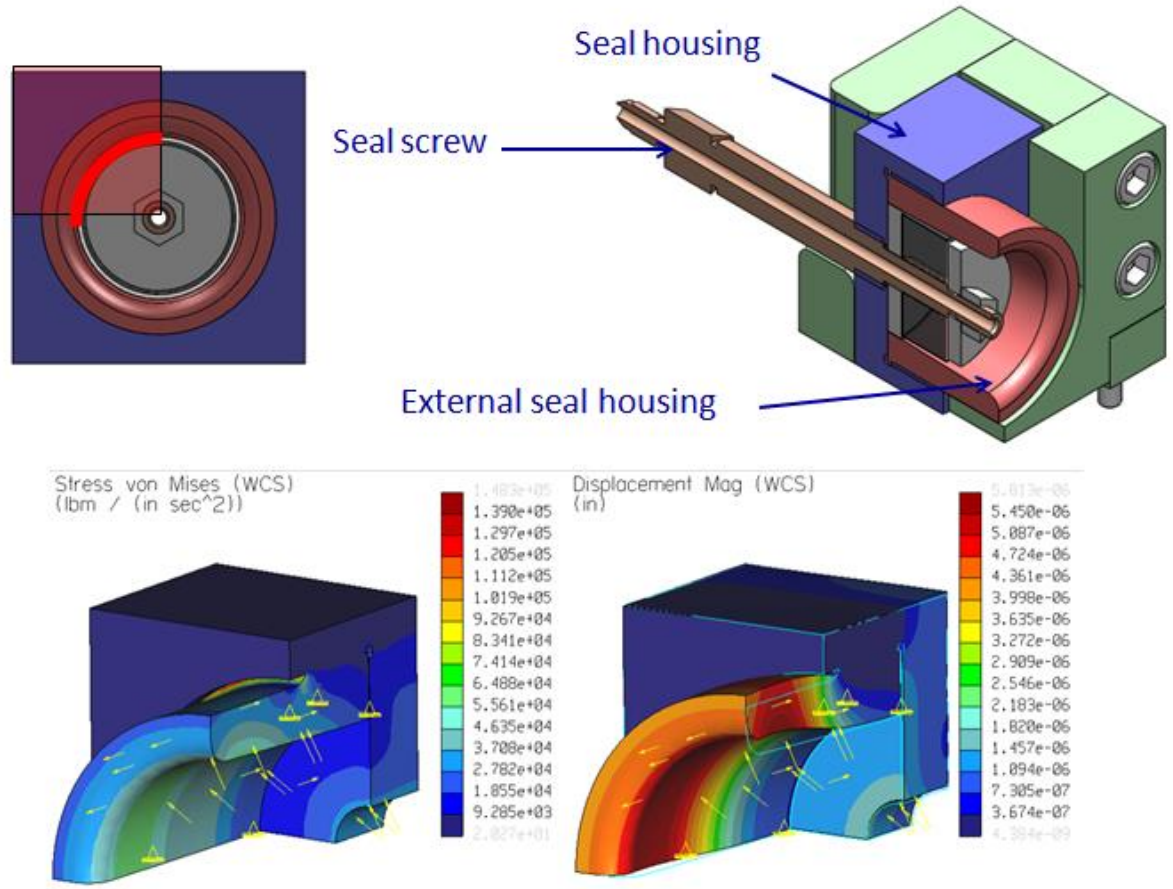

Figure 2.11: Finite element analysis of the end-block external seal housing. This is a quarter model, the maximum stress is 65 KSI. The stress concentration is an artifact due to the geometry of the threaded region.

The ends of the tube must be constrained circumferentially to prevent the tube from expanding and compromising the seal. The external seal housings are similar to the hydroforming dies since they are in contact with the tube surface and are subjected to the internal working pressure. These external seals are made of 4140 steel, and cause a metal-to-metal seal on the exterior surface of the tube. The design of the seal has been analyzed as an axisymmetric, thick wall pressure vessel with open ends. This analysis can be found in Appendix C. Additionally, the strength requirement for the external seal has been

determiend using finite element models in Pro/Engineer, as seen in Figure 2.11.

Due to the required forming pressures and the possibility of fluid volume loss due to leaking seals, the UNH hydroforming machine and the internal sealing mechanism had to be carefully designed. In commercial hydroforming, the tube is sometimes not fully sealed - however the pressurization process is so rapid that the leakage volume is minimized. Due to the expected used of the tube hydroforming machine at UNH, which may pressurize slowly in some experiments, a complete watertight seal is absolutely necessary. At the tube filling stage, the ends of the tube must be sealed to create an internal cavity. The seal must be maintained as fluid is introduced for the pressure to increase. To accomplish a complete seal, the UNH hydroforming machine has an internal and external seals.

To seal the tube at low pressures, the sealing mechanism for the UNH hydroforming machine utilizes an internal polyurethane plug. The uncompressed polyurethane plug has an outer diameter of 2 inch (50.8 mm), a 2 inch (50.8 mm) length, and has a hardness of 40 shore. This is approximately equivalent to a common pencil eraser. The plug is fully reusable for multiple experiments, providing an advantage over conventional O-ring seals.

Once a tube has been loaded into the sealing mechanism, the sealing screw is turned to compress the polyurethane plug between two thick washers. The screw is designed to be tightened from the outside using the 1 inch hex head. The polyurethane plug compression is accomplished using a 1"-5 ACME thread on the seal screw and seal housing. The washers are held in place on one side by the seal housing and on the other side by a left-hand threaded 1/2"-20 UNF grade 8 nut. As the seal screw is rotated counter-clockwise, the plug compresses axially, but expands radially to seal the internal surface of

the tube. Since the nut is left-hand threaded, it will only tighten when the screw is tightened, preventing any risk of the nut unthreading during the sealing operation. The seal screw has a 0.25 inch diameter inlet through which fluid is pumped into the tube. This is illustrated in Figure 2.12.

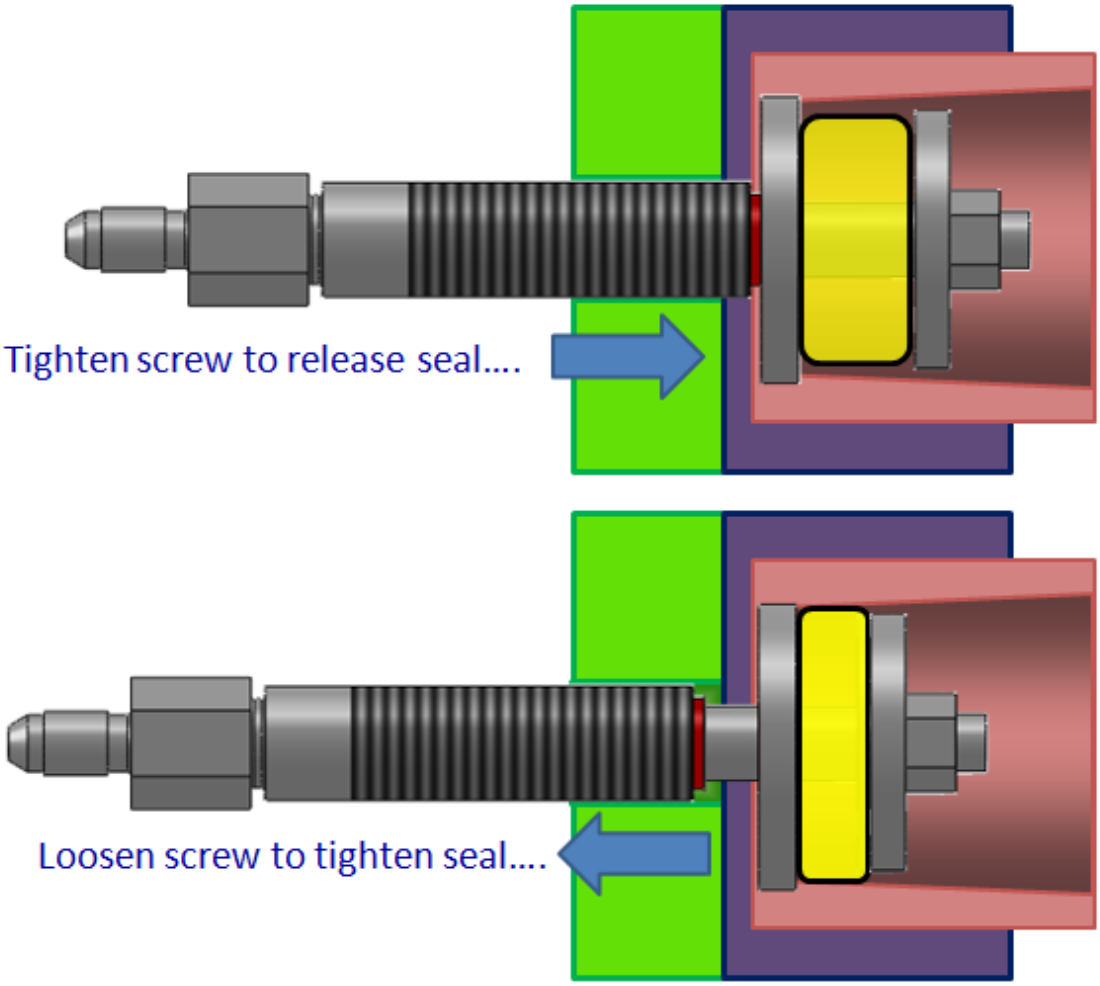

Figure 2.12: Cross-section of the sealing mechanism inside the endblock.

As the internal pressure increases, the urethane continues to compress axially, which

improves the sealing against the internal surface of the tube (self-help design principle). The exterior of the tube is constrained by the external metal-to-metal seal of the external seal housing. As the pressure becomes high, the tube is swaged against the external seal, creating a metal-to-metal self-help seal that increases effectiveness with pressure.

The external seal housing is threaded into the seal housing with a 3 3/4"-8 UN thread (visible in the cross section shown in Figure 2.11). This thread is not designed to take any load, as the external seal housing is threaded until firmly seated on the back of the seal housing. This is to allow future external seal housings to be fabricated for new tube outer diameters and be fully interchangeable within the machine.

In order to maintain the position of the plug and integrity of the seal, the seal housing must be attached to the base plate. This is accomplished using an end-block assembly in which the seals are placed. Each end-block assembly consists of T-components, a back plate and a front plate. These components can all be seen in Figure 2.13. All end-block components are produced from 4140 steel for strength. The T-components are fastened using a 3/4 inch shear pin to prevent axial displacement and four grade 8, 3/8"-16 UNC socket head cap screws to prevent rotation due to the moment. The 3/8"-16 UNC socket head cap screws are preloaded to 61 foot-pounds to prevent separation due to the elastic stretching of the bolts during full load. The preload creates a frictional force between the bottom of the T-component and the base plate, which reduces the shear load on the 3/4 inch shear pin.

The end-blocks provide the reaction forces necessary to maintain the seal, but also allow the specimen to be loaded and the formed tube to be removed without disassembly.

In the event that a formed tube becomes swaged inside the machine, the back plates can be removed to alleviate the swage and remove the tube. The specimen and seals are loaded into the end-blocks, where the seals are kept in position by the end-block back plate, which is secured with four grade 8, 5/8"-11 UNF socket head cap screws. The back plate transfers this force from the seal housings to the T-components. The T-components then transfer the reaction to the base plate through the shear pins.

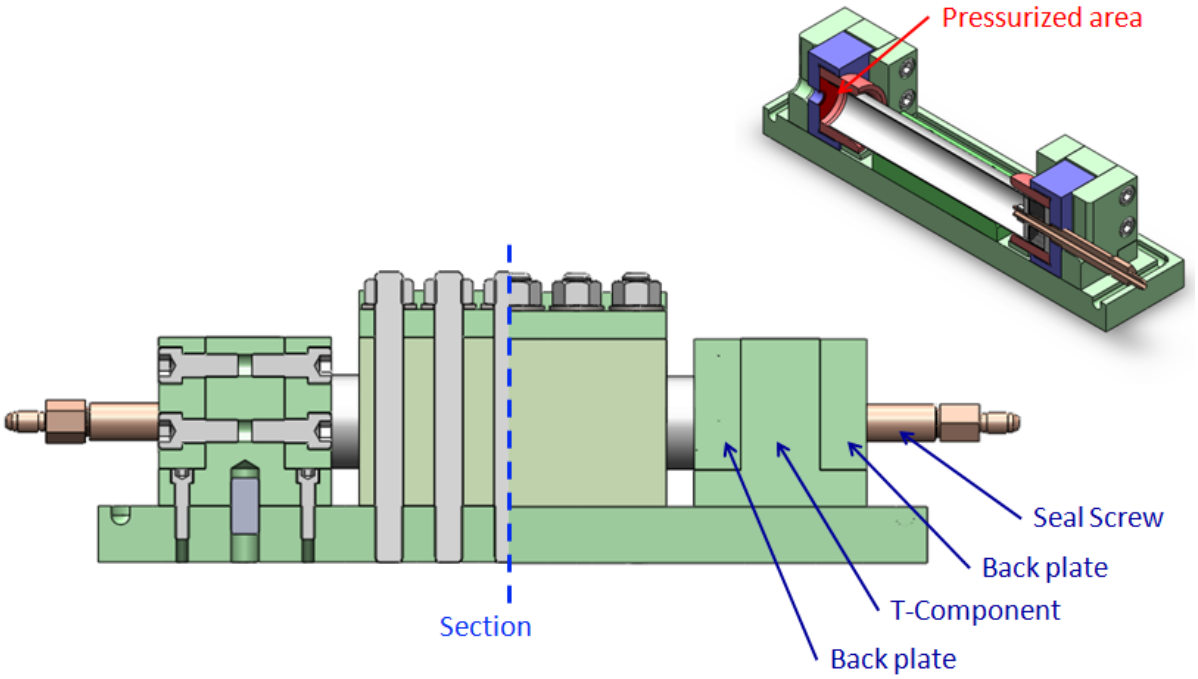

Figure 2.13: Cross-section of the sealing mechanism inside the end-block.

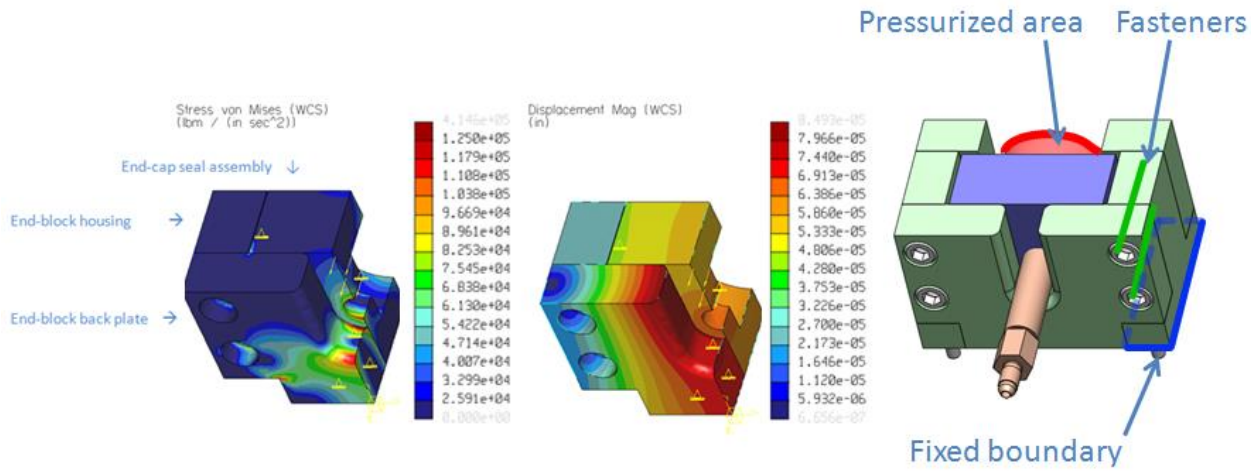

Figure 2.14: Finite element analysis of the seals and backplate. The peak stress is 125 KSI on the back plate at the plane of symmetry.

Since these components are load bearing and are critical to maintaining the integrity of the seal, the end-block assembly has been analyzed for strength using finite element analysis in SolidWorks. The results for the half model of the back plate are shown in Figure 2.14. Due to the loading and reaction forces induced by the 20 ksi pressurization, the components of the machine require very high strengths. The stiffness of steel is suitable for forming machines, and the hardenability of 4140 steel allows for heat-treatments for additional strength over low-carbon steels such as 1018.

2.3 Machining and Heat Treatments

All of the UNH tube hydroforming machine parts were machined on a Fryer MC-10 CNC with a Fanuc controller. The toolpaths were generated using MasterCam X5 for SolidWorks. Since there are multiple instances of the same component in the assembly, the CNC provides the advantage of reproducibility. The machine features a flood coolant system to cool the work piece and cutting tool. The flood coolant allows the cutting speeds

to be increased and overall machining time to be decreased as compared to conventional milling operations. Once the toolpath programs were developed, they were first run on dummy MDF (medium density fiberboard) material, to verify that there were no mistakes. The validated toolpaths were used multiple times to produce the required number of parts for the machine.

The hydroforming dies are critical to the forming results. The dies are subjected to the large internal pressure, and therefore should have both high stiffness and high strength. Many variants of steel are capable of high strengths through heat treatments; however, exotic steels can be difficult to machine with conventional mill tooling. As a result, A-2 tool steel was chosen for its balance of machinability and hardenability. After purchasing the material in the annealed state, the machining was performed on the Fryer MC-10 CNC.

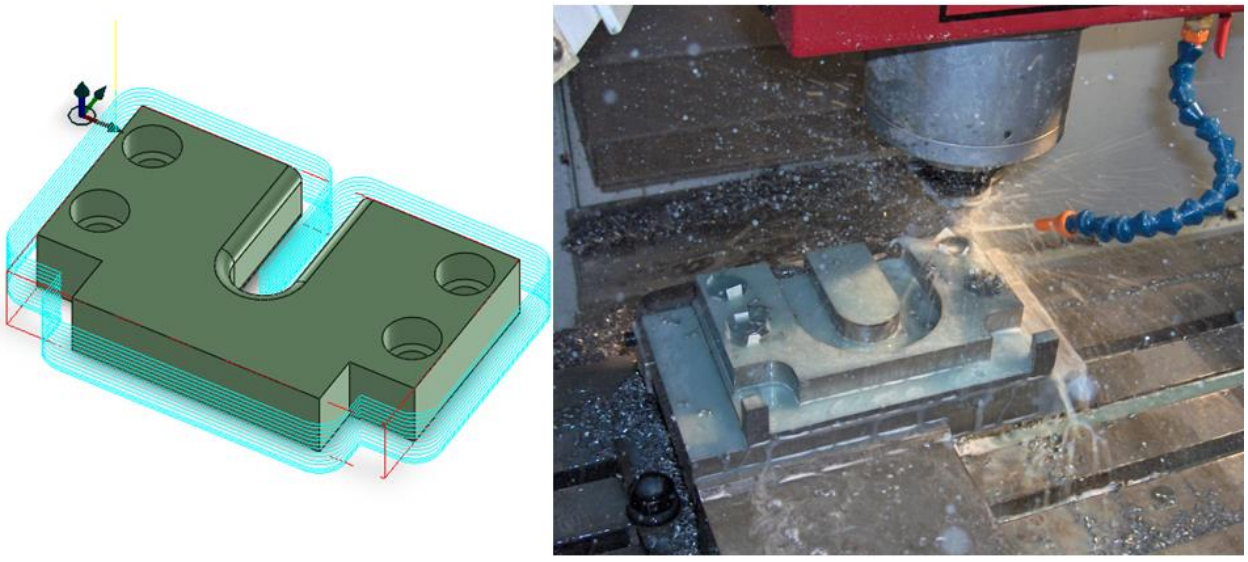

Figure 2.15: An example of the CNC machining being performed at the UNH CEPS machine shop on the Fryer MC-10.

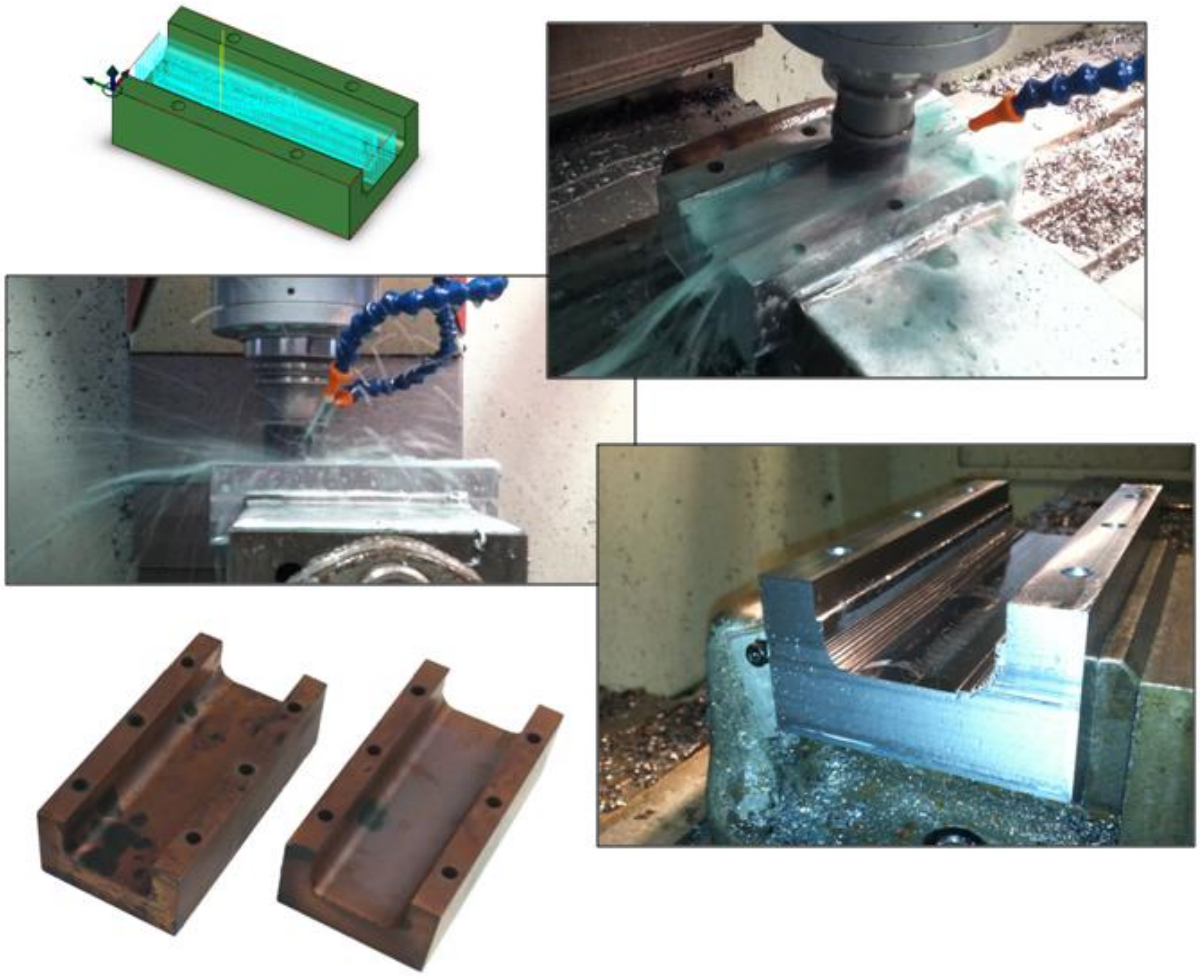

Figure 2.16: The rough cutting of the hydroforming dies in the Fryer MC-10 CNC machine at the University of New Hampshire.

The dies require a smooth surface finish to mitigate friction during forming. The dies were rough cut using a 2 inch (50.8 mm) Sandvik carbide insert tool holder, and finishing using carbide ball mills for the appropriate corner radii (see Figure 2.16). The roughing and finishing passes combined with carbide tools led to obtaining a smooth surface finish for the tube hydroforming dies.

The dies also require a hard surface to prevent gouging and scoring. The annealed

A2 material does not have the strength required for the full loading of the machine. To obtain the desired yield strength and surface hardness, the hydroforming dies were outsourced for heat treatments by BodyCote Thermal Processing in Laconia, NH. They recommended a gas quench at 1050°F in order to obtain a hardness of 62-63 HRC. This is approximately equivalent to the 225 ksi (1551 MPa) yield stress required for the part.

In addition to the dies, several parts for the hydroforming machine required greater strength than the strength of annealed 4140 steel (61 ksi / 421 MPa). The FEA for the top plate, T-components, and back plates showed that the required strengths were as high as 125 ksi. These parts were outsourced to BodyCote to be quenched and tempered at 800°F. Targeting a strength of 156-177 ksi (1075-1220 MPa), BodyCote obtained the equivalent Rockwell C hardness of approximately 36-37 HRC. Additionally, a 2.25 x 2 x 1.5 inch (57.2 x 50.8 x 38.1 mm) test coupon was included for hardness testing and future strength verification (see Figure 2.17).

The hardness of the test specimen was verified in the UNH Metallurgy laboratory using the Rockwell diamond indenter. Using a sample 4140 steel Hardness tests were performed on the surface of the piece; the readings were approximately 41 HRC. The specimen was then cut in half using the dropsaw, and the hardness evaluated through the 1.25” thickness of the test specimen. This was the smallest dimension of the specimen, and therefore, the limiting thickness for the heat to be conducted through during the treatment.

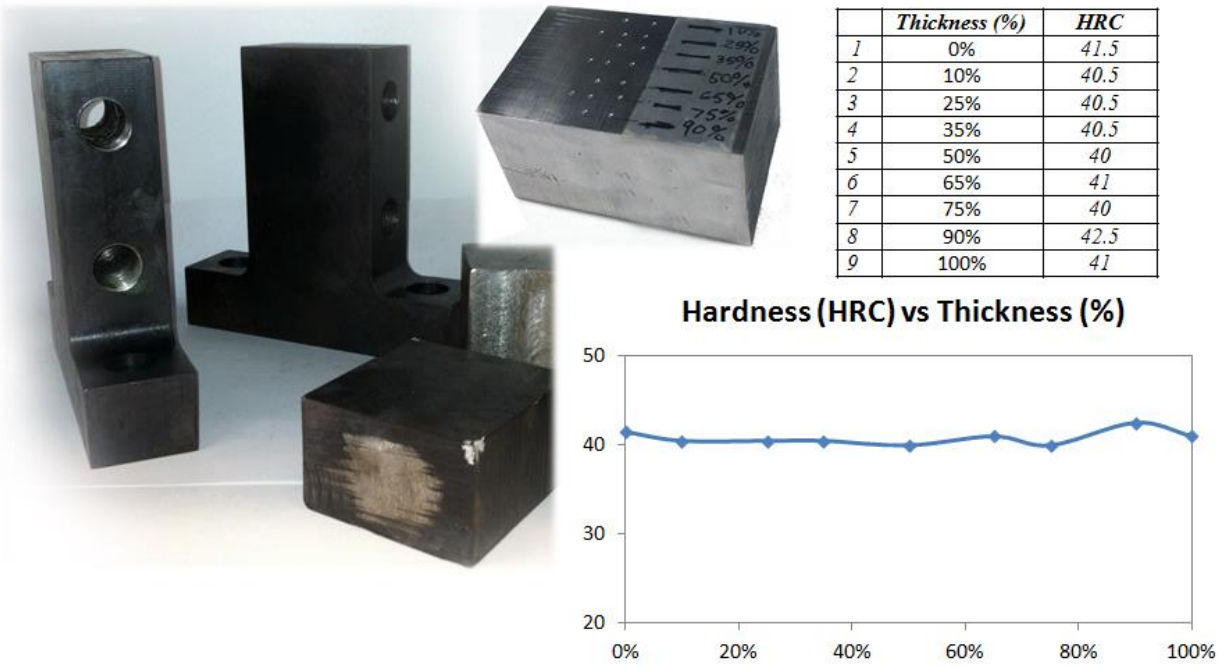

	Thickness (%)	HRC
1	0%	41.5
2	10%	40.5
3	25%	40.5
4	35%	40.5
5	50%	40
6	65%	41
7	75%	40
8	90%	42.5
9	100%	41

Figure 2.17: Validation of heat treated components from BodyCote.

A minimum of two hardness tests were performed for each data point. Some variation in the hardness readings is to be expected due to the nature and age of the Rockwell C tester available in the lab. The 4140 steel has been heat treated using an oil-based quench and tempered from an annealed condition to a hardened condition. The hardness of the material was targeted around 36-37 HRC, and the verified readings hard found the hardness of the material to be uniformly 41 HRC through the thickness of the 1.25 inch (31.8 mm) specimen. A hardness of 36 HRC is approximately equivalent to a yield stress of 165 ksi (1137.6 MPa), while 41 HRC hardness is approximately 189 ksi (1303 MPa). Both strengths are sufficient for the parts for the hydroforming machine.

The off-the-shelf hardware, including the 5/8"-11 UNF bolts, 3/8"-16 UNC bolts, and #10-32 bolts were purchased with a SAE grade 8 certification. The threaded rods for clamping the forming dies between the top plate and base plate are custom ordered 3/4"-

16 UNF. The eight inch long, heat treated 4140 steel rods haves two inches of threads on each end. Rolled threads are preferred for high strength and fatigue applications; however, due to the size of the studs and the capabilities of the manufacturer, the threads could not be rolled. The cut threads should have sufficient strength, but a spare set of ten studs was ordered, in case fatigue or accidental overloading becomes an issue. The threaded rods were independently certified to be grade 8 strength.

The strength was also validated at UNH using the 1 MN (220 KIP) Instron servohydraulic load frame available from the Civil Engineering department. A reduced section was cut from the 3/4" nominal diameter to bring the diameter down to 3/8". The test data and results are provided in Appendix D. The results are shown in Figure 2.18.

Test performed by:	Gage Diameter (in)	Max Load (lbf)	Tensile Stress (psi)	Yield (0.2%) (psi)	Elongation (%)	Surface Hardness (rC)
All-Ohio Threaded Rod Co.	0.356	17761.0	180000	162000	14	39
UNH	0.375	19910.5	178000	164000	16.95	-
SAE J429-1999 Grade 8	-	-	> 150000	> 130000	-	-

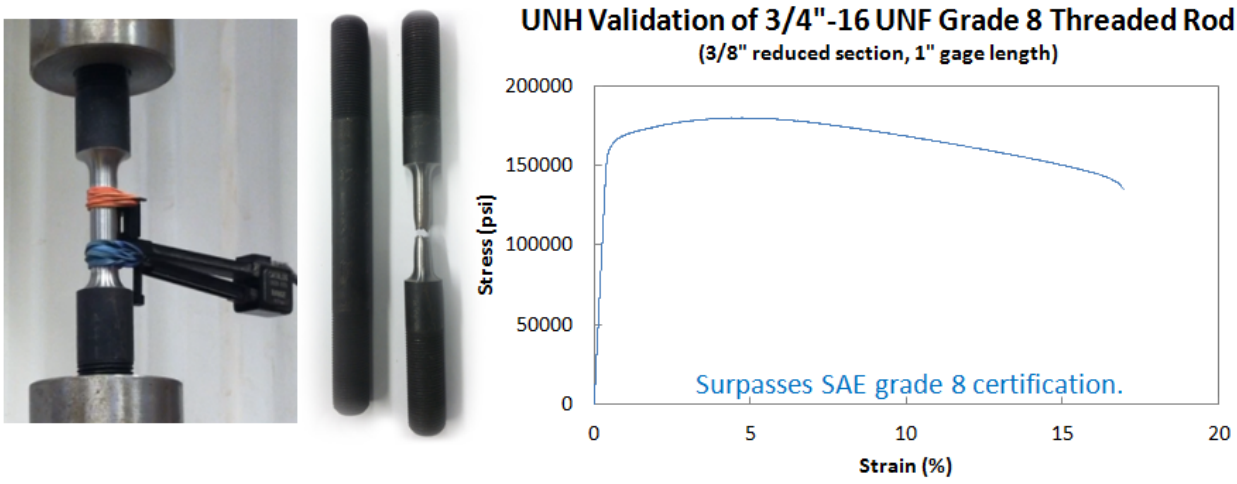

Figure 2.18: SAE grade 8 certification validations performed by the University of New

Hampshire and independently by All-Ohio Threaded Rod.

2.4 Workpiece Preparation

The tubular blank to be formed is referred to as the workpiece. The workpiece is first cut to length. The maximum length for the 2.25 inch (50.8 mm) diameter seals is 13.75 inches (349.3 mm). Specimens may be as short as 12 inches (305 mm), however the maximum length should be used to provide the largest contact area for the internal polyurethane seal. This is because as the tube is formed, the ends will contract and the length of the tube in contact with the inner and outer seal will decrease. As a result, the tube length should be maximized when possible.

Once the tube is cut to length, the thickness of the wall should be recorded prior to the experiment. A ball micrometer or ultrasonic thickness gage is suitable to measure the nominal thickness and wall eccentricity tolerance. Although not required for operation, for research purposes the specimen geometry should be measured and the thinnest region of the wall should be noted and marked as a potential zone for failure. If possible, the positions of the tube's manufacturing seams should be noted.

Some specimens may require a 2° taper on the ends if they are too eccentric or too large for the seal housings. Again, the tube should be seated as deep inside the seal as possible so the maximum length should be used when possible.

2.5 Machine Assembly

There are several steps included in the assembly of the hydroforming machine in order to load or unload a workpiece, detailed in Figure 2.19. The sealing components must

be assembled first. This includes the interior seal cap, the exterior seal housing, and the sealing screw, shown in Figure 2.3. The interior seal cap is externally threaded and is inserted into the square external seal housing first. The external seal housings should be fully threaded into the seal housings (Figure 2.19(A)) so they are seated flush against the back of the housing. Next, the seal screw can be inserted through the inside of the interior seal cap and the components of the seal screw added and tightened. The sealing screw is comprised of the screw itself, a press fit ring, large washer, polyurethane block, small thread washer, and left hand thread nut, assembled in that order (Figure 2.3). The left-threaded nut should not be fully tightened, as it will also tighten when the seal screw is tightened by being rotated counter-clockwise.

The tubular blank workpiece is going to be inserted into each seal, and then the seal screw tightened to seal the interior or the tube against the polyurethane plug. The base plate is assembled next. The lower die is secured, followed by the T-components (Figure 2.5), whose 3/8"-16 UNC bolts must be preloaded to 61 foot-pounds. Once the T-components are secured, the front plate can be secured using the 5/8"-11 UNF bolts. The 3/4"-16 UNF studs can be fully threaded into the base plate, so that the first thread is beginning to protrude from the bottom of the base plate. The aluminum sidewalls can be placed over the threaded rods (Figure 2.19(A)).

Separately, the upper die should be secured to the top plate using the #10-32 screws. To load the specimen, the seal housings and workpiece are dropped into the end-block assemblies. The external seal housings should sit in the U-shaped channel of the front plate, and should not be touching the hydroforming dies. Once the seals are in place, the

back plates (Figure 2.19(C)) can be secured using the 5/8"-11 UNF bolts. Finally, the top plate and upper die can now be placed onto the machine and secured using the grade 8 nuts and washers preloaded to 361 foot-pounds (489 N-m). Figure 2.19 describes the major steps in the assembly process.

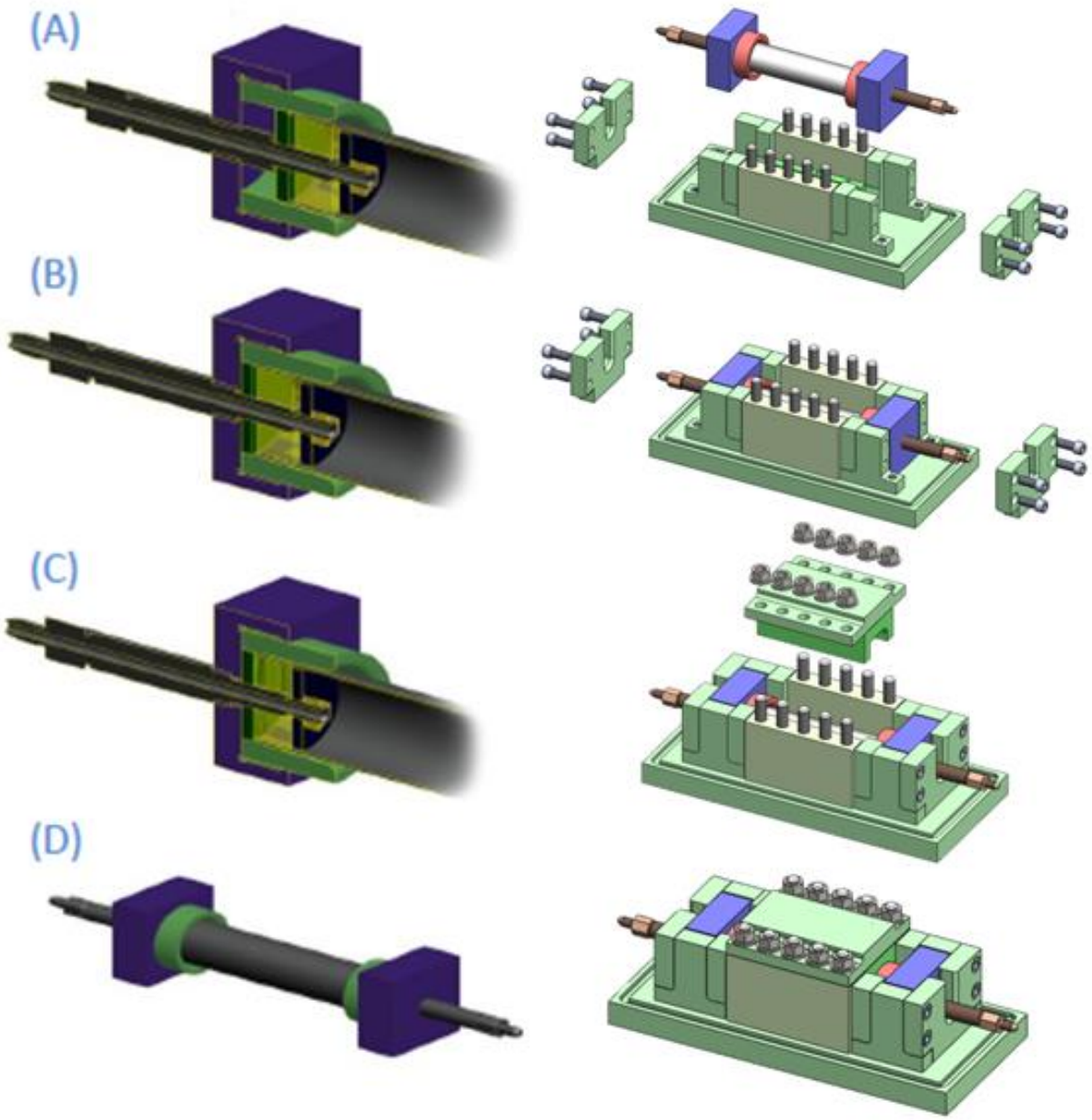

Figure 2.19: Assembly of seals and end-blocks for replacing workpiece.

2.6 Control System Overview

The tube hydroforming machine requires a method to pressurize the tube. Due to the mechanics of the forming process, a critical pressure exists where the tube will continue to deform without additional load or pressure. It is not always possible to run the experiment in pressure control, since the pressure would need to decrease if the tube reaches a plastic instability before making contact with the die. For accurate and useful experiments, the tube hydroforming machine should be operated by controlling the volume of fluid introduced. As the volume is incremented, the pressure is determined by the equilibrium state between the internal pressure and the stress in the tube wall about the circumference. For basic experiments at low pressures, a hand-pump may be used to add fluid volume to the tube in a controlled manner, but there is often no way to meter or measure the volume in hand-pumps. For ease of use, an automated solution using an electric pump with volume control feedback is the ideal solution.

Due to the pressure capacity of the machine, standard hydraulics are not suitable because typical systems operate at 3,000 psi (207 bar). To reach higher pressures, a second hydraulic loop with a pressure intensifier should be utilized. Figure 2.20 shows an example of this system, which consists of two loops. The low pressure loop is a closed loop that utilizes standard hydraulics, such as the MTS pump rated at 3,000 psi (207 bar), and is powering the low-pressure side of the pressure intensifier. The intensifier stores all the fluid necessary form the tube, and is an open line connected to the tube hydroforming machine. The low-pressure hydraulics are used to displace the cylinder inside the intensifier, which is instrumented with an LVDT so that the cylinder position and therefore

cylinder volume can be accurately controlled. The output of the intensifier is a single high pressure line which is used to form the tube. This system can operate with the MTS controller in either pressure or volume control. The control system allows for more complex experiments such as pulsed pressurization instead of a simple monotonic profile.

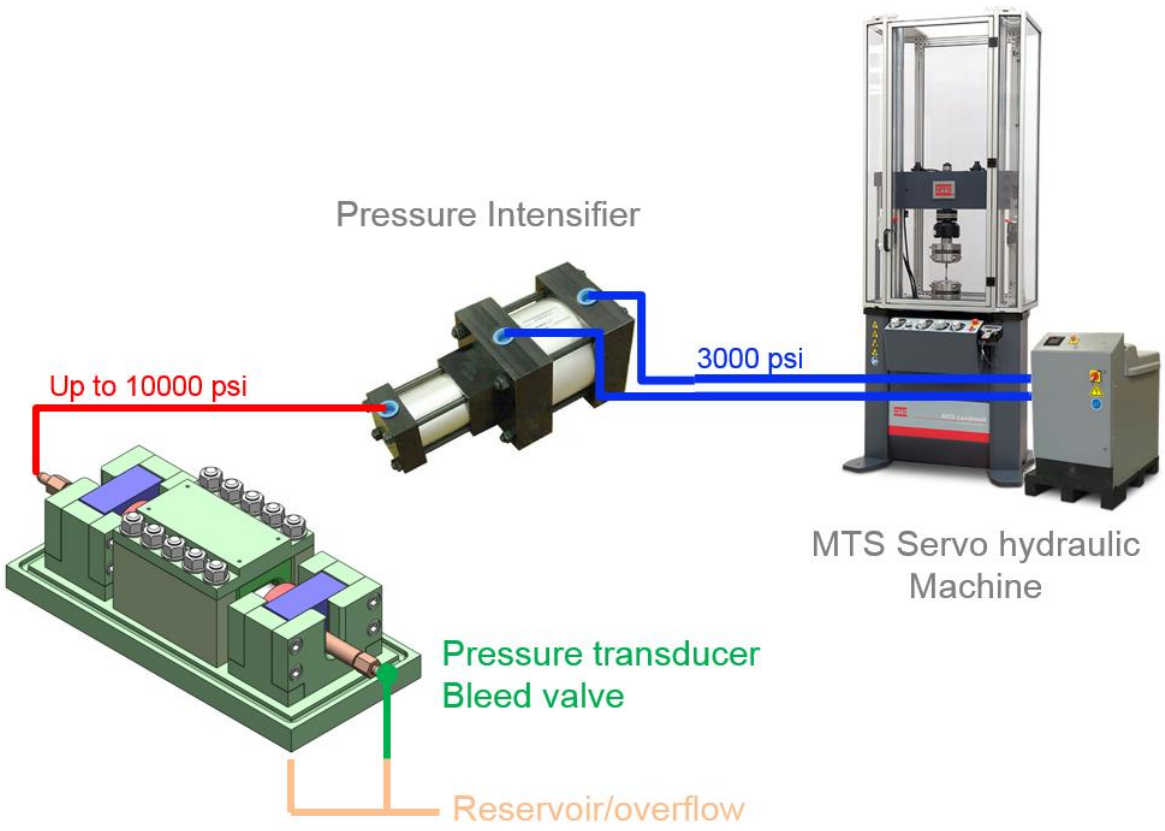

Figure 2.20: Proposed high-pressure control system for the tube hydroforming machine.

CHAPTER 3

TUBE FORMABILITY

3.1 Formability Overview

The tubes used in this study are cold extruded Al-6061-T4. The tubes were obtained from Ford Motor Company, which had previously studied the stress-strain behavior. Aluminum is of interest due to its high strength to weight ratio when compared to parts traditionally manufactured out of steel. On the other hand, it is a difficult material to form because of the low ductility.

Tube formability is a qualitative metric that refers to the degree of plastic deformation achievable during a process without failure. Tube formability is an important evaluation of the applicability of a certain tube for tube hydroforming, since the strains in the circumference may be quite large. The formability of a tube can limit the design of the hydroforming die - as a result, a thorough evaluation of the tube formability is invaluable to manufacturing process engineers, and can provide insight towards the success or failure of a particular hydroforming process. Tube formability is linked to the tube's manufacturing process. There are several manufacturing techniques used to create tubes, each affecting the tube's material, strength, ductility, thickness, uniformity, and eccentricity. Tubes can be categorized by their manufacturing method, which falls into two categories: welded or seamless.

Welded tubes typically originate as strips from hot or cold rolled coils, as illustrated in Figure 3.1. The strips are fed through a series of forming rollers that progressively curl the

outside edges of the strip inward towards each other. In a process referred to as electric resistance welding (ERW), these edges are welded together using a high electric current passing through the strip. This leaves a region of thickened flash from the weld on the inside of the tube. The welded tube may undergo further finishing to size the final dimensions of the tube. The quality of the tubes can be improved through temperature treatments, straightening, and other finishing operations to increase the thickness uniformity, such as drawn over mandrel (DOM) forming or honing.

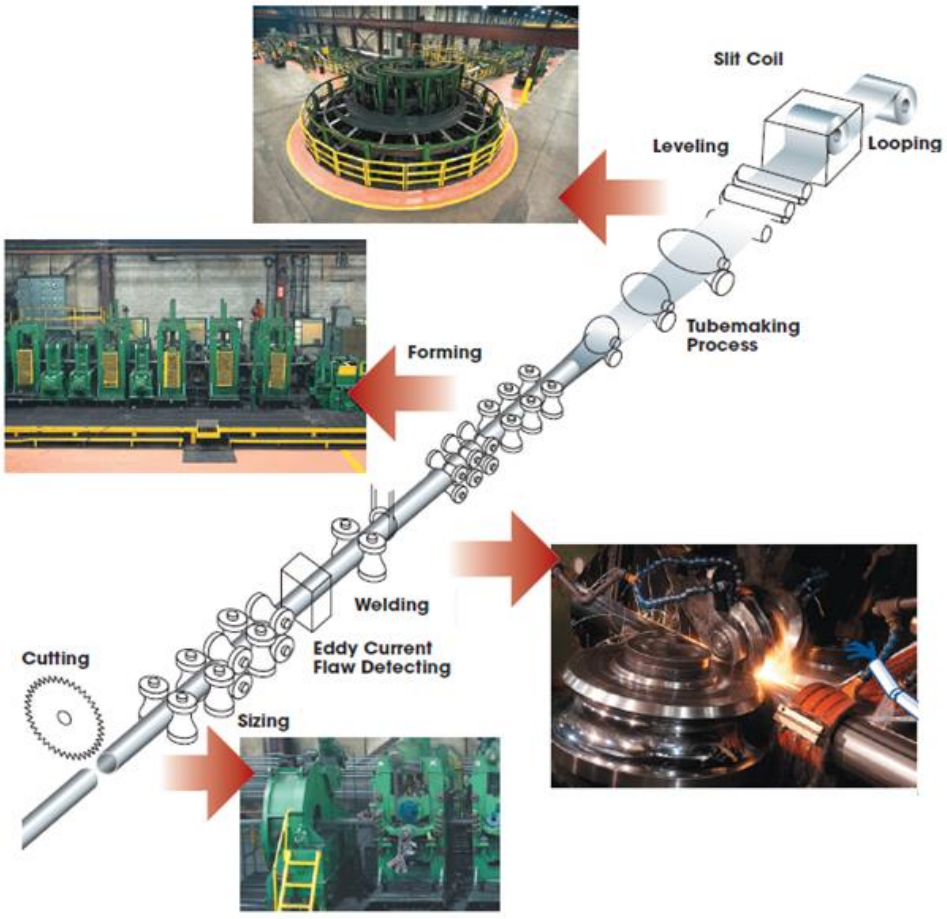

Figure 3.1: Manufacturing process for electric resistance welded tubes. The tubes progressively shaped into cylindrical tubes and welded (http://www.leavitt-tube.com/manufacturing.html).

Figure 3.2: Example of the extrusion dies for making tubes (not actual die used for the Al-6061-T4 of this work). Legs holding the billet cause cold-welds in the extrusion profile [27].

Seamless tubes are produced from a variety of extrusion and pilgering processes. The tube originates as solid stock and is drawn through a die or series of dies to form the final cross section. The internal diameter cavity is formed by a forming billet. Many times, small legs are used to hold the billet in place as seen in Figure 3.2. These legs (known as a spider die) cause the extruded material to divide, flow around the leg, and then cold-weld together again after the leg. As a result, weld lines can often be observed in micrographs for extruded "seamless" tubes, but not by the naked eye.

Aluminum tubes are commonly produced by extrusion, while steel tubes are typically available in as-welded ERW or higher-quality DOM variants. The Al-6061-T4 tubes used in this research have three cold-welds due to the extrusion process. The impact on formability

for weld lines in extruded seamless tubes is less severe compared to electric resistance welded tubes; however, the presence of the welds in both cases can lead to longitudinal splitting of the tube during hydroforming.

The formability of extruded tubes is different than electrically welded tubes. The temperature treatment during the extrusion process determines the grain structure and the degree of work hardening for the formed material, allowing additional control over the strength and temper of the final tube. The electrically welded tubes contain a heat-effected zone near the weld which may have different material properties. Although the material properties of the extruded tube are more uniform, the wall thickness and eccentricity are more difficult to control compared to welded tubes. Some researchers, such as Hosford [14], generically state that welded tubes are preferred over seamless tubes due to the thickness uniformity of the wall, which has a more significant impact on the forming process than the difference in material strength at the welds. This opinion does not hold true for all hydroforming researchers however. There are several ways to evaluate tube formability as well as characterize the tube material. These include standard material tests such as ASTM tensile testing for strips and ring specimens, as well as flaring and free expansion tests, which are helpful for analyzing biaxial stress states common in hydroforming. The ASTM experiments can be used to individually characterize the axial and circumferential directions of the tube material, as well as the degree of anisotropy in the tube.

3.2 Tube Material

The Al-6061-T4 tubes used in this research have three cold-welds due to the extrusion process. The welds cannot be distinguished with the naked eye on either the tube

surface of the tube or through the cross section on the tube wall. To locate the welds, a metallographic treatment should be used to etch the grain boundaries. In order to locate the welds, several etches were tried, however, ultimately a macro-scale caustic etch or a micro-scale Keller's reagent produced the most visible results. In order to perform these etchings, ring specimens were cut from the tubes and finish cut on a lathe. The rings were then polished by wet sanding with 400 grit, then 800 grit, and finally 4000 grit. The final polishing was performed using a diamond pad with diamond paste in an oil suspension. The resulting weld lines are visible to both the naked eye and under a 5x magnification, as documented by Figure 3.3. The welds on the full tubes were marked using the ring specimens to map the corresponding locations on the stock Al-6061-T4 tubes. The welds were approximately equally spaced by 120 degrees about the tube circumference.

The welds from electric resistance welded tubes are typically the weakest material in tube wall. Cold-welds in extruded tubes are typically of slightly higher strength that the rest of the tube; however, imperfections in the weld itself can lead to failure of the weld seam. In both cases, longitudinal splitting of the tube wall along the weld is a concern.

The tubes had an approximate outer diameter of 60mm and a nominal thickness of 3 mm. The variation of the wall thickness is due to a slight eccentricity of the mandrel during the extrusion process, however, the variation was found to be systematic in the batch of Al-6061-T4 that was received. The thickness of the tube was measured in 12 places equally spaced about the tube circumference (see Figure 3.4).

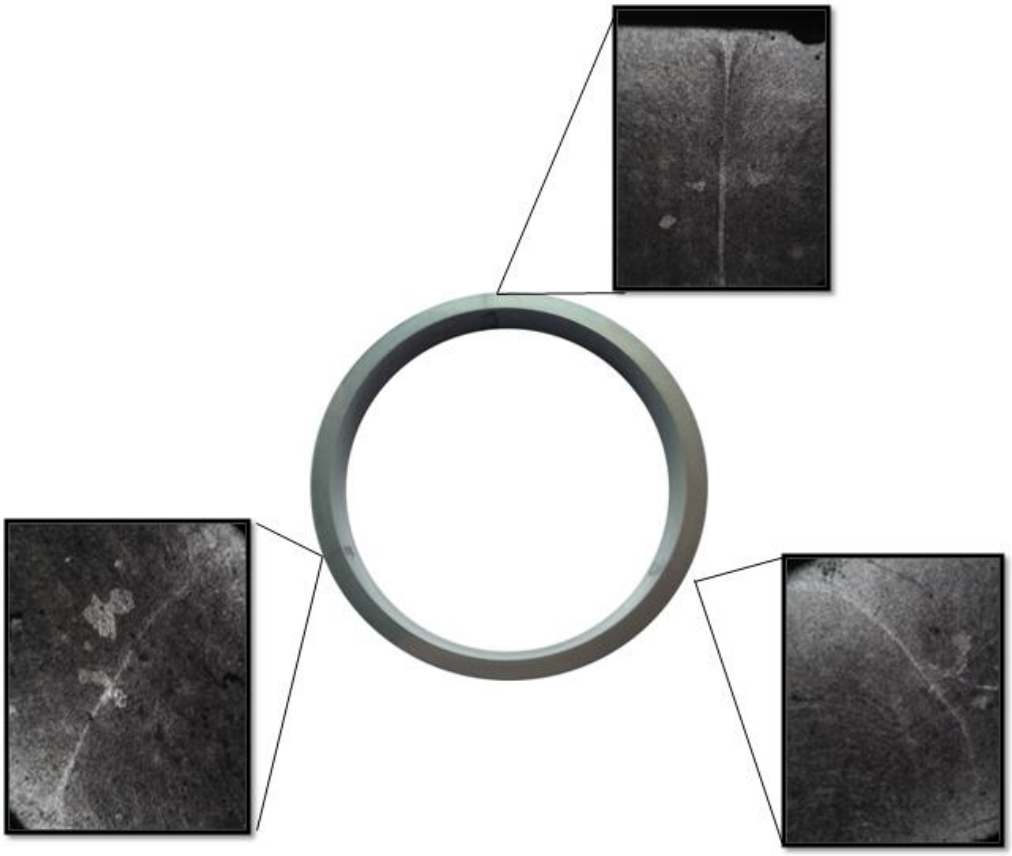

Figure 3.3: Micrographs of cold-weld lines from cold-extrusion of the aluminum tubes exposed using a Keller's reagent to etch polished specimens.

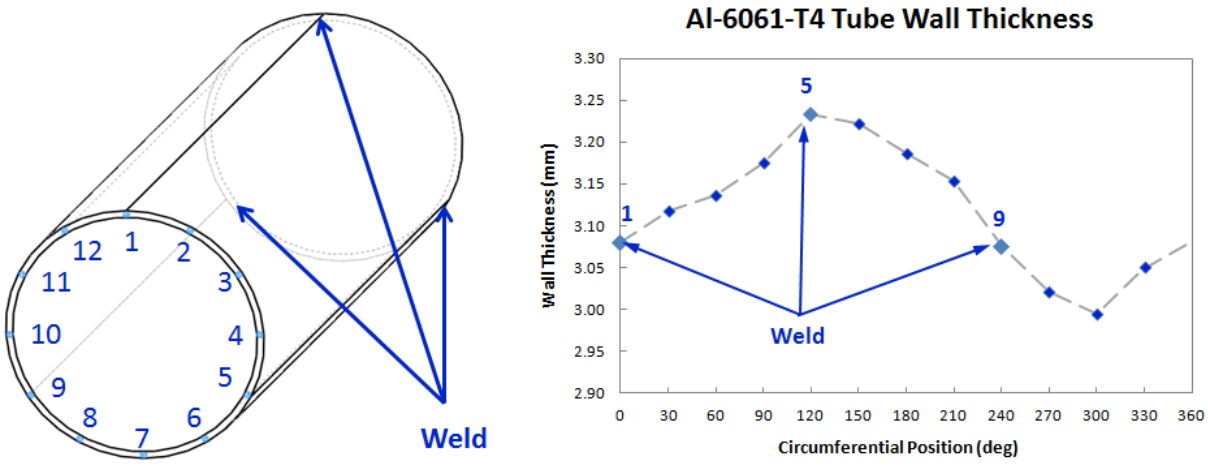

Figure 3.4: Distribution of wall thickness about the circumference of the stock aluminum tube, characteristic of all tubes in the received batch.

3.3 Axial Tension Tests

The uniaxial tension test provides information on the strength and ductility of the tube in the axial direction. A strip can be cut from the tube parallel to the axis of the tube. The strip is then machined into an ASTM E8 subsize specimen [26]. Subsize specimens were chosen to minimize the effect of the tube curvature as the wider the specimen, the larger the deviation from flatness. Smaller specimens will have less curvature, which will aid in both specimen preparation and specimen gripping in the servohydraulic machine. The subsize specimens were prepared using a CNC milling machine with flood coolant. The edges were deburred to remove defects from the machined edges.

Six specimens were cut from the tube every 60°. Specimens #1, #3, and #5 were cut from the welded region, while the remaining specimens came from the material between the welds. The Al-6061-T4 tube was first cut into longitudinal strips using a bandsaw, which was able to maintain parallel orientation perpendicular to the open face of the tube. These strips were then CNC machined as shown in Figure 3.5. The jig used to hold the curved strip from the tube was also rounded in order to accommodate the curvature of the blank. Some tensile specimens were milled flat, however this was later adbandoned due to the possibility of the machining altering the mechanical properties.

The specimens were loaded using the MTS Landmark 370 servohydraulic load frame. The specimens were clamped using MTS hydraulic grips. The crosshead force was recorded using a 250 kN (56200 lbf) MTS load cell. The peak load for all axial tension testing of Al-6061-T4 specimens was less than 5 kN (1124 lbf).

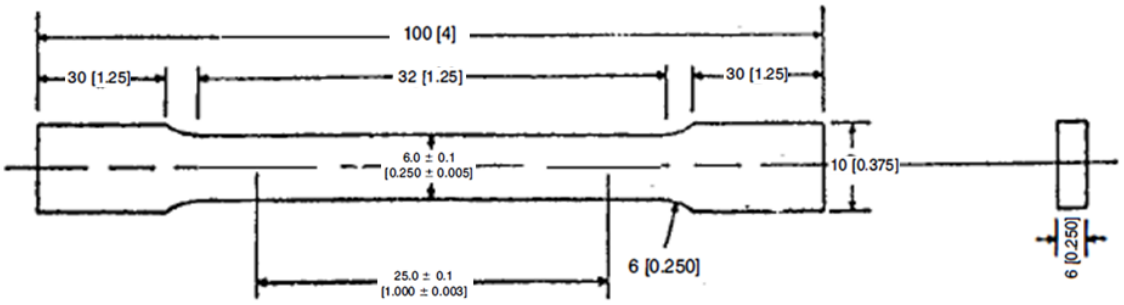

Dimensions in mm [in].

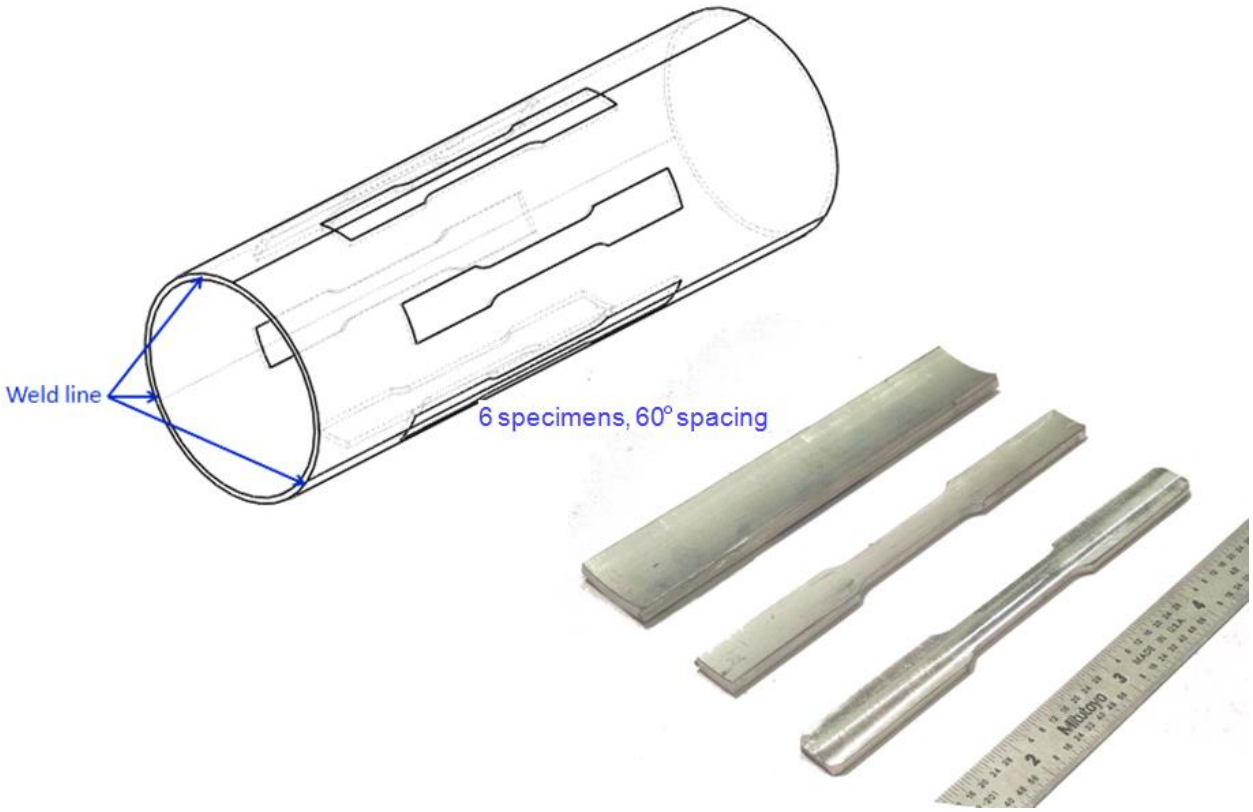

Figure 3.5: Extraction of axial ASTM E8 subsize specimens from tube. Tensile specimen dimensions reprinted from ASTM E8 publication [26].

The specimens were tested using a crosshead velocity of 10^{-3} in/s. On average, the experiments lasted around 275 seconds. Grip pressure was maintained between 800 and 1000 psi. The engineering strain was measured using an MTS extensometer with as 25.4 mm (1 inch) gage length. The extensometer displacement resolution is 2.713×10^{-4} mm (1.068×10^{-5} in), and the strain resolution is 1.068×10^{-5} for the given gage length and the full ±10 V scale of the 16 bit A/D converter in the MTS controller.

The results of testing the first set of specimens are given in Figure 3.6 and Figure 3.7. They show negligible variation in the material behavior around the circumference of the tube for the base material. Two of the three weld material specimens failed on the extensometer leg, so the post UTS stress-strain behavior is not comparable to other tests. However, the remaining weld specimen (Al61T4-W3) showed a discernibly different post-UTS response. As a result of this observation, the stress-strain results for the welded specimens were investigated further.

During tensile testing, a few subsize specimens failed near the ends of the gage length, likely due to small errors/defect from the milling process. As the specimen reaches its ultimate tensile strength, the localization would occur either outside the extensometer gage or directly on the extensometer leg, resulting in incorrect stress-strain relationships after this point. The post-UTS portion of the curve is important for extrapolation of the strains beyond those achievable in the uniaxial tension test. This post-UTS portion of the curve is also important for accurate matching of FEA models to experiments. There is also variation in the UTS achieved in the different tests, indicating slight material variation about the circumference of the tube.

In order to obtain the post-UTS portion of the stress-strain curve, small 3.125 mm (0.123 inch) radius notches were filed into the sides of a second batch of specimens (designated Batch D) to encourage localization within the extensometer gage length. The post-UTS behavior of these notched specimens allows further calibration of material models and more accurate material extrapolation. The results of these specimens are labeled “notch” and are included in Figures 3.8 and 3.9. The three notch specimens for the welded tube failed in the gage length and had more similar stress-strain behavior than the un-notched specimens.

To summarize the uniaxial tension experiments, the base material tests achieved nominal strains of 15% before localization occurred. The ultimate tensile strength of the base material was 258.3 ± 6.3 MPa (37.5 ± 0.9 ksi). The average yield stress was 153.3 ± 3.7 MPa (22.2 ± 0.5 ksi). A single specimen, A6, failed near the outside of the extensometer and post-UTS strains are not meaningful. The strains seen in A6 are artificially small; however the UTS is still valid.

Only one of three welded specimens failed in the gage length (~15% nominal strain), but the average the average UTS of these tests was 263.1 ± 1.8 MPa (38.2 ± 0.26 ksi). The average yield stress was 152.2 ± 0.6 MPa (22.1 ± 0.1 ksi). The failure in the only valid weld specimen from Figure 3.7 fails earlier than the base material specimens. The weld material notch specimens in Figure 3.8, when compared to the equivalent base material notch specimen in Figure 3.9, demonstrate that the weld material has a different failure behavior after UTS than the base material. These relatively small differences may be useful for improving the numerical modeling of the hydroforming experiments.

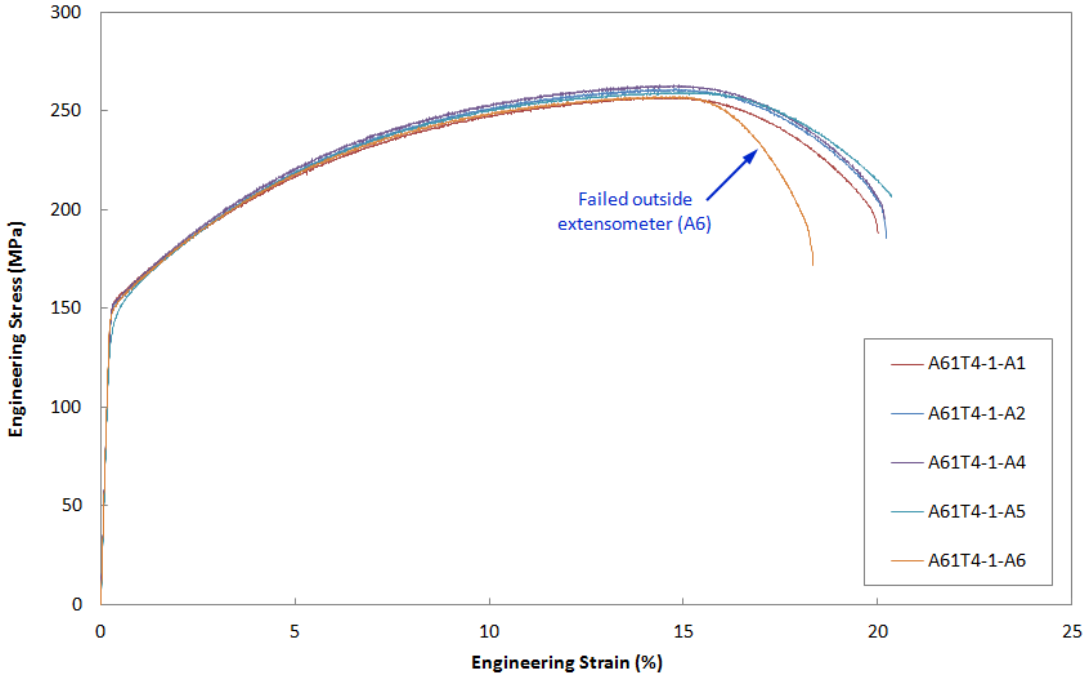

Figure 3.6: Axial tension specimens for Al-6061-T4, base material.

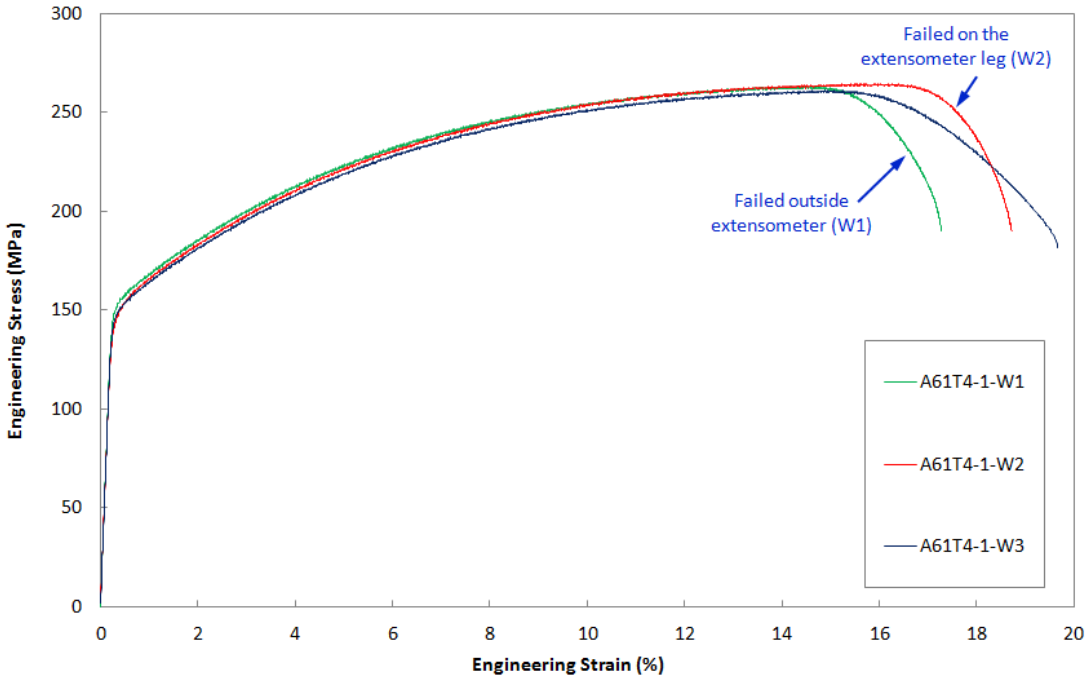

Figure 3.7: Axial tension specimens for Al-6061-T4, welded material.

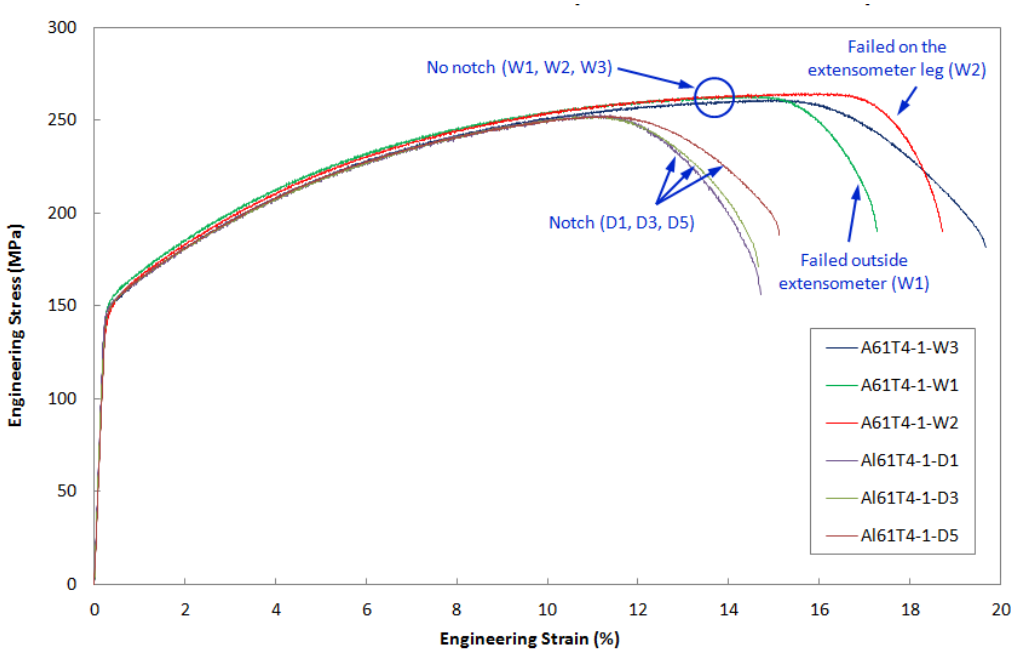

Figure 3.8: Comparison of axial tension specimens with notch (D) and no notch (W) for Al-6061-T4, welded material.

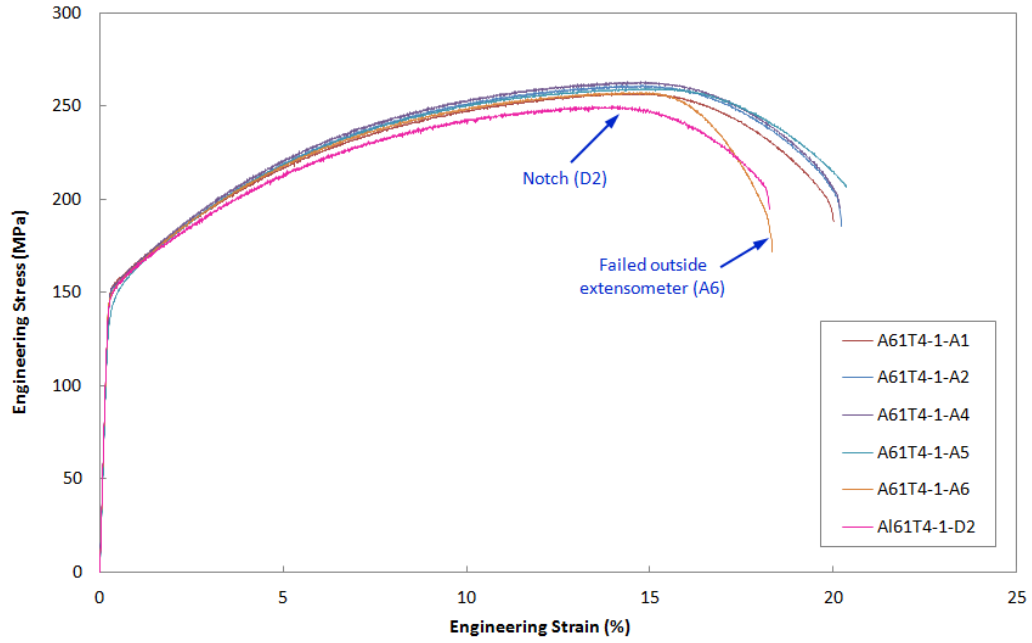

Figure 3.9: Comparison of axial tension specimens with notch (D) and no notch (A) for Al-6061-T4, base material.

The variation in the material test curves seen in all tests from Figure 3.6 to Figure 3.9 should be noted. This variation is likely due to true variation of the material circumferentially around in the tube wall, which can be expected from the "seamless" extrusion process. Despite correcting for the true measured thickness of the specimens, the results indicate slight material variation about the circumference of the tube.

3.4 Strain-Rate Tension Tests

Due to unique geometries during the tube hydroforming process, the material in each region can deform at different rates. By tracking different points on the tube surface, different strain paths and rates can be observed. As a result, it is important to investigate the material's sensitivity to different strain-rates.

During the standard uniaxial tension tests, the crosshead velocity is maintained at a constant value, which subjects the material inside the gage length to a specific strain-rate. After UTS, the material in the localized deformation zone is deforming faster than the material outside the localized deformation zone, and therefore is subjected to different strain-rates. As a result, the material's strain-rate dependence should be investigated and quantified for accurate material modeling.

Using the MTS Landmark 370 load frame, the ASTM E8 subsize specimen was subjected to a tensile test in which the crosshead velocity would be altered during the tension test. By changing the crosshead velocity, the rate is effectively changed inside the gage length. If the material is sensitive to strain-rates, then the material stress behavior should reflect the sensitivity via jumps in the work-hardening on the stress-strain curve.

The Al-6061-T4 specimens were tested at four crosshead rates; $5x10^{-4}$, 10^{-3}, $5x10^{-2}$, 10^{-2} /s. The initial rate was 10^{-3} /s, followed by 10^{-2}, $5x10^{-4}$, $5x10^{-2}$, and then returned back to 10^{-3} /s. This alternating order was chosen to allow any deformation-induced heating from the faster rates to dissipate during the slower rates. The results of the test are similar to the tensile tests at constant rates for both the weld and base metal specimens. The deviations in the curve are due to the instantaneous changes in crosshead velocity. As a result, the Al-6061-T4 shows very little strain-rate sensitivity. Notably, the specimens failed outside the extensometer region similar to previous tension specimens - this failure occurred around ~14-15% nominal strain as seen in Figure 3.10.

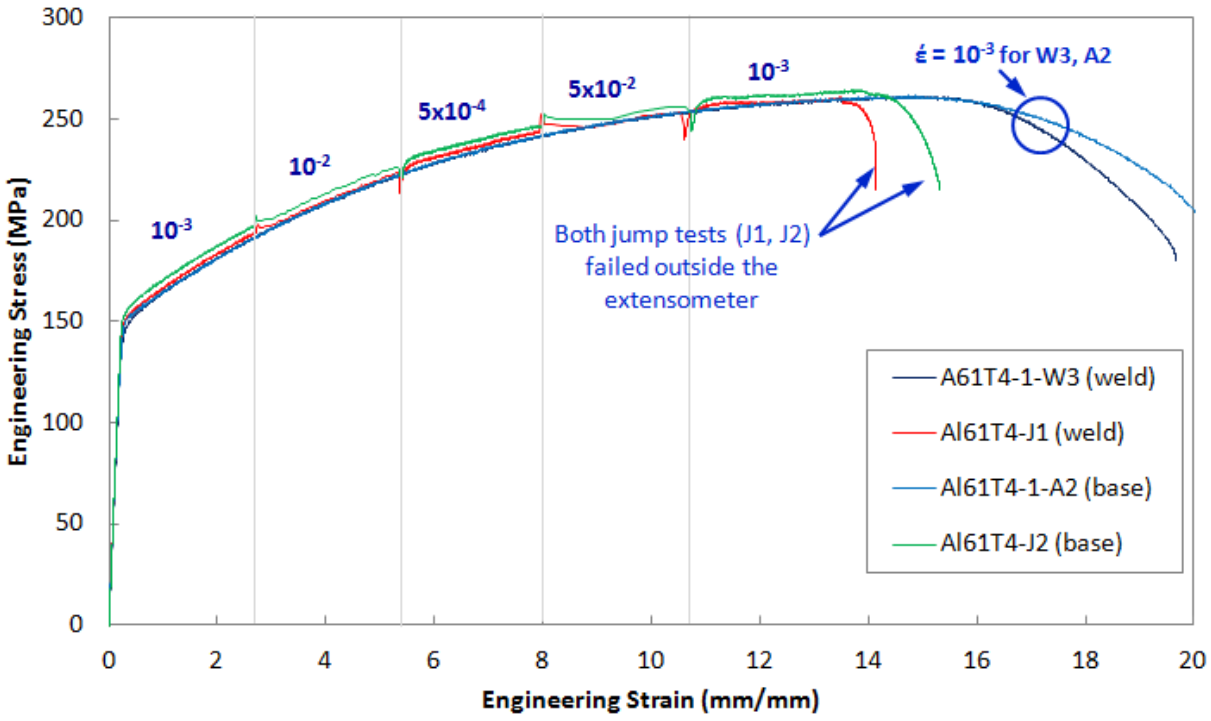

Figure 3.10: Effect of strain-rate on material work hardening. The stress-strain curve demonstrates negligible strain-rate sensitivity for the Al-6061-T4 axial specimens (base or weld material).

3.5 Elastic Tension Tests

The elastic modulus (E), Poisson's ratio (v), and yield stress (σ_{ys}) of the Al-6061-T4 tubes should be evaluated in order to fully characterize the tube material. The published elastic modulus for Al-6061-T4 is 68.9 GPa (9.99 x 10^6 psi). The published Poisson's ratio is 0.33 [28]). The published yield stress for Al-6061-T4 is 152 MPa (22 ksi) ([29]). The elastic modulus and yield stress can be found using the 0.2% strain-offset method as specified by ASTM E8 standard [26].

Due to the stiffness of the load train in the MTS machine and the 16 bit resolution of the A/D converter for the load cell and MTS extensometer, the results for the elastic modulus and yield stress were obtainable from the tension test data. In these tests, the engineering strain was measured using an MTS extensometer with as 1 inch (25.4 mm) gage length. Presented in Figure 3.11 are the results for the measured elastic modulus from three previous tensile tests. The graph illustrates that the resolution of the strain and force measurements are enough to successfully obtain the elastic modulus for the aluminum specimens. For these tests (weld and base), the overall average elastic modulus was 66.9 GPa (9.70 x 10^6 psi) and the yield stress was 152.8 MPa (22.1 ksi).

To obtain Poisson's ratio, the lateral contraction must be measured as well as the axial extension. Due to the smaller magnitude of the lateral strains, the MTS extensometer is does not provide adequate resolution to confidently resolve the strains. Also, the presence of the axial MTS extensometer would interfere with the placement of a second extensometer to measure the lateral strains. Additionally, only a single MTS extensometer was readily available.

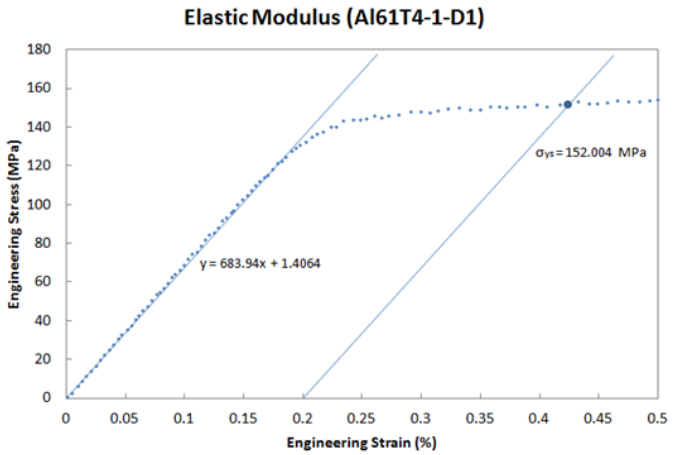

Specimen	Elastic Modulus (GPa)	Yield Stress (MPa)
Al61T4-1-D1	69.37	152.004
Al61T4-1-D3	67.60	152.132
Al61T4-1-D5	68.47	152.798
AVERAGE	68.48	152.311

(weld)

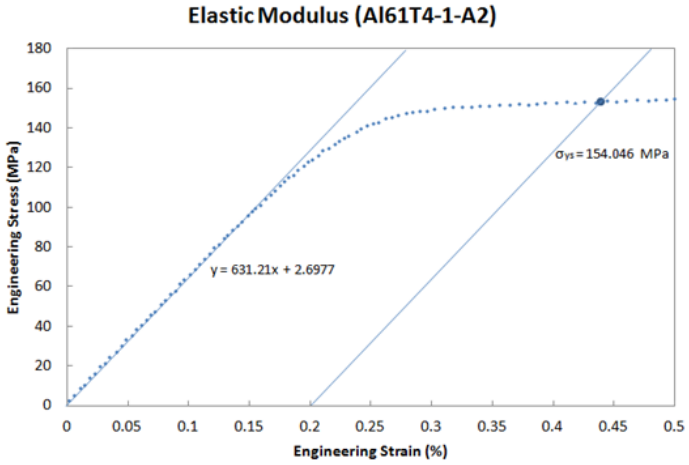

Specimen	Elastic Modulus (GPa)	Yield Stress (MPa)
Al61T4-1-A1	69.37	155.77
Al61T4-1-A2	67.60	154.05
Al61T4-1-A4	67.51	155.16
Al61T4-1-A5	64.21	148.47
Al61T4-1-A6	65.31	152.92
AVERAGE	65.27	153.34

(base)

Figure 3.11: Evaluation of elastic modulus and the 0.2% offset yield stress. The data is from the tensile specimens that were tested until failure.

In order to measure such small magnitudes, a strain gage was mounted onto one surface of a subsize specimen, in the center of the gage length. The Micro-Vishay CAE-06-062LT-350 strain gage is a stacked T-rosette gage that features an axial and transverse strain gage on a single backing. The backing is approximately 5 mm x 5 mm (0.2 inch x 0.2 inch) and the lead wires are provided with the gage. In order to amplify and record the strains, the MTS A/D converter was used in combination with two quarter Wheatstone bridges. The first quarter bridge recorded the axial strains, while the second recorded the transverse strains. Both signals were sampled using two 16 bit A/D inputs on the MTS controller, and the values were recorded along with load, extensometer strain, and crosshead displacement. A third A/D input monitored the excitation voltage used by both Wheatstone bridges. The experimental setup is shown in Figure 3.12.

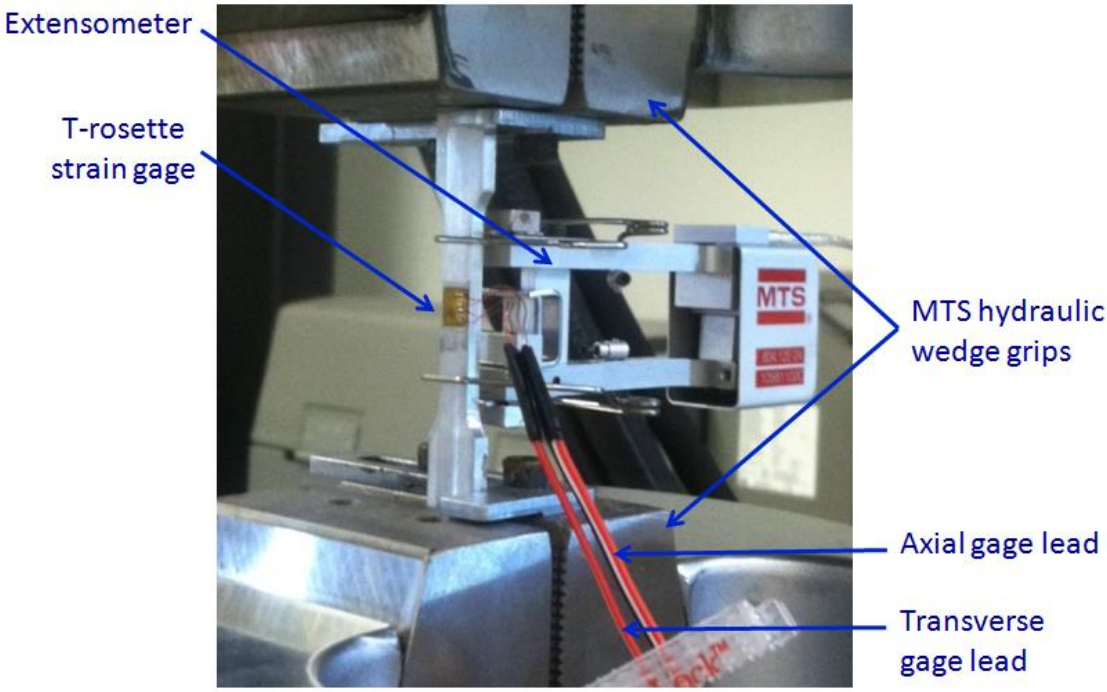

Figure 3.12: Elastic experimental setup utilizing a stacked Poisson's gage to measure axial and transverse strains.

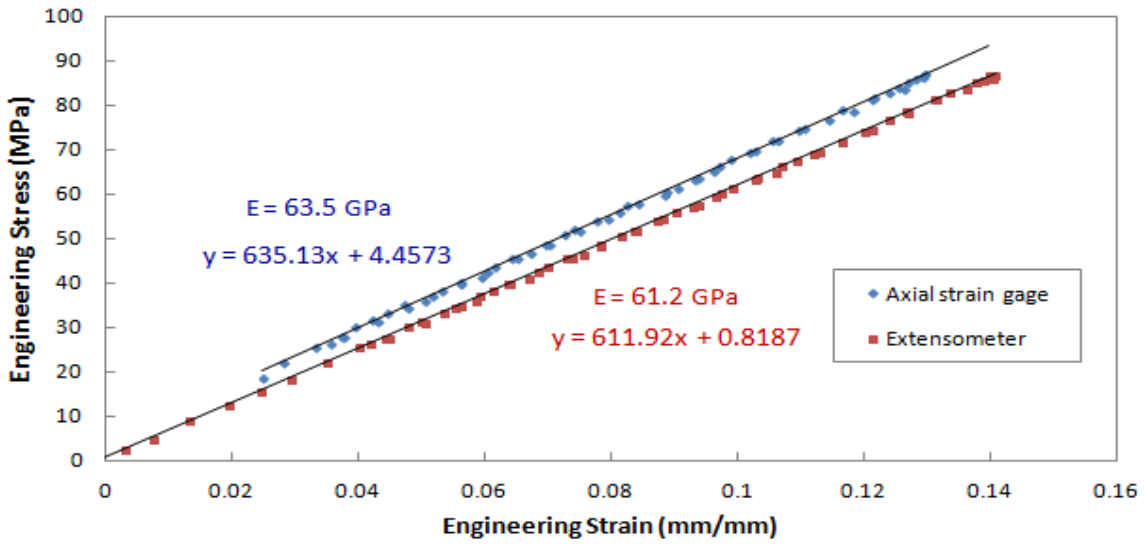

Figure 3.13: Elastic modulus from the axial strains measured by the strain gage. The extensometer is included for comparison.

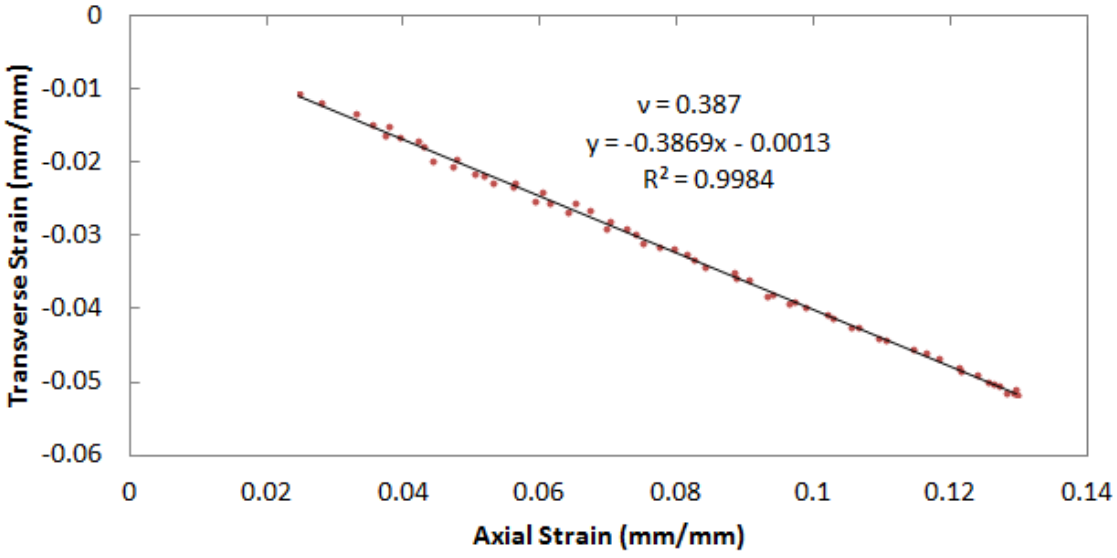

Figure 3.14: Poisson ratio from the elastic experiments as measured by the strain gage.

In order to maximize the resolution for the ±10V scale of the 16 bit A/D converter in the MTS controller, the excitation voltage and A/D gain must be carefully chosen to utilize the full range of the A/D. The minimum voltage resolution of the A/D converter is 0.305 mV. The Al-6061-T4 begins to deviate from proportional loading around 0.15% axial strain, therefore the expected strains for the elastic test are 0.13% axially and 0.05% transverse . The transverse voltage signal will be smaller than the axial signal, and therefore should be analyzed as the worst case when calculating the resolution. A 10V excitation voltage was chosen in order to obtain sufficient resolution while also minimizing temperature effects. The expected transverse voltage from the quarter bridge for the 0.15% strain using the 10V excitation is 76.875 mV axially, and 25.625 mV transverse. The MTS gain could be increased to 10 or even 100 in order to increase the resolution; however, with a minimum resolvable voltage of 0.305 mV, the MTS A/D has sufficient resolution to resolve the strains with a gain of 1.0. This is outlined in Appendix E.

The results of the tests are shown in Figure 3.13 and Figure 3.14. The elastic modulus was 63.5 GPa, and the Poisson's ratio was 0.387. The elastic modulus seems low compared to earlier tests using the extensometer. Also, the Poisson's ratio is unusually high. A small non-linear region was noticed in the initial strain behavior, leading to low confidence in the test. The artificially high Poisson's ratio may be due to poor alignment of the strain gage with the loading axis or bad adhesion of the gage to the specimen, but also could be due to: work-hardening of the material during machining of the specimen, caused by bending effects due to misalignment of specimen grips, or self-heating of the strain gages on the specimen. As a result, the published value of 0.33 will be used in future analysis for Poisson's ratio.

3.6 Ring Hoop Tension Test (D-Blocks)

The tube hydroforming process causes the tubes to expand circumferentially. As a result, the principal loading direction is in the hoop or circumferential direction of the tube. The geometry of a tube is such that specimens are easily prepared from the axial direction, however the hoop direction proves more difficult to test using ASTM standard methodologies such as uniaxial tension testing. The ASTM E8 standard suggests specimens should be cut from the circumferential direction and flattened. The flattening of the specimen induced plastic strains due to bending, which are potentially significant with small diameter tubes. The ring hoop tension test is an alternative method for loading the un-flattened specimen in order to preserve the original properties of the material.

The ring hoop tension test has been proposed by Arsene and Bai [30-31] and further developed by Dick and Korkolis [32]). The test uses circumferential rings with a reduced gage section. The rings are mounted onto two semi-circular mandrels, referred to as D-blocks. The gage length is kept on the upper D-block, completely above the seam. The curvature of the gage length does not change during loading, therefore the gage section is in tension and is not subjected to bending. Using this method, the circumferential direction can be tested in uniaxial tension. An example specimen is shown in Figure 3.15.

The specimen was developed to be similar to the tensile subsize specimens. ASTM E8 standard states the gage to width ratio must be greater or equal to 4. Since the axial tension specimens have approximately a 6 mm (0.234 inch) width, the minimum recommended gage length for the ring hoop tension specimens is 24 mm (0.945 inch).

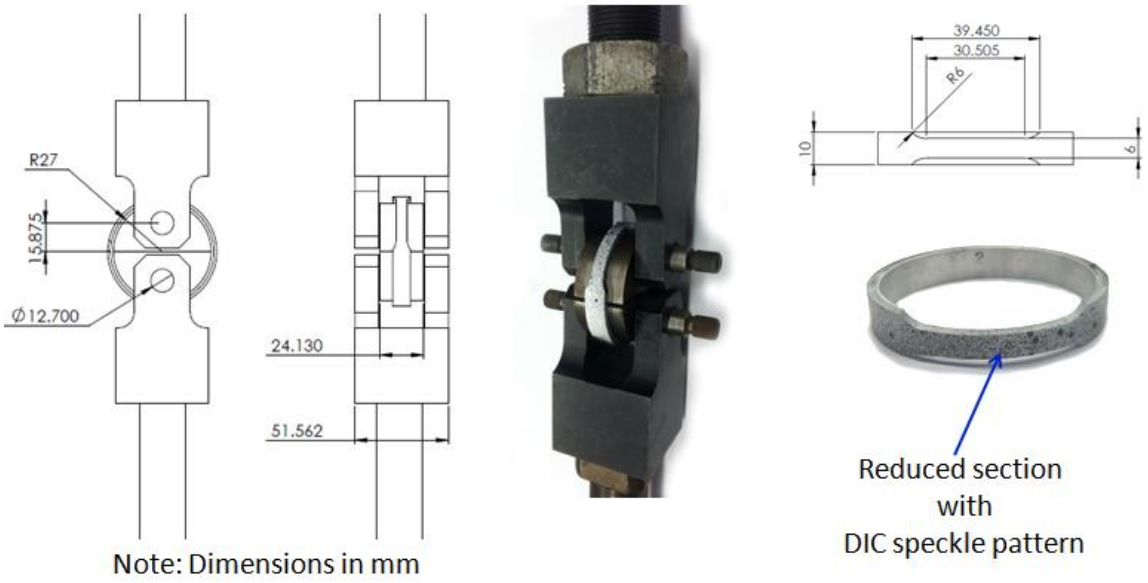

Figure 3.15: D-block assembly for circumferential tension test. The reduced section is oriented onto one half of the fixture.

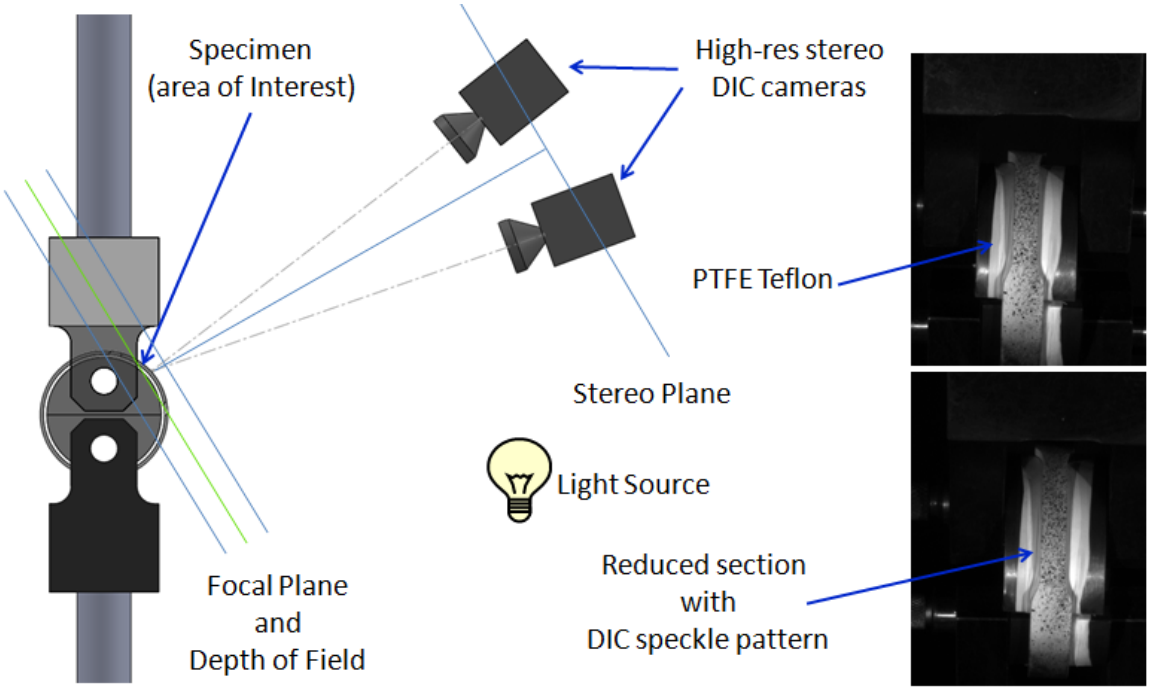

Figure 3.16: Positioning of DIC camera system for strain field acquisition.

This approach has a few unique problems. The inside surface of the ring is inaccessible for mounting the extensometer to measure the elongation of the gage length. The inside surface of the ring is also subjected to friction due to contact with the D-blocks mandrel. As a result, the strain inside the gage length is neither uniform nor appropriately measurable with a point-based system like an extensometer. Both problems can be solved by utilizing a field-based system to measure strains.

Digital Image Correlation (DIC) is an optical, non-contact technique used to evaluate deformation and rigid body motion. This method compares the pixel values of successive images in order to measure full-field displacements and strains. To provide unique pixel patches for the images, a high contrast random black and white speckle pattern is added to the area of interest on the specimen. The Correlated Solutions VIC-3D system allows surface positions along the specimen to be triangulated into 3D coordinates using the images taken from two mounted cameras. From these coordinates, 3D displacements, velocities, strains, and strain-rates can be measured and analyzed.

In order to maximize the viewable region of the gage, the cameras were arranged at a 15 degree stereo angle in the plane of the ring as shown in Figure 3.16. The view from the cameras is shown in Figure 3.17. The VIC Snap software was used to capture the images. The specimens were loaded using the university's Instron 1350 servohydraulic testing frame. The force data from a 100 kN (22480 lbf) load cell was logged using the Instron Fast Track Console and Fast Track DAX software. The load cell data will be through-put to the VIC Snap software in order to synchronize the strain calculations with the load.

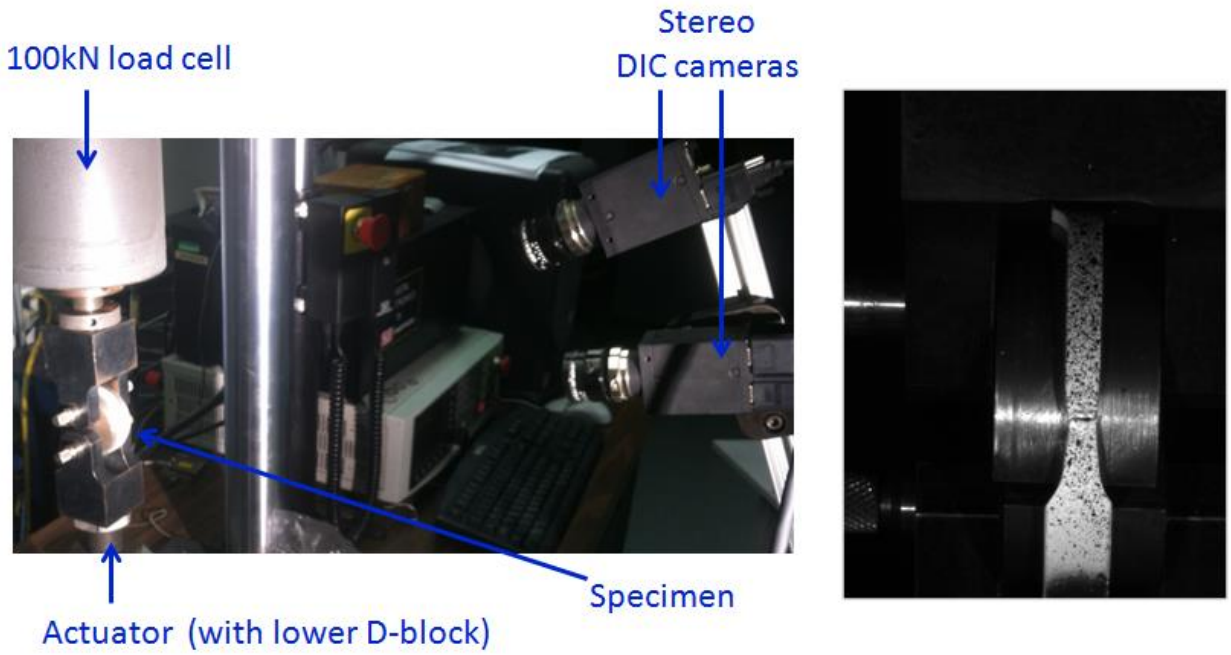

Figure 3.17: Experimental setup for D-block circumferential tension test utilizing stereo cameras for digital image correlation.

During the experimental setup and initial tests, a few problems were encountered with the tube-mandrel interface. Low viscosity lubricants had a tendency to gravitate to the lower block, and thicker greases occasionally obscured the gage length from the cameras as the specimen was loaded. PTFE Teflon tape supplemented with oil lubricant was the most consistent to work with.

The experiments presented below were performed at a crosshead rate was 10^{-3} in/s. At failure, the experiment should be immediately stopped so as to prevent unbending on tubular specimen. To supplement the existing wall thickness measurements in Figure 3.4, the thickness and width along the gage was measured at 5 equal spaced locations along the reduced section of the specimen. The weld (location #9, 270 degrees in Figure 3.4) was placed inside the gage length for these tests.

After perfecting the procedure during the first few tests, the stress-strain curves for two ring hoop tension test specimens are shown below in Figure 3.18. In Figure 3.19, the tests are compared to the uniaxial tension tests. The results show good agreement with both ultimate tensile strength and fracture strain with the base material from the longitudinal material specimens. The curves for a weld material specimen is also shown in Figure 3.19, it is difficult to say which post-UTS behavior is more characteristic. The notch specimens failed at a lower ultimate tensile stress and fracture strain, and therefore are not compared here.

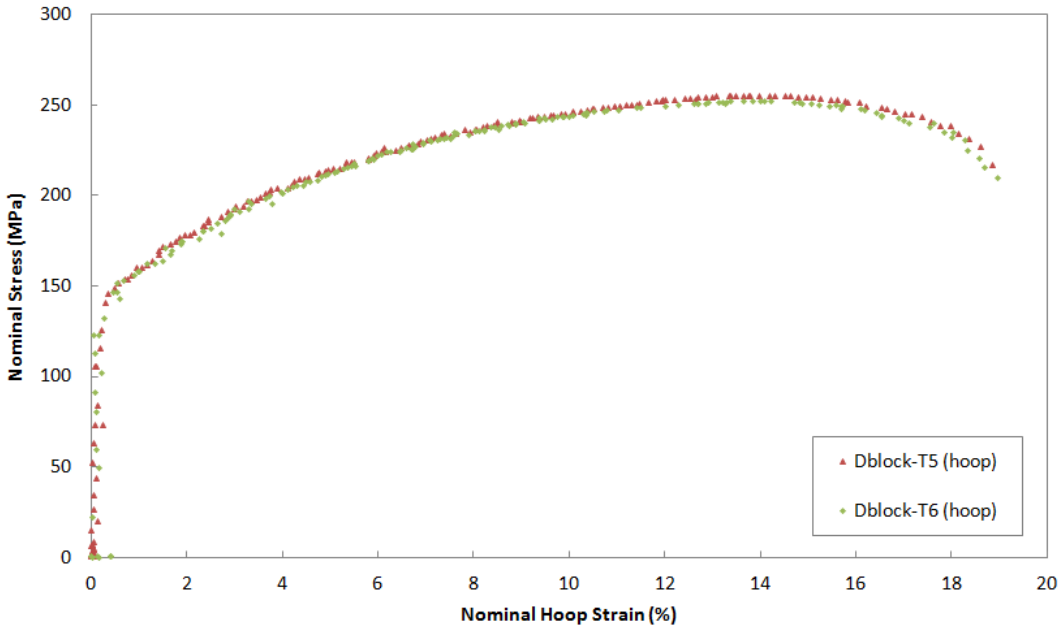

Figure 3.18: The stress-strain results for the circumferential tension test (RHTT).

Overall, it appears the circumferential properties of the tube can be modeled reliably using the properties extracted from the longitudinal specimens from the base material region of the tube in the axial orientation. There is some anisotropy in the material, and the load/stress in the gage length should be corrected for friction between the interface to

obtain a more accurate material model in the future. The axial material tests show higher UTS than the RHTT tests, indicating that the material may be weaker in the hoop direction than the axial - even before correcting for friction.

When evaluating the specimen's strain with the DIC software, the distribution of strain along the gage length can be quantified. Due to the presence of friction, the axial force varies along the gage length, which leads to non-uniform strain before the specimen reaches the ultimate tensile strength (UTS). The gage length should be selected to minimize non-uniform strain. The best results were obtained using the same gage length as the axial tension tests, as illustrated in Figure 3.20.

When comparing the experiments, the length of the gage length should be similar. If a smaller gage length is used, the size of the localized deformation after UTS is large relative to the gage length. This non-uniform strain is naturally averaged with the strain in the remaining gage length, therefore the size of the gage length should also be kept as close to the uniaxial test as possible. When evaluating the specimens load, the crosshead force is distributed through the specimen on either side of the mandrel interface. The width of the specimen is constant between the two sides; however there are minor variations in the thickness and there are differences in frictional surface area due to the reduced gage length. The load (for calculating the nominal stress) is assumed to be evenly distributed between the two sides for these tests, but small variations in the load are to be expected.

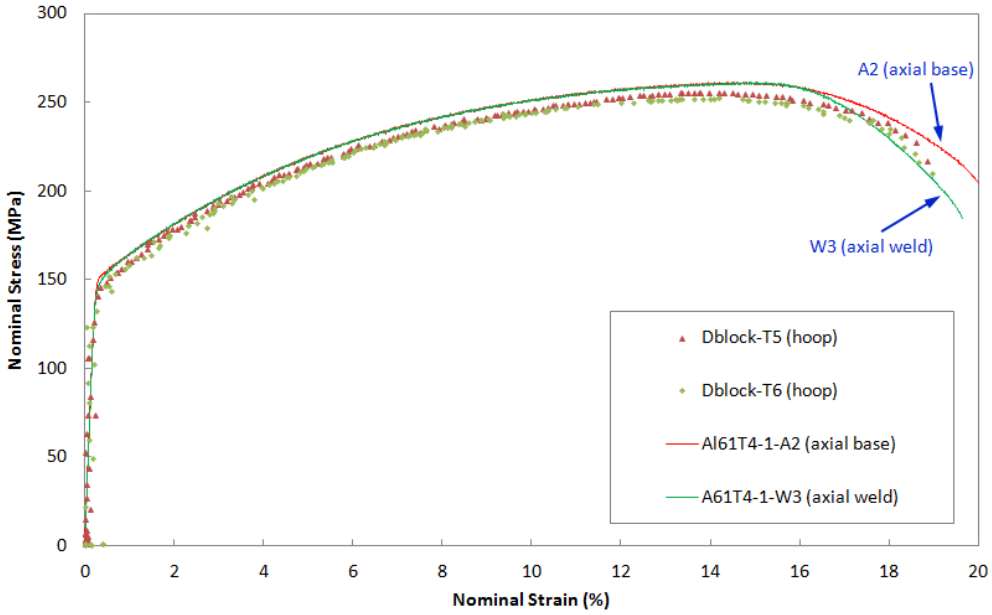

Figure 3.19: A comparison of the stress-strain results for the circumferential tests and the uniaxial tests (base material).

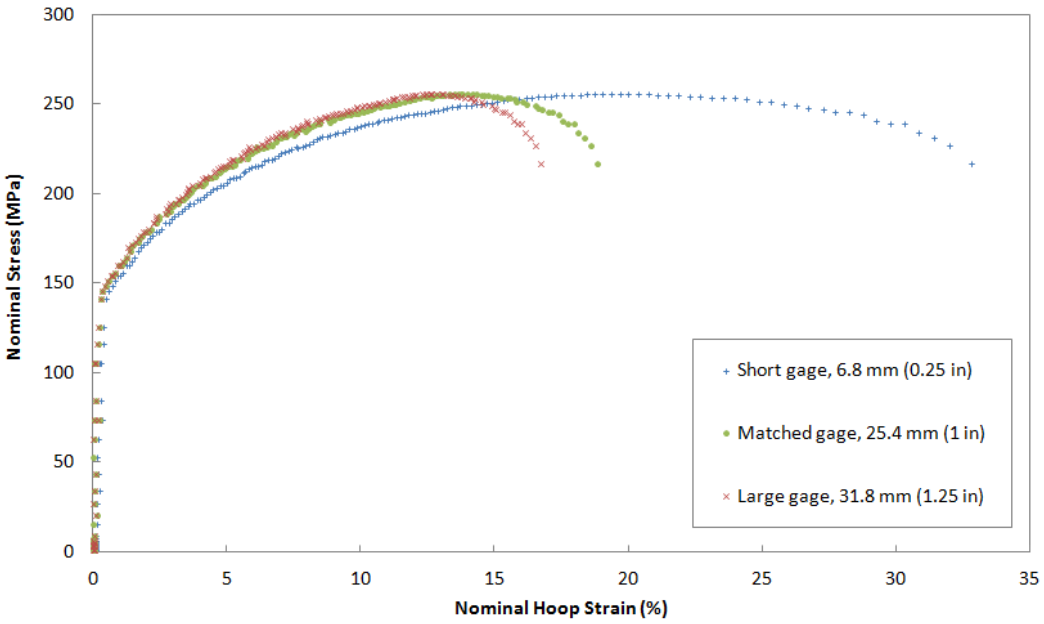

Figure 3.20: The effect of varying the gage length for the RHTT, using D-block test specimen 5 as an example.

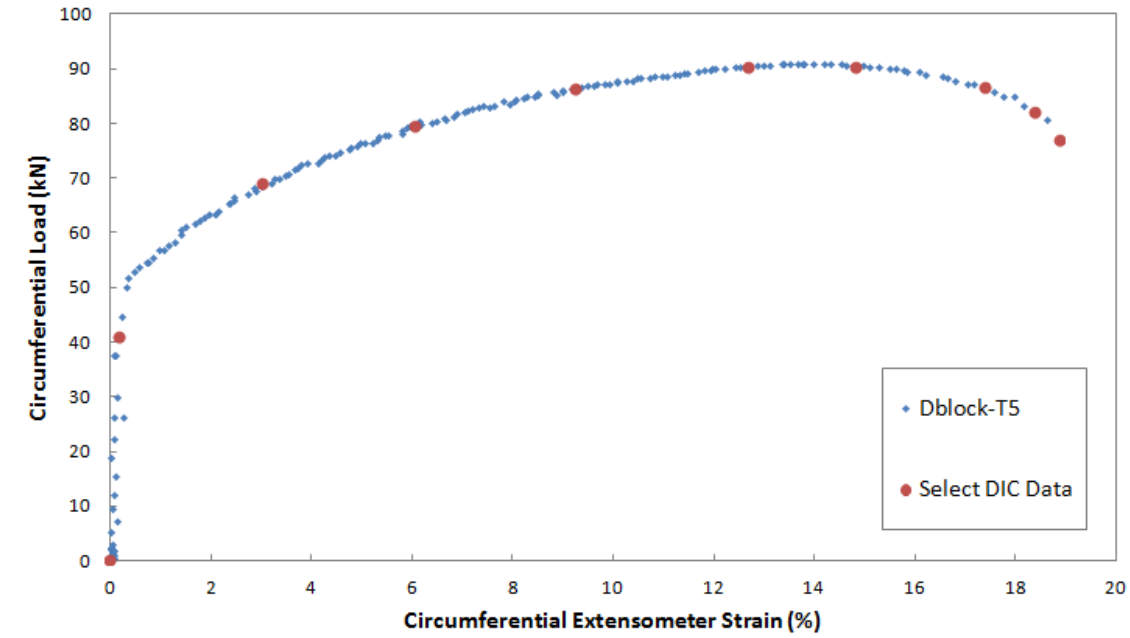

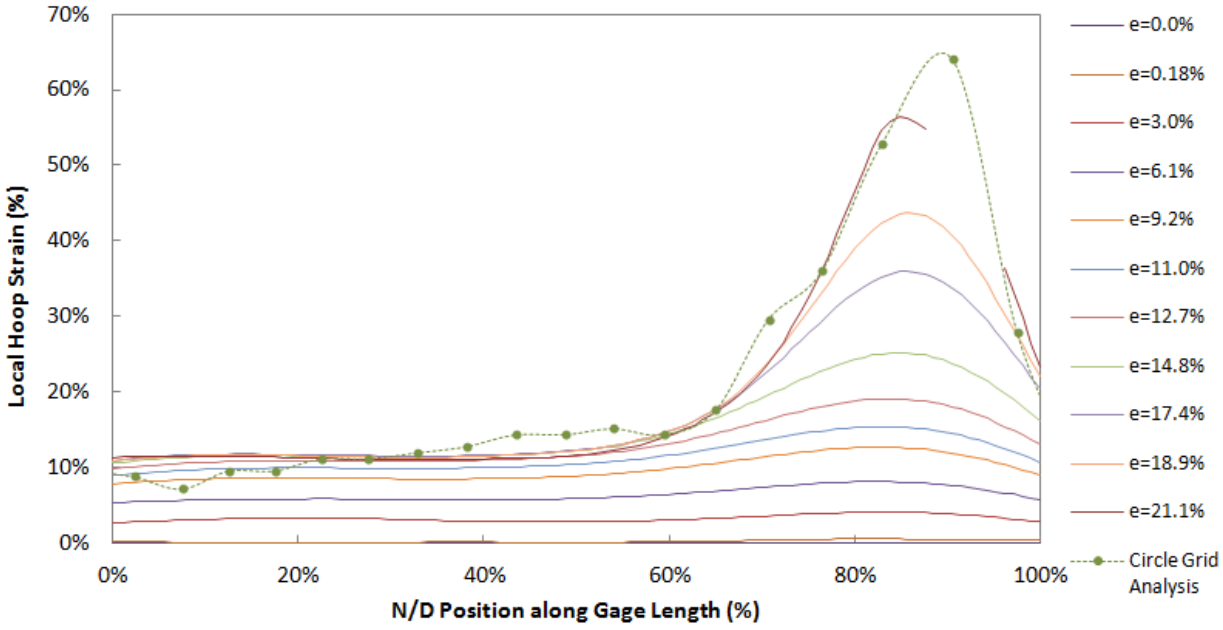

Figure 3.21: The evolution of strain for the RHTT specimen DBlock-T5. Some variation in the strain distribution before localization is exhibited.

The DIC data can not only to compute the nominal strain with a virtual extensometer, but can view the strain distribution through the gage length at any point on the stress-strain curve (see Figure 3.21). There is substantial localization before ~10% nominal strain in this test. This is likely due to a combination of friction with the mandrel interface and a variation in the thickness distribution. Circle grid analysis was used to validate the DIC data. The 0.1 inch grid was etched onto the specimen beneath the DIC speckle pattern, and measured after the test was complete. Good agreement is reached between the DIC strains after fracture (e=21.1%) and the circle grid major strain. A visualization of the distribution is given in Figure 3.22.

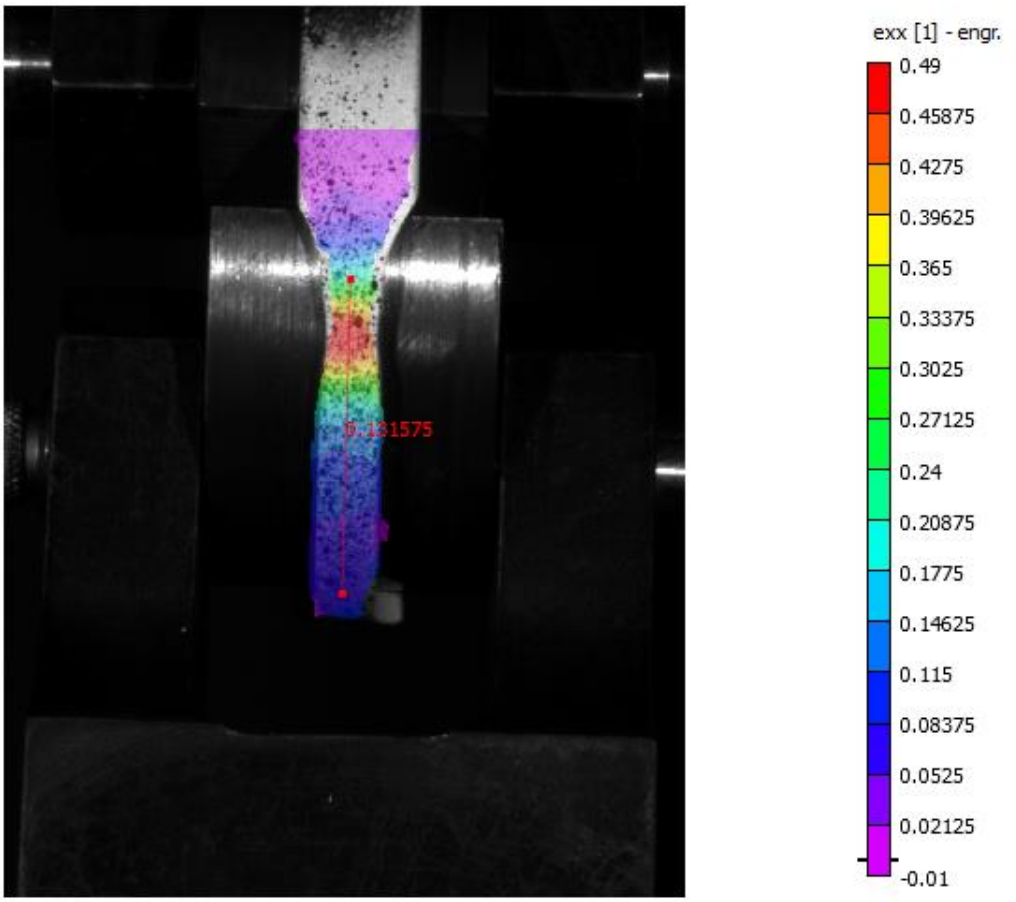

Figure 3.22: The distribution of hoop strain within the RHTT specimen.

3.7 Flaring Tests

Another method for testing the circumferential direction of the tube, especially with regards to formability, is to perform a flaring test. In this test, a short length of tube is expanded by inserting a conical punch into the tube end. A common flaring mode known as end flaring or expansion flaring has been studied due to its applications in part manufacturing, conical sealing [2], crash elements/energy absorption [33], and material behavior testing. As the punch contacts the tube wall, the material is stretched circumferentially and compressed axially by the conical punch. The punch continues to stretch the tube radially and compress the tube axially until the experiment is stopped at failure when the tube wall fractures. The friction on interface between the tube and the punch can lead to strain localization(s) in the hoop direction [34]. This complicates the stress-strain and formability evaluation; however some useful observations can be made about the Al-6061-T4 tubes from a good experimental setup:

- Obtain the maximum circumferential strain limit of flaring a stock tube.
- Obtain the major and minor strains using Circle Grid Analysis.
- Determine the strain field around the weld lines using 3D DIC.
- Determine where failure occurs in the circumference of the tube.
- Observe multiple localized necks around the circumference of the tube.

For this experiment, a 60 degree punch was machined from 4140 steel and hardened by quench and tempering at 800°F [28]. The punch utilizes an adapter so that it can be held

in the MTS hydraulic wedge grips on the MTS Landmark 370. A self-aligning platen was used to seat the tube during the flaring test. The punch is lubricated with oil for each experiment. The crosshead force was recorded from the 250 kN MTS load cell via the 16 bit A/D converter at 500 ms intervals. The experimental setup is shown in Figure 3.23.

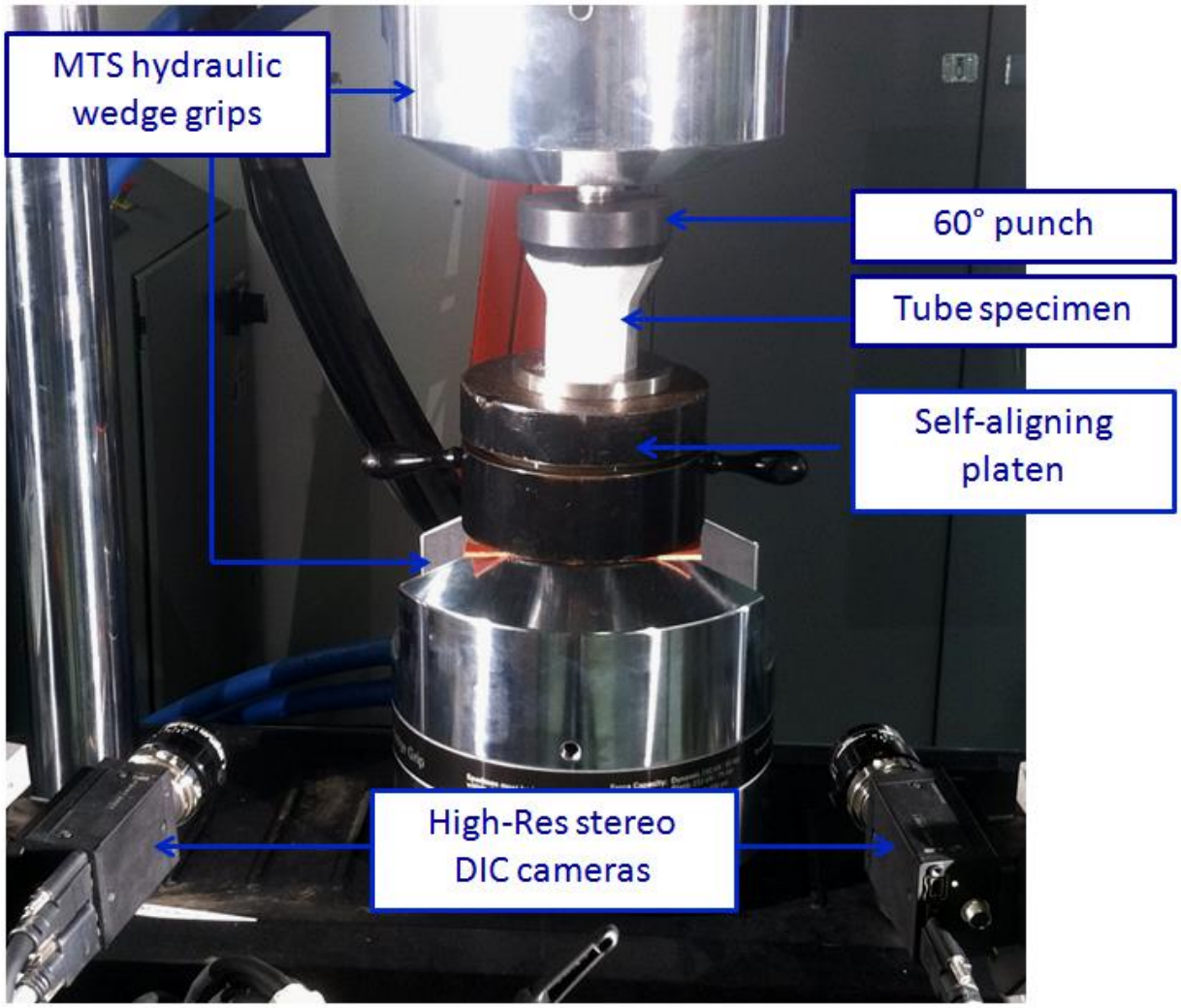

Figure 3.23: Setup for flaring experiments.

The length of the specimen was 64 mm (2.52 inches) and the outer diameter approximately 60.325 mm (2.375 inches), which was sufficient to prevent failure due to Euler or concertina buckling. The positions of the three welds are marked on the inner tube

surface. The specimens are prepared using a lathe to lightly sand the exterior (400 grit paper) and bevel the upper inside wall of the tube with a 30° taper. The taper is chosen to match the punch angle and aids in aligning the specimen with the punch. It also increases the surface area when the punch initially contacts the tube and allows the punch to slide in without interference from burrs or other debris.

The entire circumference is etched with a 0.1 inch (2.5 mm) circular grid to allow Circle Grid Analysis. Additionally, a speckle pattern for DIC analysis is painted onto 1/3 of the circumference. This pattern is positioned in order to capture the weld closest to the thinnest region of the tube wall in order to increase the likelihood of capturing the failure in this region. It is important to capture the failure in order to observe the maximum major and minor strain limits for the material. Circle grid analysis is performed on the specimen after failure and compared to the final strain fields in the DIC analysis. It is convenient that the speckle pattern for the DIC analysis can be removed after the experiment in order to expose the underlying circle grid.

The circumferential (hoop) strain evolves non-uniformly due to friction. Additionally, the hoop strain decreases from a maximum strain at the upper edge of the specimen (rim) to the end of the deformed region. As a result, the selection of gage length must be small in order to prevent excessive averaging (which creates artificially low strains). In other words, the strain must be evaluated on a local level. For circle grid analysis, the gage length is the diameter of each circle. The DIC analysis, the strain field can be calculated using subpixel increments and the post-processing of the data allows the selection of any virtual gage length for the purposes of calculating an average strain. The entire circumference can

be considered to calculate the overall circumferential strain - however there are typically multiple regions of localized thinning (necks) and the strains around the circumference are non-uniform.

The crosshead speed is calculated in order to target an average circumferential strain of $1x10^{-3}$ /s. In order to calculate the crosshead rate, the calculation uses the target strain-rate along with the punch taper angle and the initial radius of the tube. The calculated crosshead speed was $2.362x10^{-3}$ in/s (0.06 mm/s) and can be found in Appendix F. This calculation neglects any axial compression of the tube, which would lower the actual circumferential strain-rate seen by the tube wall. The material has not previously exhibited strain-rate dependence (see Figure 3.10), therefore small differences in the actual strain-rate are considered negligible.

The crosshead advance is stopped when tube wall ruptures. This failure is precipitated by localized thinning in the region (necking) before the tube wall fractures at the rim. When considering the failure limit of the material, the upper rim region should be considered, as this region fails while the rest of the tube is intact. The regions below the rim fail due to the propagation of the previously formed crack and are not indicative of the failure limit of the hoop material in this forming process.

The crosshead force for the tube end flaring process is well documented to have 5 characteristic regimes in the load-displacement curve [35-37]. The first regime is the elastic deformation due axial compression and circumferential elastic stretching from the initial contact force of the punch on the rim. At a certain load, plastic deformation begins but the curve is relatively flat. This regime is characterized by bending deformation as the

uppermost circumferential sections of the rim begin to plastically deform. The load then begins to increase as the further portions of the tube wall come into contact with the punch. The next regime is characterized by a linear load-displacement curve as the tube enters a regime of steady-state expansion. At the peak of the curve, the specimen reaches its final regime as failure of the specimen due to buckling or fracture occurs and the load drops off sharply. These regimes are labeled on the test data for the 6 flaring test specimens presented below in Figure 3.24.

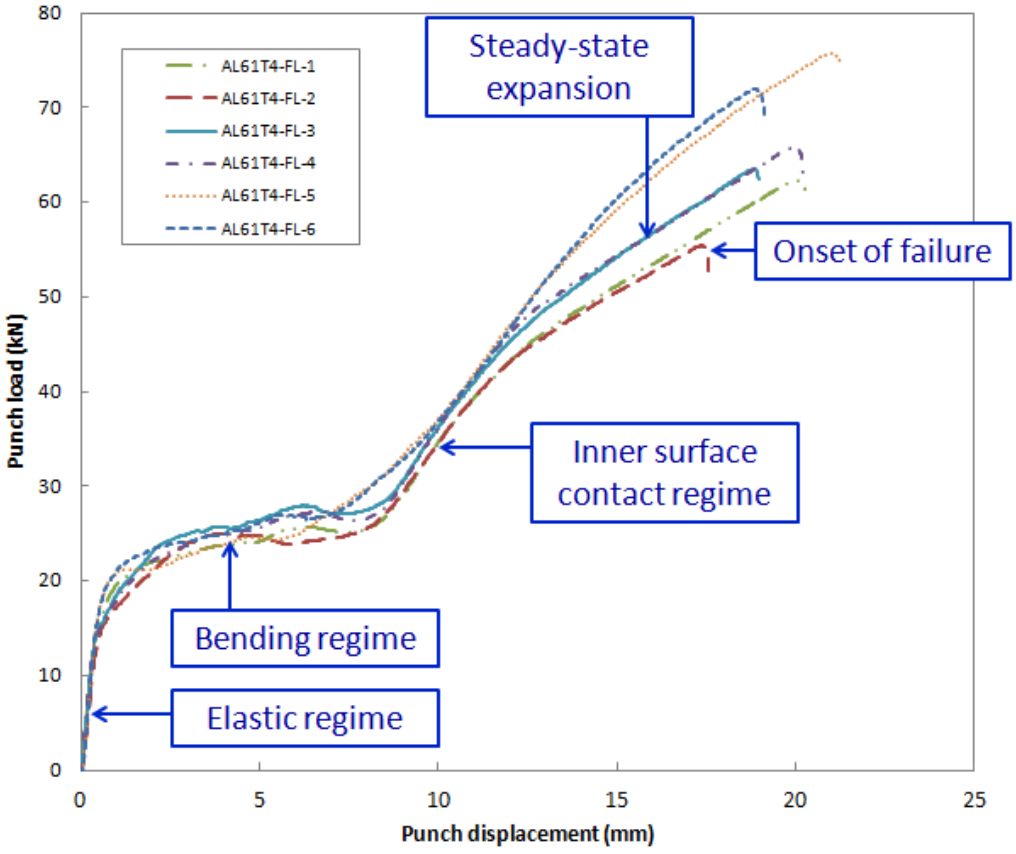

Figure 3.24: Load-displacement curve for Al-6061-T4 tube flaring experiments.

One of the better test specimens was specimen #5 (Figure 3.25), which failed predictably within the DIC region and was minimally deformed after the initial fracture of the rim. The circle grid under the DIC paint was sampled at the locations in Figure 3.26. The major and minor strains were calculated for the first 5 circles from the rim along the tube axis in increments of 5-degrees. The measurements also include the circles on each side of the fracture. These are organized into a failure envelope with safe and fail zones identified in Figure 3.27. The envelope is commonly used in sheet metal forming as per Graf and Hosford [38].

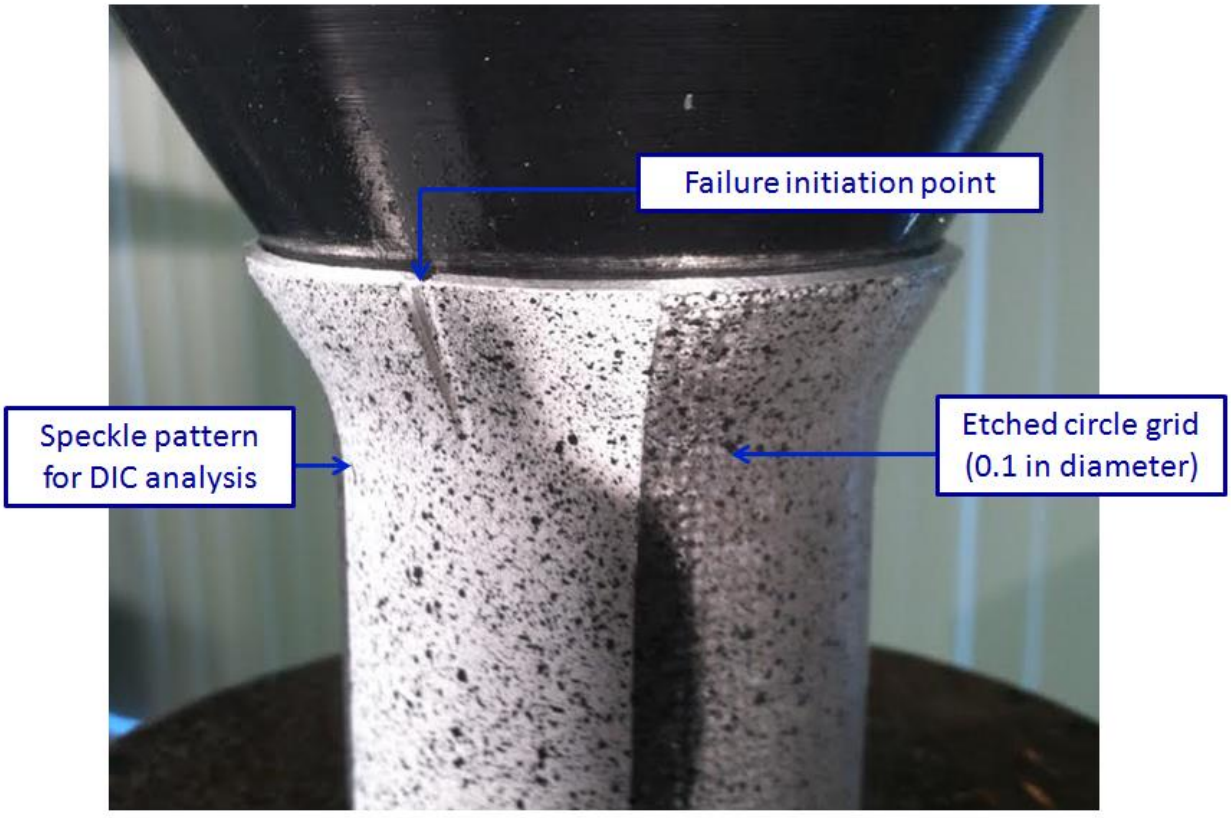

Figure 3.25: Flaring specimen Al61T4-FL-5 at failure.

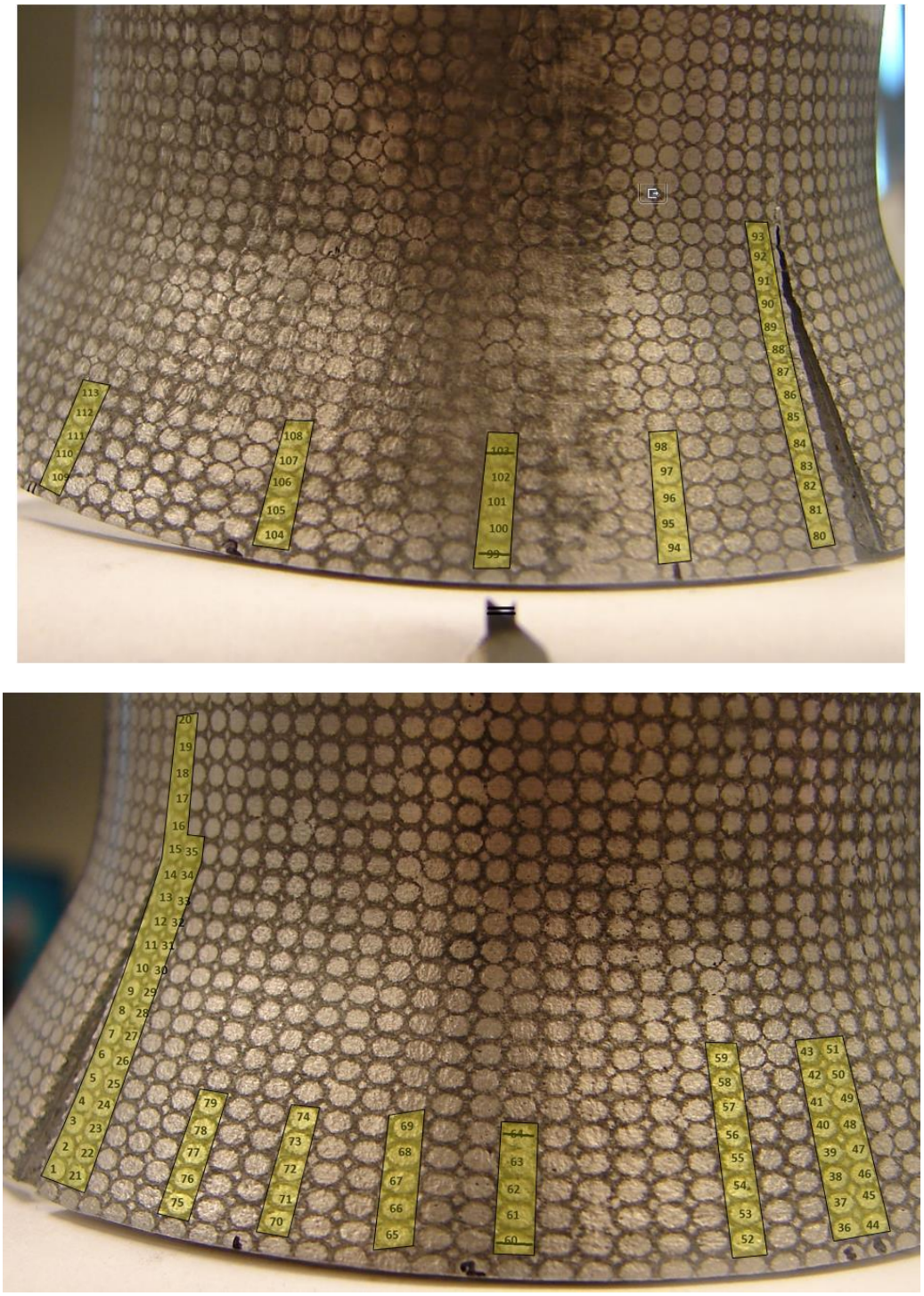

Figure 3.26: Regions of interest for circle grid analysis of Al61T4-FL-5 flaring.

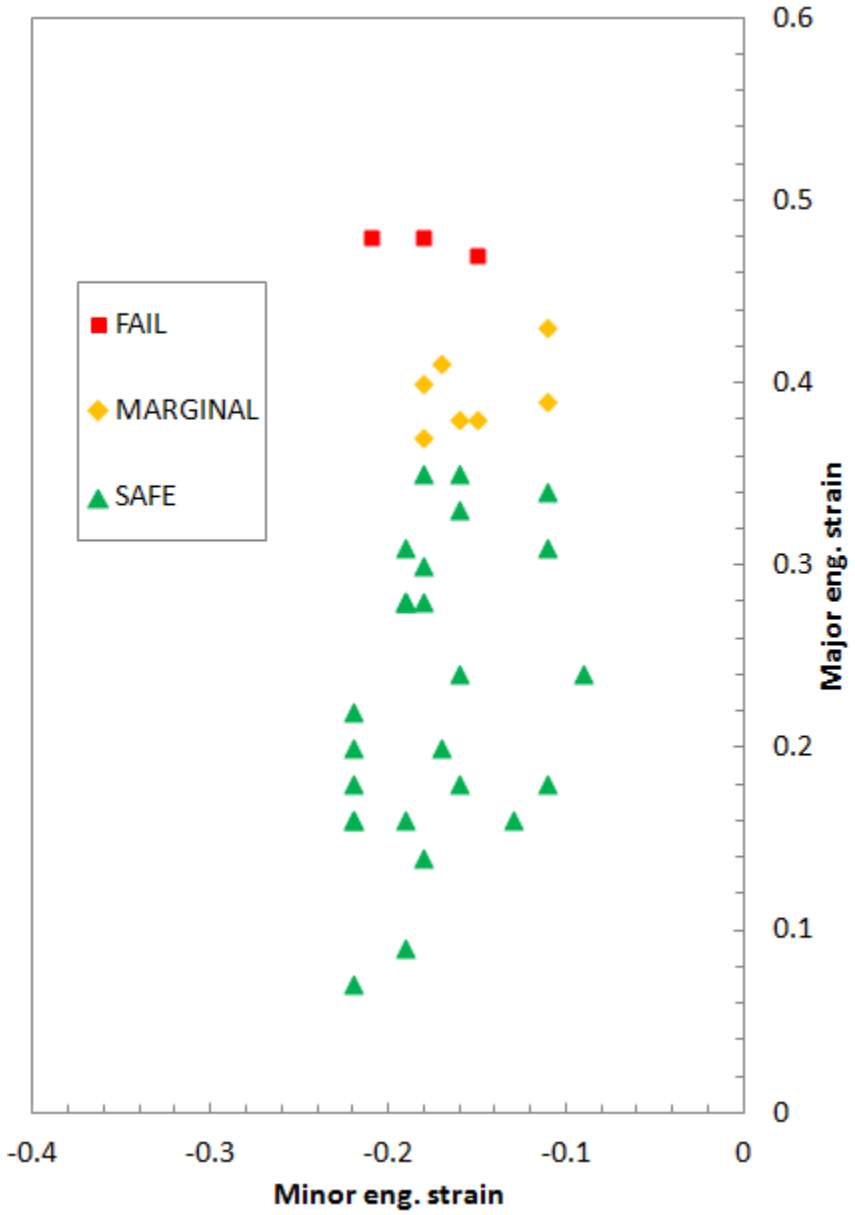

Figure 3.27: Failure envelope for end flaring of Al61T4-FL-5 specimen.

The DIC analysis for hoop-strain field for specimen 5 at the point of failure is shown below in Figure 3.28. The DIC hoop-strain field is engineering strain. This data is further detailed in Figure 3.29, where the DIC strains are reported along the circumference of the specimen for several sections along the axial length of the tube. The engineering strains from the CGA are overlaid for comparison. Despite the relatively small gage length (0.1 inch / 2.5 mm) of the circles, it is important to note that the circles average over a region both vertically and horizontally. Figure 3.29 demonstrates a large strain gradient along the tube axis, so differences in the CGA values are expected. It is also quite difficult to accurately measure such small circles. Overall, the circle grid analysis with 0.1 inch (2.5 mm) circles corresponds well with the strains measured by DIC.

The strain limit found from the flaring test is higher than the strains seen in both the tensile test and the ring hoop tension test. The latter tests evaluate strain over a comparatively larger span (gage length) and are accurate as long as the gage is uniformly strained. Once localized areas of high strain occur, the strain evaluated with the extensometer in the tensile test and the virtual extensometer in the D-block tests is not indicative of the actual strains in the material. DIC analysis of the lower sections of the tube show there are sections of the tube where the strain is uniform about the circumference. Localization begins to develop before 20% strain ("Bottom line" in Figure 3.26), which corresponds reasonably well with the strain at UTS in the tensile tests. It is likely that the localization seen with flaring is similar to the localization seen previously in RHTT test (Figure 3.21). The DIC data should be examined at strains around 10% to see if the localization has occurred before the 20% "Bottom line" in Figure 3.26.

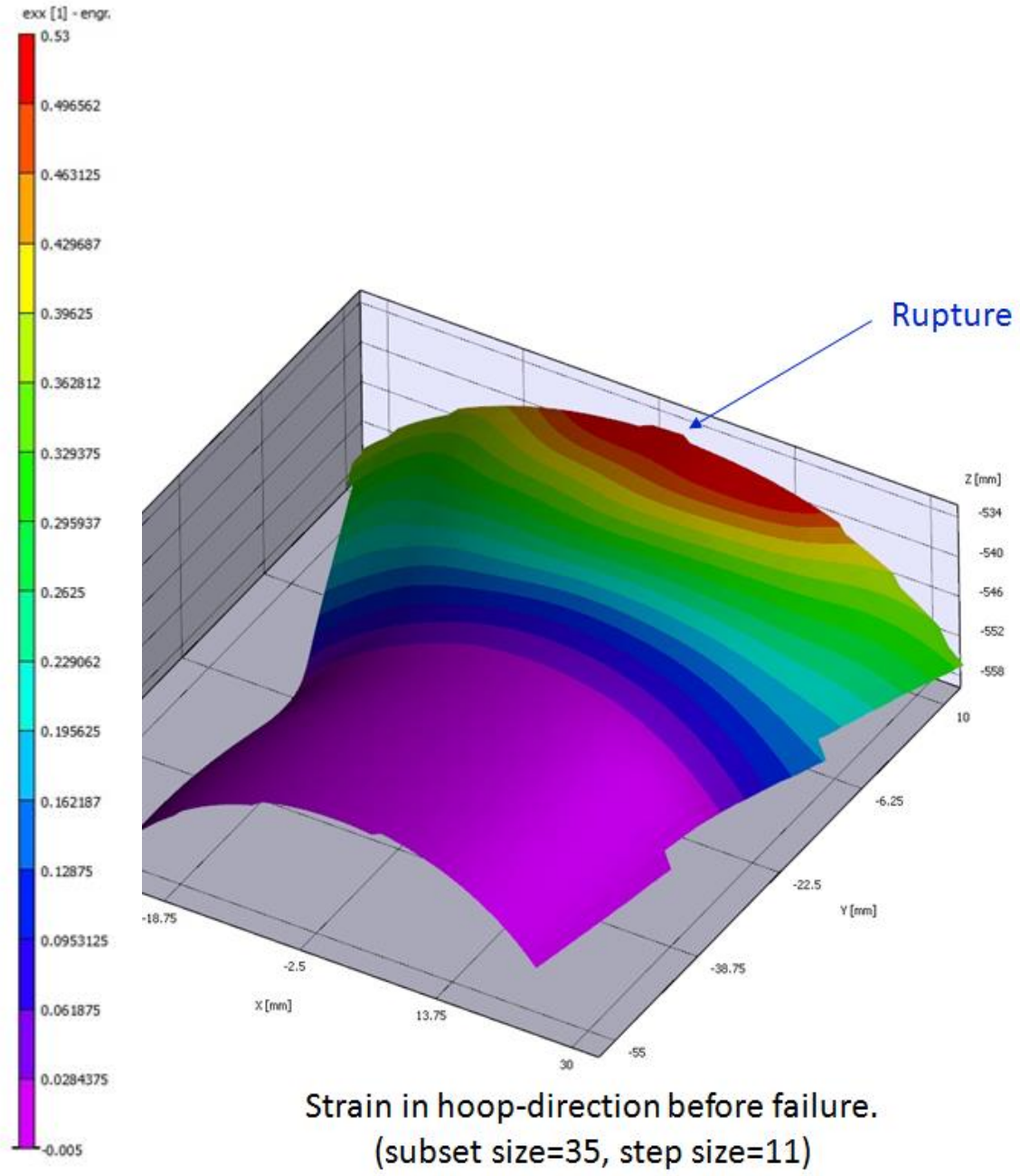

Figure 3.28: DIC analysis of hoop strain at failure for flaring Al61T4-FL-5 specimen.

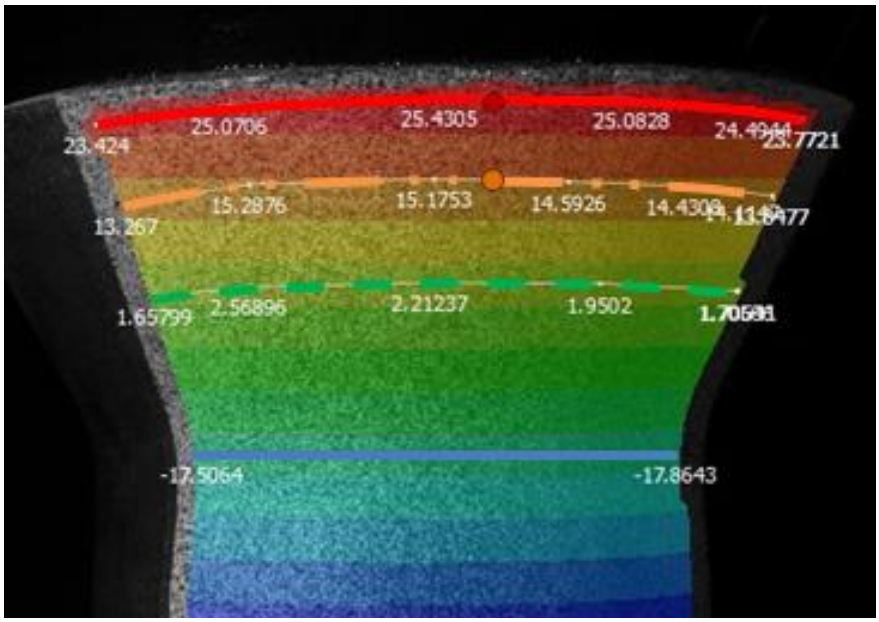

Note: This image is taken at an intermediate punch displacement to illustrate the nominal measurement bands in VIC 3D. The image is prior to failure.

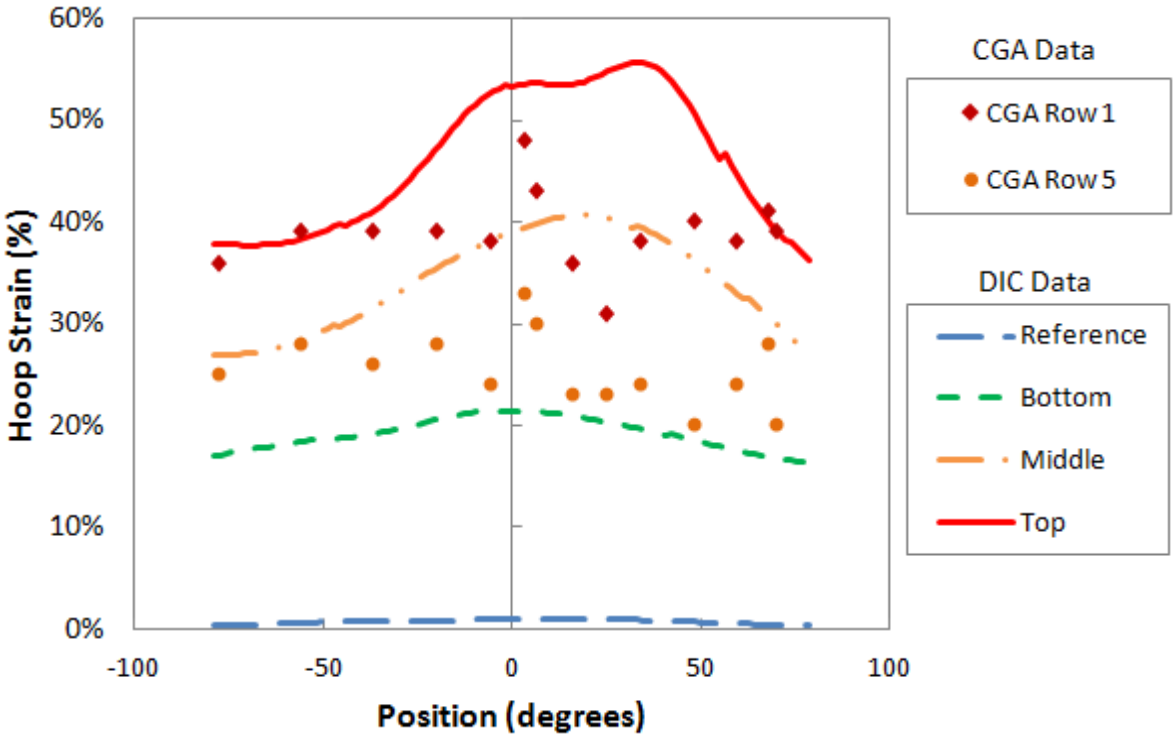

Figure 3.29: Analysis of eng. hoop strain at failure for flaring Al61T4-FL-5 specimen at various axial sections along the tube axis, at the final punch displacement.

CHAPTER 4

NUMERICAL SIMULATIONS

4.1 Analysis Overview

In this chapter, the tube hydroforming process is modeled by finite element analysis. The simulations offer a viable solution to detailed plasticity problems such as thinning, necking, and corner filling, which cannot be easily solved with simple models or approximate analyses. The finite element models described in this chapter are used to evaluate the suitability of specific tube geometries (OD and thickness), tube materials, die configurations, and fluid pressure and volume requirements for the experimental tube hydroforming machine. The axial tension test and ring hoop tension test are also valuable finite element models for calibrating material plasticity curves. These models are part of a greater research into improving the formability of tubes during the hydroforming process.

The resulting geometry from the finite element model can be correlated back to the physical experiment. Once calibrated, a finite element model can be used for feasibility studies, die development, forming pressure and volume requirements, and even qualitative analysis of different lubricants and tube materials. The results can be compared using the distributions of circumferential strain and wall thickness at selected cross sections. These values can be calculated from the physical experimental tube using a variety of measurement techniques including: CMM measurements of the tubes outer dimensions, circle grid analysis on the tube surface for strain calculations, measurement of cross-sections using a profile projector, and calculation of 3D displacements and strains via digital image correlation.

The finite element models for the tube hydroforming machine were developed with Simulia Abaqus CAE (v6.10), a non-linear finite element package. The numerical codes are known as Abaqus/Standard and Abaqus/Explicit. Abaqus CAE refers to the graphical editor that supplements the codes usability. Abaqus CAE and the codes are Windows compatible. These simulations have been executed on two modest platforms: UNH Nozomi Server running Linux OS (Ubuntu 11.04 64-bit), 2 CPU, 8 Cores, 32GB RAM (+32GB Swap), and a PC running Windows OS (Windows 7 Professional 64-bit), 1 CPU, 4 cores, 16GB RAM (+16GB Swap).

The Abaqus code is well-suited for hydroforming simulations due to its detailed plasticity models for when the material exceeds its yield point and begins ductile, non-recoverable deformation. Additionally, the load manager allows multi-step simulations, which can be helpful for modeling the hydroforming process.

More importantly, Abaqus includes a specialized feature for simulating fluid-filled cavities. The cavity surface is defined with a surface element knows as a “hydrostatic element”. The cavity surface is coincident with other geometric elements (in this case, the tube and the seals of the device) and transfers the pressure as an evolving boundary condition. In hydroforming simulations, the cavity pressure or volume can be specified over time – analogous to the input of actual hydraulic control systems. As the geometric elements deform, the hydrostatic elements defining the cavity displace accordingly.

These elements will be described in detail for in the latter sections of this chapter. The simulations were used to determine the forming die dimensions and evaluate commercially available tubes.

4.2 Material Model

Abaqus material models include classical isotropic metal plasticity using the von-Mises yield criterion, anisotropic metal plasticity using Hill's yield criterion, kinematic hardening, Johnson-Cook, and User-Defined yield functions. Temperature and strain-rate dependence are included in many material models.

Development of accurate material models is vital to any analysis, whether finite element, analytical models, or hand-calculations. Abaqus will be used to compare two material models for the Al-6061-T4 tubes. Two of these material models correspond to the axial tension tests – one for the base material specimen and one for the specimen with the weld. The axial material with the weld line has a similar overall strain before UTS, but a more rapid failure after localization (Figure 3.8 and Figure 3.9 in Chapter 3). The hoop direction of the material as tested by the ring hoop tension test has a slightly different response, but not enough to warrant a separate material model.

Relative to the overall cross section of the Al-6061-T4 tubes, the volume of the weld is small compared to the volume of base material. It is true that the presence of the weld can lead to premature failures due to strain localization, especially in the circumferential direction of the tube. However, it should be noted that the variation in the wall thickness is also a driving factor in strain localization, and that the occurrence of maximum wall thickness is directly between two of the aluminum welds. In flaring experiments from Chapter 3, it was often seen that the thinnest region of the tube wall before deformation was the location of the failure. As a result, it may be considered a safe assumption to omit the weld volume from the model. Due to the added complexity involved of including the

weld material in the tube model, it will be neglected. The material model of the weld, both axial and circumferential, may be used in future refinements of the model.

Abaqus requires the user to define the material's elastic and plastic properties. The elastic modulus and Poisson's ratio are used to define the elastic material definition. The elastic modulus for the Al-6061-T6 tube material was defined as 68.3 GPa (9.9 ksi) and the Poisson's ratio was defined as 0.33 (see Elastic Tension Tests in Chapter 3).

The plasticity model uses true stress and effective plastic strain [39]. The raw data from the axial tension experiments are used to calculate the engineering stress and strain. These values are transformed into true stress and true strain. The elastic strain is removed from the true strain to find the effective plastic strain. True stress and strain will be calculated from the plastic components of the engineering stress-strain:

Eng. stress:	$\sigma_{Nominal} = F_{crosshead} / A_{gage}$	in units of MPa.
Eng. strain:	$\varepsilon_{Nominal} = D_{extensometer} / L_{gage}$	in units of mm/mm.
True strain:	$\varepsilon_{True} = \ln(1 + \varepsilon_{Nominal})$	
True stress:	$\sigma_{True} = \sigma_{Nominal} (1 + \varepsilon_{Nominal})$	
Plastic strain:	$\varepsilon_{Plastic} = \varepsilon_{Nominal} - \varepsilon_{Elastic}$	

Where:

L_{gage} is the initial distance between the extensometer legs in mm.

A_{gage} is the characteristic cross-sectional area of the gage in mm^2.

$F_{crosshead}$ is the axial force measured by the crosshead in Netwons.

$D_{extensometer}$ is the displacement measured by the extensometer in mm.

$\varepsilon_{Elastic}$ is the 0.2% strain offset used to calculate the initial yield stress.

σ_{Yield} is the yield stress (engineering) at the 0.2% strain offset.

Since Abaqus uses the plastic portion of the true stress curve, the true stress value at zero plastic strain is the first point in the definition. From that point, the plastic strain and the true stress must increase with each data point in the definition.

Due to noise in the data, the raw data must be smoothed so that Abaqus can use a monotonically increasing material curve. In the Al-6061-T6 tensile experiments, there are about 2600 data points for each test. The number of samples in the dataset is difficult to work with, therefore the points for the final material curve can also be reduced via curve fitting and data regressions.

In order to regress and smooth the plasticity data into a usable curve, a MATLAB script was employed to create the plasticity curve. The first script, named *Main_SingleCurve.m* (see Appendix G is used to smooth the data and ensure it is monotonically increasing. A low pass filter was applied using the “filtfilt” function in MATLAB, which removes most of the high-frequency noise from the curve but maintains

the characteristic curve shape. Next, the resulting data is checked to ensure that the filtered curve monotonic increases in stress by at least 0.01 MPa for each data point. The exceptions are removed and the curve is re-checked until the resulting curve is truly monotonic. A second MATLAB script called *CurveSmoothingForAbaqus.m* (see Appendix H is used to spline and reevaluate the curve. The spline allows the number of points to be reduced and evaluated at "observer-friendly" strain increments (e.g. 0.01, 0.02, 0.03, etc.).

The axial tensile data reached about 15% nominal strain before strain localization near UTS. Once the strain becomes non-uniform, the true stress and strain calculations derived from the engineering curve are no longer reflective of the state of stress in the material. In tube hydroforming simulations, the tube will commonly fail due to localized thinning of the tube wall. In this region, the strain of individual elements will greatly exceed the nominal value from the axial tension test. As a result, the plasticity model will be extrapolated to 100% true strain.

It is common practice to use plastic region of the curve prior to ultimate tensile strength in order to extrapolate the work-hardening behavior at high strain values. In order to verify the extrapolation, the axial tension experiment can be simulated. The engineering stress-strain curve for the simulation (with the strain calculated from a virtual extensometer over the gage length) is compared to the experiment, and the extrapolation is manually adjusted until there is good agreement between the curves after the ultimate tensile strength has been reached and strain localization occurs. This process is largely trial and error, where the researcher manually observes the response and corrects the extrapolation on the next iteration.

Base material axial tension tests Al-6061-T4-A2 and Al-6061-T4-A5 were processed through the MATLAB script. Those results were averaged to create the initial points in the base material curve. The final extrapolation of the hardening curve for the base material is shown in Figure 4.1, along with the test datas and comparative models for linear and perfectly plastic hardening models. To create the weld material model, tests Al-6061-T4-D1 and Al-6061-T4-D5 were processed and averaged. Similarly, the final extrapolation and comparisons are shown in Figure 4.2.

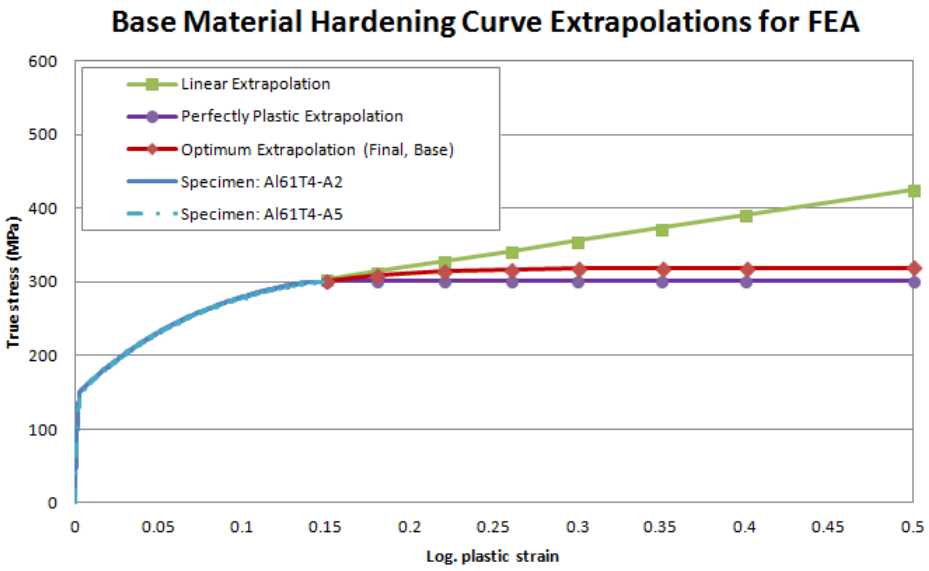

Figure 4.1: FEA hardening curve for base material.

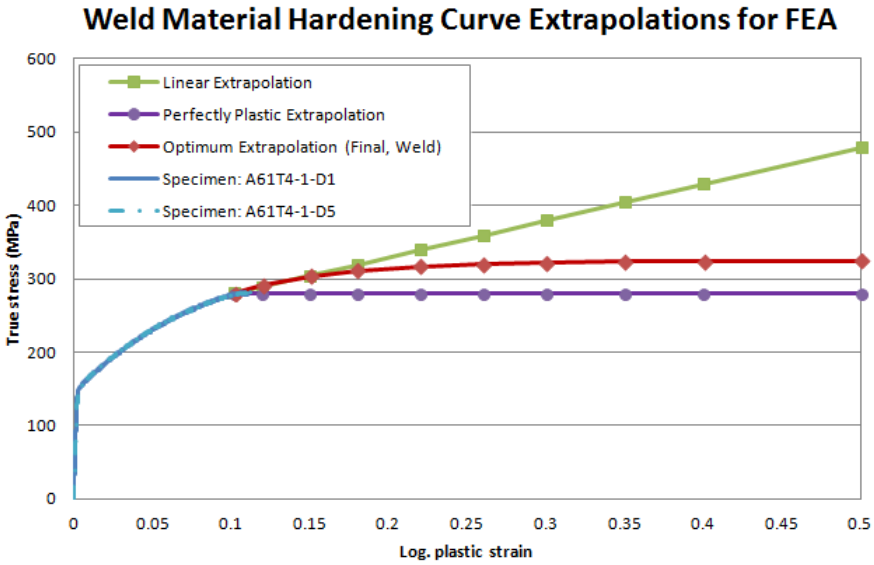

Figure 4.2: FEA hardening curve for weld material.

The final Abaqus material definition for the base material and the weld material can be found in Appendix I. Figure 4.3 shows a comparison of the two material definitions. There is a divergence between the two curves at 13.96%, where the weld material curve

finally exceeds the base material. This intersection is shown in Figure 4.4. This material data point will certainly be encountered in the simulations, so it is interesting to note that the extrapolated material behavior deviates from this plastic strain onward.

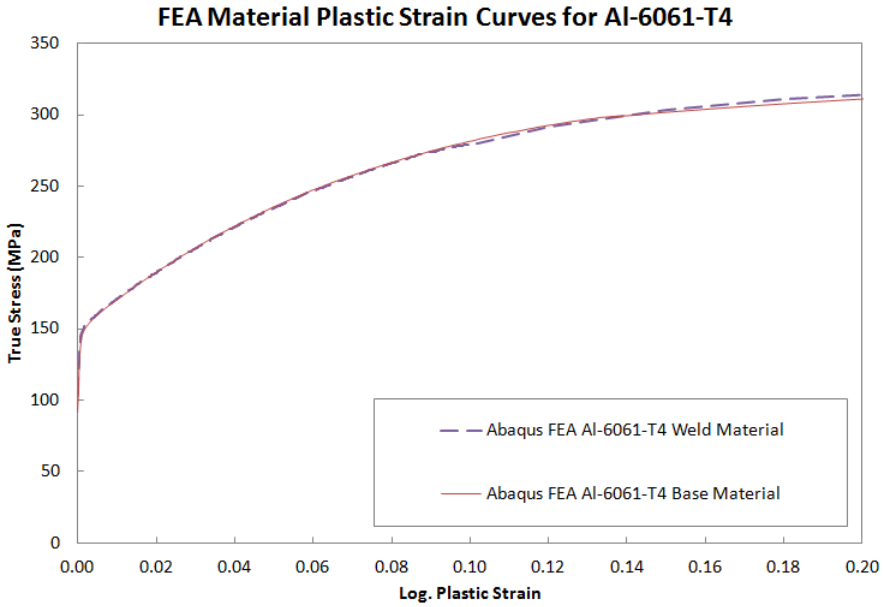

Figure 4.3: FEA plastic material for Al-6061-T4 base and weld regions.

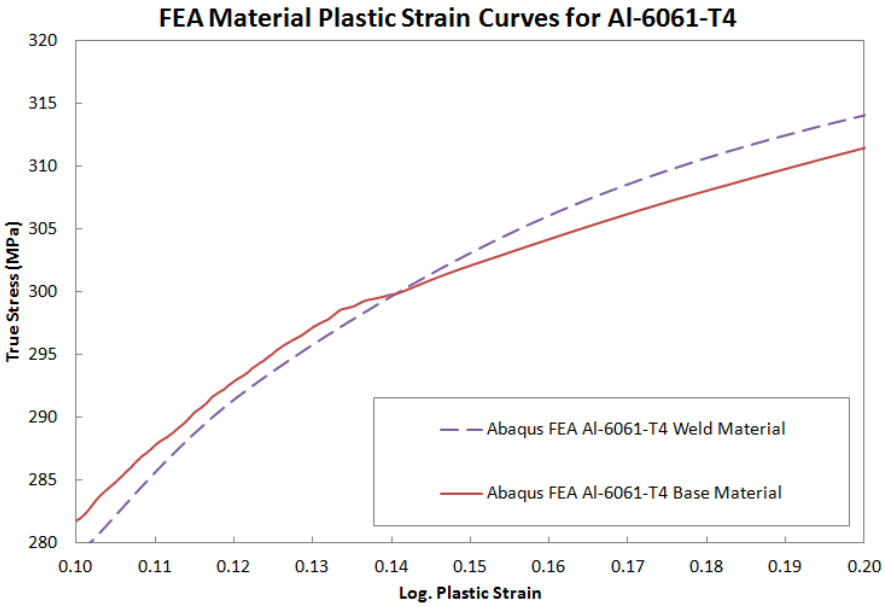

Figure 4.4: Intersection point in Al-6061-T4 base and weld FEA materials.

4.3 Simulation of the Tensile Test

An axial tension finite element model was created using the geometry of the ASTM E8 Standard subsize specimen with Abaqus/Standard (i.e., implicit). The gage length and grip regions of the model were partitioned separately in order to implement boundary conditions and provide some local control of mesh density in those areas. Symmetry was utilized through the thickness and along the meridian of the model (parallel to the gage length) to reduce the mesh to a minimum of 1472 C3D20R hex elements with quadratic integration points and reduced integration. The mesh was 3 elements thick to the symmetry plane.

To model the tensile force applied by grips of the servo-hydraulic machine, two boundary conditions were created at the top and bottom of the specimen. In order to simplify the summation of forces, kinematic couplings where utilized on both the top surface nodes and the lower surface nodes. Kinematic couplings link the degrees of freedom for a preselected set of nodes to the corresponding displacement of a master node. The lower coupling is a rigid body with pinned nodes, labeled *RP-Fixed*. The upper coupling is also a rigid body with pinned nodes, labeled *RP-Load*. This setup allows us to prescribe the displacement of the crosshead by prescribing a displacement to RP-Fixed. It also allows the output of the force seen by the crosshead - the coupling automatically sums the force of each individual node.

The master node for the lower fixed (no degrees of freedom). The crosshead is simulated by applying a prescribed displacement in the Y direction (U2) and fixing all other degrees of freedom.

A maximum number of 500 increments were sufficient for the analysis to complete. The time step was automatically adjusted by the software and the initial time increment size was 10^{-4}, with a minimum step size of 10^{-10} and a maximum step size of 6×10^{-3} (all in units of time). The Abaqus/Standard code was used and non-linear geometry was enabled. The load was ramped linearly over the total time period. The prescribed displacement is 10 mm (0.394 inch).

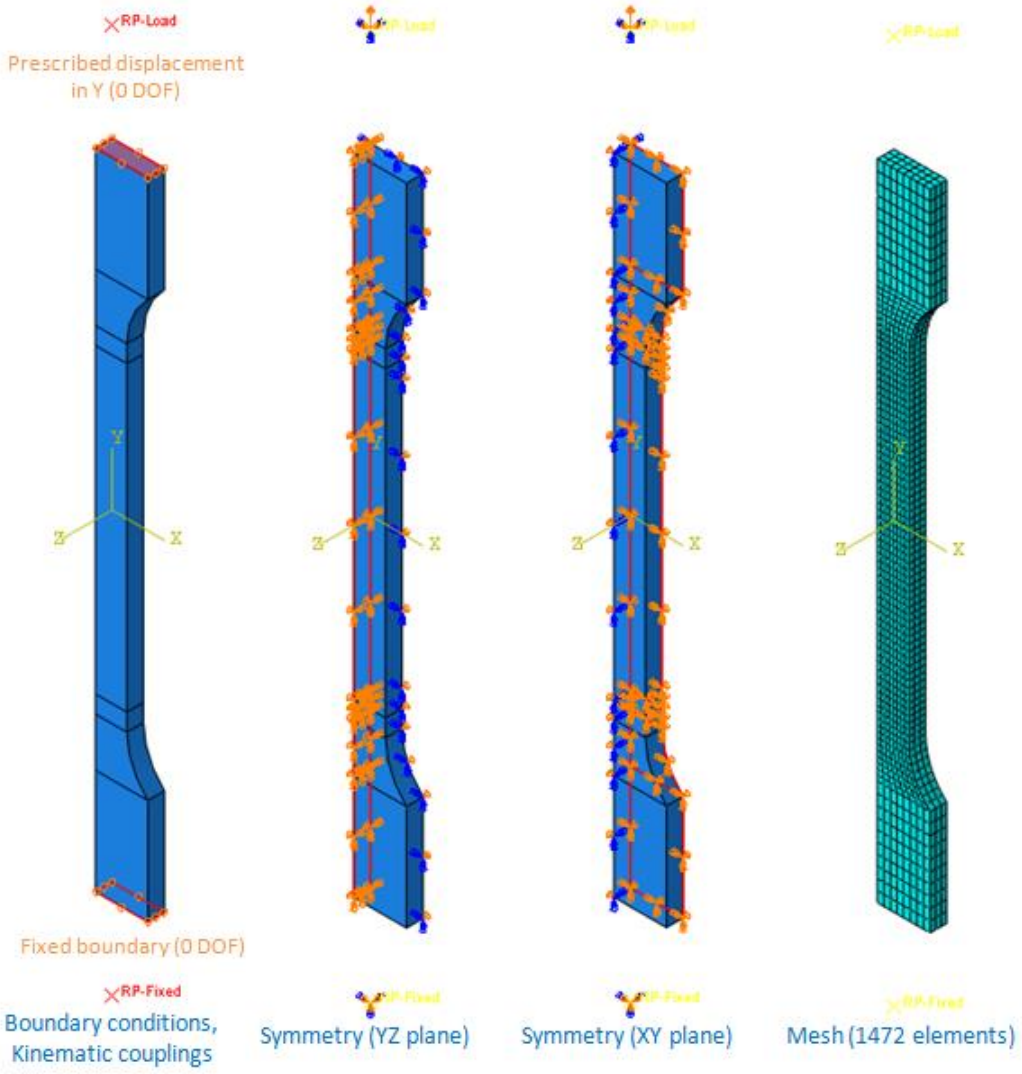

Figure 4.5: Boundary conditions, symmetry, and mesh for the finite element model of the axial tensile test.

This axial model was used simulate the axial tension experiments for the Al-6061-T4 specimens - the first, using a specimen cut from the uniform base material of the tube wall, and the second using a specimen that represented the weld region material of the tube wall. In order to recreate each physical experiment, the FEA model gage area dimensions were updated to the average thickness and width of the gage for each axial tension experiment. The FEA models use the material extrapolations from Figure 4.3 for all presented simulations. The material model was primarily derived from the un-notched axial specimen Al61T4-1-A5, as it was one of the few un-notched base material tests to fail inside the gage length (see Figure 3.6). The FEA results match well for this test; therefore other tests (such as A61T4-1-D2) are included to demonstrate the accuracy of the extrapolation for slight variations in specimen geometry. The differences in the pre-necking region between the FEA and the test data is expected, as there was similar variation between experimental tensile curves in these tests.

In Figure 4.6, two experiments of the base material specimens from Chapter 3 are compared to the finite element model. The A61T4-1-A5 specimen is a standard ASTM E8 specimen. A61T4-1-D2 is an ASTM E8 specimen with a notch to promote failure in the center of the gage length. The corresponding Abaqus models include the as-measured variations in specimen thickness for both models, and the notch depth for the D2 specimen.

Figure 4.7 shows two experiments on the weld material specimens and the corresponding finite element models. Both of these are ASTM E8 specimens with notches, which were added because none of the tensile experiments on the weld specimens from Chapter 3 failed within the gage length.

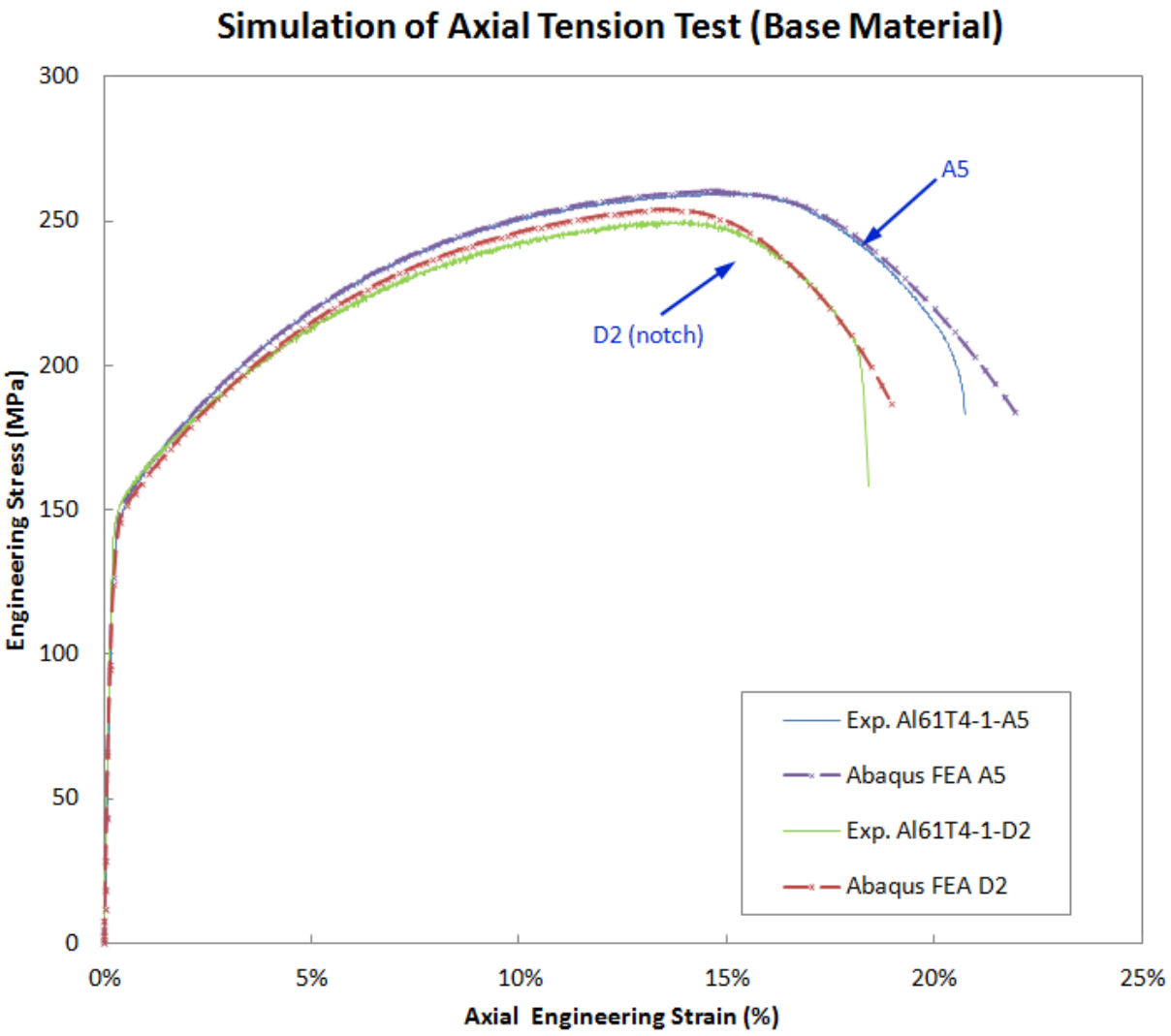

Figure 4.6: Axial tensile results of Al-6061-T4 tube base material, comparison of FEA model for two experiments of ASTM E8 subsize specimen with (D2) and without (A5) notch.

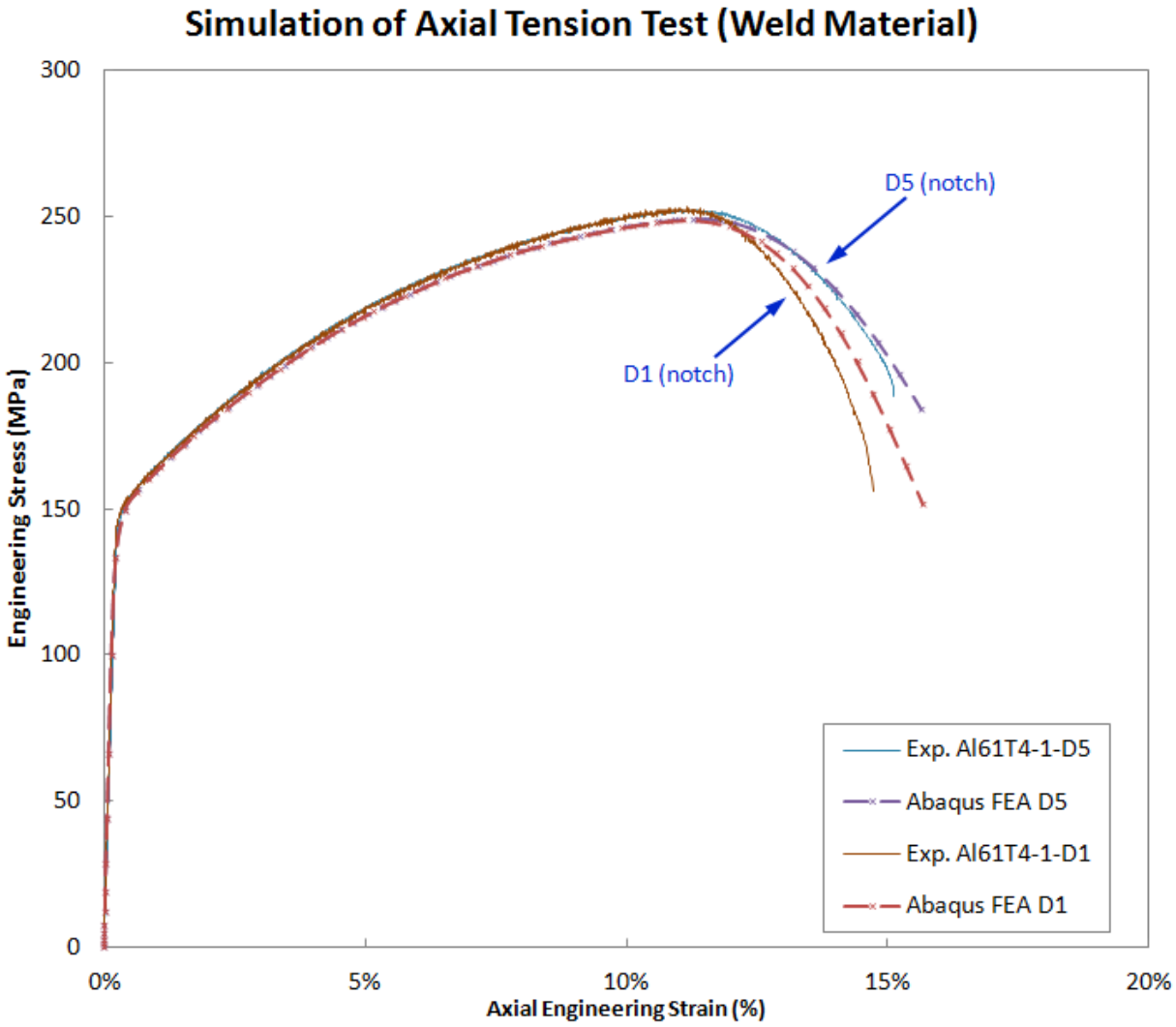

Figure 4.7: Axial tensile results of Al-6061-T4 tube weld material, comparison of FEA model for two experiments with notches (D1 and D5).

4.4 Ring Hoop Tension Test Simulation

The RHTT model was created using the geometry of the D-block specimen as specified in Chapter 3. The geometric model for the specimen includes the variation in wall thickness as measured on each test specimen. Due to the simulation of contact, Abaqus Standard/Explicit was used. The inner diameter was modeled as a perfect circle, i.e., any eccentricity in the inner diameter was neglected. All the eccentricity of the tube thickness is on the outer dimension. This variation is shown in Figure 4.8. The reduced section was created with a planar cut to mimic the milled profile. The gage length was partitioned and the nodes representing the extensometer defined along the centerline on the outside gage surface. Symmetry was utilized along the centerline of the specimen. The specimen was meshed with a minimum of 28680 C3D8R linear hexahedral elements with reduced integration. The mesh was 8 elements thick.

The upper and lower D-block mandrels were modeled as analytical rigid surfaces. Each is 53.5 mm (2.106 inch) radius semi-circle with a 1 mm (0.039 inch) fillet radius on each corner (to prevent contact singularities). Each D-block instance has a reference point that can be used to calculate the net force on the rigid body - this will be used to calculate the crosshead force seen by the load cell.

The upper D-block has a fixed boundary condition that prevents displacement and rotation (0 DOF). The lower D-block has a prescribed displacement of -10 mm (0.394 inch) in the Y-direction. Surface-to-surface contact is used between the D-block (master) and the nodes of the inside surface of the specimen (slave). A coefficient of friction was specified as 0.05.

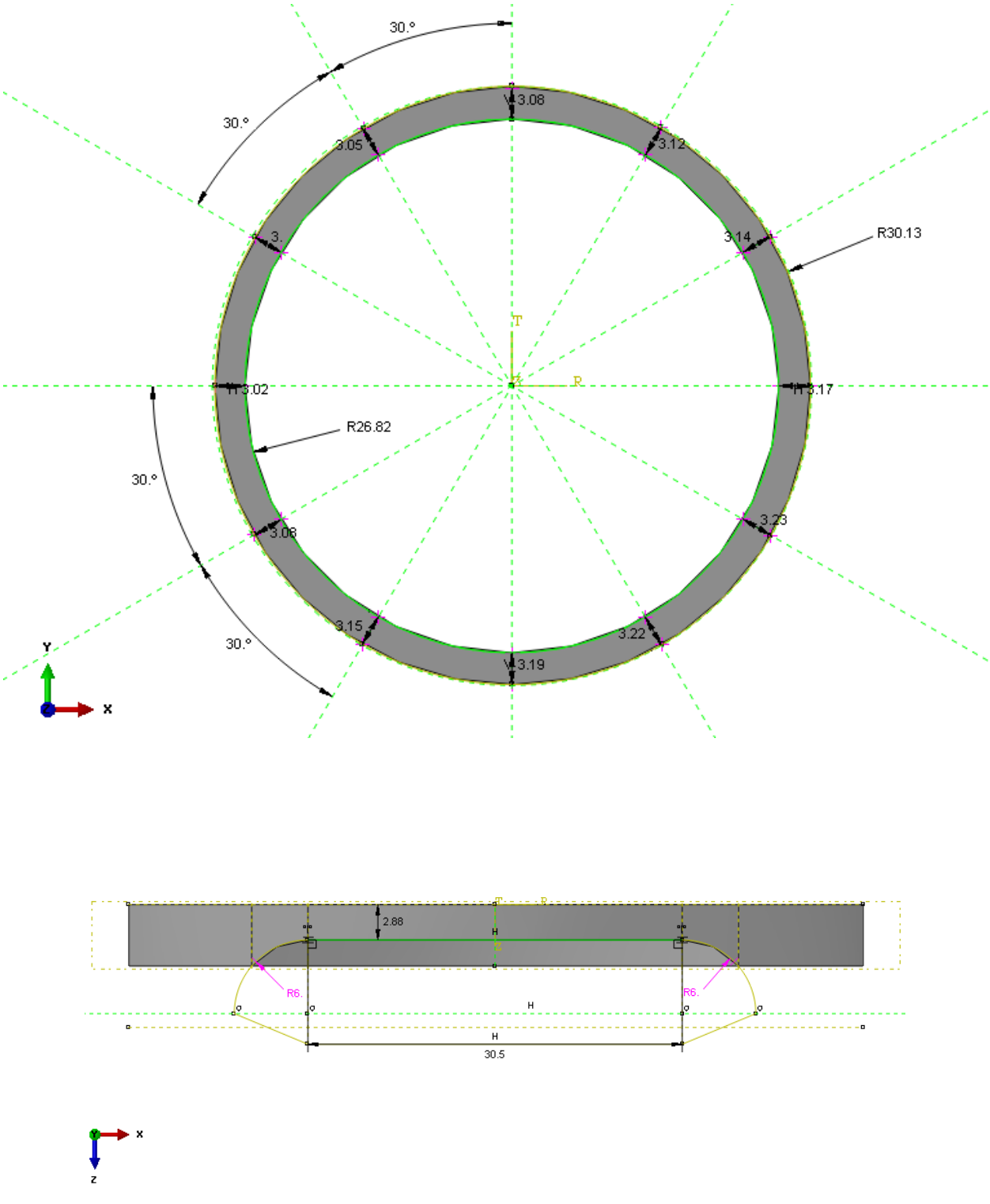

Figure 4.8: An example of the finite element model for the RHTT, including the variation of wall thickness and the planar cut that creates the reduced section.

In order to recreate the experiment, we will have to use a virtual extensometer similar to the one selected from the DIC data, which was a 25.4 mm (1 inch) span. These nodes were created on the outer surface at the center of the gage length. To mimic the post-processing of the DIC data, the nominal strain will be evaluated using the integrated distance along the surface between the two points. The linear distance would give artificially lower strains. Since the gage stretches along the constant circumference of the mandrel, the angle and radius of each reference point can be calculated (from the nodes' X and Y position). The average radius and angle of each node is used to calculate the change in the arc-length, S, which provides the nominal strain for the RHTT finite element model. This is illustrated below in Figure 4.9.

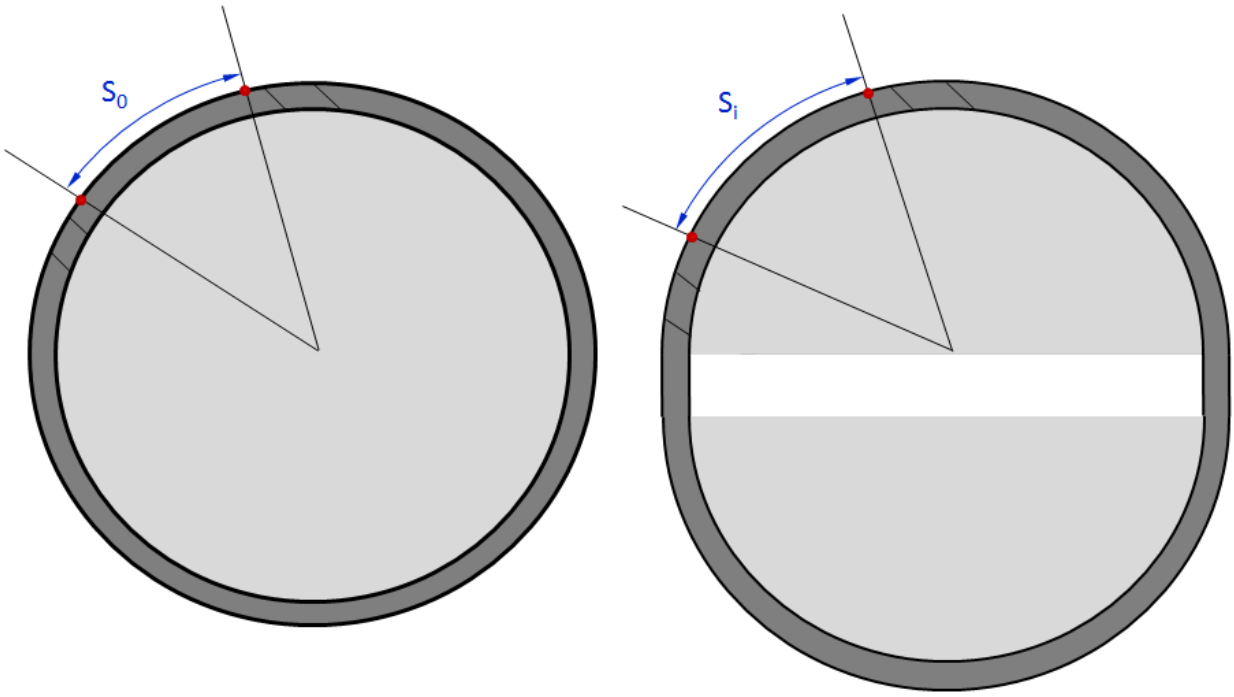

Figure 4.9: Illustration of how the change in arc-length of the reduced section is used to calculate the nominal strain in the Ring Hoop Tension Test.

In an earlier study that used simulations with a similar Al-6061-T4 tube material but thinner wall thickness of 1.59 mm (0.0625 in), the friction was examined to determine the influence on cross head force. Friction contributes to the crosshead force, however the friction cannot reasonably be decreased below a coefficient of 0.05 (the published value of PTFE tape). This relationship with the friction and the crosshead force is explored in Figure 4.10. The trend is very linear for a specimen of this surface area. The friction has a more significant effect on the localization of strain, which is apparent by the different positions of the UTS for the different friction coefficients shown in Figure 4.11 (Note: the strains have been calculated based on a linear span between the gage-length end-points and is artificially low). This relationship indicates that the frictional coefficient could be calibrated by matching the experimental crosshead force.

The next FEA models were updated with the specimen tube wall thickness of 3 mm (0.118 in) and run with the axial material data to see how close the results are to the RHTT experimental load curves. The response from the FEA model does not match the test data well, as seen in Figure 4.12. This is possibly due to the selection of gage length in the original data, as determined by the analytical strain field shown in Figure 3.22. The DIC analysis shows that the selected gage length captures the failure region, while the failure does not occur within the 25.4 mm (1 inch) gage length shown in Figure 4.13. A second 32 mm (1.25 inch) gage length was selected to capture the failure, which more closely matches the strains seen in the experiment. The presence of the failure within the gage length creates large differences in the calculated strain. This is apparent in Figure 4.12 when the curves deviate.

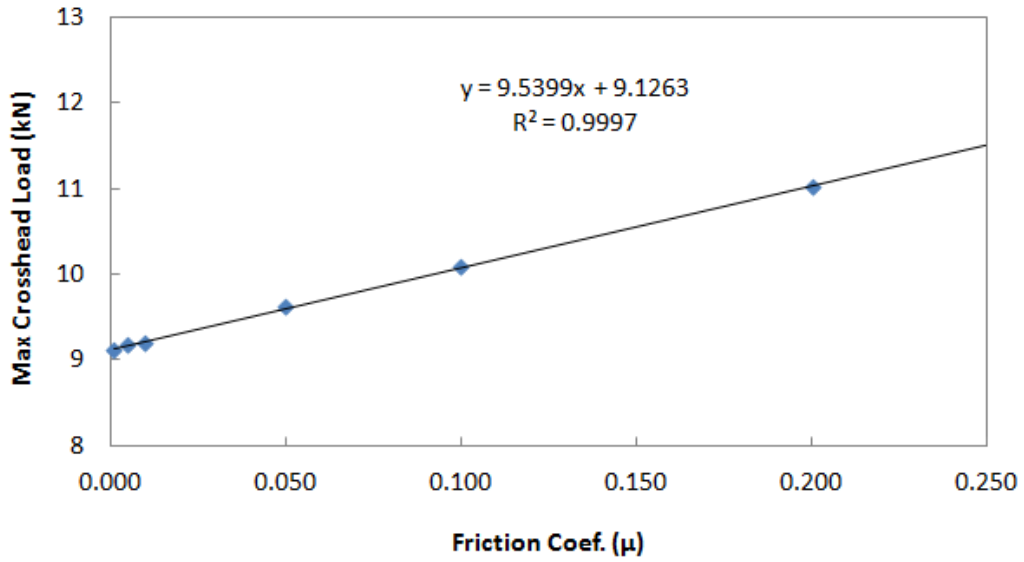

Figure 4.10: The effect of the coefficient of friction in the RHTT FEA model on the maximum crosshead force.

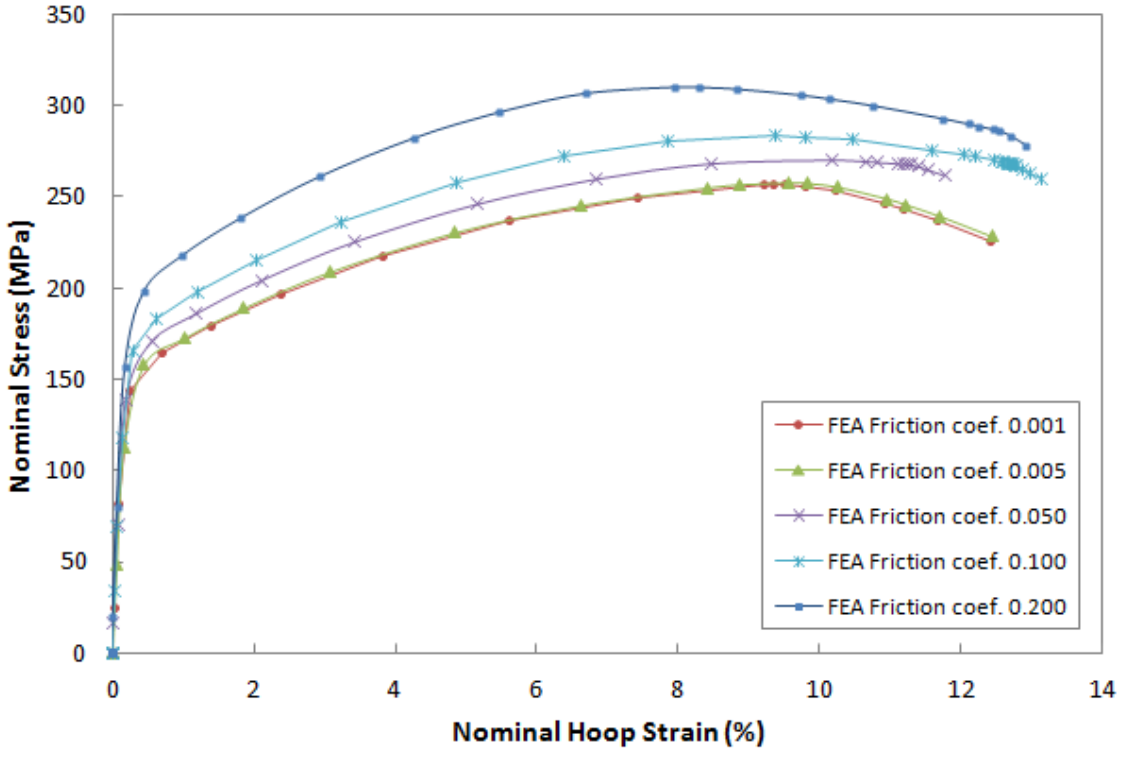

Figure 4.11: The effect of friction on the stress-strain curve for the RHTT FEA model.

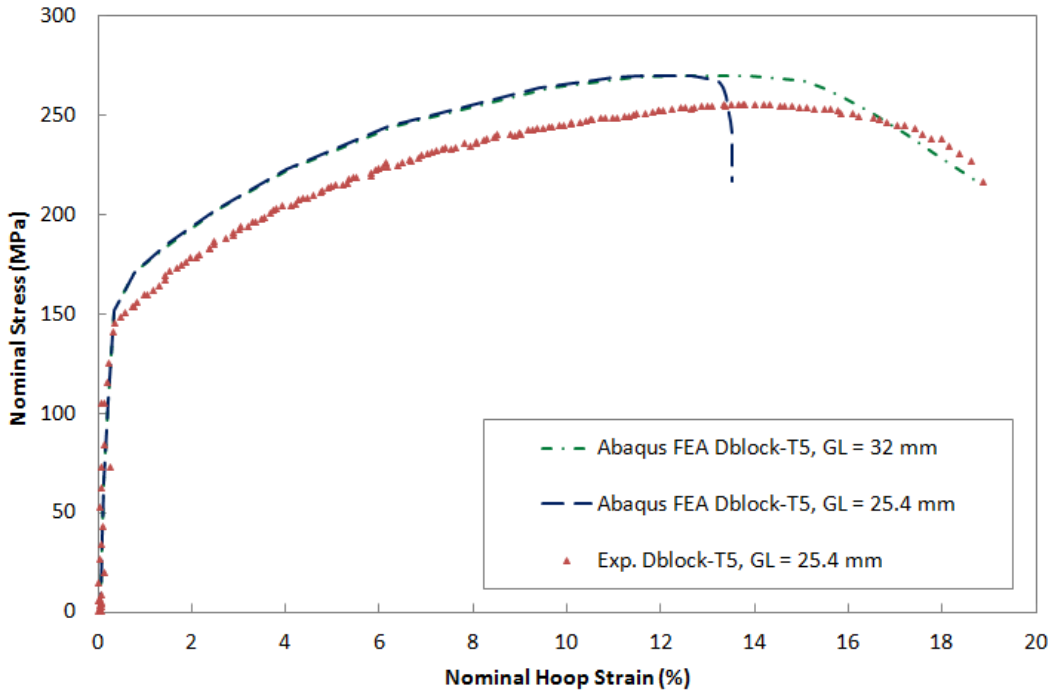

Figure 4.12: The engineering stress-strain curve of RHTT FEA compared to the experimental Dblock-T5 test specimen.

The crosshead force for the DBlock-T5 experiment was 9.10 kN, and the FEA model predicts 9.56 kN. In this case, it is not possible to calculate the friction with the numerical FEA model using the axial material definition. The comparison in Chapter 3, Figure 3.18 already shows that the material is slightly weaker in the hoop direction; however the crosshead force remains inexplicably large. In six RHTT tests, the average peak crosshead force was 9.59 kN +- 0.27 kN. The disagreement in the FEA model response (both the strain response as well as the crosshead force) demonstrates the need for a new material curve and true-stress plastic strain extrapolation. This material model should be based on the original test data from the RHTT in Chapter 3. This FEA model can be used in the future to refine the extrapolation of the plastic curve after strain localization in the experiment.

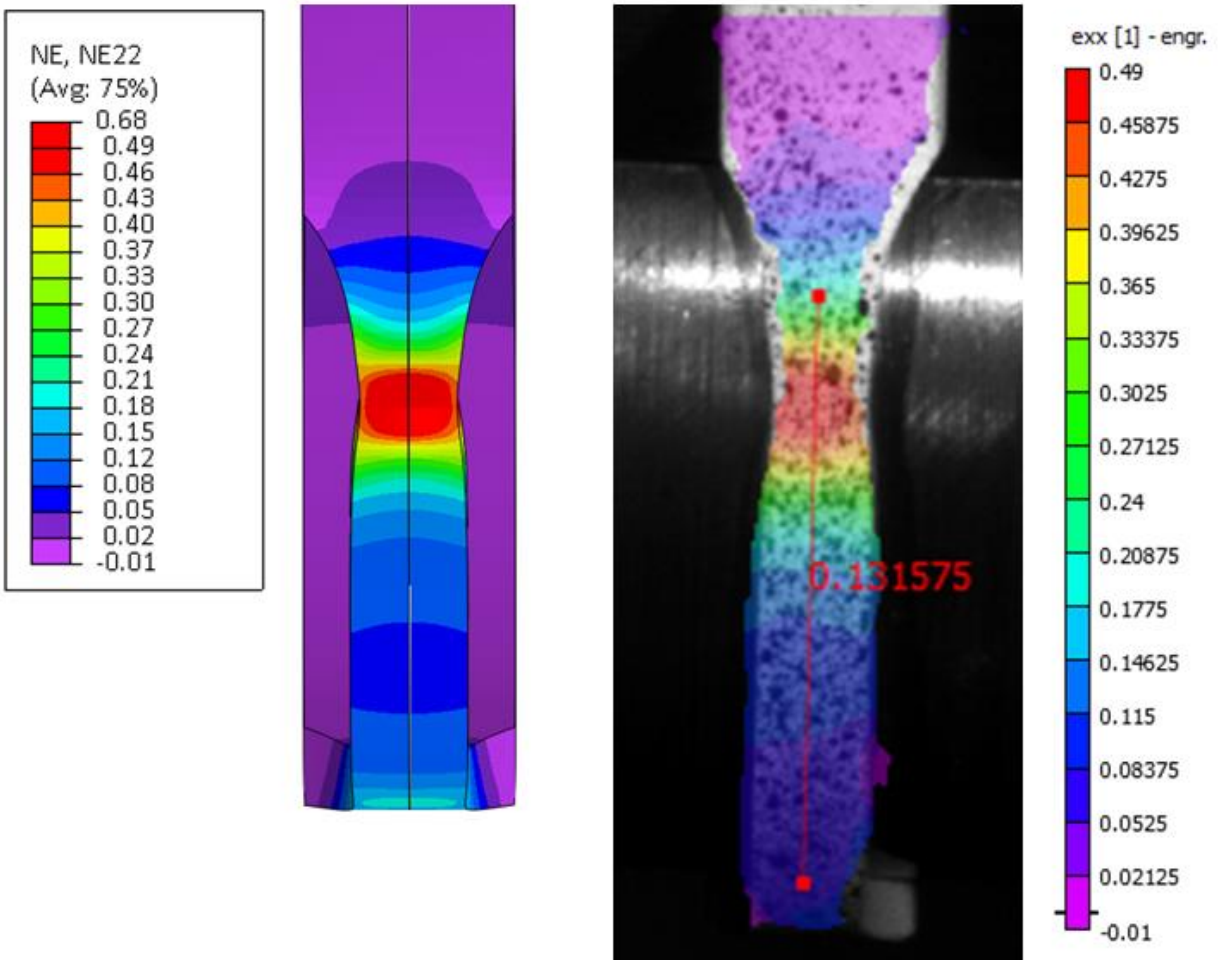

Figure 4.13: An example of the FEA nominal hoop strain contours for Dblock-T5.

Despite the differences in the stress-strain response of the gage length measurement, the necking phenomenon is fully captured and the contours of nominal strain show reasonable agreement at 13.15% nominal hoop strain. This is illustrated in Figure 4.13 This indicates the failure behavior of the model is working well. This model also demonstrates the sensitivity of the specimen formability to an accurate material curve - and suggests that despite the similarity between the axial tension and RHTT curves, the differences are significant enough to warrant a separate material plasticity curve (or an anisotropic material model).

4.5 2D (Plane-Strain) Simulation of Tube Hydroforming

The Abaqus material models for the axial and circumferential properties of the tube can be used for simulating the THF experiments performed with the device described in this thesis. The first hydroforming FEA model is a 2D plane-strain model, i.e., one that considers only the hoop-radial deformation of the tube and assumes that the axial strain is zero (or uniformly prescribed). This model provides an initial estimate of the required forming pressure and formed specimen dimensions of the actual experiment. The plane-strain model is also conservative, since the tube ends will contract towards the forming die despite the friction from the seal surfaces.

An Abaqus/Explicit model of the complete 2D cross section was developed. Since each radius on the forming die is unique, the full forming die cross section will be used and no symmetry will be implemented. The forming die is modeled as a rigid analytical surface and is fixed (0 DOF). Each radius is modeled with the dimensions of the device shown in Figure 4.14. The die-span is 63.50 mm (2.5 in). The tube is modeled with uniform wall thickness, 3 mm (0.118 in) thick comprised of 6 elements through the thickness. The entire tube is meshed with 2136 CPE4R linear reduced integration plane-strain quadrilateral elements.

The coefficient of friction is estimated as 0.2, which was calibrated from similar hydroforming experiments on Al-6260-T4 tubes at the University of Texas at Austin [22]. There is surface-to-surface contact between the outer surface elements of the tube (slave) and the analytical die surface (master). The normal direction contact over-closure was handled using the hard contact algorithm. Separation after contact must be allowed so that

the elements in the necking region can deform freely.

Using a full 2D cross section requires some unique boundary conditions to prevent rigid body movement of the tube. Unlike a quarter cross section model which has symmetry conditions on the X and Y planes, the full cross section must be restrained to prevent movement before contact with the die surfaces. Without restraint, numerical imbalances in the contact forces can cause movement of the cross section and problems with simulation convergence. As a result, a special step is used with boundary conditions that force the tube to expand radially. These conditions are shown in Figure 4.14

The tube is loaded with a uniform pressure load increased to 690 bar (10 ksi) over the total simulation time. The first simulation step includes a boundary condition to prevent displacement in X on a radial ray of nodes along the Y axis (Ux=0) and a second boundary condition to prevent displacement in Y on a radial ray of nodes along the X axis (Uy=0). This first simulation step lasts for 0.11 until the tube comes into contact with the die. These two boundary conditions are suspended for the second simulation step after the tube comes into contact with the die. Necking occurs before the tube has expanded to any of the die corner radii. Thinning of the tube wall occurs in the freely deforming region of the tube, immediate to the contact with the die surfaces. Eventually localized necking is seen to occur simultaneously in multiple regions. This is illustrated in Figure 4.15. The 2D model is simple and executes very fast, so it can be used for preliminary part and die design. However, the fact that it cannot capture the axial straining requires a fully 3D model for detailed deformation and failure analysis, and for detailed die design.

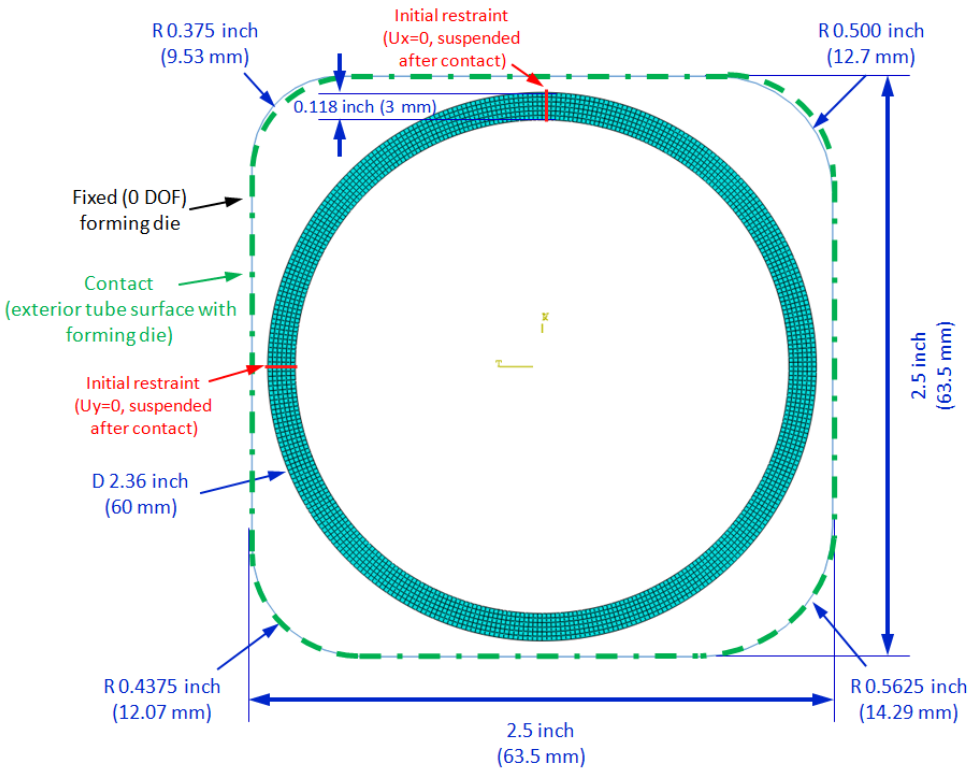

Figure 4.14: Dimensions and mesh for the 2D plane-strain model.

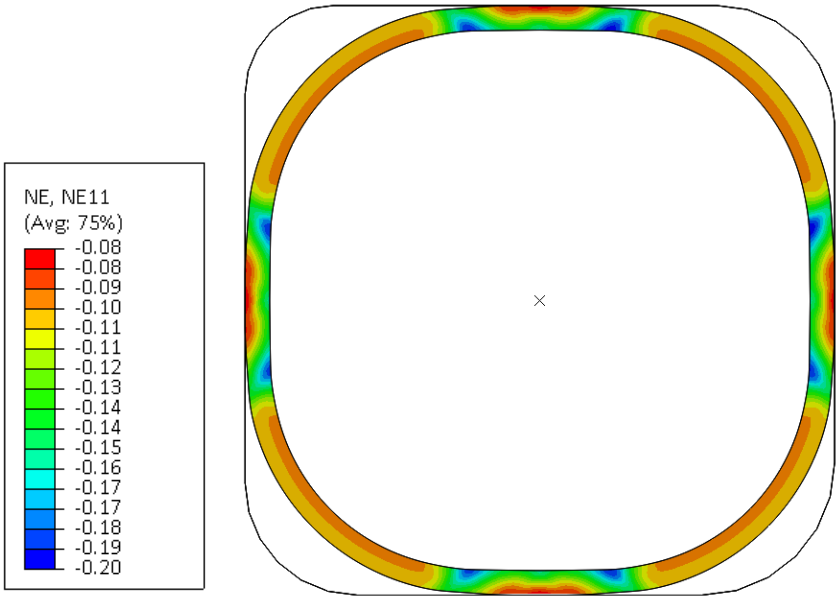

Figure 4.15: Through-thickness nominal strain for the 2D plane-strain model. The pressure is 398 bar (5.77 ksi).

4.6 3D Simulation of Tube Hydroforming

A 3D Abaqus FEA model of the hydroforming process for the Al-6061-T4 tubes was developed with Abaqus/Explicit. Symmetry can always be used at the mid-span cross section of the tube to reduce computational expense. The 2D simulations show that the tube does not rotate about its axis after contact with the asymmetric die wall. Furthermore, it indicates that localization sets in before any die corner has been filled. As a result, it is possible to utilize symmetry and model the smallest corner of the forming die, resulting in a 1/8 model. The forming die and seals can be modeled as analytical rigid surfaces. Contact is defined between the outer tube surface and the seals/forming die surfaces (Figure 4.16).

This model also has some unique elements for the hydroforming process related to the loading of the tube. The table-top hydroforming device will be run under volume control (as opposed to pressure control). The pump will introduce fluid incrementally regardless of the pressure within the tube. Additionally, available hydroforming pressure curves [1] show that the forming pressure reaches a maximum pressure peak and then decreases. This decrease is easy to understand in the case of a rupture of the tube wall, which allows the fluid to escape. The decrease in pressure can also occur once the tube reaches plastic instability (i.e. once the tube wall thins to the point that it is unable to hold the load without continuously expanding). If the point of plastic instability is reached anywhere in the tube wall, the specimen is likely to fail unless it makes contact with the die surface. Interestingly, when the tube wall contacts the die surface, it stabilizes the initial region of contact but causes localization to develop in the immediate vicinity of the tube wall not in contact with the die. The region near the start of the corner of each radius is noticeably thinner than the rest of the tube wall in these simulations.

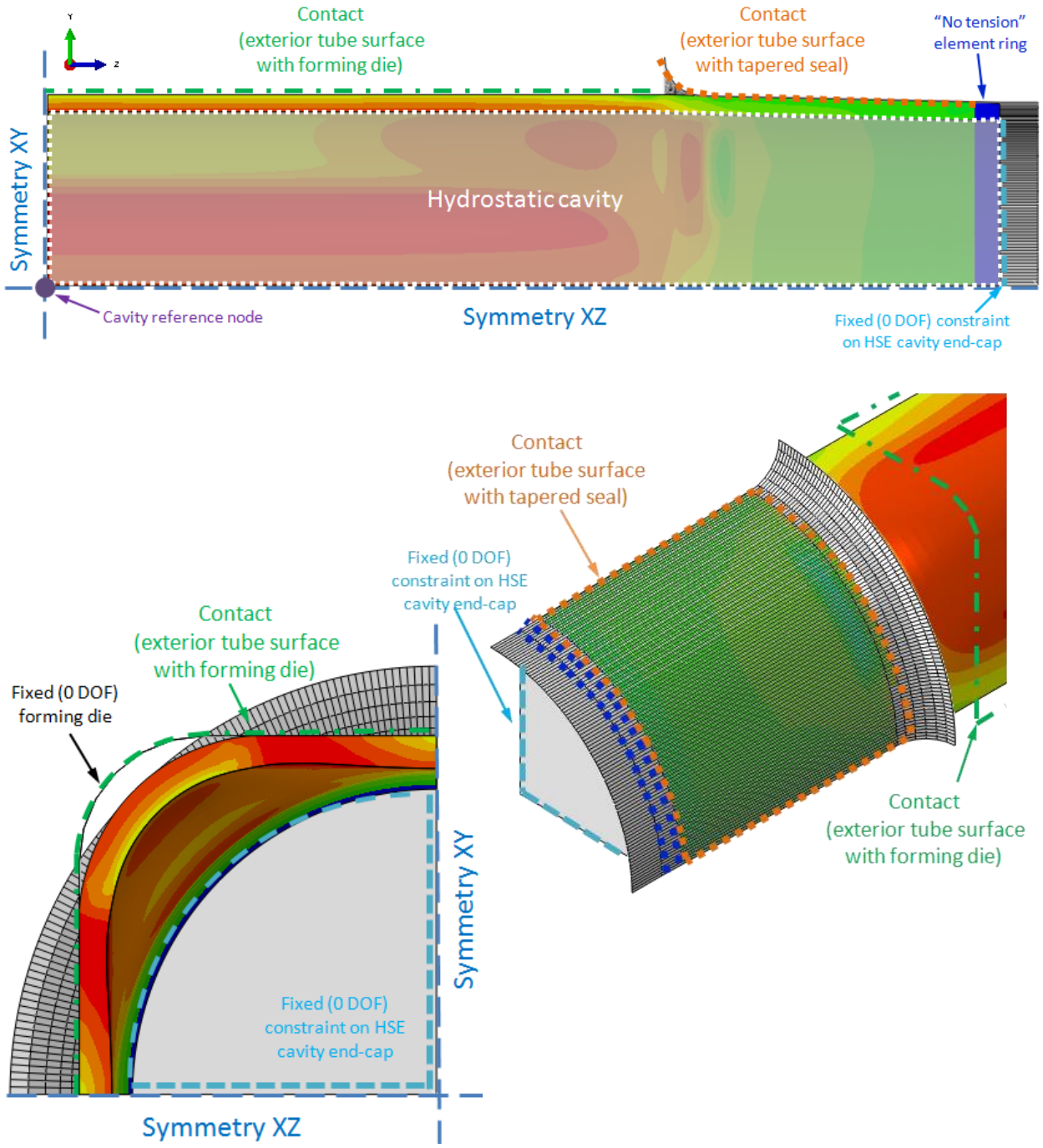

Figure 4.16: The boundary conditions for 1/8 THF FEA model.

Due to the risk of reaching the point of plastic instability before the specimen fills the corners of the die, the simulation must also be run with volume control. Instead of using a pressure load as a boundary condition on the internal surface of the tube cross-section, a cavity representing the internal fluid volume will be defined. This cavity is defined using a feature in Abaqus known as “hydrostatic elements” (HSE), and the properties of the cavity (volume or pressure) can be controlled using a reference node. This allows the cavity volume to be linearly increased with each time step, and the pressure response of the cavity drives the loading along the tube interface. There are some considerations when using hydrostatic elements:

1. Hydrostatic elements must share the same nodes as the solid surfaces they interact with.

2. A reference node must be included inside the cavity defined by the hydrostatic elements. This node defines the loading properties of the fluid cavity.

3. The reference node must lie on the planes of symmetry, if present.

The full procedure for creating the hydrostatic elements is provided in Appendix J. In 3D FEA models, the cavity elements are specialized F3D4 4-node quadrilateral shell elements. The fluid density is defined as 1000 kg/m^3 (0.036 lbf/in^3) for water.

The Abaqus CAE editor does not yet support the hydrostatic elements in the user interface; however the functionality is fully implemented in the Abaqus solver. The HSE must be manually added to the Abaqus Input file (*.*inp*). With nodes and elements in the thousands, this is a difficult task to define manually. To define the cavity for Abaqus 6.11,

a MATLAB program was created to find the HSE nodes in the Abaqus input file, create the hydrostatic elements to define the cavity, and add the necessary boundary conditions for volume control. There are two programs provided in Appendix K. The subroutine, *ExtractSection.m*, is used to find all nodes on the interior cavity surface by searching for the requested named set. The script *HSE_Generator_Envelope_FordAl6061.m* replaces the material with the appropriate material model, defines the HSE cavity and reference node, sets the volume input rate, and defines the history output for the regions of interest.

The cavity must be sealed; therefore the ends of the tube are a difficult area to implement a boundary condition that constrains the cavity elements from expanding without interfering with the ends of the tube's material elements. To solve this, the cavity end cap is fixed with 0 DOF. To accommodate axial contraction of the tube ends, the first ring of material elements are defined with a special material condition that allows element compression but not tension. This ring of elements resists being crushed by the compressive load of the HSE, but allows the tube ends to contract by the un-resisted stretching the elements. This region of "no tension" is labeled in Figure 4.16. It should be noted that the model omits the interior urethane seal within the interior of the cavity (see Chapter 2). This seal would be in contact with the tube's internal surface in the experiment, but is not relevant to the simulation. The added complexity of the interior seal is neglected from this model - its presence in the experiment is believed to add some resistance to any induced axial contraction of the tube ends.

In order to establish confidence in the finite element simulations, the mesh was refined until the solution converged to calculate the same change in thickness at select points in

the tube wall. The mesh is shown in Figure 4.17 and the mesh parameters are outlined in Table 4.1. In previous convergence studies, the onset of localized necking was primarily dependent on the number of circumferential elements - therefore, for this study, only the circumferential elements will be varied. This study uses a 1018 steel material curve and a 2.25 inch (57.15 mm) diameter, 0.080 inch (2 mm) wall thickness tube. The geometry and material was selected from a preliminary evaluation of available tubes that could be successfully formed within the working pressures of the laboratory hydroforming machine. This case provides a good basis for a convergence study that would be representative of the simulation set. The contours of through-thickness engineering strain are shown in Figure 4.18.

Table 4.1: The number of elements for the tube in the FEA model for a quarter 3D.

	Coarse	Selected	Medium	Fine
Circumference elements	60	100	120	200
Thickness elements	5	5	5	5
Length elements	80	80	80	80
Total elements	24,000	40,000	48,000	80,000

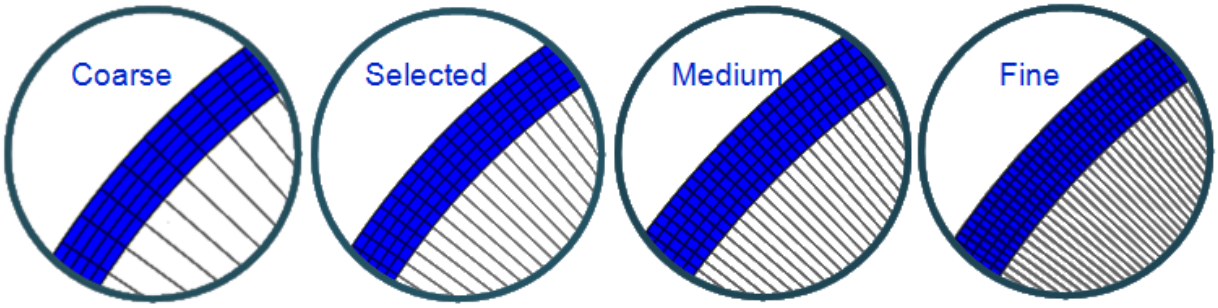

Figure 4.17: Examples of the mesh density for the quarter FEA model of the tube.

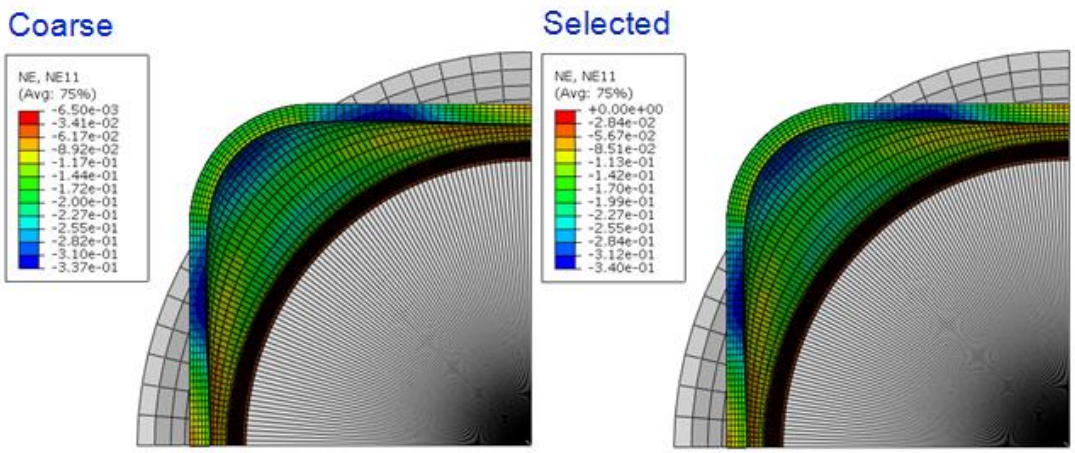
Coarse
NE, NE11
(Avg: 75%)
-6.50e-03
-3.41e-02
-6.17e-02
-8.92e-02
-1.17e-01
-1.44e-01
-1.72e-01
-2.00e-01
-2.27e-01
-2.55e-01
-2.82e-01
-3.10e-01
-3.37e-01
Selected
NE, NE11
(Avg: 75%)
+0.00e+00
-2.84e-02
-5.67e-02
-8.51e-02
-1.13e-01
-1.42e-01
-1.70e-01
-1.99e-01
-2.27e-01
-2.55e-01
-2.84e-01
-3.12e-01
-3.40e-01

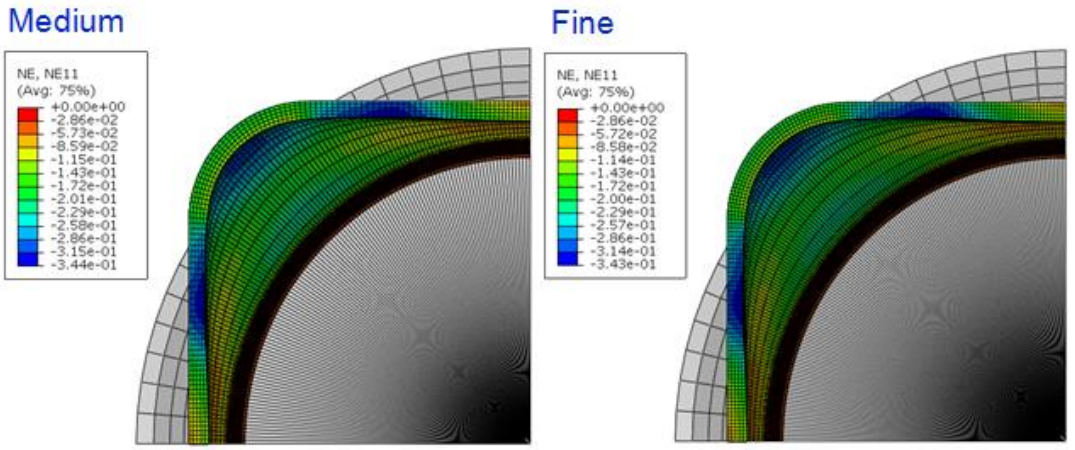
Medium
NE, NE11
(Avg: 75%)
+0.00e+00
-2.86e-02
-5.73e-02
-8.59e-02
-1.15e-01
-1.43e-01
-1.72e-01
-2.01e-01
-2.29e-01
-2.58e-01
-2.86e-01
-3.15e-01
-3.44e-01
Fine
NE, NE11
(Avg: 75%)
+0.00e+00
-2.86e-02
-5.72e-02
-8.58e-02
-1.14e-01
-1.43e-01
-1.72e-01
-2.00e-01
-2.29e-01
-2.57e-01
-2.86e-01
-3.14e-01
-3.43e-01

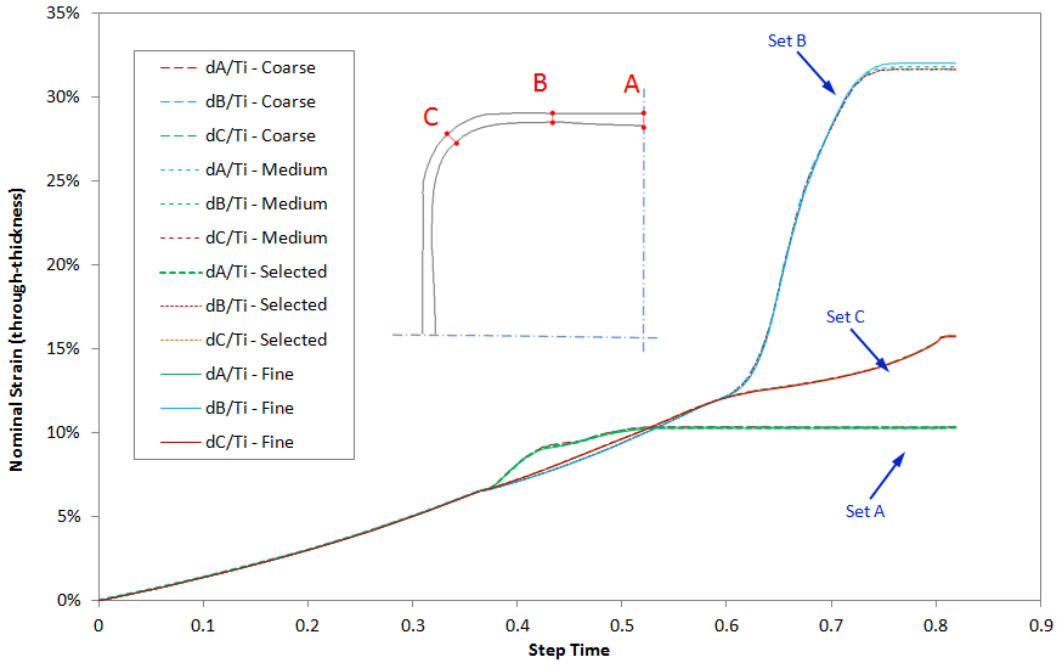
35%
30%
25%
20%
15%
10%
5%
0%
Nominal Strain (through-thickness)
0
0.1
0.2
0.3
0.4
0.5
0.6
0.7
0.8
0.9
Step Time
dA/Ti - Coarse
dB/Ti - Coarse
dC/Ti - Coarse
dA/Ti - Medium
dB/Ti - Medium
dC/Ti - Medium
dA/Ti - Selected
dB/Ti - Selected
dC/Ti - Selected
dA/Ti - Fine
dB/Ti - Fine
dC/Ti - Fine
A
B
C
Set A
Set B
Set C

Figure 4.18: Mesh convergence via monitoring of wall thinning (A - C).

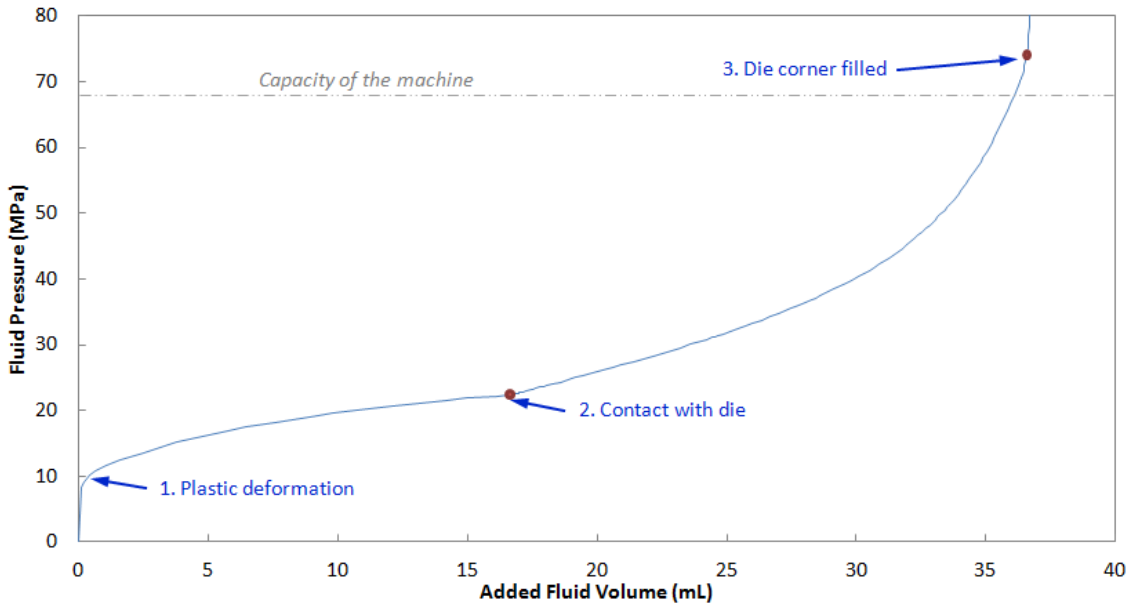

Figure 4.19: Pressure response of the FEA model in the mesh convergence study.

The pressure response from this model is also of interest. Figure 4.19 shows the resulting pressure from the fine mesh. It should be noted that there is no discernible difference in the pressure-volume curve for the difference meshes, so these curves cannot be used to monitor convergence in future mesh studies. Between points 1-2, the mid-span cross section of the tube is expanding freely. After making contact with the forming die wall at point 2, the expanding tube begins a corner filling process until the tube material is fully in contact at point 3. After point 3, the forming primarily occurs at the unconstrained transition region between the forming die and the end seal.

At the machine's pressure limit (10,000 psi / 690 bar), the corner is nominally filled with around 0.008 inch (0.2 mm) distance between the tube and the die corner at the mid-span cross-section. The FEA model also shows that the first point of contact with the tube and the die is at the mid-span, while the corner is first filled near the edge of the forming

die. This occurs at 10,600 psi (731 bar) and is illustrated in Figure 4.20. The values of contact pressure (CPRESS) in Figure 4.20 appear extraordinary low and should be probed in more detail in the future. For now, CPRESS is used as a visual confirmation of corner filling only.

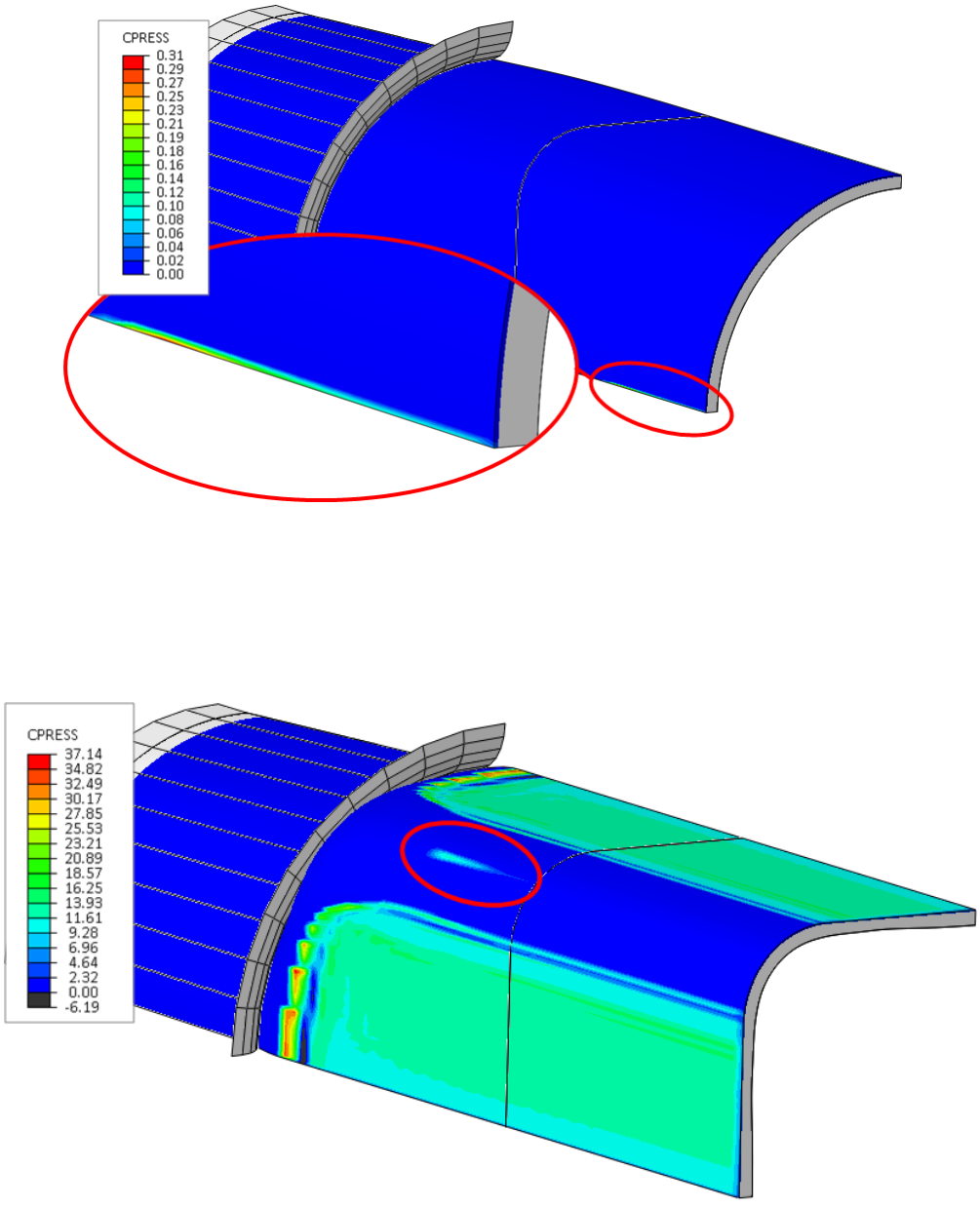

Figure 4.20: The contact pressure (in psi) of the initial contact of the tube and die

(upper image) and the initial contact of the die corner radius (lower image).

The next set of simulations was developed to determine the possible thickness for Al-6061-T4 tubes that could be formed by the machine using 690 bar (10,000 psi) input pressure. The example specifically explores the applicability of 57.15 mm (2.25 in) OD tubes. The results presented in Figure 4.21 demonstrate the effect of thickness on the tube formability for Al-6061-T4 material.

If the tube material is too thin, the tube material cannot be fully formed without localized thinning and subsequent failure. The thinning is similar to necking and causes the time-increments to become extremely small as the material rapidly fails. Many times, this causes the simulation to abort due to exceeding the minimum time-increment limit (Figure 4.21 (a), Thickness = 0.89mm (0.035 in)). If the tube material is too thick, the required forming pressure will be greater than 690 bar (10,000 psi) and the tube will only be partially formed (Figure 4.19 (c), Thickness = 2.41 mm (0.095 in) and 3.2 mm (0.125 in)).

The Al-6061-T4 tubes provided by Ford are 60 mm OD and 3 mm thick, so they will not be able to fill the corners of the die without exceeding the working pressure limit desired for operating the table-top tube hydroforming machine. There are two potential solutions to this problem: reduce the die span or anneal the Al-6061-T4 tubes back to a softer Al-6061-O condition.

Thickness = 0.035 inch (0.89 mm) / Pressure = 2787 psi (19.2 MPa) / NE11 = -39.3%
Simulation failed because time increment required is less than the minimum specified (10e-7).

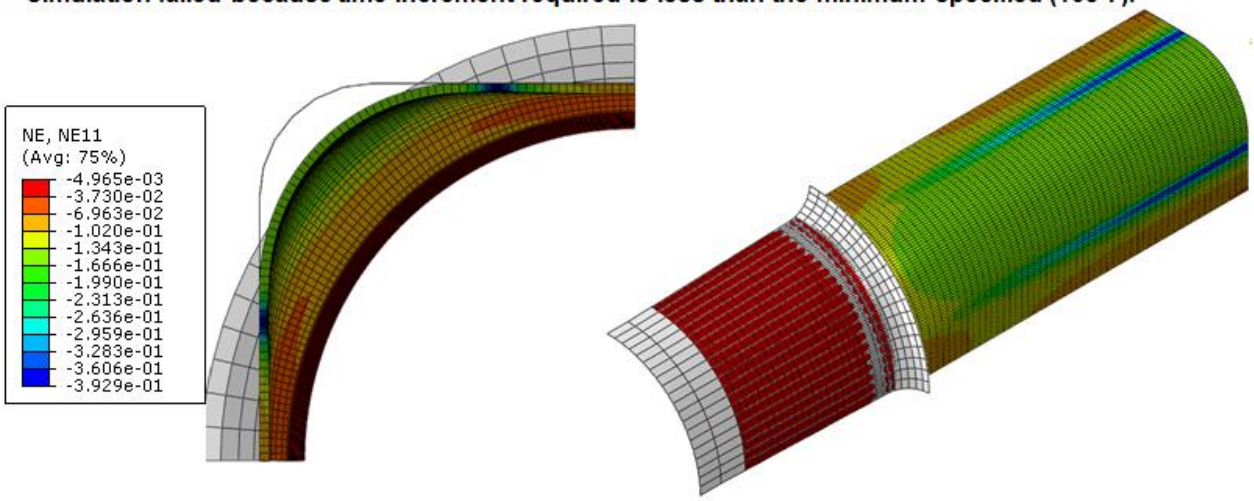

(a)

Thickness = 0.065 inch (1.65 mm) / Pressure = 10000 psi (68.3 MPa) / NE11 = -35.16%
Simulation completed successfully, just filling the corner at 10000 psi (68.3 MPa) .

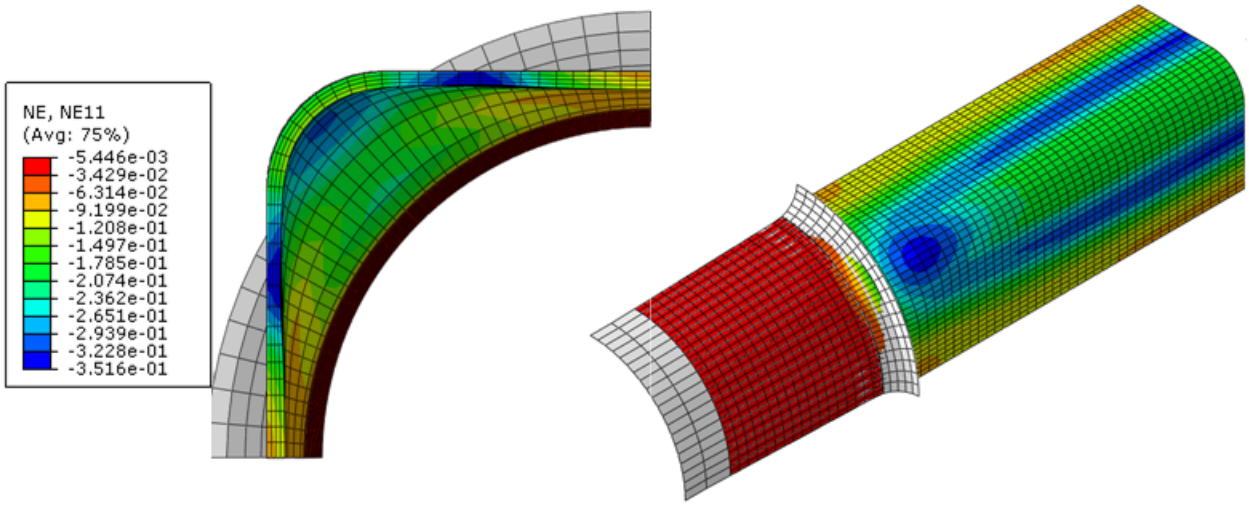

(b)

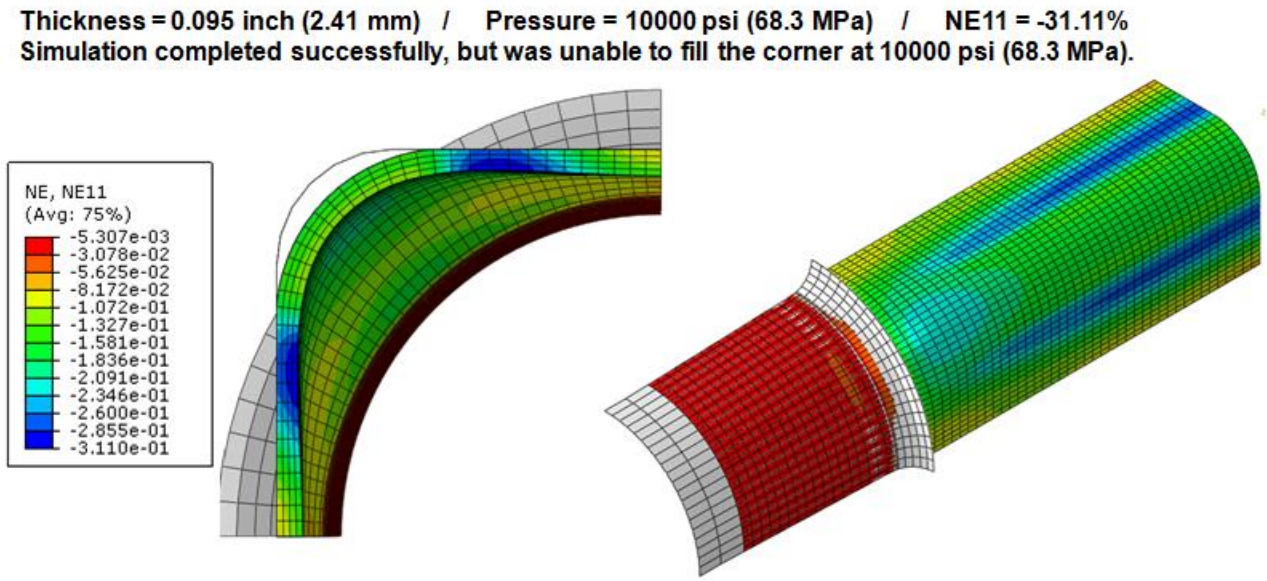

(c)

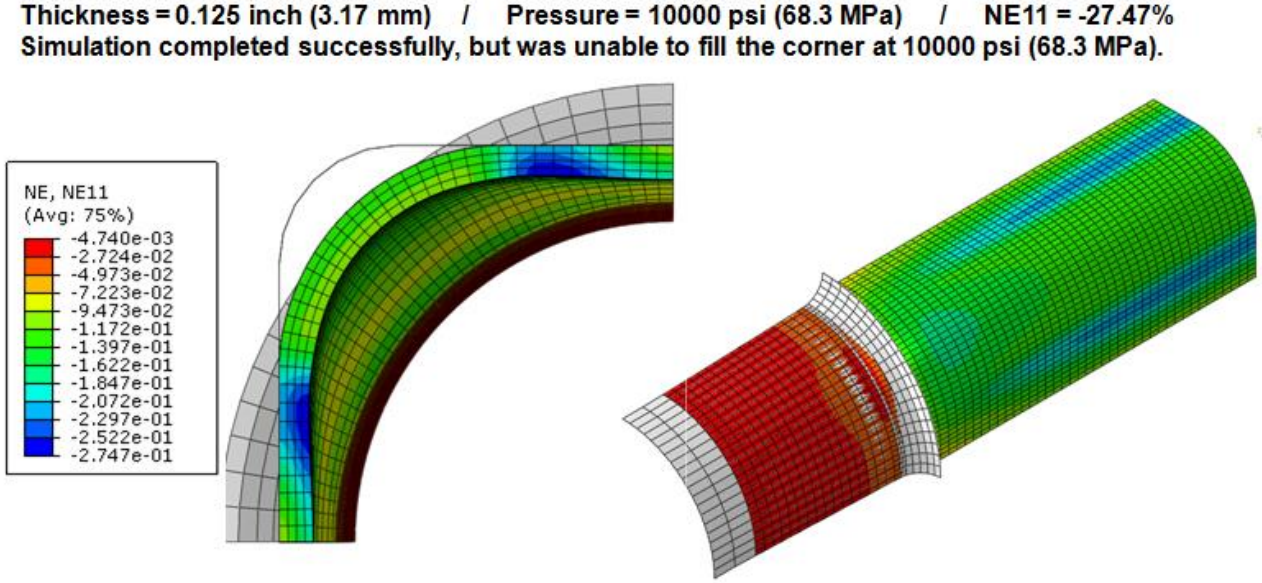

(d)

Figure 4.21: Numerical simulations of 60 mm (2.362 in) OD tubes of varying wall thickness: (a) 0.89 mm (0.035 inch), (b) 2.65 mm (0.065 inch), (c) 2.41 mm (0.095 inch) and (d) 3.17 mm (0.125 inch).

CHAPTER 5

SUMMARY AND CONCLUSIONS

5.1 The Hydroforming Process

Tube hydroforming is an increasingly popular manufacturing process that utilizes fluid pressure and forming dies to expand sections of tubes into specific parts. The tube hydroforming process is used to produce a variety of parts from specialized pipe fittings to automotive. It is a viable alternative for parts with hollow cross-sections that would otherwise be cast in a single piece or assembled from stamped/welded assemblies of smaller components. Additionally, hydroformed parts benefit from reduced tooling wear and improved surface finishes compared to stamped parts and castings.

Despite humble beginnings from serpentine boiler tubes and pipe-fitting manufacturing patents dating back to the first decades of the 1900's, tube hydroforming is increasingly popular with the automotive industry. Many automotive companies have successfully used hydroformed parts to replace multiple-part assemblies and reduce the weight of their vehicles. Examples include the aluminum chassis of the Chevrolet Corvette Z06, the factory roll bar in the Porsche Boxster, door frame members in the Ford F150, and the rear-axel subframe for the BMW 7-series.

As a result of its rising popularity, advances in tube hydroforming are of interest to researchers and manufacturers alike. The development of a small laboratory hydroforming machine allows researchers to investigate the process in detail and improve the understanding and simulation of the forming process.

5.2 The UNH Hydroforming Machine

The first phase of this project required the finalization of the original design concept into a final form suitable for manufacture and use at the University of New Hampshire. The original design required several changes including (but not limited to): an increase in the number, size, and strength of the vertical bolts securing the top plate and base plate; reduction in upper plate thickness to accommodate vertical bolts; determine the minimum radius of the forming die; calculate the preload force and select the sidewall material to prevent separation of the dies; FEA of the end-plates and T-blocks for suitable safety factors while including the effects of preloaded counterbored fasteners; FEA analysis of the outer seal and end block housing to ensure sufficient strength for the 60.3 mm Al-6062-T4 tubes; and adapter design for connection to standard high-pressure hydraulic fittings. After many changes, the final design drawings for machining the device's parts were drafted.

All the parts were machined in-house at the CEPS Machining Center in Kingsbury Hall. CNC tool paths were developed and executed on the Fryer MC-10 for most parts, while the rest were produced on a traditional lathe. The parts were sent out for heat-treatments and powder coating and finally assembled into the full machine in the Fall of 2012. The machine has undergone successful forming tests on Al-6061 tubes at pressures up 3,000 psi (207 bar) using a hydraulic hand-pump.

Although time prevented the execution of a series of hydroforming experiments, the next step in the research should be to perform the forming experiments with the current 2.5 inch die span. In the future, the machine can be integrated with a high-pressure hydraulic booster and a standard hydraulic control system, which will be helpful for recording the

pressure and volume of the fluid cavity.

5.3 Tube Formability

This thesis has largely focused on evaluating a potential candidate tube for hydroforming with the experimental device. These tubes, provided by Ford Motor Company, are 60.3 mm/2.37 inch OD, 3 mm/0.118 inch thick Al-6061-T4 tubes. They are a suitable size for use in the UNH hydroforming machine. These tubes are formed by an extrusion process through a spider die that leaves 3 equally spaced cold welds in the tube wall.

The tube material was evaluated using three tests: axial tension (specimen along the length of the tube), ring hoop tension (circumferential specimen), and tube flaring (tubular specimen). Additionally, a rate dependence test was performed on the axial specimen and the elastic properties were also derived using a strain gage.

The results of the axial tension tests (measured with an extensometer) included specimens taken from the welded regions of the tube, as well as several specimens from the base material region. Due to failures occurring outside the gage length on many welded specimens, a small notch was introduced to encourage localization in the center of the gage length. This failure near the radius at the top of the gage is most likely due to machining errors with the tensile specimens, although no significant reductions in width were found during hand-inspection with dial calipers. While both specimens achieved a nominal engineering strain of 15% before localization, the failure behavior of the welded material occurred more quickly.

The RHTT is a unique test that was developed to evaluate the hoop direction material properties. The experimental setup positions a reduced section (gage length) on a ring specimen about a circular mandrel of similar diameter. This prevents bending at the gage region and loads the specimen in tension. Since the gage length is wrapped about a cylinder, a traditional extensometer is difficult to mount. Alternatively, the strain field was recorded with stereo-cameras and analyzed using Digital Image Correlation with Vic-3D. The gage length points were tracked from the engineering hoop strain field to create a virtual extensometer to calculate the nominal hoop strain for the experiment. The location of strain localization and failure occurred near the radius at the bottom of the gage length - this is attributed to the additional force due to friction with the mandrel as this region stretches. The post-processed results showed comparable stress-strain curves to the previous uniaxial tension tests, indicating (at least initially) that the axial tension tests were characteristic of the hoop direction as well.

The RHTT experiment is worthy of further exploration. To better understand the test, the influence of the contact pressure/friction with the mandrel on the distribution of stress within the gage length should be examined. Additionally, a circle grid would aid in measuring the non-uniformity of the strains along the gage length outside of the failure zone.

Short tubular specimens were also tested via expansion flaring with a 60° conical punch. The strains were recorded using stereo cameras with 3D DIC analysis as well using an etch grid of circles. One end of the tube was flared until failure via localized thinning and rupture of the tube wall. The load curve from the tests match the characteristics of typical

flaring load curves, exhibiting several distinct regions as the region of contact and loading on the specimen advance. The major engineering strains (hoop direction) from the circle grid were compared with the DIC strain field, which serve to verify the 3D DIC analysis and show good agreement. The DIC analysis shows that the hoop strain develops uniformly until before 20%, which agrees well with the axial tension tests and ring hoop tension tests.

The flaring test and resulting failure envelope may prove useful in future comparisons to CGA on a hydroformed tubular specimen.

5.4 Numerical Simulations

The enclosed nature of the tube during hydroforming experiments makes it difficult to capture the evolution of the forming process. Circle grid analysis and measurements of the formed tube dimensions can provide insight of the strains within the material at the final stage, but numerical simulations allow researchers to calibrate models and track the evolution of the forming process over time. Several finite element models were developed to evaluate potential tube material candidates but also to compliment a future set of hydroforming experiments.

The material model is universal to all models and two material models were developed based on the axial tension tests (for the base material and weld region respectively). The development of these material models was aided by MATLAB scripts to smooth, spline, and extrapolate the raw test data into a true stress-plastic strain curve required for Abaqus, the FEA package used for these models.

In order to calibrate the extrapolation to high plastic strains, the axial tension test was

recreated with an FEA model. The resulting engineering stress-strain curve matched very well with the original test data for both many different tests. The specimen thickness and material was replicated for several tests presented in Chapter 4 and both the base material and weld material were well characterized by the final extrapolations.

The RHTT was also recreated using an Abaqus FEA model, however the same material curve derived from the axial data was used. The failure in the model occurred just on the edge of the original gage length used in the experiment, and as a result there was some difficultly matching up the engineering hoop strain results with the experimental data. Additionally, the crosshead load in the simulation was higher than the recreated experiment, even with a low coefficient of friction. These results indicate that the RHTT model is sensitive to the difference between the axial material and hoop material response. Despite the differences in the nominal stress-strain curves, the failure phenomenon was captured in the FEA model and the contours of engineering hoop strain were comparable to the DIC images. In the future, the model should be used in along with the RHTT raw data to create a new true stress-plastic strain extrapolation for Abaqus in order to improve the response of the numerical models.

The first FEA model of the tube hydroforming process was a 2D plane-strain model (of the full cross section at the mid-span of the die), which simulated zero prescribed displacement of the tube ends. The results showed that localized thinning occurred in multiple regions of the tube wall before any section of the tube material reached the die radius. Although this is a simple model, it indicates that the tubes will not be able to be successfully formed to the final die dimensions before failure. This model is useful in the

future because it is extremely fast in evaluating potential tube candidates.

The 3D FEA model included the ends of the tubes constrained in the outer seals. This model features a simulated fluid cavity created by hydrostatic elements that allow the pressure to be applied as a dynamic boundary condition based on a controlled volume approach. This allows the pressure of the cavity to decrease (while the volume continues to increase), which will happen in certain cases. The 3D model mesh was calibrated using a parametric study that varied the circumferential elements while monitoring the change in the wall thickness at particular locations in the mid-span. The results showed that a 1/8 model mesh of 100 circumferential elements, 5 thickness elements, and 80 length elements was sufficient to see convergence of the results by monitoring the thickness at 3 critical locations. The same 3D model was also used to perform a thickness study on 60 mm (2.36 mm) tubes of varying thicknesses. The results showed that the ideal thickness for a fully formed tube is around 0.065 inch (1.65 mm) for the current die setup, and thicker tubes (such as the candidates explored in Chapter 3) will not be able to be completely formed within the pressure capacity of the machine. In the future, this model can be correlated back to actual hydroforming experiments using the UNH tube hydroforming machine.

REFERENCES

[1] Koc M. *Hydroforming for Advanced Manufacturing*. Cambridge, England: Woodhead Publishing; 2008.

[2] Singh H. *Fundamentals of Hydroforming*. Dearborn, Michigan: Society of Manufacturing Engineers; 2003.

[3] Kocanda A. Sadlowska, H. “Automotive component development by means of hydroforming”. *Archives of Civil and Mechanical Engineerin*g 2008, Vol. 8, pp. 55-72.

[4] Gerard D. "Materials and processes in the Z06 Corvette". *Advanced Materials & Processes*, January 2008, pp. 30-33.

[5] Mortimer J. "BMW breaks new ground with hydroforming", *Assembly Automation* 2001, Vol. 21, pp. 317-320.

[6] Tschätsch H. *Metal Forming Practice: Processes – Machines – Tools*. New York, NY: Springer Publishing; 2006.

[7] Korkolis Y.P. Formability and hydroforming of anisotropic aluminum tubes. *PhD Dissertation*. University of Austin, Texas; 2009.

[8] Park K. “Apparatus for forming serpentine hollow bodies". *US Patent US731124A*, June 1903.

[9] Liddell J. "Method and apparatus for die shaping metal". *US Patent 1448457*, March 1923.

[10] Parker A. “Apparatus for making wrought metal T’s”. *US Patent 2027285*, October 1936.

[11] Gray J. “Apparatus for making wrought metal T’s”. *US Patent 2203868*, June 1940.

[12] Davis E. “Yield and fracture of medium-carbon steel under combined stress”. *Journal of Applied Mechanics*; March 1945.

[13] Sauer W., Gotera A., Robb F., Huang, P.. "Free bulge forming of tubes under internal pressure and axial compression". *Proceedings of the Sixth North American Metalworking Research Conference NAMRC*, 1978, pp. 228 - 235.

[14] Hosford W., Cadell, R. *Metal Forming - Mechanics and Metallurgy*. New York, NY: Cambridge University Press; 2011.

[15] Hosford, W. “On yield loci of anisotropic cubic metals”. *Proceedings of the 7th North American Metalworking Research Conference NAMRC*, Society of Manufacturing Engineers, Dearborn, MI, pp. 191-96. 1979.

[16] Karafillis, A., Boyce, M. “A general anisotropic yield criterion using bounds and a transformation weighting tensor”. *Journal of Mechanics and Physics of Solids,* Vol. 41, pp. 1859-1886. 1993.

[17] Barlat F., Brem J., et al. “Plane stress function for aluminum alloy sheets - part I: theory”. *International Journal of Plasticity*, Vol. 19, pp. 1297-1319. 2003.

[18] Korkolis Y.P, Kyriakides S. “Inflation and burst of anisotropic aluminum tubes for hydroforming applications”, *International Journal of Plasticity*, Vol. 24/3 pp. 509-543. 2008.

[19] Korkolis Y.P, Kyriakides S. “Inflation and burst of anisotropic aluminum tubes, part II: an advanced yield function including deformation-induced anisotropy”. *International Journal of Plasticity*, Vol. 24/9, pp. 1625-1637. 2008.

[20] Korkolis Y.P, Kyriakides S. “Path-dependent failure of inflated aluminum tubes”. *International Journal of Plasticity*, Vol. 25/11, 2059–2080. 2009.

[21] Korkolis Y.P, Kyriakides S. “Hydroforming of anisotropic aluminum tubes. Part I: experiments & analysis”. *International Journal of Mechanical Sciences* Vol. 53/2, pp. 75-82. 2011.

[22] Korkolis Y.P, Kyriakides S. “Hydroforming of anisotropic aluminum tubes. Part II: advanced constitutive models”, *International Journal of Mechanical Sciences*, Vol. 53/2, pp. 83-89. 2011.

[23] Manabe K, Fujita K, Tada K. “Experimental and numerical study on warm hydroforming for t-shape joint of AZ31 magnesium alloy”. *Journal of the Chinese Society of Mechanical Engineers*, Vol. 31/4, pp. 281-287. 2010.

[24] Mori K, Patwari, A, Maki S. Improvement of formability by oscillation of internal pressure in pulsating hydroforming of tube. *CIRP Annals – Manufacturing Technology*, Vol. 53/1, pp. 215-218. 2004.

[25] Rípodas F. “Manufacturing tubes for hydroforming applications.” *Tube & Pipe Technology*, May/June, pp. 114-119. 2003.

[26] ASTM Standard E8, "E8 Standard Test Methods of Tension Testing of Metallic Materials," *ASTM International*, West Conshohocken, PA, 2008.

[27] "Extrusion." Wikipedia. Wikimedia Foundation, n.d. Web. 03 Dec. 2016.

[28] *Metals Handbook Volume 1 Properties and Selection: Irons and Steels*. Metals Park, Ohio: American Society for Metals, 1978.

[29] "Aluminum 6061-T4; 6061-T451", ASM Aerospace Specification Metals, Inc. Web. Sep. 2011.

[30] Arsene S, Bai J. "A new approach to measuring transverse properties of structural tubing by a ring test", *Journal of Testing and Evaluation*, Vol. 24(6), pp. 386-391. 1996.

[31] Arsene S, Bai J. "A new approach to measuring transverse properties of structural tubing by a ring test – experimental investigation", *Journal of Testing and Evaluation* Vol. 26 pp. 26-30. 1998.

[32] Dick C.P, Korkolis Y.P. "Mechanics and full-field deformation study of the Ring Hoop Tension Test", *International Journal of Solids and Structures*, Vol. 51/18, pp. 3042-3057. 2014.

[33] Kyriakides S, Corona E. *Mechanics of Offshore Pipelines - Vol. I Buckling and Collapse*. Elsevier, 2007.

[34] Jang W, Kuk I. "Flare Test and Stress Analysis of Alloy 600/690 Tubes", *Journal of Korean Nuclear Society*, Vol. 29/2, pp. 138-147. 1997.

[35] Alves M, Almeida B, et al. "End forming of thin-walled tubes", *Journal of Materials Processing Technology*, Vol. 177, pp. 183-187. 2006.

[36] Fischer F, Rammerstorfer F, Daxner T, "Flaring – An Analytical Approach", *Intl. Journal of Mechanical Sciences*, Vol. 48, pp. 1246-1255. 2006.

[37] Fischer F, Daxner T, Rammerstorfer F. "Instability phenomena during the conical expansion of circular cylindrical shells", *Computer Methods in Applied Mechanics and Engineering*, Vol. 194, pp. 2592-2603. 2005.

[38] Graf A, Hosford W. "Effect of changing strain paths on forming limit diagrams of Al 2008-T4", *Metallurgical Transactions A*, Vol. 24, pp. 2503-2512. 1993.

[39] Abaqus 6.11 Documentation. Dassault Systemes/Simulia, 2010.

[40] Lee M-G, Korkolis Y.P, Kim J.H. "Recent developments in hydroforming technology", *Journal of Engineering Manufacture*, Vol. 229(4), pp. 572-596. 2015.

[41] Kronis M, Kubec V, Korkolis Y.P. “Hydroforming of extruded and fully-annealed 6061 aluminum tubes: experiments and analysis”, 12th NUMIFORM, Troyes, France, Jul. 4-7, 2016.

[42] Dick C, Korkolis Y.P. "Strength and ductility evaluation of cold-welded seams in aluminum tubes extruded through porthole dies", *Materials and Design*, Vol. 67, pp. 631-636. 2015.

[43] Dick C, Korkolis Y.P. "Anisotropy of thin-walled tubes by a new method of combined tension and shear loading", International Journal of Plasticity, Vol. 71, pp. 87-112. 2015.

APPENDIX A

TUBE HYDROFORMING MACHINE DRAWINGS

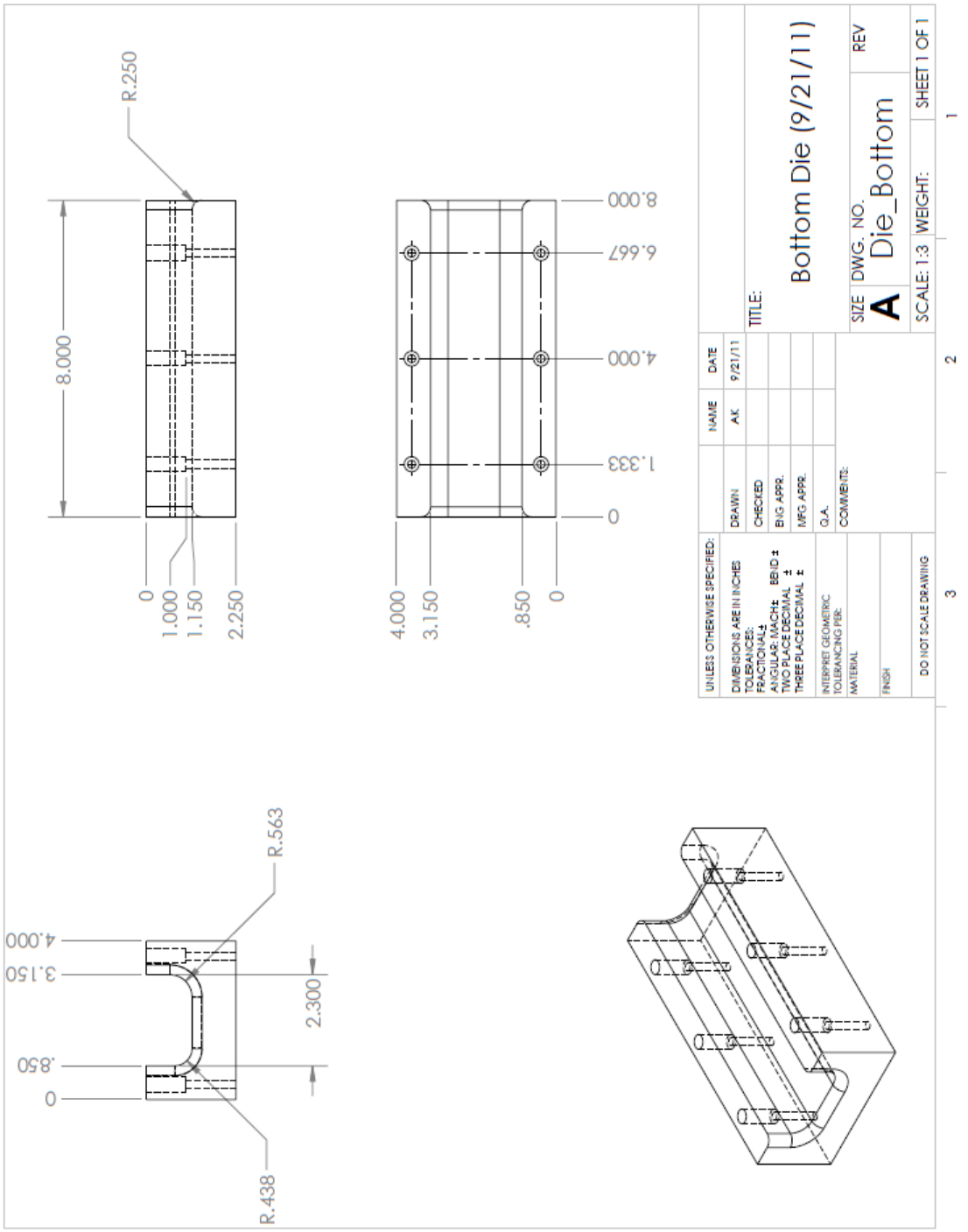

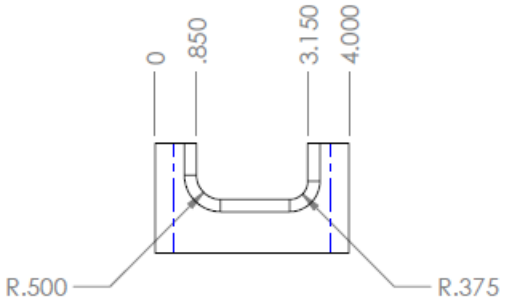

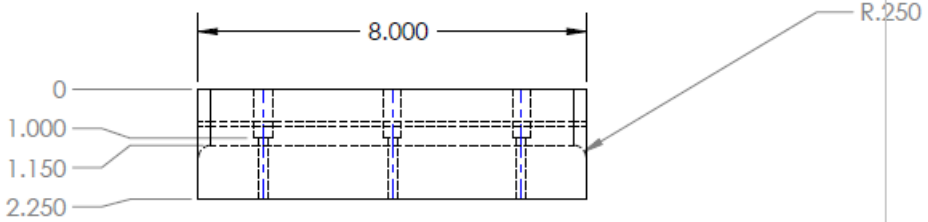

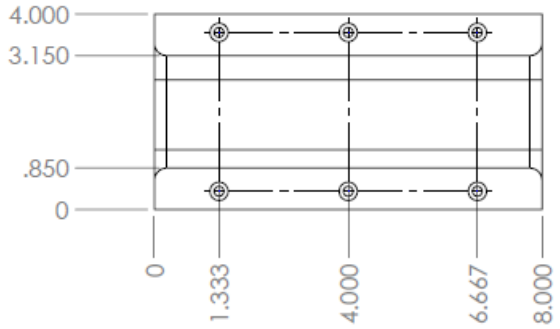

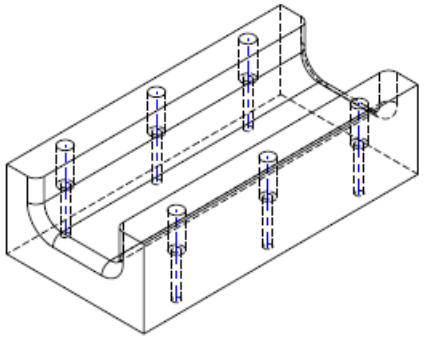

UNLESS OTHERWISE SPECIFIED:		NAME	DATE
DIMENSIONS ARE IN INCHES TOLERANCES: FRACTIONAL ± ANGULAR: MACH ± BEND ± TWO PLACE DECIMAL ± THREE PLACE DECIMAL ±	DRAWN	AK	9/27/10
	CHECKED		
	ENG APPR.		
	MFG APPR.		
INTERPRET GEOMETRIC TOLERANCING PER:	Q.A.		
MATERIAL	COMMENTS:		
FINISH			
DO NOT SCALE DRAWING			

TITLE:

TOP DIE (9/21/11)

SIZE	DWG. NO.	REV
A	Die_Top	

SCALE: 1:3	WEIGHT:	SHEET 1 OF 1

3 2 1

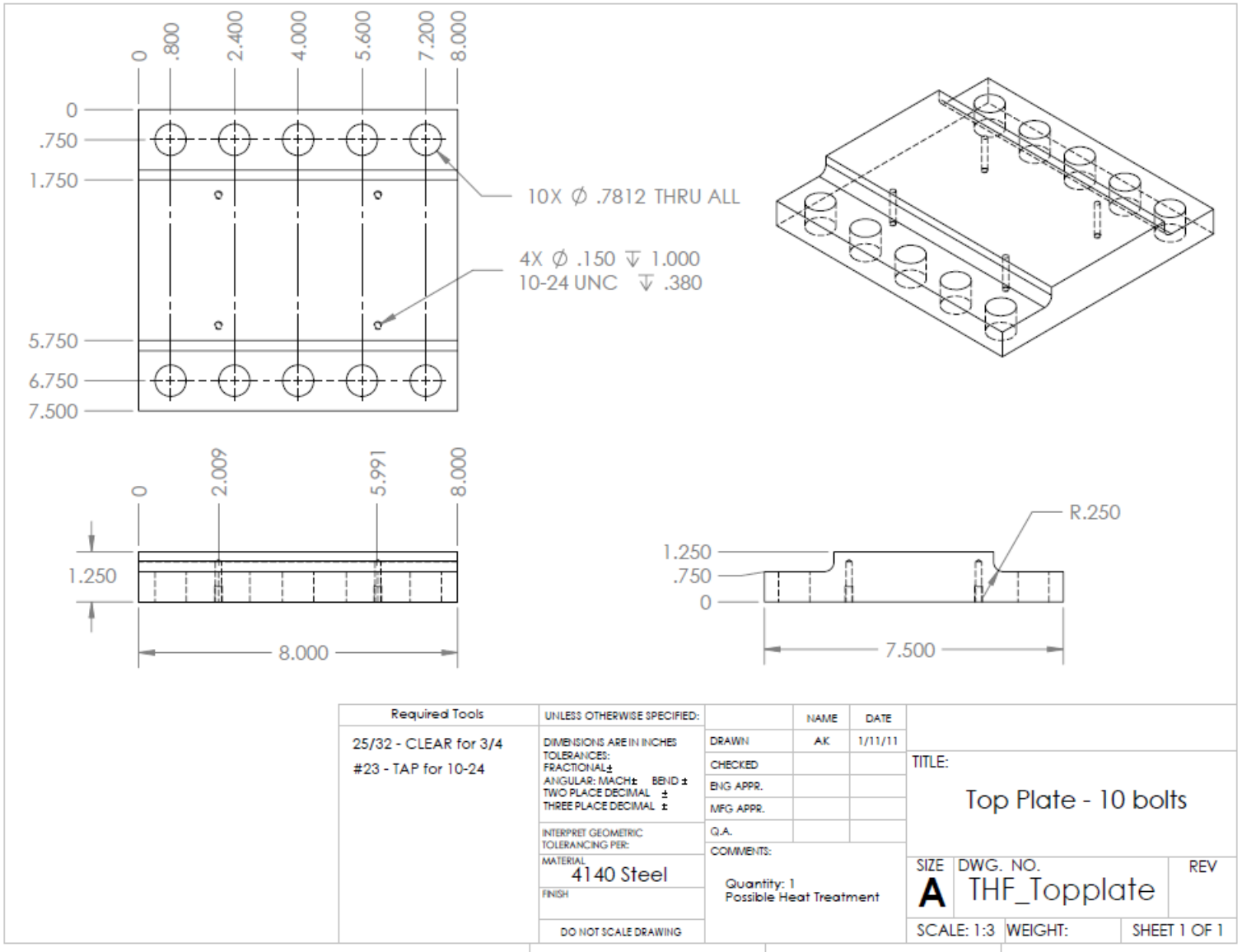
0
.800
2.400
4.000
5.600
7.200
8.000
0
.750
1.750
5.750
6.750
7.500
10X Ø .7812 THRU ALL
4X Ø .150 ↧ 1.000
10-24 UNC ↧ .380
0
2.009
5.991
8.000
1.250
8.000
R.250
1.250
.750
0
7.500
Required Tools
25/32 - CLEAR for 3/4
#23 - TAP for 10-24
UNLESS OTHERWISE SPECIFIED:
DIMENSIONS ARE IN INCHES
TOLERANCES:
FRACTIONAL ±
ANGULAR: MACH ± BEND ±
TWO PLACE DECIMAL ±
THREE PLACE DECIMAL ±
INTERPRET GEOMETRIC TOLERANCING PER:
MATERIAL
4140 Steel
FINISH
DO NOT SCALE DRAWING
NAME
DATE
DRAWN
AK
1/11/11
CHECKED
ENG APPR.
MFG APPR.
Q.A.
COMMENTS:
Quantity: 1
Possible Heat Treatment
TITLE:
Top Plate - 10 bolts
SIZE
A
DWG. NO.
THF_Topplate
REV
SCALE: 1:3
WEIGHT:
SHEET 1 OF 1
3
2
1

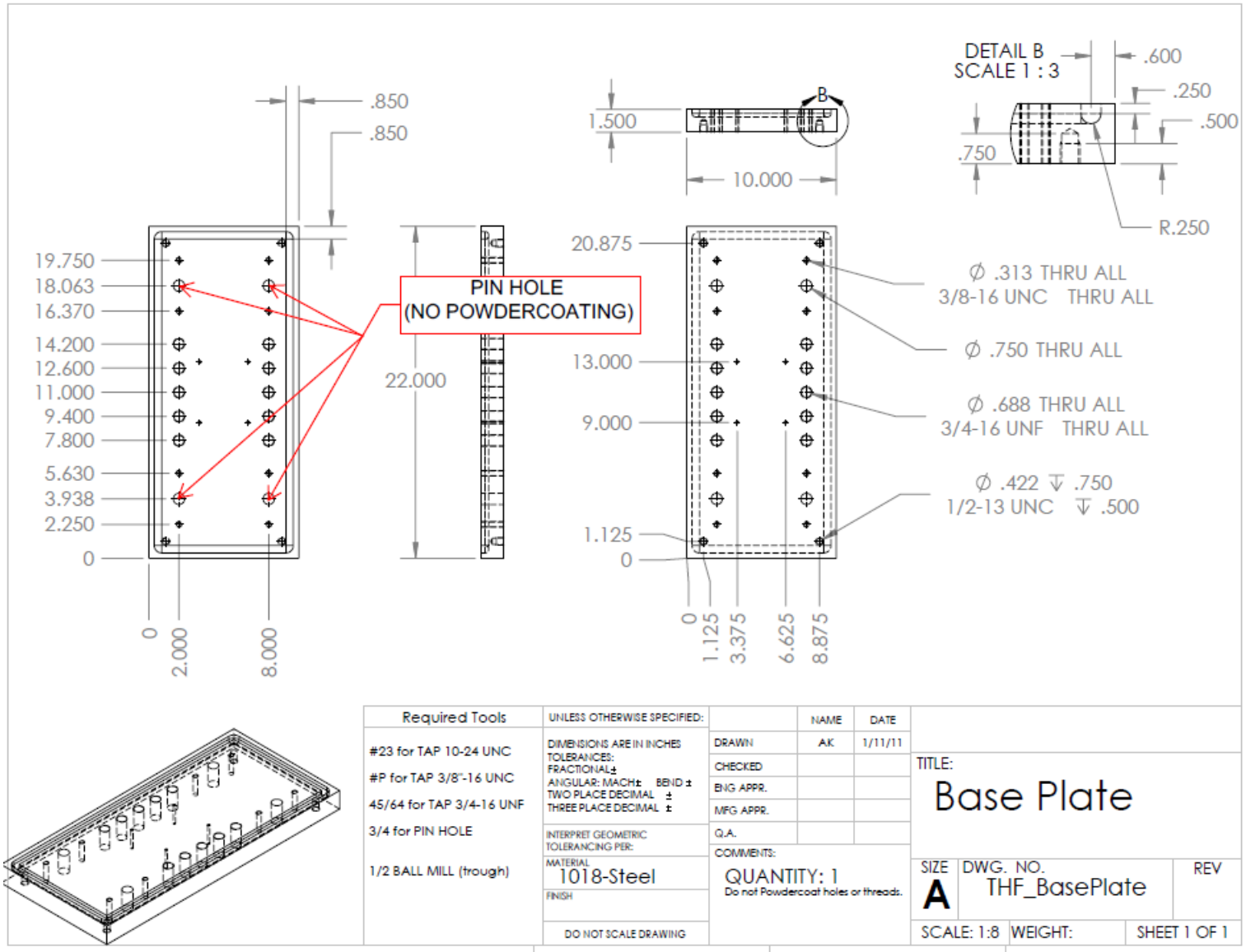

Required Tools	UNLESS OTHERWISE SPECIFIED:		NAME	DATE
#23 for TAP 10-24 UNC	DIMENSIONS ARE IN INCHES TOLERANCES: FRACTIONAL ± ANGULAR: MACH ± BEND ± TWO PLACE DECIMAL ± THREE PLACE DECIMAL ±	DRAWN	AK	1/11/11
#P for TAP 3/8"-16 UNC		CHECKED		
45/64 for TAP 3/4-16 UNF		ENG APPR.		
3/4 for PIN HOLE		MFG APPR.		
1/2 BALL MILL (trough)		Q.A.		
	INTERPRET GEOMETRIC TOLERANCING PER:	COMMENTS:		
	MATERIAL 1018-Steel	QUANTITY: 1 Do not Powdercoat holes or threads.		
	FINISH			
	DO NOT SCALE DRAWING			

TITLE:

Base Plate

SIZE	DWG. NO.	REV
A	THF_BasePlate	
SCALE: 1:8	WEIGHT:	SHEET 1 OF 1

3 2 1

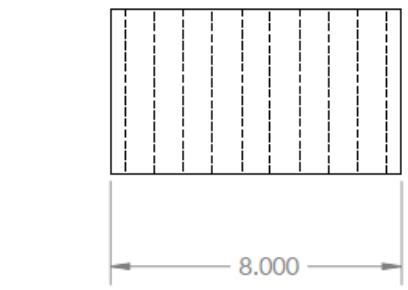

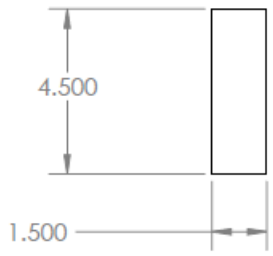

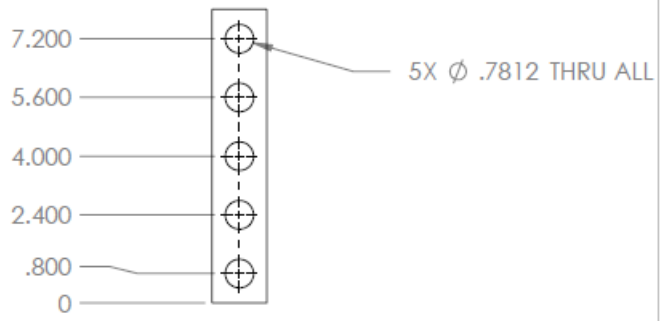

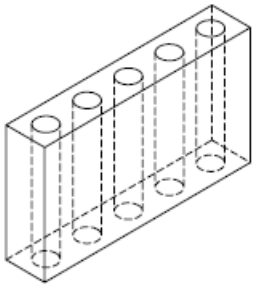

Required Tools	UNLESS OTHERWISE SPECIFIED:		NAME	DATE	
25/32 CLEAR 3/4-16 UNF	DIMENSIONS ARE IN INCHES TOLERANCES: FRACTIONAL ± ANGULAR: MACH ± BEND ± TWO PLACE DECIMAL ± THREE PLACE DECIMAL ±	DRAWN	AK	1/11/11	TITLE: Vertical Support Wall
		CHECKED			
		ENG APPR.			
		MFG APPR.			
	INTERPRET GEOMETRIC TOLERANCING PER:	Q.A.			
	MATERIAL: AL-6061 or 1018-Steel	COMMENTS: Quantity: 2			SIZE A | DWG. NO. THF_Support_Wall | REV
	FINISH				SCALE: 1:4 | WEIGHT: | SHEET 1 OF 1
	DO NOT SCALE DRAWING				

3 2 1

8.50 in

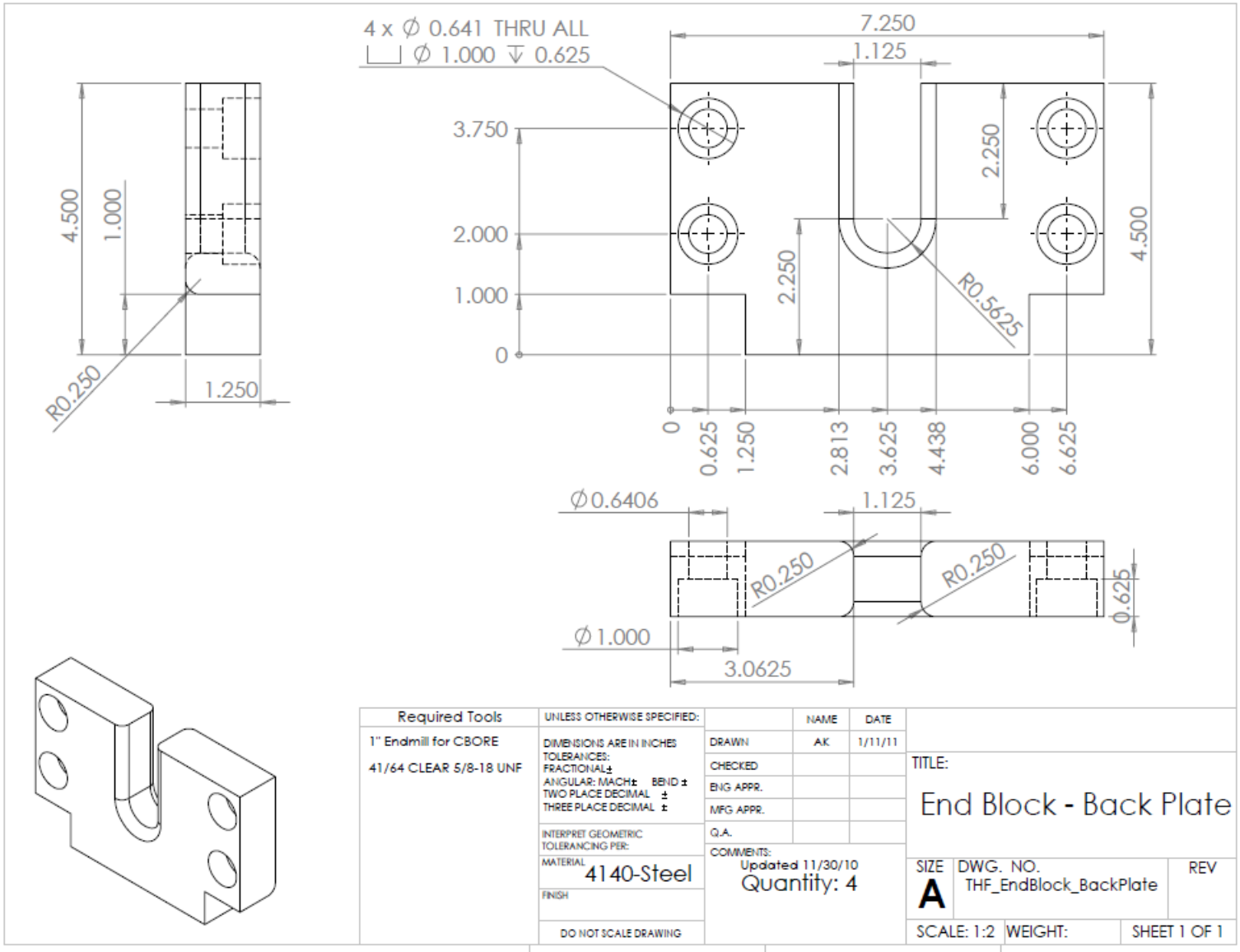

Required Tools	UNLESS OTHERWISE SPECIFIED:		NAME	DATE
1" Endmill for CBORE 41/64 CLEAR 5/8-18 UNF	DIMENSIONS ARE IN INCHES TOLERANCES: FRACTIONAL ± ANGULAR: MACH ± BEND ± TWO PLACE DECIMAL ± THREE PLACE DECIMAL ±	DRAWN	AK	1/11/11
		CHECKED		
		ENG APPR.		
		MFG APPR.		
		Q.A.		
	INTERPRET GEOMETRIC TOLERANCING PER:	COMMENTS: Updated 11/30/10 Quantity: 4		
	MATERIAL 4140-Steel			
	FINISH			
	DO NOT SCALE DRAWING			

TITLE:

End Block - Back Plate

SIZE	DWG. NO.	REV
A	THF_EndBlock_BackPlate	

SCALE: 1:2 | WEIGHT: | SHEET 1 OF 1

3 2 1

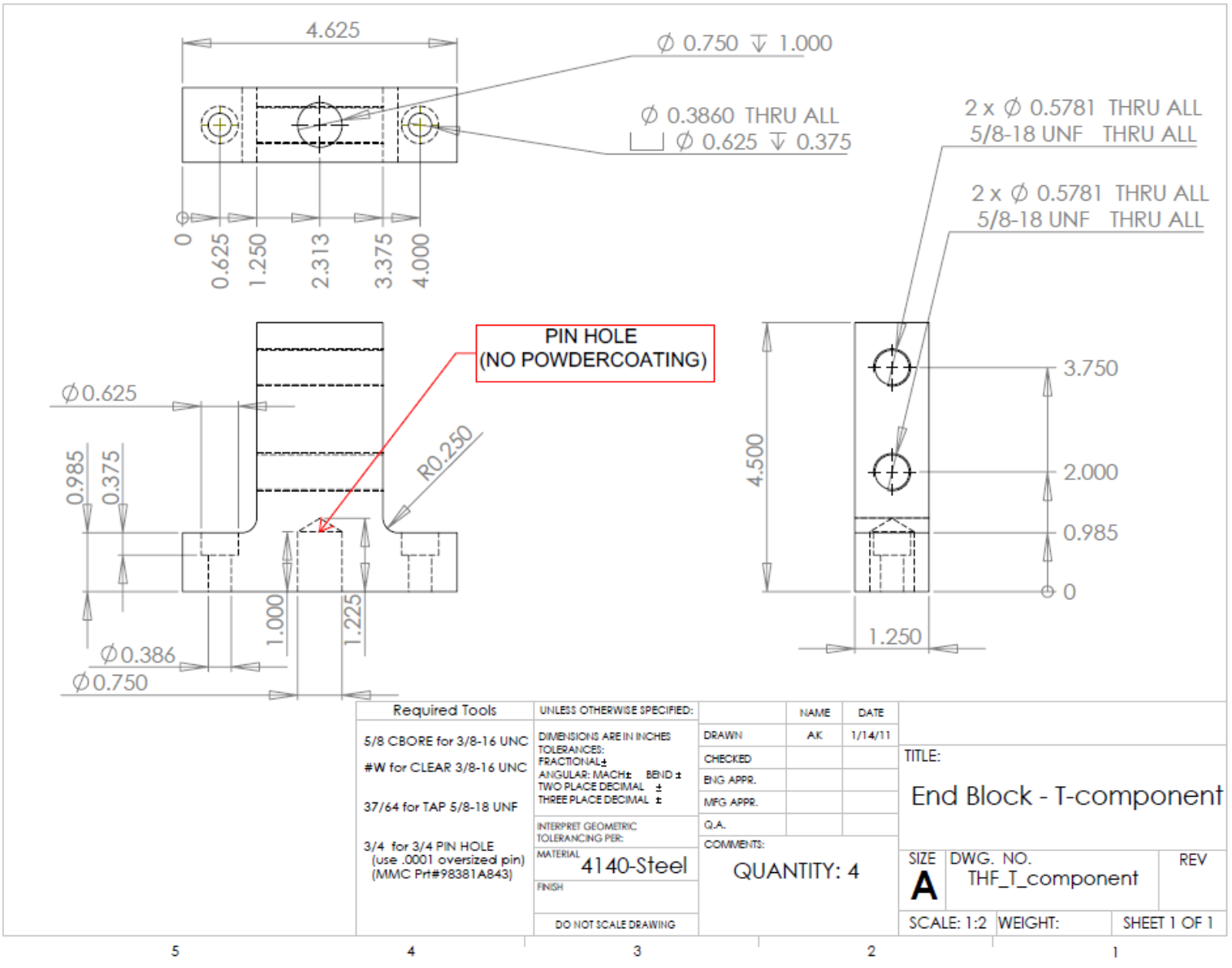
4.625
∅ 0.750 ↧ 1.000
∅ 0.3860 THRU ALL
⌴ ∅ 0.625 ↧ 0.375
2 x ∅ 0.5781 THRU ALL
5/8-18 UNF THRU ALL
2 x ∅ 0.5781 THRU ALL
5/8-18 UNF THRU ALL
0
0.625
1.250
2.313
3.375
4.000
PIN HOLE
(NO POWDERCOATING)
∅0.625
R0.250
0.985
0.375
1.000
1.225
∅0.386
∅0.750
4.500
3.750
2.000
0.985
0
1.250
Required Tools
5/8 CBORE for 3/8-16 UNC
#W for CLEAR 3/8-16 UNC
37/64 for TAP 5/8-18 UNF
3/4 for 3/4 PIN HOLE
(use .0001 oversized pin)
(MMC Prt#98381A843)
UNLESS OTHERWISE SPECIFIED:
DIMENSIONS ARE IN INCHES
TOLERANCES:
FRACTIONAL ±
ANGULAR: MACH ± BEND ±
TWO PLACE DECIMAL ±
THREE PLACE DECIMAL ±
INTERPRET GEOMETRIC TOLERANCING PER:
MATERIAL
4140-Steel
FINISH
DO NOT SCALE DRAWING
NAME
DATE
DRAWN
A.K.
1/14/11
CHECKED
ENG APPR.
MFG APPR.
Q.A.
COMMENTS:
QUANTITY: 4
TITLE:
End Block - T-component
SIZE
A
DWG. NO.
THF_T_component
REV
SCALE: 1:2
WEIGHT:
SHEET 1 OF 1
5
4
3
2
1

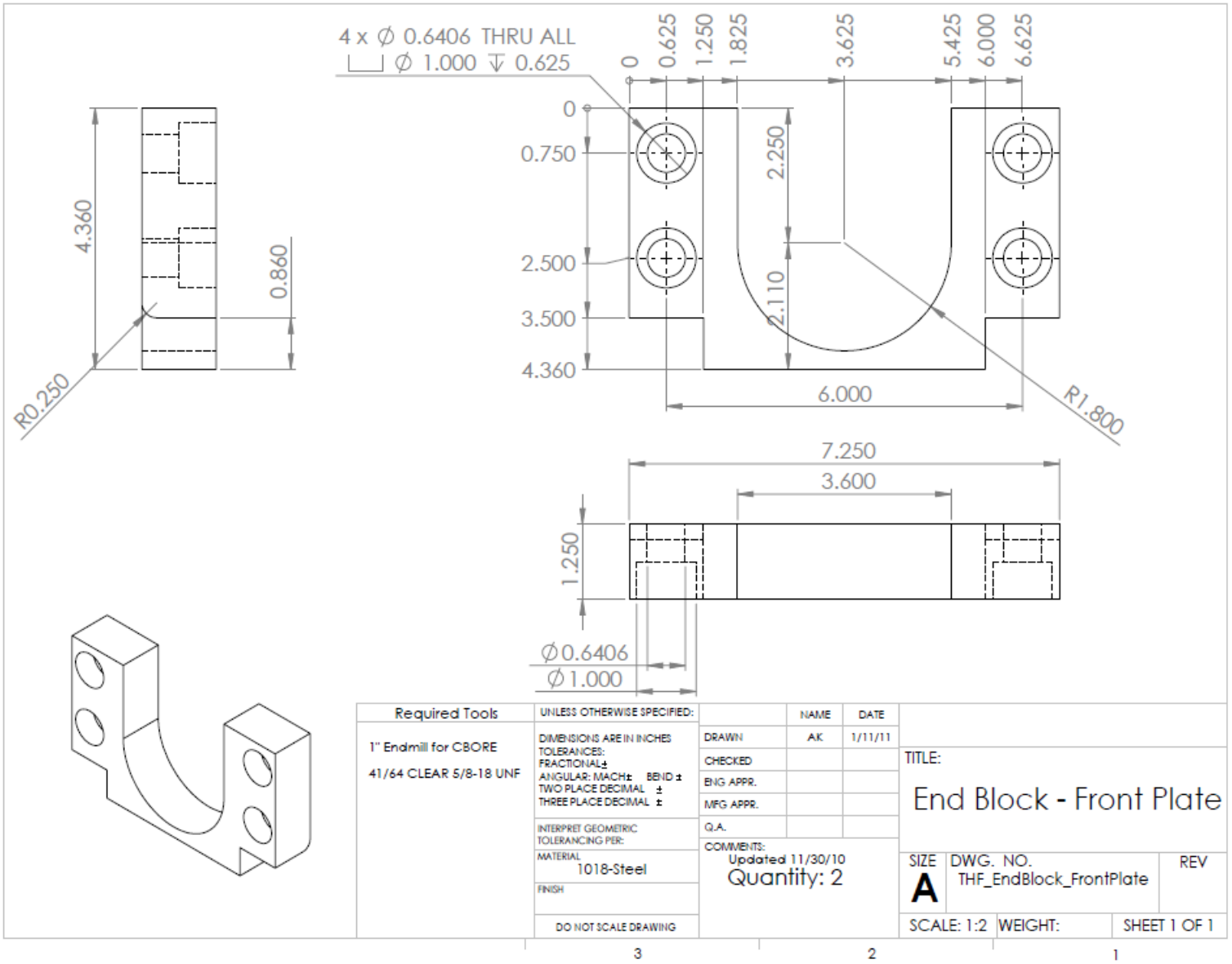
4 x ∅ 0.6406 THRU ALL
⌴ ∅ 1.000 ↧ 0.625
0
0.625
1.250
1.825
3.625
5.425
6.000
6.625
0
0.750
2.500
3.500
4.360
2.250
2.110
6.000
R1.800
4.360
0.860
R0.250
7.250
3.600
1.250
∅0.6406
∅1.000
Required Tools
1" Endmill for CBORE
41/64 CLEAR 5/8-18 UNF
UNLESS OTHERWISE SPECIFIED:
DIMENSIONS ARE IN INCHES
TOLERANCES:
FRACTIONAL ±
ANGULAR: MACH ± BEND ±
TWO PLACE DECIMAL ±
THREE PLACE DECIMAL ±
INTERPRET GEOMETRIC TOLERANCING PER:
MATERIAL
1018-Steel
FINISH
DO NOT SCALE DRAWING
NAME
DATE
DRAWN
AK
1/11/11
CHECKED
ENG APPR.
MFG APPR.
Q.A.
COMMENTS:
Updated 11/30/10
Quantity: 2
TITLE:
End Block - Front Plate
SIZE
A
DWG. NO.
THF_EndBlock_FrontPlate
REV
SCALE: 1:2
WEIGHT:
SHEET 1 OF 1
3
2
1

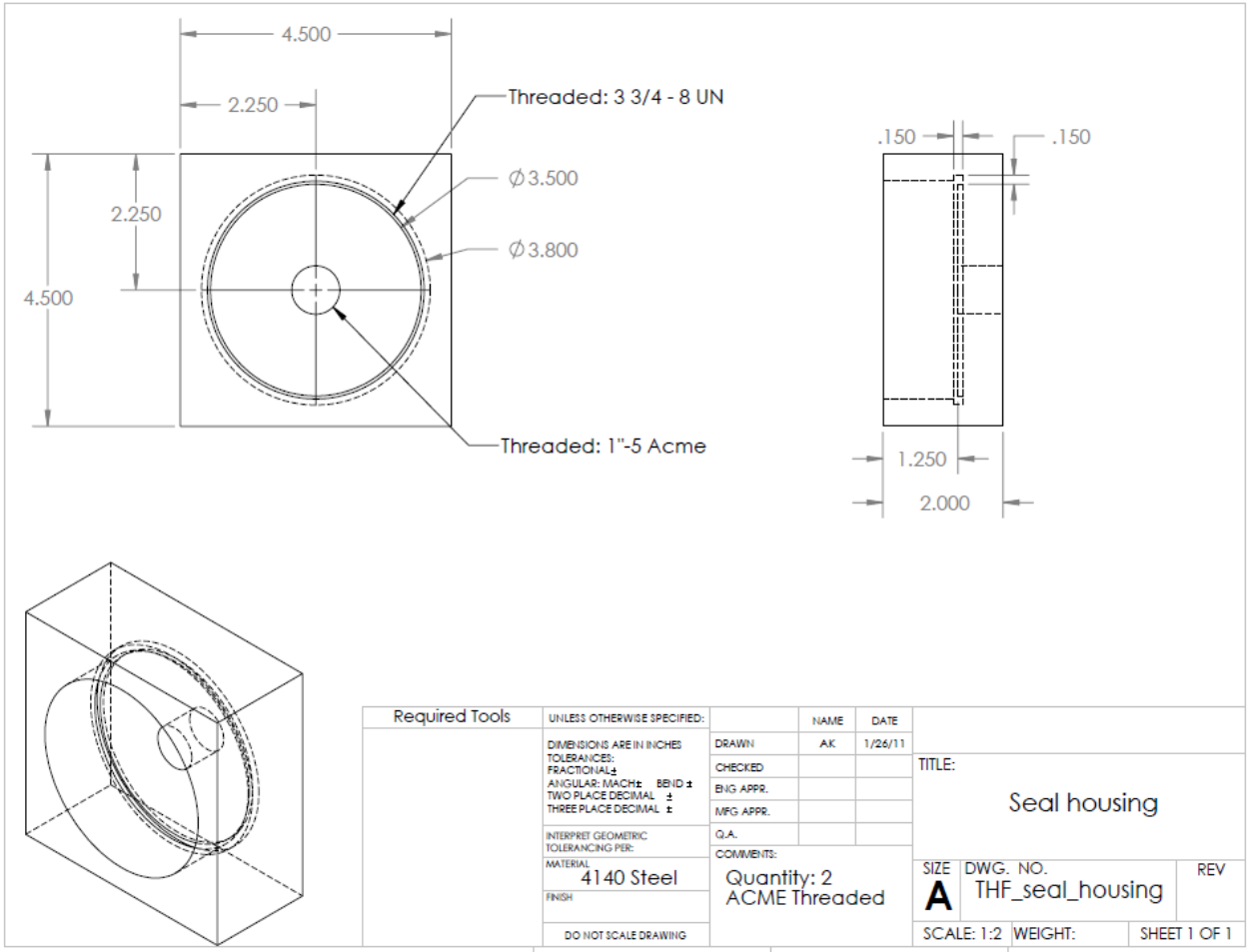

Required Tools	UNLESS OTHERWISE SPECIFIED:		NAME	DATE
	DIMENSIONS ARE IN INCHES TOLERANCES: FRACTIONAL ± ANGULAR: MACH ± BEND ± TWO PLACE DECIMAL ± THREE PLACE DECIMAL ±	DRAWN	AK	1/26/11
		CHECKED		
		ENG APPR.		
		MFG APPR.		
	INTERPRET GEOMETRIC TOLERANCING PER:	Q.A.		
	MATERIAL 4140 Steel	COMMENTS: Quantity: 2 ACME Threaded		
	FINISH			
	DO NOT SCALE DRAWING			

TITLE: Seal housing		
SIZE A	DWG. NO. THF_seal_housing	REV
SCALE: 1:2	WEIGHT:	SHEET 1 OF 1

3 2 1

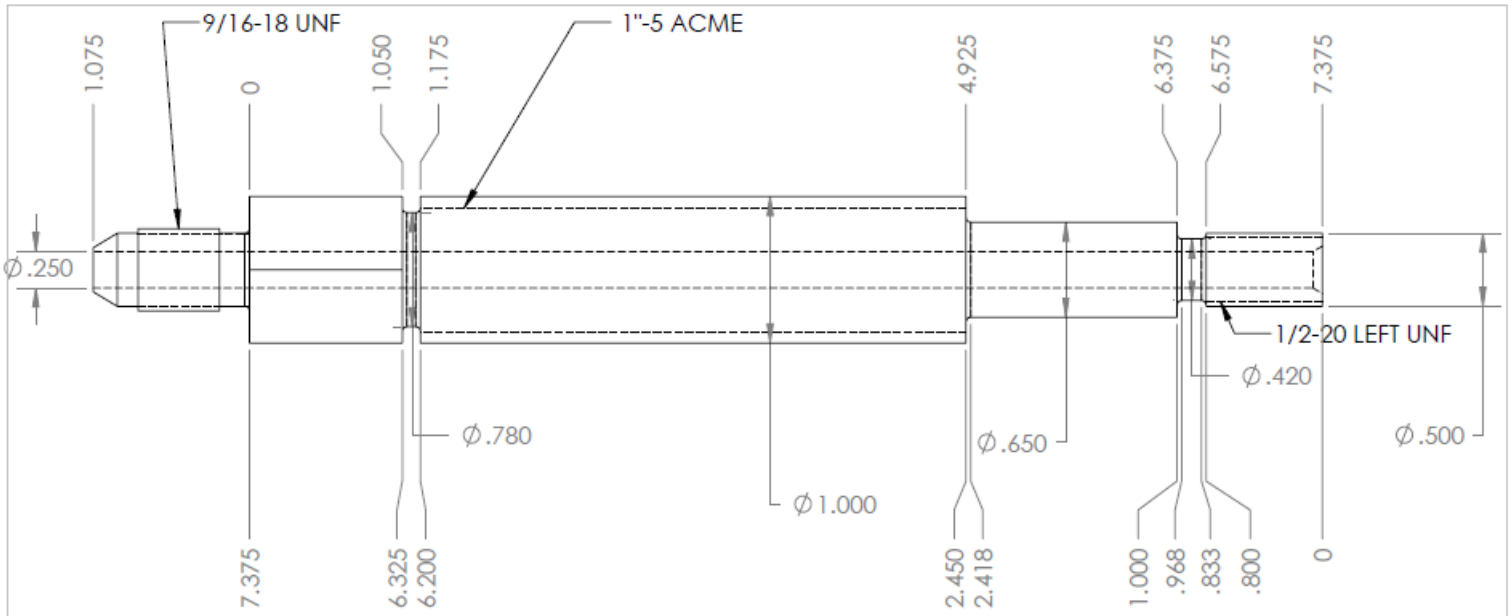

All fillets at diameter reductions are R0.0325"

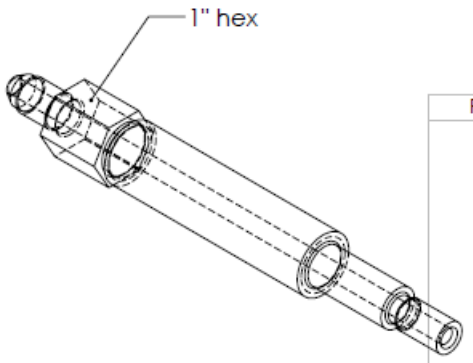

Required Tools	UNLESS OTHERWISE SPECIFIED:		NAME	DATE
	DIMENSIONS ARE IN INCHES TOLERANCES: FRACTIONAL± ANGULAR: MACH± BEND ± TWO PLACE DECIMAL ± THREE PLACE DECIMAL ±	DRAWN	AK	6/15/11
		CHECKED		
		ENG APPR.		
		MFG APPR.		
	INTERPRET GEOMETRIC TOLERANCING PER:	Q.A.		
	MATERIAL 4140 - 1" hex stock	COMMENTS: Quantity: 2		
	FINISH			
	DO NOT SCALE DRAWING			

TITLE: Threaded sealing screw

SIZE	DWG. NO.	REV
A	THF_seal_screw_Machining	

SCALE: 1:1 | WEIGHT: | SHEET 1 OF 1

3 2 1

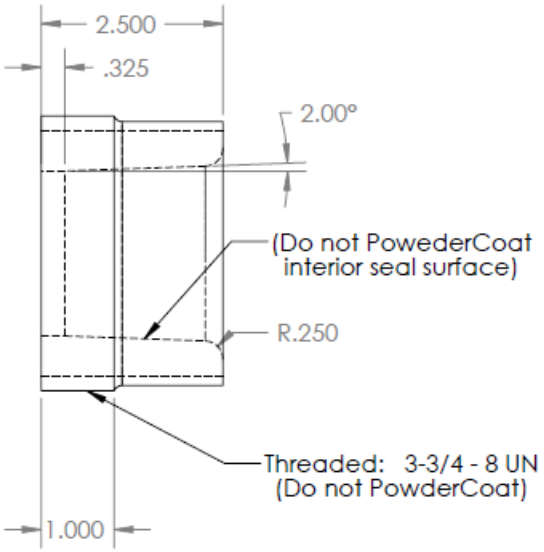

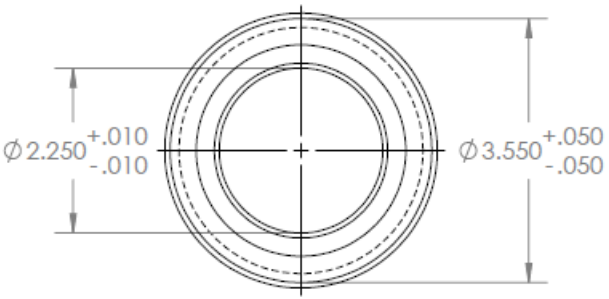

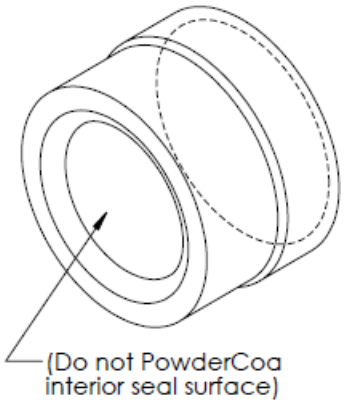

Required Tools	UNLESS OTHERWISE SPECIFIED:		NAME	DATE
	DIMENSIONS ARE IN INCHES TOLERANCES: FRACTIONAL ± ANGULAR: MACH ± BEND ± TWO PLACE DECIMAL ± THREE PLACE DECIMAL ±	UPDATED	AK	7/5/2011
		CHECKED		
		ENG APPR.		
		MFG APPR.		
		Q.A.		
	INTERPRET GEOMETRIC TOLERANCING PER:	COMMENTS:		
	MATERIAL 4140 steel	Quantity: 2		
	FINISH	Interior surface not PowderCoated		
	DO NOT SCALE DRAWING			

TITLE: Interior Seal Cap

SIZE	DWG. NO.	REV
A	THF_Seal_Cap	

SCALE: 1:2 | WEIGHT: | SHEET 1 OF 1

3 2 1

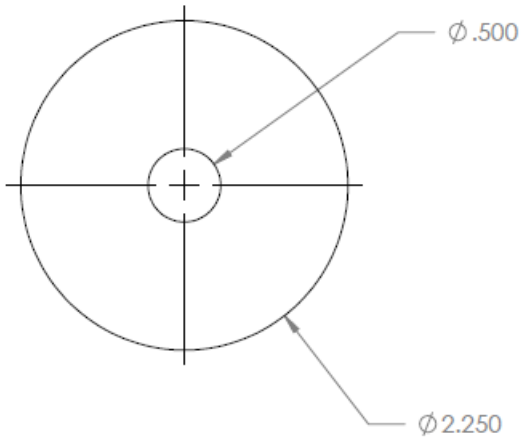

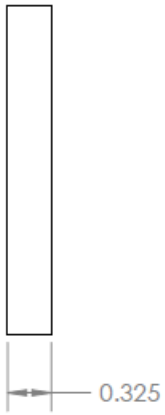

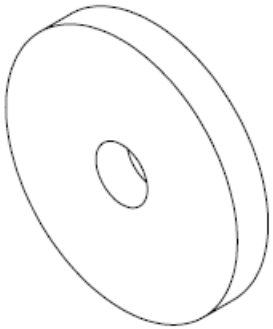

UNLESS OTHERWISE SPECIFIED:		NAME	DATE
DIMENSIONS ARE IN INCHES TOLERANCES: FRACTIONAL ± ANGULAR: MACH ± BEND ± TWO PLACE DECIMAL ± THREE PLACE DECIMAL ±	DRAWN	AK	5/24/11
	CHECKED		
	ENG APPR.		
	MFG APPR.		
INTERPRET GEOMETRIC TOLERANCING PER:	Q.A.		
MATERIAL	COMMENTS: Quantity: 4		
FINISH			
DO NOT SCALE DRAWING			

TITLE: Small Washer

SIZE	DWG. NO.	REV
A	leftthreadwash	

SCALE: 1:1 | WEIGHT: | SHEET 1 OF 1

3 2 1

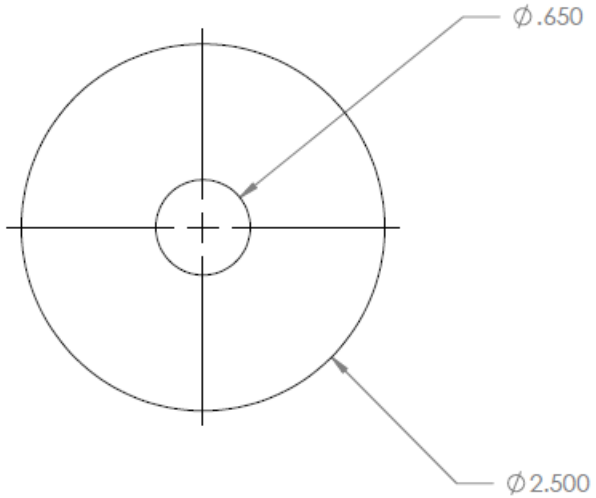

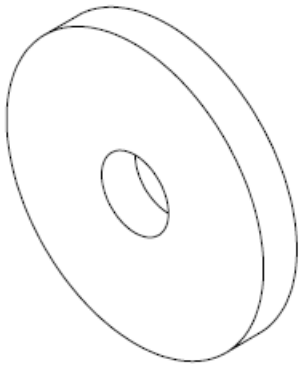

UNLESS OTHERWISE SPECIFIED:		NAME	DATE
DIMENSIONS ARE IN INCHES TOLERANCES: FRACTIONAL ± ANGULAR: MACH ± BEND ± TWO PLACE DECIMAL ± THREE PLACE DECIMAL ±	DRAWN	AK	9/27/10
	CHECKED		
	ENG APPR.		
	MFG APPR.		
INTERPRET GEOMETRIC TOLERANCING PER:	Q.A.		
MATERIAL	COMMENTS:		
FINISH			
DO NOT SCALE DRAWING			

TITLE:

SIZE	DWG. NO.	REV
A	tubeendwash	

SCALE: 1:1	WEIGHT:	SHEET 1 OF 1

3 2 1

APPENDIX B

TUBE HYDROFORMING MACHINE STRENGTH ANALYSIS

MathCAD evaluation of different stud strengths, sidewall materials, and preloads

Case 1 Use 10 x 3/4"-16 UNF Studs (40 kips each) with Grade 8 rating.
Use steel for material around bolt (E=30e6, Sy=130 KSI)

Assume: Stud is fully theaded (5.75" threaded)

	INPUTS			RESULTS	
Preload	78%		Preload	34.9	kips
d1	0.75	in	Torque	458.2	lbft
d2	0.75	in	C	0.2196	
At	0.373	in2	σ bolt	117.2	ksi
l1	5	in	Sfy	1.11	
l2	0	in	Sfsep	1.12	
D1	1.5	in			
D2	1.5	in			
L1	5.75	in			
L2	0	in			
l3	0.75	in			

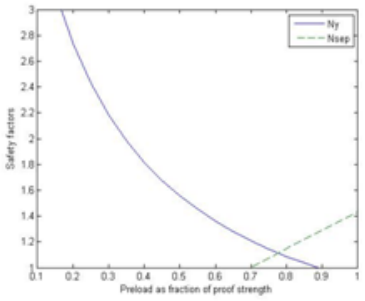

Case 2 Use 10 x 3/4"-16 UNF Hex bolt
Use steel for material around bolt (E=30e6, Sy=130 KSI)

Assume: Partial Threading (5" shank, 0.75" thread)
Shank @ major diam (d2=0.75")

	INPUTS			RESULTS	
Preload	70%		Preload	33.6	ki
d1	0.75	in	Torque	440.6	lb
d2	0.75	in	C	0.2456	
At	0.373	in2	σ bolt	116	ks
l1	0	in	Sfy	1.12	
l2	5	in	Sfsep	1.11	
D1	1.5	in			
D2	1.5	in			
L1	5.75	in			
L2	0	in			
l3	0.75	in			

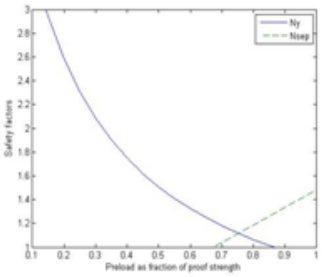

Case 3 Use 10 x 3/4"-16 UNF Reduced Shank Hex bolt
Use steel for material around bolt (E=30e6, Sy=130 KSI)

Assume: Partial threaded (5" shank, 0.75" thread)
Reduced shank @ minor diam (d2=0.6688")

NOTE: Highest bolt stress occurs at reduced diameter cross section.
This case requires a higher preload to prevent seperation.
78% produces best balance of Sfy and Sfsep

	INPUTS			RESULTS	
Preload	75%		Preload	33.6	kips
d1	0.75	in	Torque	440.6	lbft
d2	0.6688	in	C	0.2108	
At	0.373	in2	σ bolt	119.5	ksi
l1	0	in	Sfy	1.09	

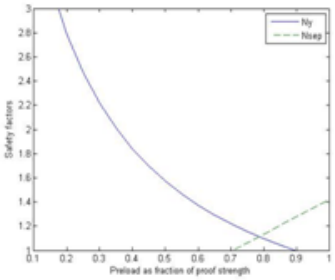

l2	5	in	Sfsep	1.06	
D1	1.5	in			
D2	1.5	in			
L1	5.75	in			
L2	0	in			
l3	0.75	in			

Case 4 Re-do Case 1 with Aluminum sidewalls
Use AL-6061 around bolt (E=10.1e6, Sy=35 KSI)

Assume: Stud is fully theaded (5.75" threaded)
NOTE: Total flange load is 116.9486 lbf
58% produces best balance of Sfy and Sfsep

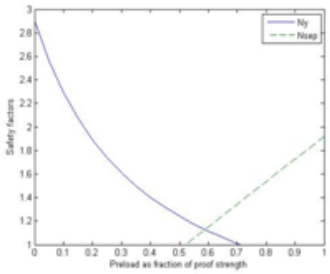

INPUTS			RESULTS		
Preload	60%		Preload	26.9	kips
d1	0.75	in	Torque	352.5	lbft
d2	0.75	in	C	0.417	
At	0.373	in2	σ bolt	116.7	ksi
l1	0	in	Sfy	1.11	
l2	5	in	Sfsep	1.15	
D1	1.5	in			
D2	1.5	in			
L1 (Steel)	1.25	in			
L2 (Al)	4.5	in			
l3	0.75	in			

Case 5 Re-do Case 2 with Aluminum sidewalls
Use AL-6061 around bolt (E=10.1e6, Sy=35 KSI)
Assume: Partial Threading (5" shank, 0.75" thread)
Shank @ major diam (d2=0.75")
NOTE: This case requires a lower preload to prevent yielding.

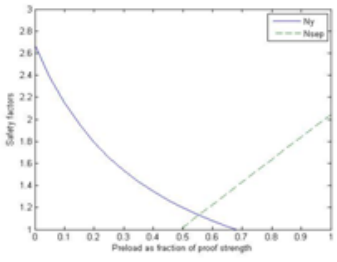

INPUTS			RESULTS		
Preload	55%		Preload	24.6	kips
d1	0.75	in	Torque	323	lbft
d2	0.75	in	C	0.4528	
At	0.373	in2	σ bolt	114.6	ksi
l1	0	in	Sfy	1.14	
l2	5	in	Sfsep	1.125	
D1	1.5	in			
D2	1.5	in			
L1	1.25	in			
L2	4.5	in			
l3	0.75	in			

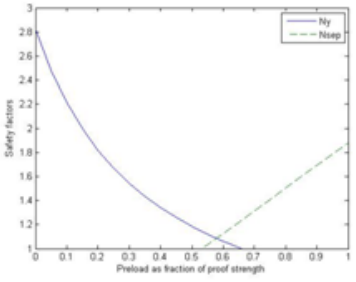

Case 6 Re-do case 3 with Aluminum sidewalls
Use AL-6061 around bolt (E=10.1e6, Sy=35 KSI)
Assume: Partial threaded (5" shank, 0.75" thread)
Reduced shank @ minor diam (d2=0.6688")
Highest bolt stress occurs at reduced diameter cross section.
NOTE: This case requires a lower preload to prevent yielding.

NOTE: This case requires a lower preload to prevent yielding.

INPUTS			RESULTS		
Preload	58%		Preload	26.9	kips
d1	0.75	in	Torque	340.7	lbft
d2	0.6688	in	C	0.4044	
At	0.373	in2	σ bolt	119.9	ksi
l1	0	in	Sfy	1.09	
l2	5	in	Sfsep	1.09	
D1	1.5	in			
D2	1.5	in			
L1	1.25	in			
L2	4.5	in			

MatLab Cases (*.m files)

```
%Case 1 - Use 10 x 3/4"-16 UNF Studs (40 kips each)
% This is a more general case than Fig. 14-23, p.836 (or Example 14-2) from
% Norton, R. Machine Design: An Integrated Approach, 3rd Edition.
% Prentice Hall, New York, NY 2005. Bolt can have a reduced section,
% as well as the flanges can have unequal areas.
% Units: in., lbf, psi, etc
%
% Preloaded Fasteners in Static Loading
%
%%%%%% Given:
% Bolt (note: l3=L1+L2-l1-l2, see below)
d1 = 0.75; At = 0.373; d2 = 0.75; l1 = 5.0; l2 = 0;

% Flange (aka material)
D1 = 1.5; D2 = 1.5; L1 = 5.75; L2 = 0.;
% Applied load (per bolt)
'Applied load, P [lbf]:'
P = 40000    % lbf
%
%%%%%% Assumptions
%Steel sidewall
E = 30e6; Sp = 120*1000; fraction = 0.78; Sy = 130*1000;
%
%%%%%% Solution
%
l3 = L1+L2-l1-l2;           % in
A2 = (pi * d2^2) / 4;       % in2
Fi = @(fp) fp * Sp * At;    % lbf
preload = Fi(fraction)      % lbf
torque = 0.21 * preload * d1 / 12 % ft-lbf, lubr.threads (Norton p.855)
%
% Stiffnesses of bolt and flange (aka material)
kb = 1/(( (l1+l3) / (E*At)) + (l2 / (E*A2)));  % lbf / in
km = 1/( L1/(E*(pi/4)*(D1^2 - d1^2)) + L2/(E*(pi/4)*(D2^2 - d1^2)));  %lbf/in
%
% Joint stiffness
'Joint stiffness, C:'
C = kb / (km + kb)
```

```
'Portions of the external load felt on bolt and flange:'
%
% Loads in bolt & flange
Pb = C * P          % lbf
Pm = (1 - C) * P    % lbf
Fb = @(fp) Fi(fp) + Pb;  % lbf
'Total bolt load [lbf]:', Fb(fraction)   % lbf
SIGb = @(fp) Fb(fp) / At;    % psi
'Stress in the bolt [psi]:', SIGb(fraction)
Fm = @(fp) Fi(fp) - Pm;  % lbf
'Total flange load [lbf]', Fm(fraction)   % lbf
%
% Safety factors
Ny = @(fp) Sy ./ SIGb(fp);
'Safety factor for yielding'
Ny(fraction)
P0 = @(fp) Fi(fp) / (1 - C);   % lbf
'Separation load'
P0(fraction)
Nsep = @(fp) P0(fp) ./ P;
'Safety factor for separation'
Nsep(fraction)
%
%%%%%% Plots
%
fp = 0:0.05:1;
NyPlot = Ny(fp);
NsepPlot = Nsep(fp);

plot(fp,NyPlot,'-',fp,NsepPlot,'--')
xlabel('Preload as fraction of proof strength')
ylabel('Safety factors')
ylim([1 3])
legend('Ny','Nsep')


% Case 2 - Use 10 x 3/4"-16 UNF Hex bolts
% This is a more general case than Fig. 14-23, p.836 (or Example 14-2) from
% Norton, R. Machine Design: An Integrated Approach, 3rd Edition.
% Prentice Hall, New York, NY 2005. Bolt can have a reduced section,
% as well as the flanges can have unequal areas.
% Units: in., lbf, psi, etc
%
% Preloaded Fasteners in Static Loading
%
%%%%%% Given:
% Bolt (note: l3=L1+L2-l1-l2, see below)
d1 = 0.75; At = 0.373; d2 = 0.75; l1 = 0.; l2 = 5.;
% Flange (aka material)
D1 = 1.5; D2 = 1.5; L1 = 5.75; L2 = 0.0;
% Applied load (per bolt)
'Applied load, P [lbf]:'
P = 40000    % lbf
%
%%%%%% Assumptions
%Steel sidewall
```

```
E = 30e6; Sp = 120*1000; fraction = 0.75; Sy = 130*1000;
%
%%%%%% Solution
%
l3 = L1+L2-l1-l2;           % in
A2 = (pi * d2^2) / 4;       % in2
Fi = @(fp) fp * Sp * At;    % lbf
preload = Fi(fraction)      % lbf
torque = 0.21 * preload * d1 / 12 % ft-lbf, lubr.threads (Norton p.855)
%
% Stiffnesses of bolt and flange (aka material)
kb = 1/(( (l1+l3) / (E*At)) + (l2 / (E*A2)));  % lbf / in
km = 1/( L1/(E*(pi/4)*(D1^2 - d1^2)) + L2/(E*(pi/4)*(D2^2 - d1^2)) );  % lbf /
in
%
% Joint stiffness
'Joint stiffness, C:'
C = kb / (km + kb)
'Portions of the external load felt on bolt and flange:'
%
% Loads in bolt & flange
Pb = C * P          % lbf
Pm = (1 - C) * P    % lbf
Fb = @(fp) Fi(fp) + Pb;  % lbf
'Total bolt load [lbf]:', Fb(fraction)   % lbf
SIGb = @(fp) Fb(fp) / At;    % psi
'Stress in the bolt [psi]:', SIGb(fraction)
Fm = @(fp) Fi(fp) - Pm;  % lbf
'Total flange load [lbf]', Fm(fraction)   % lbf
%
% Safety factors
Ny = @(fp) Sy ./ SIGb(fp);
'Safety factor for yielding'
Ny(fraction)
P0 = @(fp) Fi(fp) / (1 - C);   % lbf
'Separation load'
P0(fraction)
Nsep = @(fp) P0(fp) ./ P;
'Safety factor for separation'
Nsep(fraction)
%
%%%%%% Plots
%
fp = 0:0.05:1;
NyPlot = Ny(fp);
NsepPlot = Nsep(fp);

plot(fp,NyPlot,'-',fp,NsepPlot,'--')
xlabel('Preload as fraction of proof strength')
ylabel('Safety factors')
ylim([1 3])
legend('Ny','Nsep')
```

```
% Case 3 - 10 x 3/4"-16 UNF Reduced Shank Hex bolt
% This is a more general case than Fig. 14-23, p.836 (or Example 14-2) from
% Norton, R. Machine Design: An Integrated Approach, 3rd Edition.
% Prentice Hall, New York, NY 2005. Bolt can have a reduced section,
% as well as the flanges can have unequal areas.
% Units: in., lbf, psi, etc
%
% Preloaded Fasteners in Static Loading
%
%%%%%% Given:
% Bolt (note: l3=L1+L2-l1-l2, see below)
d1 = 0.75; At = 0.373; d2 = 0.6688; l1 = 0; l2 = 5;
% Flange (aka material)
D1 = 1.5; D2 = 1.5; L1 = 1.25; L2 = 4.5;
% Applied load (per bolt)
'Applied load, P [lbf]:'
P = 40000    % lbf
%
%%%%%% Assumptions
%Steel sidewall
E = 30e6; Sp = 120*1000; fraction = 0.75; Sy = 130*1000;
%
%%%%%% Solution
%
l3 = L1+L2-l1-l2;          % in
A2 = (pi * d2^2) / 4;      % in2
Fi = @(fp) fp * Sp * At;   % lbf
preload = Fi(fraction)     % lbf
torque = 0.21 * preload * d1 / 12 % ft-lbf, lubr.threads (Norton p.855)
%
% Stiffnesses of bolt and flange (aka material)
kb = 1/(( (l1+l3) / (E*At)) + (l2 / (E*A2)));  % lbf / in
km = 1/( L1/(E*(pi/4)*(D1^2 - d1^2)) + L2/(E*(pi/4)*(D2^2 - d1^2)));%lbf/in
%
% Joint stiffness
'Joint stiffness, C:'
C = kb / (km + kb)
'Portions of the external load felt on bolt and flange:'
%
% Loads in bolt & flange
Pb = C * P          % lbf
Pm = (1 - C) * P    % lbf
Fb = @(fp) Fi(fp) + Pb;  % lbf
'Total bolt load [lbf]:', Fb(fraction)   % lbf
SIGb = @(fp) Fb(fp) / A2;    % psi
'Stress in the bolt [psi]:', SIGb(fraction)
Fm = @(fp) Fi(fp) - Pm;  % lbf
'Total flange load [lbf]', Fm(fraction)   % lbf
%
% Safety factors
Ny = @(fp) Sy ./ SIGb(fp);
'Safety factor for yielding'
Ny(fraction)
P0 = @(fp) Fi(fp) / (1 - C);   % lbf
'Separation load'
P0(fraction)
Nsep = @(fp) P0(fp) ./ P;
```

```
'Safety factor for separation'
Nsep(fraction)
%
%%%%%% Plots
%
fp = 0:0.05:1;
NyPlot = Ny(fp);
NsepPlot = Nsep(fp);

plot(fp,NyPlot,'-',fp,NsepPlot,'--')
xlabel('Preload as fraction of proof strength')
ylabel('Safety factors')
ylim([1 3])
legend('Ny','Nsep')


%Case 4 - Use 10 x 3/4"-16 UNF Studs (40 kips each)
%       - Aluminum 6061 Sidewalls
% This is a more general case than Fig. 14-23, p.836 (or Example 14-2).
% Bolt can have a reduced section, as well as the flanges can have unequal
% areas.
% Units: in., lbf, psi, etc
% Preloaded Fasteners in Static Loading
%
%%%%%% Given:
% Bolt
d1 = 0.75; At = 0.373; d2 = 0.75; l1 = 5.75; l2 = 0; % then l3=L1+L2-l1-l2, see
below
% Flange (aka material)
D1 = 1.5; D2 = 1.5; L1 = 5.75; L2 = 0.;
% Applied load (per bolt)
'Applied load, P [lbf]:'
P = 40000    % lbf
%
%%%%%% Assumptions
% Steel bolts, aluminum walls.
E = 30e6; Sp = 120*1000; fraction = 0.7; Sy = 130*1000;
E_mat = 10.1e6;
%
%%%%%% Solution
%
l3 = L1+L2-l1-l2;           % in
A2 = (pi * d2^2) / 4;       % in2
Fi = @(fp) fp * Sp * At;    % lbf
preload = Fi(fraction)      % lbf
torque = 0.21 * preload * d1 / 12 % ft-lbf, lubr.threads (Norton p.855)
%
% Stiffnesses of bolt and flange (aka material)
kb = 1/(( (l1+l3) / (E*At)) + (l2 / (E*A2)));  % lbf / in
km = 1/( L1/(E_mat*(pi/4)*(D1^2 - d1^2)) + L2/(E_mat*(pi/4)*(D2^2 - d1^2)) );
% lbf / in
%
% Joint stiffness
'Joint stiffness, C:'
C = kb / (km + kb)
'Portions of the external load felt on bolt and flange:'
```

```
%
% Loads in bolt & flange
Pb = C * P          % lbf
Pm = (1 - C) * P    % lbf
Fb = @(fp) Fi(fp) + Pb;  % lbf
'Total bolt load [lbf]:', Fb(fraction)   % lbf
SIGb = @(fp) Fb(fp) / At;    % psi
'Stress in the bolt [psi]:', SIGb(fraction)
Fm = @(fp) Fi(fp) - Pm;  % lbf
'Total flange load [lbf]', Fm(fraction)   % lbf
%
% Safety factors
Ny = @(fp) Sy ./ SIGb(fp);
'Safety factor for yielding'
Ny(fraction)
P0 = @(fp) Fi(fp) / (1 - C);   % lbf
'Separation load'
P0(fraction)
Nsep = @(fp) P0(fp) ./ P;
'Safety factor for separation'
Nsep(fraction)
%
%%%%%% Plots
%
fp = 0:0.05:1;
NyPlot = Ny(fp);
NsepPlot = Nsep(fp);

plot(fp,NyPlot,'-',fp,NsepPlot,'--')
xlabel('Preload as fraction of proof strength')
ylabel('Safety factors')
ylim([1 3])
legend('Ny','Nsep')


% Case 5 - Use 10 x 3/4"-16 UNF Hex bolts
%       - Aluminum 6061 Sidewalls
% This is a more general case than Fig. 14-23, p.836 (or Example 14-2).
% Bolt can have a reduced section, as well as the flanges can have unequal
% areas.
% Units: in., lbf, psi, etc
% Preloaded Fasteners in Static Loading
%
%%%%%% Given:
% Bolt
d1 = 0.75; At = 0.373; d2 = 0.75; l1 = 0.; l2 = 5.; % then l3=L1+L2-l1-l2, see
below
% Flange (aka material)
D1 = 1.5; D2 = 1.5; L1 = 1.25; L2 = 4.5;
% Applied load (per bolt)
'Applied load, P [lbf]:'
P = 40000    % lbf
%
%%%%%% Assumptions
%
E = 30e6; Sp = 120*1000; fraction = 0.55; Sy = 130*1000;
```

```
E_al = 10.1e6;
%
%%%%%% Solution
%
l3 = L1+L2-l1-l2;           % in
A2 = (pi * d2^2) / 4;       % in2
Fi = @(fp) fp * Sp * At;    % lbf
preload = Fi(fraction)      % lbf
torque = 0.21 * preload * d1 / 12 % ft-lbf, lubr.threads (Norton p.855)
%
% Stiffnesses of bolt and flange (aka material)
kb = 1/(( (l1+l3) / (E*At)) + (l2 / (E*A2)));  % lbf / in
km = 1/( L1/(E*(pi/4)*(D1^2 - d1^2)) + L2/(E_al*(pi/4)*(D2^2 - d1^2)));% lbf /
in
%
% Joint stiffness
'Joint stiffness, C:'
C = kb / (km + kb)
'Portions of the external load felt on bolt and flange:'
%
% Loads in bolt & flange
Pb = C * P          % lbf
Pm = (1 - C) * P    % lbf
Fb = @(fp) Fi(fp) + Pb;  % lbf
'Total bolt load [lbf]:', Fb(fraction)   % lbf
SIGb = @(fp) Fb(fp) / At;    % psi
'Stress in the bolt [psi]:', SIGb(fraction)
Fm = @(fp) Fi(fp) - Pm;  % lbf
'Total flange load [lbf]', Fm(fraction)   % lbf
%
% Safety factors
Ny = @(fp) Sy ./ SIGb(fp);
'Safety factor for yielding'
Ny(fraction)
P0 = @(fp) Fi(fp) / (1 - C);   % lbf
'Separation load'
P0(fraction)
Nsep = @(fp) P0(fp) ./ P;
'Safety factor for separation'
Nsep(fraction)
%
%%%%%% Plots
%
fp = 0:0.05:1;
NyPlot = Ny(fp);
NsepPlot = Nsep(fp);

plot(fp,NyPlot,'-',fp,NsepPlot,'--')
xlabel('Preload as fraction of proof strength')
ylabel('Safety factors')
ylim([1 3])
legend('Ny','Nsep')
```

```
%Case 6 - 10 x 3/4"-16 UNF Reduced Shank Hex bolt
%       - Aluminum 6061 Sidewalls
% This is a more general case than Fig. 14-23, p.836 (or Example 14-2).
% Bolt can have a reduced section, as well as the flanges can have unequal
% areas.
% Units: in., lbf, psi, etc
% Preloaded Fasteners in Static Loading
%
%%%%%% Given:
% Bolt
d1 = 0.75; At = 0.373; d2 = 0.6688; l1 = 0; l2 = 5; % then l3=L1+L2-l1-l2, see
below
% Flange (aka material)
D1 = 1.5; D2 = 1.5; L1 = 1.25; L2 = 4.5;
% Applied load (per bolt)
'Applied load, P [lbf]:'
P = 40000    % lbf
%
%%%%%% Assumptions
%
E = 30e6; Sp = 120*1000; fraction = 0.58; Sy = 130*1000;
E_al = 10.1e6;
%
%%%%%% Solution
%
l3 = L1+L2-l1-l2;          % in
A2 = (pi * d2^2) / 4;      % in2
Fi = @(fp) fp * Sp * At;   % lbf
preload = Fi(fraction)     % lbf
torque = 0.21 * preload * d1 / 12 % ft-lbf, lubr.threads (Norton p.855)
%
% Stiffnesses of bolt and flange (aka material)
kb = 1/(( (l1+l3) / (E*At)) + (l2 / (E*A2)));  % lbf / in
km = 1/( L1/(E*(pi/4)*(D1^2 - d1^2)) + L2/(E_al*(pi/4)*(D2^2 - d1^2)) );  % lbf
/ in
%
% Joint stiffness
'Joint stiffness, C:'
C = kb / (km + kb)
'Portions of the external load felt on bolt and flange:'
%
% Loads in bolt & flange
Pb = C * P          % lbf
Pm = (1 - C) * P    % lbf
Fb = @(fp) Fi(fp) + Pb;  % lbf
'Total bolt load [lbf]:', Fb(fraction)   % lbf
SIGb = @(fp) Fb(fp) / A2;    % psi
'Stress in the bolt [psi]:', SIGb(fraction)
Fm = @(fp) Fi(fp) - Pm;  % lbf
'Total flange load [lbf]', Fm(fraction)   % lbf
%
% Safety factors
Ny = @(fp) Sy ./ SIGb(fp);
'Safety factor for yielding'
Ny(fraction)
P0 = @(fp) Fi(fp) / (1 - C);   % lbf
'Separation load'
```

```
P0(fraction)
Nsep = @(fp) P0(fp) ./ P;
'Safety factor for separation'
Nsep(fraction)
%
%%%%%% Plots
%
fp = 0:0.05:1;
NyPlot = Ny(fp);
NsepPlot = Nsep(fp);

plot(fp,NyPlot,'-',fp,NsepPlot,'--')
xlabel('Preload as fraction of proof strength')
ylabel('Safety factors')
ylim([1 3])
legend('Ny','Nsep')
```

APPENDIX C

ESTIMATION OF FASTNER FORCES

End plate bolts

Known Values:

$P := 20ksi$ $BoltCount := 4$ $Diam := 2.5in$ $AreaTubeEndCap := \pi \cdot \left(\frac{Diam}{2}\right)^2$

Properties for SAE Grade 8 UNC 5/8-11 Hex Bolt

$MinProofStrength := 120ksi$ $TensileArea := 0.2260in^2$

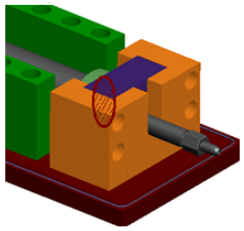

Calculate force per bolt

$ForceTotal := P \cdot AreaTubeEndCap = 98.175kip$

$ForcePerBolt := \frac{ForceTotal}{BoltCount} = 24.544kip$ $StressPerBolt := \frac{ForcePerBolt}{TensileArea} = 108.6ksi$

Since 108.6 KSI is less than the proof strength of 120 KSI, selection is valid!

$SafetyFactor := \frac{MinProofStrength}{StressPerBolt} = 1.105$

Top plate bolts

Known Values:

$P := 20ksi$ $BoltCount := 8$ $TopPlateArea := 24in^2$

Properties for SAE Grade 8 UNC 1-8 Hex Bolt

$MinProofStrength := 120ksi$ $TensileArea := 0.6057in^2$

Calculate force per bolt

$ForceTotal := P \cdot TopPlateArea = 480kip$

$ForcePerBolt := \frac{ForceTotal}{BoltCount} = 60kip$ $StressPerBolt := \frac{ForcePerBolt}{TensileArea} = 99.059ksi$

Since 99 KSI is less than the proof strength of 120 KSI, selection is valid!

$SafetyFactor := \frac{MinProofStrength}{StressPerBolt} = 1.211$

Initial evaluation of bolting solutions for vertical bolts (neglecting sidewall compression)

Adam Kaplan
Hydroforming Project

11/15/2009

Bolt Specifications

Source: Ch.14 - Table 14.1 of Norton, R. 2009. "Machine Design." Pearson Prentice Hall.

Type	UNC - Course	UNC - Course	UNC - Course	UNC - Course
Size	1 1/2	1 1/4	1	3/4
Major Diam (d)	1.5 in	1.25 in	1 in	0.75 in
Threads per In.	6	7	8	10
Minor Diam (dr)	1.1585 in2	1.0644 in2	0.8376 in2	0.6201 in2
Tensile Area (At)	1.4053 in2	0.9691 in2	0.6057 in2	0.3345 in2

SAE Specifications and Strengths

Source: Ch.14 - Table 14.6 of Norton, R. 2009. "Machine Design." Pearson Prentice Hall.

SAE Grade	1	2	2	4	5	5	5.2	7	8	8.2
Outside Diam Min (in)	0.25	0.25	0.875	0.25	0.25	1.125	0.25	0.25	0.25	0.25
Outside Diam Max (in)	1.5	0.75	1.5	1.5	1	1.5	1	1.5	1.5	1
Minimum Proof Strength (kpsi)	33	55	33	65	85	74	85	105	120	120
Minimum Yield Strength (kpsi)	36	57	36	100	92	81	92	115	130	130
Minimum Tensile Strength (kpsi)	60	74	60	115	120	105	120	133	150	150

Pressure Input

Plow (Pl)	10	kpsi
Phigh (Ph)	20	kpsi
Area of die	24	in^2
ForceLow (Fl)	240	k-lbf
ForceHigh (Fh)	480	k-lbf

Bolt Analysis

Number of Bolts	4 bolts	4 bolts	4 bolts	6 bolts
ForceL per bolt	60 k-lbf	60 k-lbf	60 k-lbf	40 k-lbf
ForceH per bolt	120 k-lbf	120 k-lbf	120 k-lbf	80 k-lbf
Tensile stress low (at 10kpsi)	42.69551 kpsi	61.913115 kpsi	99.05894 kpsi	119.5815 kpsi
Tensile stress high (at 20kpsi	85.39102 kpsi	123.82623 kpsi	198.1179 kpsi	239.1629 kpsi

Summary of Possible Solutions

Number of Bolts	4	4	4	6
UNC Bolt Diameter	1 1/2	1 1/4	1	3/4
UNC Minor Diameter	1.1585	1.0644	0.8376	0.6201
Required Grade (at 10kpsi)	4	4	7	8
Required Grade (at 20kpsi)	7	n/a	n/a	n/a

Estimation of vertical force for threaded studs

Force due to pressurization on die span:

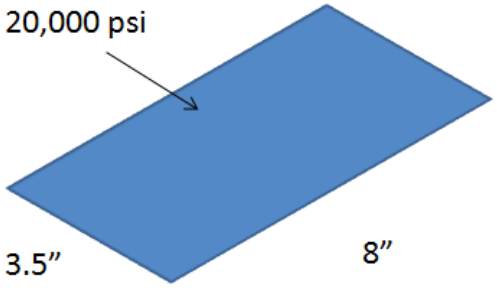

Pressure = 20 ksi

Area = 3.5*8 = 28 in^2

Total Force F_{total} = Pressure * Area = 560 kips

Bolt strength check and minimum diameter calc:

Proof strength (SAE grade 8) σ_{poof} = 120 ksi (Table 14.1, Norton, “Machine Design”)

Force per bolt $F_{bolt} = F_{total} / \#Bolts$

Required area $A_R = F_{bolt} / \sigma_{poof}$

		Approximate bolt diameter with greater tensile area:
6 bolts: F_{bolt} = 93.3 kips	A_R = 0.788 in^2	D_{bolt} = 1 $^1/_8$ in UNC
8 bolts: F_{bolt} = 70 kips	A_R = 0.583 in^2	D_{bolt} = 1 in UNC

End-block shear pin sizing

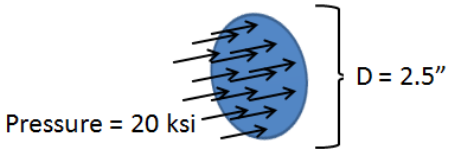

End-block force:

$F_{Horz} = P\ (\pi\ D^2)/4 = 98$ kips (= 436 kN)

Use dowel pins to take shear component of F_{horz}

2 pins, $F_{pin} = 49$ kips

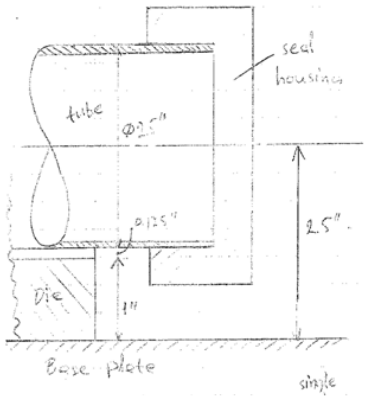

Shear pin sizing:

Machine pin strength $\tau = 120$ ksi
(Machinery Handbook p. 1577)

$\tau = F_{pin} / A_{pin}$

➔ $d_{min} = \sqrt{[(4/\pi)\ (Fpin/2)]} = 0.693”$

Use ¾” shear pins

Calculation of End-block Friction force:

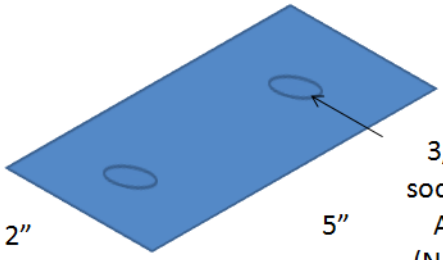

3/8” – 16 UNC
socket head bolts
$A_T = 0.775$ in^2
(Norton Pg. 816)

Bolt preload $\sigma_{preload} = 120$ ksi (Norton Pg. 834)

Force preload $F_{bolt} = \sigma_{preload} * A_T = 9.3$ kips

Bolt Torque $T_{bolt} = 0.21*F*Dbolt = 732$ in*lb = 61 ft-lb

Per Bolt (2x)

Assume $\mu = 0.4$ (Machinery Handbook, p. 189, Steel on steel, dry = 0.8)

2 bolts: $F_{total} = F_{bolt} * 2 = 18.66$ kips

$F_{friction} = \mu * F_{total} = 7.43$ kips

4 bolts: $F_{total} = F_{bolt} * 4 = 37.33$ kips

$F_{friction} = \mu * F_{total} = 14.86$ kips

APPENDIX D

TENSILE TEST FOR THREADED RODS

Tensile test of grade 8 threaded rod (strength validation of vertical studs)

Dimension : Diameter	0.3	in	Dreduced	0.375	
Dimension : Length	2.25	in	Areduced	0.110447	
Dimension : Final diameter	0.2	in			
Dimension : Final length	3	in	Max Load	19910.5	(lbf)
			Max		
Dimension : Geometry	Circular		Stress	180024.8	(psi)
Strain : Axial Gauge Length					
(Strain Source)	1	in	Yield	164073	(psi)
Test : Rate 1	0.045	in/min			

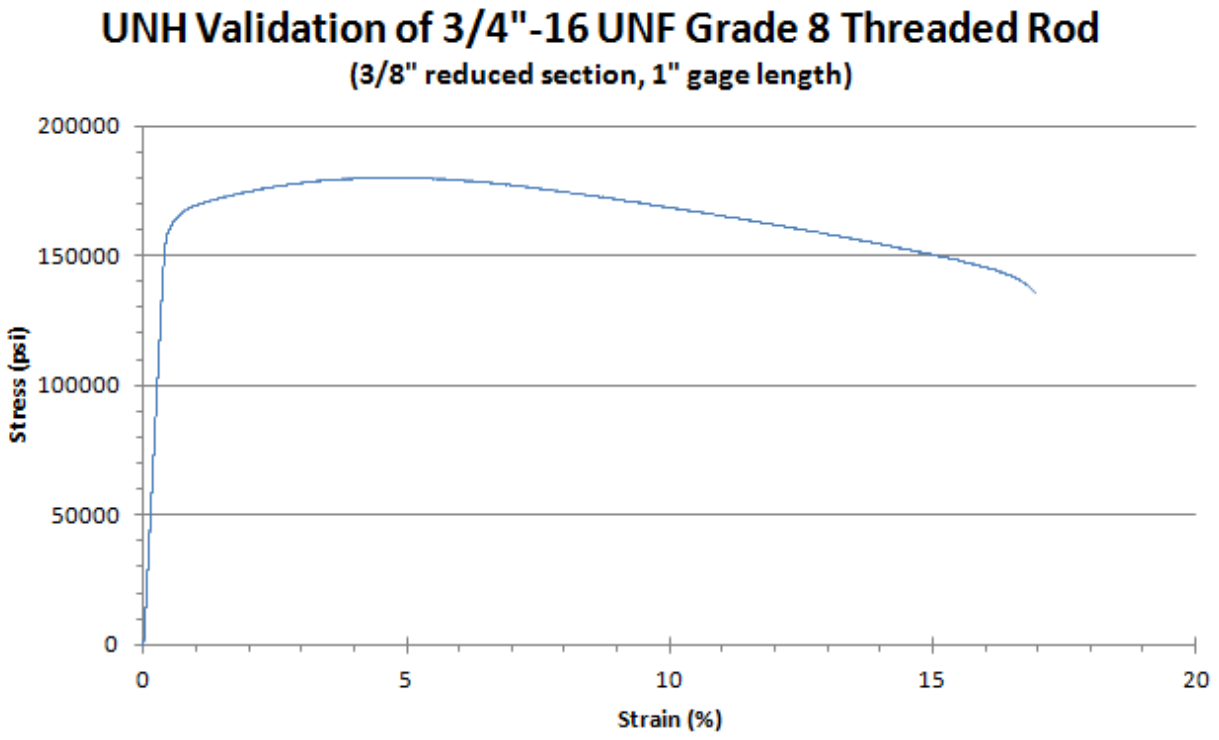

APPENDIX E

INSTRON DAQ RESOLUTION CALCULATIONS

Load cell and strain resolution for elastic testing of Al-6061-T4 specimens.

Instron Loadcell (X-monitor out to NI 9215 DAQ)

A/D Converter Properties

dblMinRange := −10V

dblMaxRange := 10V

dblRange := dblMaxRange − dblMinRange = 20 V

$dblResolution := 2^{16} = 6.554 \times 10^{4}$

$dblMinResolution := \frac{dblRange}{dblResolution} = 0.305 \cdot mV$

Loadcell Properties

dblMinRange := −100kN

dblMaxRange := 100kN

dblRange := dblMaxRange − dblMinRange = 200·kN

$dblResolution := 2^{16} = 6.554 \times 10^{4}$

$dblMinResolution := \frac{dblRange}{dblResolution} = 3.052 \cdot N$

A/D Converter Properties

dblVoltageRange := 20V (+/- 10 V)

dblGageLength := 25.4mm

dblMinRange := −15%

dblMaxRange := 55%

dblStrainRange := dblMaxRange − dblMinRange = 70·%

dblExtensometerRange := dblStrainRange·dblGageLength = 17.78·mm

$dblResolution := 2^{16} = 6.554 \times 10^{4}$

$dblMinExtensometerResolution := \frac{dblExtensometerRange}{dblResolution} = 2.713 \times 10^{-4} \cdot mm$

$dblMinStrainResolution := \frac{dblStrainRange}{dblResolution} = 1.068 \times 10^{-5} \cdot \frac{mm}{mm}$

Strain gage resolution for C2A-06-062LT-350 T-rosette Wheatstone quarter bridge

A/D Converter Properties

dblMinRange := −10V

dblMaxRange := 10V

dblRange := dblMaxRange − dblMinRange = 20V

$dblResolution := 2^{16} = 6.554 \times 10^{4}$

$dblMinResolution := \frac{dblRange}{dblResolution} = 0.305 \cdot mV$

Strain Gage Properties (C2A-06-062LT-350)

GF := 2.05

Elastic Test Properties

dblMaxStrain := 5%

dblDesiredVoltage := 10V

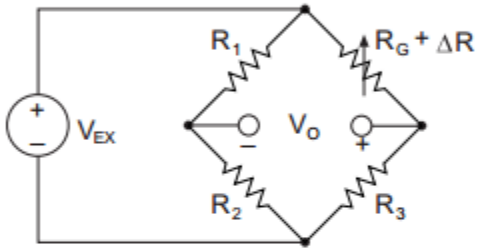

Wheatstone Bridge Properties

$R_1 := 350\Omega$

$R_2 := 350\Omega$

$R_3 := 350\Omega$

$R_G := 350\Omega$

$V_{excite} := 10V$

$$\frac{V_O}{V_{EX}} = -\frac{GF \bullet \varepsilon}{4}\left(\frac{1}{1 + GF \bullet \frac{\varepsilon}{2}}\right)$$

$$V_{Out} := \frac{-GF \cdot dblMaxStrain}{4} \cdot \left(\frac{1}{1 + GF \cdot \frac{dblMaxStrain}{2}}\right) \cdot V_{excite} = -0.244\,V$$

$$V_{out2} := \frac{R_1 \cdot R_2}{(R_1 + R_2)^2} \cdot (-GF \cdot dblMaxStrain) \cdot V_{excite} = -0.256\,V$$

$$V_{out3} := \frac{GF \cdot dblMaxStrain}{4 + 2 \cdot GF \cdot dblMaxStrain} \cdot V_{excite} = 0.244\,V$$

APPENDIX F

RHTT STRAIN RATE CALCULATION

Distance: $D_{crosshead} := 18\,mm$

Time: $T_{crosshead} := 300s$

INPUT VARIABLE(S)

Crosshead velocity: $V_{crosshead} := \frac{D_{crosshead}}{T_{crosshead}}$ $V_{crosshead} = 2.362 \times 10^{-3}\,\frac{in}{s}$

Punch Angle: $\theta_{punch} := 30deg$

Initial Radius: $r_i := \frac{60mm}{2}$ $r_i = 1.181\,in$

Initial Circumference: $C_i := 2 \cdot \pi \cdot r_i$ $C_i = 7.421\,in$

Gage Length: $GageLength := C_i$

Final Radius: $r_f := r_i + D_{crosshead} \cdot \sin(\theta_{punch})$ $r_f = 39\,mm$

Initial Circumference: $C_f := 2 \cdot \pi \cdot r_f$ $C_f = 245.044\,mm$

Change in Length: $\Delta C := C_f - C_i$ $\Delta C = 56.549\,mm$

Circumference Strain: $\varepsilon_{circumference} := \frac{\Delta C}{GageLength}$ $\varepsilon_{circumference} = 0.3$

Strain Rate: $\varepsilon_{dot} := \frac{\varepsilon_{circumference}}{T_{crosshead}}$

$\varepsilon_{dot} = 1 \times 10^{-3}\,\frac{1}{s}$

APPENDIX G

MATLAB ROUTINE FOR STRESS-STRAIN CURVE FILTERING

```
clc;
clear all;
close all;
fprintf('** BEGIN CURVE SMOOTHING! **\n');
      % SETTINGS AND CONTROLS %
%%%%%%%%%%%%%%%%%%%%%%%%%%%%%%%%%%%%%%%%%%%%
dblMinStressIncrease = .1;  %%%%%%%%%%
%%%%%%%%%%%%%%%%%%%%%%%%%%%%%%%%%%%%%%%%%%%%
dblMaxStrain = .188;             %%%%%%%%%%
%%%%%%%%%%%%%%%%%%%%%%%%%%%%%%%%%%%%%%%%%%%%
intNumPointsOut = 100;       %%%%%%%%%%
%%%%%%%%%%%%%%%%%%%%%%%%%%%%%%%%%%%%%%%%%%%%

strSource1='SOURCE\\Al-6061-T4-D1.csv';
%strSource2='SOURCE\\Al-6061-T4-D4.csv';
strFilteredOutput='OUTPUT\\Al-6061-T4-D-AvgFilt.csv';

%Spline the curves at the same strain values.
strOutput1 = SplinePoints(strSource1, dblMaxStrain, intNumPointsOut);
%strOutput2 = SplinePoints(strSource2, dblMaxStrain, intNumPointsOut);

%Read curve data from files
MyData1 = csvread(strOutput1);
%MyData2 = csvread(strOutput2);

%Average the splined values to find the effective curve.
%MyDataOut = zeros(intNumPointsOut,2);
%Stress= zeros(intNumPointsOut,1);
%Strain= zeros(intNumPointsOut,1);
%for i=1:intNumPointsOut
%    Stress(i) = (MyData1(i,1) +  MyData2(i,1))/2.0;
%    Strain(i) = (MyData1(i,2) +  MyData2(i,2))/2.0;
%    MyDataOut(i,1)= Stress(i);
%    MyDataOut(i,2)= Strain(i);
%end
MyDataOut =  MyData1;

%Smooth data using low pass filter.
order=5;
B = 1/order*(ones(order,1));
MyDataFilt = filtfilt(B,1,MyDataOut);
intNumFilteredPoints = length(MyDataFilt(:,1));
```

```
%Check to make sure filtering resulted in monotonic increasing stress.
%Remove non-monotonic values that are less than specified delta stress:
%%%%%%%%%%%%%%%%%%%%%%%%%%%%%%%%%%%%%%%%
%dblMinStressIncrease = 0.01;  %%%%%%%%%%
%%%%%%%%%%%%%%%%%%%%%%%%%%%%%%%%%%%%%%%%
intRemoved = 999;
MyDataReFilt = MyDataFilt;
intNumFilteredPoints = intNumPointsOut;
intLoopCount = 1;
while (intRemoved > 0)
    %Check to make sure filtering resulted in monotonic increasing stress.
    %Remove non-monotonic values
    intRemoved = 0;
    intFilterIndex = 2;
    for i=2:length(MyDataReFilt(:,1));
        dblDelta = MyDataReFilt(intFilterIndex,1) -
MyDataReFilt(intFilterIndex-1,1);
        if(dblDelta<=dblMinStressIncrease)
            MyDataReFilt(intFilterIndex,:)=[];
            intRemoved = intRemoved + 1;
            intFilterIndex = 2;
        end
        intFilterIndex = intFilterIndex +1;
    end
    intLoopCount = intLoopCount +1;
end

intNumFilteredPoints = length(MyDataReFilt(:,1));
fprintf([num2str(intLoopCount) ' items removed during data check.\n']);

% intRemoved = 0;
MyDataPlastic = MyDataReFilt;
intNumFilteredPoints = length(MyDataPlastic(:,1));

%plot and check data
%Compare all the curves to the resultant curve.
plot(MyData1(:,2),MyData1(:,1),'-r',MyDataOut(:,2),MyDataOut(:,1),'-g');

%Compare entire curve for filtered and unfiltered curves
figure;
plot(MyDataFilt(:,2),MyDataFilt(:,1),'-r',MyDataOut(:,2),MyDataOut(:,1),'-
g');

%Compare elastic-plastic transition for filtered and unfiltered curves
figure;
intStart=1;
intEnd=100;
plot(MyDataFilt(intStart:intEnd,2),MyDataFilt(intStart:intEnd,1),'-
r',MyDataOut(intStart:intEnd,2),MyDataOut(intStart:intEnd,1),'-g');

%Save files
csvwrite(strOutput, MyDataOut);
csvwrite(strFilteredOutput, MyDataPlastic);
fprintf('** COMPLETE! **\n');
```

APPENDIX H

MATLAB ROUTINE FOR STRESS-STRAIN SMOOTHING AND EXTRAPOLATION

CurveSmoothingForAbaqus.m (subroutine)

```
function [strOutput] = SplinePoints(strSource, dblMaxStrain, intNumPointsOut)

%dblMaxStrain = max(Strain1);
%Must hardcode max strain so that strain increment is the same
%dblMaxStrain = 18;
%intNumPointsOut = 1000;
%strSource1='SOURCE\\Al-6061-T4-A1.csv';

MyData = csvread(strSource1);

intNumRows = length(MyData);
for i=1:intNumRows
    Stress1(i) = MyData(i,1);
    Strain1(i) = MyData(i,2);
end


SStress1(1)=0;
SStrain1(1)=0;
for i=2:intNumPointsOut
    dblStrain = (i-1)*dblMaxStrain/intNumPointsOut;
    SStress1(i) = spline(Strain1, Stress1, dblStrain);
    SStrain1(i) = dblStrain;

end

strOutput = strSource
intLength = length(strSource)-4;
strOutput = [sprintf(['%.' num2str(intLength) 's'],strSource) '_TEMP.csv']

return;
```

SmoothBaseMaterial.m (example script using single test data set)

```
clc;
clear all;
close all;

fprintf('** BEGIN CURVE SMOOTHING! **\n');

      % SETTINGS AND CONTROLS %
%%%%%%%%%%%%%%%%%%%%%%%%%%%%%%%%%%%%%%%%
dblMinStressIncrease = .1;  %%%%%%%%%%
%%%%%%%%%%%%%%%%%%%%%%%%%%%%%%%%%%%%%%%%
dblMaxStrain = .13;             %%%%%%%%%%
%%%%%%%%%%%%%%%%%%%%%%%%%%%%%%%%%%%%%%%%
intNumPointsOut = 100;       %%%%%%%%%%
%%%%%%%%%%%%%%%%%%%%%%%%%%%%%%%%%%%%%%%%
strFilteredInput='OUTPUT\\Al-6061-T4-A-AvgFilt-Input.csv';
strFilteredOutput='OUTPUT\\Al-6061-T4-A-AvgFilt-Final.csv';
MyDataOut = csvread(strFilteredInput);
%Spline the curves at the same strain values.
strOutput1 = SplinePoints2(strFilteredInput, dblMaxStrain, intNumPointsOut);

%Read curve data from files
MyDataOut = csvread(strOutput1);
MyDataFilt =  MyDataOut;
%Smooth data using low pass filter.
% order=4;
% B = 1/order*(ones(order,1));
% MyDataFilt = filtfilt(B,1,MyDataOut);
% intNumFilteredPoints = length(MyDataFilt(:,1));

%Check to make sure filtering resulted in monotonic increasing stress.
%Remove non-monotonic values that are less than specified delta stress:
%%%%%%%%%%%%%%%%%%%%%%%%%%%%%%%%%%%%%%%%
%dblMinStressIncrease = 0.01;  %%%%%%%%%%
%%%%%%%%%%%%%%%%%%%%%%%%%%%%%%%%%%%%%%%%

intRemoved = 999;
MyDataReFilt = MyDataFilt;
intNumFilteredPoints = intNumPointsOut;
intLoopCount = 1;
while (intRemoved > 0)
    %Check to make sure filtering resulted in monotonic increasing stress.
    %Remove non-monotonic values
    intRemoved = 0;
    intFilterIndex = 2;
    for i=2:length(MyDataReFilt(:,1));
        dblDelta = MyDataReFilt(intFilterIndex,1) -
MyDataReFilt(intFilterIndex-1,1);
        if(dblDelta<=dblMinStressIncrease)
            MyDataReFilt(intFilterIndex,:)=[];
            intRemoved = intRemoved + 1;
            intFilterIndex = 2;
        end
```

```
        intFilterIndex = intFilterIndex +1;
    end
    intLoopCount = intLoopCount +1;
end

intNumFilteredPoints = length(MyDataReFilt(:,1));
fprintf([num2str(intLoopCount) ' items removed during data check.\n']);


% intRemoved = 0;
MyDataPlastic = MyDataReFilt;
% for i=2:intNumFilteredPoints
%     dblDelta = MyDataReFilt(i,1) - MyDataReFilt(i-1,1);
%     if(dblDelta<=0)
%         MyDataPlastic(i-intRemoved,:)=[];
%         intRemoved = intRemoved + 1;
%     end
% end
% fprintf([num2str(intRemoved) ' items removed from 2nd data check']);

intNumFilteredPoints = length(MyDataPlastic(:,1));

%plot and check data
%Compare all the curves to the resultant curve.
plot(MyDataOut(:,2),MyDataOut(:,1),'-
r',MyDataPlastic(:,2),MyDataPlastic(:,1),'-g');

%Compare elastic-plastic transition for filtered and unfiltered curves
figure;
intStart=10;
intEnd=100;
plot(MyDataPlastic(intStart:intEnd,2),MyDataPlastic(intStart:intEnd,1),'-
r',MyDataOut(intStart:intEnd,2),MyDataOut(intStart:intEnd,1),'-g');


%Save files
csvwrite(strFilteredOutput, MyDataPlastic);
fprintf('** COMPLETE! **\n');
```

SmoothBaseMaterialFromTwoTests.m (example script using two sets of test data)

```
clc;
clear all;
close all;

fprintf('** BEGIN CURVE SMOOTHING! **\n');

      % SETTINGS AND CONTROLS %
%%%%%%%%%%%%%%%%%%%%%%%%%%%%%%%%%%%%%%%%
dblMinStressIncrease = .1;     %%%%%%%%%%
%%%%%%%%%%%%%%%%%%%%%%%%%%%%%%%%%%%%%%%%
dblMaxStrain = .18;            %%%%%%%%%%
%%%%%%%%%%%%%%%%%%%%%%%%%%%%%%%%%%%%%%%%
intNumPointsOut = 500;         %%%%%%%%%%
%%%%%%%%%%%%%%%%%%%%%%%%%%%%%%%%%%%%%%%%

strSource1='SOURCE\\Al-6061-T4-A2.csv';
strSource2='SOURCE\\Al-6061-T4-A5.csv';
strOutput='OUTPUT\\Al-6061-T4-A-Base-Avg.csv';
strFilteredOutput='OUTPUT\\Al-6061-T4-A-Base-AvgFilt.csv';

%Spline the curves at the same strain values.
strOutput1 = SplinePoints(strSource1, dblMaxStrain, intNumPointsOut);
strOutput2 = SplinePoints(strSource2, dblMaxStrain, intNumPointsOut);

%Read curve data from files
MyData1 = csvread(strOutput1);
MyData2 = csvread(strOutput2);

%Average the splined values to find the effective curve.
MyDataOut = zeros(intNumPointsOut,2);
Stress= zeros(intNumPointsOut,1);
Strain= zeros(intNumPointsOut,1);
for i=1:intNumPointsOut
    Stress(i) = (MyData1(i,1) +  MyData2(i,1))/2.0;
    Strain(i) = (MyData1(i,2) +  MyData2(i,2))/2.0;
    MyDataOut(i,1)= Stress(i);
    MyDataOut(i,2)= Strain(i);
end

%Smooth data using low pass filter.
order=2;
B = 1/order*(ones(order,1));
MyDataFilt = filtfilt(B,1,MyDataOut);
intNumFilteredPoints = length(MyDataFilt(:,1));

% intRemoved = 999;
% MyDataReFilt = MyDataFilt;
% intNumFilteredPoints = intNumPointsOut;
% intLoopCount = 1;
% while (intRemoved > 0)
%     %Check to make sure filtering resulted in monotonic increasing stress.
```

```
%     %Remove non-monotonic values
%     intRemoved = 0;
%     for i=2:intNumFilteredPoints
%         dblDelta = MyDataFilt(i,1) - MyDataFilt(i-1,1);
%         if(dblDelta<=0)
%             MyDataReFilt(i-intRemoved,:)=[];
%             intRemoved = intRemoved + 1;
%         end
%     end
%     fprintf([num2str(intRemoved) ' items removed from data check #'
num2str(intLoopCount) '\n']);
%     intNumFilteredPoints = length(MyDataReFilt(:,1));
%     intLoopCount = intLoopCount +1;
% end


%Check to make sure filtering resulted in monotonic increasing stress.
%Remove non-monotonic values that are less than specified delta stress:
%%%%%%%%%%%%%%%%%%%%%%%%%%%%%%%%%%%%%%%%
%dblMinStressIncrease = 0.01;  %%%%%%%%%%
%%%%%%%%%%%%%%%%%%%%%%%%%%%%%%%%%%%%%%%%

intRemoved = 999;
MyDataReFilt = MyDataFilt;
intNumFilteredPoints = intNumPointsOut;
intLoopCount = 1;
while (intRemoved > 0)
    %Check to make sure filtering resulted in monotonic increasing stress.
    %Remove non-monotonic values
    intRemoved = 0;
    intFilterIndex = 2;
    for i=2:length(MyDataReFilt(:,1));
        dblDelta = MyDataReFilt(intFilterIndex,1) -
MyDataReFilt(intFilterIndex-1,1);
        if(dblDelta<=dblMinStressIncrease)
            MyDataReFilt(intFilterIndex,:)=[];
            intRemoved = intRemoved + 1;
            intFilterIndex = 2;
        end
        intFilterIndex = intFilterIndex +1;
    end
    intLoopCount = intLoopCount +1;
end

intNumFilteredPoints = length(MyDataReFilt(:,1));
fprintf([num2str(intLoopCount) ' items removed during data check.\n']);




% intRemoved = 0;
MyDataPlastic = MyDataReFilt;
% for i=2:intNumFilteredPoints
%     dblDelta = MyDataReFilt(i,1) - MyDataReFilt(i-1,1);
%     if(dblDelta<=0)
```

```
%         MyDataPlastic(i-intRemoved,:)=[];
%         intRemoved = intRemoved + 1;
%     end
% end
% fprintf([num2str(intRemoved) ' items removed from 2nd data check']);

intNumFilteredPoints = length(MyDataPlastic(:,1));

%plot and check data
%Compare all the curves to the resultant curve.
plot(MyData1(:,2),MyData1(:,1),'-r',MyData2(:,2),MyData2(:,1),'-
b',MyDataOut(:,2),MyDataOut(:,1),'-g');

%Compare entire curve for filtered and unfiltered curves
figure;
plot(MyDataFilt(:,2),MyDataFilt(:,1),'-r',MyDataOut(:,2),MyDataOut(:,1),'-
g');

%Compare elastic-plastic transition for filtered and unfiltered curves
figure;
intStart=1;
intEnd=100;
plot(MyDataFilt(intStart:intEnd,2),MyDataFilt(intStart:intEnd,1),'-
r',MyDataOut(intStart:intEnd,2),MyDataOut(intStart:intEnd,1),'-g');


%Save files
csvwrite(strOutput, MyDataOut);
csvwrite(strFilteredOutput, MyDataPlastic);
fprintf('** COMPLETE! **\n');
```

APPENDIX I

Al-6061-T4 MATERIAL CURVES FOR ABAQUS

Abaqus input file (*.inp) definition for axial base material

```
** MATERIALS
**
** Material data from Batch 1.
** Extrapolation Model 1 7/24/2012
*Material, name=Al-6061-T4-Base-2016
*Elastic
69800., 0.33
*Plastic
  91.64,       0.
 106.71, 0.000255
 121.67, 0.000399
 132.76, 0.000598
 140.27, 0.000849
 144.96, 0.001142
 147.85,  0.00146
 149.77, 0.001792
 151.24, 0.002131
 152.52, 0.002472
  153.7, 0.002815
  154.8, 0.003159
 155.84, 0.003504
 156.84,  0.00385
 157.76, 0.004196
 158.64, 0.004544
 159.49, 0.004891
 160.29,  0.00524
 161.13, 0.005587
 161.91, 0.005936
 162.72, 0.006284
 163.52, 0.006633
 164.28, 0.006982
 165.07,  0.00733
  165.8,  0.00768
 166.53, 0.008029
 167.23, 0.008379
  167.9, 0.008729
 168.58,  0.00908
 169.28,  0.00943
 169.99, 0.009779
 170.69, 0.010129
 171.43, 0.010478
 172.11, 0.010829
 172.82, 0.011178
 173.55, 0.011528
 174.22, 0.011878
 174.95, 0.012227
 175.65, 0.012577
 176.32, 0.012928
 176.99, 0.013278
 177.67, 0.013628
 178.37, 0.013978
  179.1, 0.014327
 179.84, 0.014677
 180.53, 0.015027
 181.18, 0.015377
```

181.81, 0.015728
182.47, 0.016079
183.16, 0.016429
183.85, 0.016779
184.53, 0.017129
185.18, 0.017479
185.82, 0.01783
186.46, 0.018181
187.13, 0.018531
187.81, 0.018881
188.48, 0.019232
189.17, 0.019582
189.84, 0.019932
190.44, 0.020283
191.06, 0.020634
191.64, 0.020986
192.19, 0.021338
 192.8, 0.021689
193.39, 0.02204
193.98, 0.022392
194.62, 0.022743
195.25, 0.023094
195.86, 0.023445
196.48, 0.023796
197.08, 0.024147
197.67, 0.024499
198.29, 0.02485
198.93,   0.0252
199.58, 0.025551
200.19, 0.025902
200.78, 0.026254
201.34, 0.026605
 201.9, 0.026957
202.46, 0.027309
203.04, 0.027661
203.61, 0.028013
204.21, 0.028364
204.82, 0.028715
205.43, 0.029066
206.03, 0.029418
206.61, 0.029769
207.18, 0.030121
207.72, 0.030473
 208.3, 0.030825
208.86, 0.031177
209.42, 0.031528
209.97, 0.03188
 210.5, 0.032233
211.06, 0.032585
211.63, 0.032936
212.22, 0.033288
212.81, 0.033639
213.37, 0.033991
 213.9, 0.034344
214.43, 0.034696
214.95, 0.035048
215.49, 0.035401
216.03, 0.035753
216.53, 0.036106
217.07, 0.036458
217.57, 0.03681
218.06, 0.037163
218.56, 0.037516
219.04, 0.037869
219.53, 0.038222
220.07, 0.038574
220.61, 0.038926
 221.1, 0.039279
221.63, 0.039632
222.12, 0.039985
222.62, 0.040337

223.15, 0.04069
223.66, 0.041042
224.19, 0.041395
224.66, 0.041748
225.11, 0.042101
225.57, 0.042455
226.01, 0.042808
226.53, 0.043161
227.05, 0.043513
227.56, 0.043866
228.07, 0.044218
228.55, 0.044572
229.03, 0.044925
229.53, 0.045277
230.02, 0.04563
230.48, 0.045984
230.93, 0.046337
231.36, 0.046691
231.81, 0.047044
232.25, 0.047398
232.72, 0.047751
233.19, 0.048104
233.66, 0.048458
234.17, 0.04881
234.66, 0.049163
235.17, 0.049516
 235.6, 0.049869
236.02, 0.050223
236.42, 0.050578
 236.8, 0.050932
237.26, 0.051285
237.73, 0.051639
238.21, 0.051992
238.68, 0.052345
 239.1, 0.052699
239.49, 0.053053
239.88, 0.053408
240.29, 0.053762
 240.7, 0.054116
241.13, 0.054469
241.56, 0.054823
241.99, 0.055177
242.42, 0.055531
242.85, 0.055885
243.25, 0.056239
243.67, 0.056593
244.06, 0.056947
244.44, 0.057301
244.86, 0.057655
245.24, 0.05801
245.67, 0.058364
246.12, 0.058717
246.56, 0.059071
246.99, 0.059425
247.39, 0.059779
247.76, 0.060133
248.08, 0.060489
248.38, 0.060844
 248.7,   0.0612
249.01, 0.061555
249.42, 0.061909
249.87, 0.062263
250.34, 0.062616
250.77, 0.06297
251.15, 0.063324
251.51, 0.063679
251.86, 0.064034
252.26, 0.064388
252.68, 0.064742
253.03, 0.065097
253.37, 0.065452

253.69, 0.065808
253.98, 0.066163
254.37, 0.066518
254.73, 0.066873
 255.1, 0.067227
255.47, 0.067582
255.79, 0.067937
256.14, 0.068292
256.47, 0.068647
 256.8, 0.069003
257.14, 0.069358
257.46, 0.069713
257.79, 0.070068
258.14, 0.070423
258.46, 0.070779
258.81, 0.071133
259.14, 0.071489
259.44, 0.071844
259.77,   0.0722
260.09, 0.072555
260.42, 0.07291
260.79, 0.073265
261.14, 0.07362
261.51, 0.073974
261.88, 0.074329
262.21, 0.074684
262.53, 0.07504
262.81, 0.075396
263.09, 0.075752
263.39, 0.076107
 263.7, 0.076463
264.06, 0.076817
 264.4, 0.077173
264.73, 0.077528
265.06, 0.077883
265.35, 0.078239
265.64, 0.078595
265.93, 0.07895
 266.2, 0.079306
266.52, 0.079662
266.83, 0.080017
267.13, 0.080373
267.44, 0.080729
267.71, 0.081085
268.02, 0.08144
268.34, 0.081796
268.67, 0.082151
269.02, 0.082506
269.32, 0.082861
269.57, 0.083218
269.81, 0.083574
270.03, 0.083931
270.29, 0.084287
270.61, 0.084643
270.93, 0.084998
271.24, 0.085354
271.53, 0.085709
271.77, 0.086066
272.04, 0.086422
272.31, 0.086778
272.57, 0.087134
272.85, 0.08749
 273.1, 0.087847
273.35, 0.088203
273.65, 0.088559
273.93, 0.088915
274.24, 0.08927
274.56, 0.089625
274.83, 0.089982
275.12, 0.090337
275.38, 0.090694

```
 275.6,  0.09105
275.83, 0.091407
276.08, 0.091763
276.33,  0.09212
276.62, 0.092476
276.93, 0.092831
277.21, 0.093187
277.47, 0.093543
277.65, 0.093901
277.85, 0.094258
278.07, 0.094615
278.34, 0.094971
278.67, 0.095326
278.94, 0.095682
279.18, 0.096039
 279.4, 0.096395
 279.6, 0.096753
279.81, 0.097109
280.04, 0.097466
280.24, 0.097823
280.47,  0.09818
280.72, 0.098536
281.03, 0.098892
281.31, 0.099248
281.54, 0.099604
281.76, 0.099961
281.88,  0.10032
282.08, 0.100677
 282.3, 0.101033
282.55,  0.10139
282.86, 0.101745
283.15, 0.102101
283.43, 0.102457
283.67, 0.102814
283.88, 0.103171
284.08, 0.103528
284.27, 0.103885
284.47, 0.104242
284.66, 0.104599
284.86, 0.104956
285.08, 0.105313
285.28,  0.10567
285.51, 0.106027
285.73, 0.106384
285.93, 0.106741
286.19, 0.107097
286.42, 0.107454
286.63, 0.107811
286.85, 0.108168
  287., 0.108525
287.18, 0.108883
287.37,  0.10924
287.58, 0.109597
287.79, 0.109954
287.96, 0.110311
288.12, 0.110669
288.24, 0.111027
288.38, 0.111385
288.55, 0.111743
288.72,   0.1121
288.92, 0.112458
289.11, 0.112815
289.29, 0.113172
289.48, 0.113529
289.71, 0.113886
289.94, 0.114243
290.19, 0.114599
 290.4, 0.114956
290.55, 0.115314
290.71, 0.115672
 290.9, 0.116029
```

```
291.09, 0.116386
291.35, 0.116742
291.59, 0.117099
291.73, 0.117457
291.89, 0.117815
292.03, 0.118173
292.15, 0.118531
292.35, 0.118888
292.54, 0.119245
 292.7, 0.119603
292.87,  0.11996
293.01, 0.120318
293.28, 0.121034
293.43, 0.121392
293.61,  0.12175
293.84, 0.122106
293.98, 0.122464
294.15, 0.122822
294.32, 0.123179
294.43, 0.123538
294.61, 0.123895
294.79, 0.124253
294.94,  0.12461
295.15, 0.124967
295.33, 0.125325
295.47, 0.125683
295.64,  0.12604
295.77, 0.126398
 295.9, 0.126757
296.04, 0.127115
296.16, 0.127473
296.28, 0.127831
 296.4, 0.128189
296.53, 0.128547
 296.7, 0.128905
296.86, 0.129263
297.02,  0.12962
297.18, 0.129978
297.29, 0.130336
297.42, 0.130695
297.54, 0.131053
297.75,  0.13177
297.92, 0.132127
 298.1, 0.132485
298.28, 0.132842
298.46,   0.1332
298.56, 0.133558
298.67, 0.134276
298.79, 0.134995
 298.9, 0.135353
299.02, 0.135711
299.13,  0.13607
299.23, 0.136428
299.34, 0.137147
299.48, 0.138225
299.59, 0.138943
299.72, 0.139661
299.85, 0.140739
302.08,     0.15
309.05,     0.18
314.22,     0.22
316.81,     0.26
318.09,      0.3
318.83,     0.35
319.14,      0.4
319.32,      0.5
319.35,      0.6
319.36,      0.7
319.36,      0.8
319.36,      0.9
319.36,       1.
```

Abaqus input file (*.inp) definition for axial weld material

```
** MATERIALS
* Material data from Batch D.
** 7/13/2012
*Material, name=Al-6061-T4-Weld
*Elastic
69800., 0.33
*Plastic
 103.44,          0.
  116.9, 0.000127759
 127.84, 0.000229392
 136.02, 0.000370979
 141.65, 0.000549479
  145.3, 0.000756642
 147.66, 0.000982478
 149.29,  0.00121888
 150.52,  0.00146108
 151.57,  0.00170588
 152.47,  0.00195285
 153.28,  0.00220112
 154.11,  0.00244911
 154.85,   0.0026984
  155.6,  0.00294754
 156.34,  0.00319683
 156.96,  0.00344785
 157.56,  0.00369917
 158.09,  0.00395149
 158.59,  0.00420426
 159.14,  0.00445629
 159.71,  0.00470804
 160.32,  0.00495921
 160.95,  0.00521009
 161.58,  0.00546097
 162.14,  0.00571287
 162.69,   0.0059649
 163.18,  0.00621781
 163.65,  0.00647101
 164.21,   0.0067229
 164.75,  0.00697508
 165.31,  0.00722698
 165.89,  0.00747858
 166.46,  0.00773033
 166.98,   0.0079828
  167.5,  0.00823528
 167.98,  0.00848833
 168.45,  0.00874152
 168.96,  0.00899414
 169.46,   0.0092469
   170.,  0.00949909
 170.52,  0.00975156
 171.04,    0.010004
 171.57,   0.0102564
 172.07,   0.0105091
 172.55,   0.0107622
   173.,   0.0110157
 173.41,   0.0112697
 173.87,   0.0115231
 174.39,   0.0117755
 174.89,   0.0120283
 175.37,   0.0122813
 175.85,   0.0125344
 176.27,   0.0127883
 176.76,   0.0130412
 177.29,   0.0132936
 177.79,   0.0135463
 178.28,   0.0137992
  178.7,   0.0140531
```

```
179.18,   0.0143062
 179.7,   0.0145587
180.26,   0.0148106
180.85,    0.015062
181.32,   0.0153152
181.74,   0.0155691
182.14,   0.0158233
182.56,   0.0160773
183.03,   0.0163305
183.55,   0.0165829
184.01,   0.0168363
184.46,   0.0170898
184.89,   0.0173435
185.29,   0.0175977
185.76,   0.0178509
186.22,   0.0181043
186.69,   0.0183575
187.18,   0.0186104
187.59,   0.0188645
187.99,   0.0191187
188.35,   0.0193735
188.74,   0.0196278
189.25,   0.0198804
 189.8,   0.0201325
190.39,   0.0203839
190.92,   0.0206362
191.31,   0.0208906
191.65,   0.0211457
191.97,    0.021401
192.31,   0.0216561
192.74,   0.0219099
193.21,   0.0221631
193.72,   0.0224157
194.22,   0.0226685
194.69,   0.0229217
195.12,   0.0231754
 195.5,   0.0234299
195.87,   0.0236846
196.22,   0.0239395
196.62,   0.0241937
197.05,   0.0244475
197.55,   0.0247003
198.09,   0.0249525
 198.6,   0.0252051
199.11,   0.0254577
199.55,   0.0257113
199.91,   0.0259661
200.25,   0.0262212
200.58,   0.0264764
200.94,   0.0267312
201.35,   0.0269853
201.76,   0.0272393
202.22,   0.0274927
202.69,   0.0277459
203.16,   0.0279991
203.61,   0.0282525
203.99,    0.028507
204.35,   0.0287618
204.72,   0.0290165
 205.1,    0.029271
205.49,   0.0295253
 205.9,   0.0297794
206.32,   0.0300333
206.78,   0.0302867
207.25,   0.0305399
 207.7,   0.0307933
208.14,    0.031047
208.49,   0.0313019
208.88,   0.0315563
209.22,   0.0318113
209.54,   0.0320667
```

```
 209.9,   0.0323215
210.24,   0.0325766
210.63,   0.0328309
211.06,   0.0330847
211.49,   0.0333385
211.94,    0.033592
212.42,    0.033845
212.89,   0.0340982
213.32,    0.034352
213.73,   0.0346061
214.08,    0.034861
214.41,   0.0351162
214.77,    0.035371
 215.1,   0.0356262
 215.4,   0.0358819
215.67,    0.036138
215.99,   0.0363933
216.34,   0.0366483
 216.8,   0.0369016
217.32,   0.0371541
217.82,   0.0374068
218.33,   0.0376595
218.75,   0.0379134
219.12,    0.038168
219.45,   0.0384232
219.75,   0.0386789
220.05,   0.0389346
220.36,   0.0391901
 220.7,   0.0394452
220.99,    0.039701
221.28,   0.0399568
221.57,   0.0402126
221.88,   0.0404681
222.26,   0.0407226
222.69,   0.0409763
223.16,   0.0412295
223.56,   0.0414838
223.94,   0.0417383
 224.3,    0.041993
224.63,   0.0422483
225.01,   0.0425028
225.39,   0.0427573
225.76,   0.0430119
226.11,   0.0432668
226.45,   0.0435219
226.77,   0.0437773
227.11,   0.0440324
227.43,   0.0442877
227.68,   0.0445441
227.91,   0.0448008
228.16,   0.0450572
228.48,   0.0453125
 228.9,   0.0455665
229.39,   0.0458194
229.83,    0.046073
230.22,   0.0463273
230.55,   0.0465826
230.87,   0.0468379
231.21,    0.047093
231.57,   0.0473478
231.95,   0.0476023
232.28,   0.0478575
232.59,    0.048113
232.86,   0.0483691
233.09,   0.0486258
233.35,    0.048882
233.63,    0.049138
233.92,   0.0493938
234.22,   0.0496494
234.51,   0.0499052
234.81,   0.0501609
```

```
235.13,   0.0504163
235.44,   0.0506718
235.75,   0.0509273
236.01,   0.0511835
236.26,   0.0514399
236.55,   0.0516957
236.89,   0.0519508
237.26,   0.0522054
237.67,   0.0524595
238.03,   0.0527143
238.34,   0.0529698
238.65,   0.0532253
238.92,   0.0534814
239.24,   0.0537368
239.61,   0.0539914
239.96,   0.0542463
240.33,    0.054501
240.63,   0.0547566
240.87,   0.0550132
241.12,   0.0552696
 241.4,   0.0555255
241.79,   0.0557799
 242.2,   0.0560339
242.56,   0.0562887
242.86,   0.0565444
243.07,   0.0568013
243.33,   0.0570576
243.67,   0.0573126
244.06,    0.057567
244.43,   0.0578216
244.77,   0.0580767
245.06,   0.0583325
245.34,   0.0585885
245.66,   0.0588438
245.96,   0.0590995
246.24,   0.0593554
 246.5,   0.0596117
246.72,   0.0598685
246.92,   0.0601256
247.12,   0.0603827
247.36,   0.0606392
 247.6,   0.0608957
247.89,   0.0611516
248.19,   0.0614072
248.42,   0.0616639
248.65,   0.0619205
248.86,   0.0621775
249.06,   0.0624346
249.34,   0.0626906
249.62,   0.0629465
 249.9,   0.0632025
 250.2,   0.0634581
250.45,   0.0637145
250.73,   0.0639704
250.96,   0.0642271
 251.2,   0.0644836
251.48,   0.0647396
251.68,   0.0649967
251.99,   0.0652522
252.31,   0.0655076
252.62,   0.0657631
252.99,   0.0660177
253.26,   0.0662738
 253.5,   0.0665303
253.71,   0.0667873
253.87,    0.067045
254.06,   0.0673022
254.25,   0.0675595
254.49,    0.067816
254.81,   0.0680714
255.18,    0.068326
```

```
255.52,   0.0685811
255.83,   0.0688366
256.05,   0.0690934
256.19,   0.0693514
 256.4,   0.0696084
256.64,   0.0698649
256.94,   0.0701205
257.31,   0.0703752
257.62,   0.0706307
257.87,   0.0708871
258.07,   0.0711442
258.23,   0.0714019
258.35,   0.0716601
258.55,   0.0719172
258.79,   0.0721738
259.04,   0.0724301
259.39,   0.0726851
259.69,   0.0729407
259.93,   0.0731973
260.16,   0.0734539
260.36,    0.073711
260.61,   0.0739674
260.91,   0.0742231
261.21,   0.0744787
261.47,    0.074735
261.67,   0.0749921
261.86,   0.0752493
262.02,    0.075507
262.25,   0.0757637
262.46,   0.0760206
262.66,   0.0762777
262.91,   0.0765341
263.12,   0.0767911
263.31,   0.0770483
263.53,   0.0773051
263.76,   0.0775618
264.01,   0.0778182
264.29,   0.0780741
264.54,   0.0783305
264.75,   0.0785875
264.96,   0.0788444
265.19,   0.0791011
265.44,   0.0793575
 265.7,   0.0796137
265.95,   0.0798701
266.16,   0.0801271
266.33,   0.0803846
 266.5,   0.0806422
266.67,   0.0808997
 266.9,   0.0811564
267.15,   0.0814127
267.39,   0.0816693
267.63,   0.0819258
267.81,   0.0821832
267.98,   0.0824407
268.14,   0.0826984
268.31,    0.082956
268.49,   0.0832133
 268.7,   0.0834703
268.96,   0.0837265
269.26,   0.0839822
269.61,   0.0842371
269.93,   0.0844925
270.16,   0.0847492
270.34,   0.0850066
270.48,   0.0852645
270.62,   0.0855225
270.84,   0.0857793
271.11,   0.0860354
271.37,   0.0862917
271.68,   0.0865472
```

```
271.96,   0.0868031
272.21,   0.0870595
272.44,   0.0873162
272.58,   0.0875741
272.78,   0.0880912
273.05,   0.0886073
273.26,   0.0888643
273.46,   0.0891214
273.65,   0.0893787
273.78,   0.0896368
274.03,   0.0909332
274.27,   0.0911897
274.57,   0.0914453
274.84,   0.0917014
275.06,   0.0919582
275.25,   0.0922155
275.47,   0.0924723
275.67,   0.0927294
275.85,   0.0929868
276.05,   0.0932439
276.22,   0.0935014
276.44,   0.0937583
276.61,   0.0940158
276.74,   0.0942739
276.88,   0.0945319
276.99,   0.0947903
 277.1,   0.0950487
277.24,   0.0955667
277.44,   0.0960838
277.65,   0.0963407
277.92,   0.0965968
278.15,   0.0968535
278.32,    0.097111
278.44,   0.0976293
278.56,   0.0981476
278.69,   0.0984057
278.85,   0.0986634
279.06,   0.0989203
279.24,   0.0991777
279.42,   0.0994351
279.56,   0.0996931
279.67,    0.100212
279.86,    0.101249
279.97,    0.101507
280.08,    0.101766
291.46,        0.12
303.13,        0.15
310.69,        0.18
316.76,        0.22
320.11,        0.26
321.94,         0.3
 323.1,        0.35
323.64,         0.4
324.01,         0.5
324.08,         0.6
 324.1,         0.7
 324.1,         0.8
 324.1,         0.9
 324.1,          1.
```

APPENDIX J

USING HYDROSTATIC ELEMENTS WITH ABAQUS 6.11

November 15, 2011 - Tube hydroforming project documentation by **Adam Kaplan**

Abaqus CAE Model:

Previous numerical modeling attempts focused on a working model of the tube hydroforming process with the appropriate 3D contact constraints implemented. These models used a linear ramp to a prescribed pressure to deform the tube; however, this methodology is incapable of allowing the pressure to decrease after reaching maximum value. This phenomenon is due to the tube thinning and becoming easier to deform. In order to capture the additional tube deformation after the peak pressure, hydrostatic fluid elements must be incorporated into the Abaqus CAE model.

Implementing Hydrostatic Elements in Abaqus:

Abaqus CAE does not yet support the hydrostatic elements in it's user interface, however the functionality is fully implemented in the Abaqus Solver. The hydrostatic elements must be manually added to the Abaqus Input file (.inp) in order for them to be used. There are some considerations when using hydrostatic elements:

1. Hydrostatic elements must share the same nodes with the solid surfaces they interact with.
2. A reference node must be included inside the cavity defined by the hydrostatic elements. This node defines the loading properties of the fluid cavity.
3. The reference node must lie on the planes of symmetry, if present.

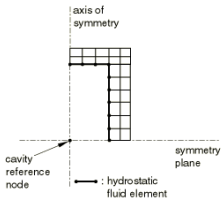

CAE does not yet support hydrostatic element implementation, however CAE can aid in the generation of nodes and elements required for the hydrostatic elements. In order to use CAE to perform most of the legwork, the following procedure should be followed:

1. Generate the solid model geometry; assign elements, materials, sections, and mesh.

2. Under the Features menu, add a **Reference Point** to control the properties of the fluid cavity. Note the XYZ coordinates of this point – the node number will need to be found in the input file. It will be used to control the fluid cavity loading.

3. Add any necessary surfaces to complete or "cap" the cavity. Surfaces can be added using the **Create Shell: Planar** from under the **Part** menu.

4. Select the hydrostatic cavity surface (for instance, the inside surfaces of a pressure vessel) and create a **Skin** named ***"CavitySkin"***. This is a surface that will share the nodes of the solid geometry.

5. Additional Planar surfaces may be required to enclose the cavity. Create as necessary.

6. Use Assign Element Type to set the skin elements to ***Shell*** **(S4R)** / ***(S3)*** / ***(S2)***.

7. Check normal of shell elements and flip as necessary.

At this point, the capabilities of CAE have been exhausted (as of version v6.11). Now the modifications will occur within the Input file (.inp). This file is located in the Temp directory on the main drive partition. The following modifications are necessary:

1. Change cavity elements from Shell to Hydrostatic Fluid and include in element set.
   For quadrilateral elements:
   The cavity is originally declared by the line: ****Element, type=S4R***
   Change this declaration to new type: ****Element, type=F3D4, elset=Cavity***
   For triangular elements:
   The cavity is originally declared by the line: ****Element, type=***S3
   Change this declaration to new type: ****Element, type=F3D3, elset=Cavity***
   For 2D line elements:
   The cavity is originally declared by the line: ****Element, type=S2***
   Change this declaration to new type: ****Element, type=F2D2, elset=Cavity***

2. The cavity **Reference Point** node number must be recorded in order to apply the load.
   Find the line with the coordinates defining the node. This is typically after the elements have been defined. For example, originally:
   **Node*
   255, 0., 0., 0.
   Change the declaration to include a node set.
   **Node, nset=CavityRef*
   255, 0., 0., 0.

3. The fluid properties must be set for the hydrostatic element set and reference node.
   Following the previous declarations, add the following:
   fluid property, elset=Cavity**, ref node=255, type=hydraulic*
   **fluid density*
   0.036

4. Find instance of the part in the assembly and record the name so part sets can be referenced.
   **Assembly, name=Assembly*
   Instance, name=Tube-3D-1**, part=Tube-3D*
   **End Instance*
   **End Assembly*

5. Under the appropriate STEP, add the loading of the fluid cavity:
   For pressure-controlled loading, use *boundary to set DOF #8:
   **boundary*
   255, 8,8, 2500
   For volume-controlled loading, use *fluid flux to set the volumetric flow rate into the cavity:
   **fluid flux*
   255, 0.1

6. Output the pressure and volume of the cavity for monitoring and post-processing. Add the following line to the Output section at the end of the file.

*node output, nset=CavityRef
pcav, cvol

The file is now setup and ready to be run through the Abaqus solver.

The following is an example of a hydrostatic fluid analysis:

```
*HEADING
…
*ELEMENT, TYPE=hydrostatic fluid element, ELSET=name_1
…
*ELEMENT, TYPE=fluid link element, ELSET=name_2
…
Define the hydrostatic fluid behavior
*PHYSICAL CONSTANTS, ABSOLUTE ZERO=
*FLUID PROPERTY, ELSET=name_1, REF NODE=number, TYPE=fluid type
The TYPE parameter is applicable only in an Abaqus/Standard
analysis.
…
*FLUID DENSITY
…
Define the compressibility and thermal expansion coefficient for a
hydraulic fluid (available only
in Abaqus/Standard)
*FLUID BULK MODULUS
…
*FLUID EXPANSION
…
Define the fluid link properties
*FLUID LINK, ELSET=name_2
…
Specify the initial conditions
*INITIAL CONDITIONS, TYPE=TEMPERATURE
…
*INITIAL CONDITIONS, TYPE=FLUID PRESSURE
…
**
*STEP
…
Change the temperature of the fluid
*TEMPERATURE
…
Change the amount of fluid in a cavity
*FLUID FLUX
…
*END STEP
```

```
*HEADING
 3D FLUID ELEMENT - a spherical fluid filled cavity in a cube
**
*PART, name=FIL-1
**
*NODE
 1,   0.,    0.,    0.
 2,  10.,    0.,    0.
 3,   0.,   10.,    0.
 4,  10.,   10.,    0.
 5,   0.,    0.,   10.
 6,  10.,    0.,   10.
 7,   0.,   10.,   10.
 8,  10.,   10.,   10.
 9,   5.,    0.,    0.
10,   0.,    5.,    0.
11,   0.,    0.,    5.
12,  3.535,  3.535,  0.
13,   0.,    3.535,  3.535
14,  3.535,  0.000,  3.535
15,  2.888,  2.888,  2.888
**
**
*ELEMENT, TYPE=C3D8,  ELSET=SURROUND
**
 1,  4,  2,  6,  8,  12,  9,  14,  15
 2,  3,  4,  8,  7,  10,  12,  15,  13
 3,  8,  6,  5,  7,  15,  14,  11,  13
**
** 4 noded Fluid elements
**
*ELEMENT, TYPE=F3D4, ELSET=FLUID
  11,  14,  15,  12,   9
  12,  15,  13,  10,  12
  13,  11,  13,  15,  14
**
*NODE, NSET=MFLUID
 880,  0, 0.
*FlUID PROPERTY, NAME=VENT,ELSET=FLUID,REF NODE=880,TYPE=hydraulic
*FLUID DENSITY
 1.E+2
*FLUID BULK MODULUS
 2.2E2
**
*SOLID SECTION, ELSET=SURROUND, MATERIAL=FIL
 1.,
*END PART
**
*assembly, name=assembly-1
*instance, name=FIL-1-1, part=FIL-1
**
*END INSTANCE
**
*NSET, NSET=BASE, INSTANCE=FIL-1-1,  internal
 2,  3,  4,  9,  10,  12
```

```
**
*NSET, NSET=YSYMM, INSTANCE=FIL-1-1,  internal
  2, 5,  6,  9,  11, 14
**
*NSET, NSET=XSYMM, INSTANCE=FIL-1-1, internal
  3, 5,  7,   10,  11,  13
**
*ELSET, ELSET=E1, internal, INSTANCE=FIL-1-1
 1, 2, 3
**
*SURFACE, TYPE=ELEMENT, name=outside
 E1, S1
**
*NSET, NSET=MFLUID, internal, INSTANCE=FIL-1-1
 880,
*end assembly
**
*MATERIAL, NAME=FIL
*ELASTIC
 1.E3 , 0.25
*DENSITY
 1600.
**
**
*BOUNDARY
 XSYMM,   1, 1,  0.
 YSYMM,   2, 2,  0.
  BASE,   3, 3,  0.
**=======================================
**
*STEP,inc=100, nlgeom
**
*STATIC, stabilize
 0.1,   1.,  1.0E-5, 0.1
**
*DSLOAD
outside,  P,  800
**
**
*Output, history
*NODE OUTPUT, NSET=MFLUID
PCAV, CVOL
**
*output, field
*node output, variable=preselect
U
*element output, variable=preselect
S, LE
*END STEP
```

An analysis with hydrostatic fluid:

```
*HEADING
…
*FLUID CAVITY, NAME=cavity_name, BEHAVIOR=behavior_name,
REF NODE=cavity_reference_node, SURFACE=surface_name
*FLUID BEHAVIOR, NAME=behavior_name
*FLUID DENSITY
Data line to define density
*FLUID BULK MODULUS
Data line to define  bulk modulus
*FLUID EXPANSION
Data line to define thermal expansion
**
*FLUID EXCHANGE, NAME=exchange_name, PROPERTY=exchange_property_name
cavity_reference_node
*FLUID EXCHANGE PROPERTY, NAME=exchange_property_name, TYPE=MASS FLUX
Data line to define mass flow rate per unit area
**
*INITIAL CONDITIONS, TYPE=TEMPERATURE
Data line to define initial temperature
*INITIAL CONDITIONS, TYPE=FLUID PRESSURE
Data line to define initial pressure
**
*STEP
**
*TEMPERATURE
Data line to define temperature
*FLUID EXCHANGE ACTIVATION
exchange_name
**
*END STEP
```

An airbag analysis with a mixture of ideal gases:

```
*HEADING
…
*FLUID CAVITY, NAME=chamber_1, MIXTURE=MOLAR FRACTION, ADIABATIC,
REF NODE=chamber_1_reference_node, SURFACE=surface_name_1
blank line
Oxygen,  0.2
Nitrogen,  0.75
Carbon_dioxide,  0.05
**
*FLUID CAVITY, NAME=chamber_2, BEHAVIOR=Air, ADIABATIC,
REF NODE=chamber_2_reference_node, SURFACE=surface_name_2
blank line
**
*FLUID BEHAVIOR, NAME=Air
*CAPACITY, TYPE=POLYNOMIAL
Data line to define heat capacity coefficient
*MOLECULAR WEIGHT
Data line to define molecular weight
**
*FLUID BEHAVIOR, NAME=Oxygen
*CAPACITY, TYPE=POLYNOMIAL
Data line to define heat capacity coefficient
*MOLECULAR WEIGHT
Data line to define molecular weight
**
*FLUID BEHAVIOR, NAME=Nitrogen
*CAPACITY, TYPE=POLYNOMIAL
Data line to define heat capacity coefficient
*MOLECULAR WEIGHT
Data line to define molecular weight
```

```
**
*FLUID BEHAVIOR, NAME=Carbon_dioxide
*CAPACITY, TYPE=POLYNOMIAL
Data line to define heat capacity coefficient
*MOLECULAR WEIGHT
Data line to define molecular weight
**
*FLUID INFLATOR, NAME=inflator, PROPERTY=inflator_property
chamber_1_reference_node
*FLUID INFLATOR PROPERTY, NAME=inflator_property,
TYPE=MASS TEMPERATURE
Data lines to define mass flow rate and gas temperature
*FLUID INFLATOR MIXTURE, TYPE=MOLAR FRACTION, NUMBER SPECIES=2
Carbon_dioxide, Nitrogen
Table to define molecular mass fraction
**
*FLUID EXCHANGE, NAME=exhaust, PROPERTY=exhaust_behavior
chamber_1_reference_node
*FLUID EXCHANGE PROPERTY, NAME=exhaust_behavior, TYPE=ORIFICE
Data line to specify orifice behavior
*FLUID EXCHANGE, NAME=leakage_1, PROPERTY=fabric_behavior
chamber_1_reference_node
*FLUID EXCHANGE, NAME=leakage_2, PROPERTY=fabric_behavior
chamber_2_reference_node
*FLUID EXCHANGE PROPERTY, NAME=fabric_behavior, TYPE=FABRIC LEAKAGE
Data line to specify fabric leakage behavior
**
*FLUID EXCHANGE, NAME=chamber_wall, PROPERTY=wall_behavior,
EFFECTIVE AREA=
chamber_1_reference_node, chamber_2_reference_node
*FLUID EXCHANGE PROPERTY, NAME=wall_behavior, TYPE=ORIFICE
Data line to specify orifice behavior
**
*AMPLITUDE, NAME=amplitude_name
Data line to define amplitude variations
*PHYSICAL CONSTANTS, UNIVERSAL GAS CONSTANT=
**
*INITIAL CONDITIONS, TYPE=FLUID PRESSURE
Data line to define initial pressure
*INITIAL CONDITIONS, TYPE=TEMPERATURE
Data line to define initial temperature
**
*STEP
**
*FLUID EXCHANGE ACTIVATION
exhaust, leakage_1, leakage_2,  chamber_wall
*FLUID INFLATOR ACTIVATION, INFLATION TIME AMPLITUDE=amplitude_name
inflator
**
*END STEP
```

APPENDIX K

MATLAB ROUTINES FOR HYDROSTATIC ELEMENTS

ExtractSection.m (subroutine)

```
function [NumLines] = ExtractSection(idSource, Key, idTempOutput)
    sLine='EMPTY';
    i=0;
    while (strcmp(sLine,Key)~=1 && ischar(sLine))
        i=i+1;
        sLine = fgets(idSource);
    end

    if(ischar(sLine)~=1)
          fprintf('     WARNING:::Requested key not found in Source File.\n')
          fprintf('     The end of the file was reached before the closing key:\n')
          fprintf('          ''%s''\n',Key(1:length(Key)-2));
          fprintf('     Please check to ensure this set is not needed. The file\n')
          fprintf('     conversion will continue and the file may (not) be usable.\n')
          NumLines=1;
          return;
    end

    %Continue until next delimeter found... '*'
    i=0;
    sLine = 'EMPTY';
    Key=sprintf('*');
    sLine = fgets(idSource); %first node values...
    while (strcmp(sLine(1),Key)~=1 && ischar(sLine))
        i=i+1;
        fprintf(idTempOutput, sLine);
        %get next line, and check while condition on next iter
        sLine = fgets(idSource);
    end

    NumLines = i;

    if(ischar(sLine)~=1)
          fprintf('     WARNING:::Requested key not found in Source File.\n')
          fprintf('     The end of the file was reached before the closing key:\n')
          fprintf('          ''%s''\n',Key(1:length(Key)-2));
          fprintf('     Please check to ensure this set is not needed. The file\n')
          fprintf('     conversion will continue and the file may (not) be usable.\n')
          NumLines=1;
          return;
    end
return;
```

HSE_Generator_Envelope_FordAl6061.m

```
clear all;
close all;
clc;
%TODO:
%TEST PRESSURE CONTROL


THICKNESS_EDGES = 1;     %(1) Full edge sets      (2) Skip
THICKNESS_SETS = 2;      %(1) 2 point node sets   (2) Skip

%*****************************************************
%TUBE MATERIAL SELECTION*******************************

strTubeMaterial='FordAl6061T4';
%strElasticMod ='9.5e+06., 0.3';
strElasticMod = '10000., 0.3'

%0.035in thick tube
strSource='SOURCE\\March_FordAl6061.inp';
strOutput=strcat('OUTPUT\\March_HSE_',strTubeMaterial,'.inp');


%*************************************************************************
%LOAD CONTROL************************************************************
V_CONTROL=1;        %Volume control using a hydrostatic element cavity
                    %otherwise Pressure control using internal dist. load.
%*************************************************************************

%*************************************************************************
%VOLUME CONTROL SPECIFIC OPTIONS*****************************************
if(V_CONTROL==1)
  NO_STIFF_PAD=1;  %No tension elements, allows axial contraction
end                %of tube while maintaining contact elements for cavity.
%*************************************************************************

%Credits!
fprintf('************************************************\n');
fprintf('************************************************\n');
fprintf('**          HSE INPUT PRE-PROCESSOR           **\n');
fprintf('**          By: Adam Kaplan                   **\n');
fprintf('************************************************\n');
fprintf('************************************************\n');
fprintf('INPUT:   ''%s''\n',strSource);
fprintf('OUTPUT:  ''%s''\n',strOutput);

%*****************************************
%(1) Default file heading
%*****************************************
idOutput = fopen(strOutput,'w');
fprintf(idOutput, '*Heading\r\n');
fprintf(idOutput, '** Generated by: ADAM KAPLAN!\r\n');
fprintf(idOutput, '*Preprint, echo=NO, model=NO, history=NO, contact=YES\r\n');
fprintf(idOutput, '**\r\n');
fprintf(idOutput, '** PARTS\r\n');
fprintf(idOutput, '**\r\n');
```

```
fprintf(idOutput, '*Part, name=Die\r\n');
fprintf(idOutput, '*End Part\r\n');
fprintf(idOutput, '**  \r\n');
fprintf(idOutput, '*Part, name=Seal-Analytical\r\n');
fprintf(idOutput, '*End Part\r\n');
fprintf(idOutput, '**  \r\n');
fprintf(idOutput, '*Part, name=Tube\r\n');

%*********************************************
%(1) open up the Source, find all Tube nodes...
%*********************************************
idSource = fopen(strSource,'r');
Key=sprintf('*Node\r\n');         %Old tag
fprintf(idOutput, '*Node\r\n');  %New tag
NumLines = ExtractSection(idSource,Key,idOutput);
fclose(idSource);

%*********************************************
%(2) open up the Source, find all Tube elements...
%*********************************************
idSource = fopen(strSource,'r');
Key=sprintf('*Element, type=C3D8R\r\n');                    %Old tag
fprintf(idOutput, '*Element, type=C3D8R, elset=Tube\r\n'); %New tag
NumLines = ExtractSection(idSource,Key,idOutput);
fclose(idSource);



%*********************************************
%(3) open up the Source, find all triangle HSE elements...
%*********************************************
if(V_CONTROL==1)
    idSource = fopen(strSource,'r');
    Key=sprintf('*Element, type=S3\r\n');    %Old tag
    fprintf(idOutput, '*Element, type=F3D3, elset=Cavity\r\n'); %New tag
    NumLines = ExtractSection(idSource,Key,idOutput);
    fclose(idSource);
end
%*********************************************
%(4) open up the Source, find all rect HSE elements...
%*********************************************
if(V_CONTROL==1)
    idSource = fopen(strSource,'r');
    Key=sprintf('*Element, type=S4R\r\n');    %Old tag
    fprintf(idOutput, '*Element, type=F3D4, elset=Cavity\r\n'); %New tag
    NumLines = ExtractSection(idSource,Key,idOutput);
    fclose(idSource);
end

%*********************************************
%(5) Add reference point
%*********************************************
fprintf(idOutput, '*Node\r\n'); %New tag
fprintf(idOutput, '   999998,           0.,           0.,           0.\r\n'); %New tag
fprintf(idOutput, '*Nset, nset=Tube-RefPt_, internal\r\n'); %New tag
fprintf(idOutput, '999998, \r\n'); %New tag

%*********************************************
%(6) Cavity Properties
%*********************************************
fprintf(idOutput, '*Node, nset=CavityRef\r\n'); %New tag
fprintf(idOutput, '    999999,           0.,           0.,           0.\r\n'); %New tag
```

```
fprintf(idOutput,     '*fluid     property,     elset=Cavity,     ref     node=CavityRef,
type=hydraulic\r\n'); %New tag
fprintf(idOutput, '*fluid density\r\n');        %New tag
fprintf(idOutput, '0.036\r\n');                 %New tag
fprintf(idOutput, '**\r\n');                    %New tag

%*******************************************
%(7) open up the Source, find all XSYM set elements...
%*******************************************
%Nodes
idSource = fopen(strSource,'r');
Key=sprintf('*Nset, nset=XSYMSET\r\n');    %Old tag
fprintf(idOutput, '*Nset, nset=XSYMSET\r\n'); %New tag
NumLines = ExtractSection(idSource,Key,idOutput);
fclose(idSource);
%Elements
idSource = fopen(strSource,'r');
Key=sprintf('*Elset, elset=XSYMSET\r\n');    %Old tag
fprintf(idOutput, '*Elset, elset=XSYMSET\r\n'); %New tag
NumLines = ExtractSection(idSource,Key,idOutput);
fclose(idSource);

%*******************************************
%(8) open up the Source, find all YSYM set elements...
%*******************************************
%Nodes
idSource = fopen(strSource,'r');
Key=sprintf('*Nset, nset=YSYMSET\r\n');    %Old tag
fprintf(idOutput, '*Nset, nset=YSYMSET\r\n'); %New tag
NumLines = ExtractSection(idSource,Key,idOutput);
fclose(idSource);
%Elements
idSource = fopen(strSource,'r');
Key=sprintf('*Elset, elset=YSYMSET\r\n');    %Old tag
fprintf(idOutput, '*Elset, elset=YSYMSET\r\n'); %New tag
NumLines = ExtractSection(idSource,Key,idOutput);
fclose(idSource);

%*******************************************
%(9) open up the Source, find all ZSYM set elements...
%*******************************************
%Nodes
idSource = fopen(strSource,'r');
Key=sprintf('*Nset, nset=ZSYMSET\r\n');    %Old tag
fprintf(idOutput, '*Nset, nset=ZSYMSET\r\n'); %New tag
NumLines = ExtractSection(idSource,Key,idOutput);
fclose(idSource);
%Elements
idSource = fopen(strSource,'r');
Key=sprintf('*Elset, elset=ZSYMSET\r\n');    %Old tag
fprintf(idOutput, '*Elset, elset=ZSYMSET\r\n'); %New tag
NumLines = ExtractSection(idSource,Key,idOutput);
fclose(idSource);



%*******************************************
%(9) open up the Source, find all TubeExterior set elements...
%*******************************************
%Nodes
idSource = fopen(strSource,'r');
Key=sprintf('*Nset, nset=TubeExterior\r\n');    %Old tag
```

```
fprintf(idOutput, '*Nset, nset=TubeExterior\r\n'); %New tag
NumLines = ExtractSection(idSource,Key,idOutput);
fclose(idSource);
%Elements
idSource = fopen(strSource,'r');
Key=sprintf('*Elset, elset=TubeExterior, generate\r\n');    %Old tag
fprintf(idOutput, '*Elset, elset=TubeExterior, generate\r\n'); %New tag
NumLines = ExtractSection(idSource,Key,idOutput);
fclose(idSource);



%*********************************************
%(10) open up the Source, find all TubeInterior set elements...
%*********************************************
%Nodes
idSource = fopen(strSource,'r');
Key=sprintf('*Nset, nset=TubeInterior\r\n');    %Old tag
fprintf(idOutput, '*Nset, nset=TubeInterior\r\n'); %New tag
NumLines = ExtractSection(idSource,Key,idOutput);
fclose(idSource);
%Elements
idSource = fopen(strSource,'r');
Key=sprintf('*Elset, elset=TubeInterior\r\n');    %Old tag
fprintf(idOutput, '*Elset, elset=TubeInterior\r\n'); %New tag
NumLines = ExtractSection(idSource,Key,idOutput);
fclose(idSource);




%*********************************************
%(11) open up the Source, find all RigidCavityEnd set elements...
%*********************************************
if(V_CONTROL==1)
    %Nodes
    idSource = fopen(strSource,'r');
    Key=sprintf('*Nset, nset=RigidCavityEnd\r\n');    %Old tag
    fprintf(idOutput, '*Nset, nset=RigidCavityEnd\r\n'); %New tag
    NumLines = ExtractSection(idSource,Key,idOutput);
    fclose(idSource);
    %Elements
    idSource = fopen(strSource,'r');
    Key=sprintf('*Elset, elset=RigidCavityEnd\r\n');    %Old tag
    fprintf(idOutput, '*Elset, elset=RigidCavityEnd\r\n'); %New tag
    NumLines = ExtractSection(idSource,Key,idOutput);
    fclose(idSource);
end



%*********************************************
%(12) open up the Source, find all NoStiffPad set elements...
%*********************************************
if(V_CONTROL==1 && NO_STIFF_PAD==1)
    %Nodes
    idSource = fopen(strSource,'r');
    Key=sprintf('*Nset, nset=NoStiffPad\r\n');    %Old tag
    fprintf(idOutput, '*Nset, nset=NoStiffPad\r\n'); %New tag
    NumLines = ExtractSection(idSource,Key,idOutput);
    fclose(idSource);
    %Elements
    idSource = fopen(strSource,'r');
    %Key=sprintf('*Elset, elset=NoStiffPad\r\n');    %Old tag
```

```
    %fprintf(idOutput, '*Elset, elset=NoStiffPad\r\n'); %New tag
    Key=sprintf('*Elset, elset=NoStiffPad, generate\r\n');    %Old tag
    fprintf(idOutput, '*Elset, elset=NoStiffPad, generate\r\n'); %New tag
    NumLines = ExtractSection(idSource,Key,idOutput);
    fclose(idSource);

    %Nodes
    idSource = fopen(strSource,'r');
    Key=sprintf('*Nset, nset=TubeElements\r\n');    %Old tag
    fprintf(idOutput, '*Nset, nset=TubeElements\r\n'); %New tag
    NumLines = ExtractSection(idSource,Key,idOutput);
    fclose(idSource);
    %Elements
    idSource = fopen(strSource,'r');
    %Key=sprintf('*Elset, elset=NoStiffPad\r\n');    %Old tag
    %fprintf(idOutput, '*Elset, elset=NoStiffPad\r\n'); %New tag
    Key=sprintf('*Elset, elset=TubeElements, generate\r\n');    %Old tag
    fprintf(idOutput, '*Elset, elset=TubeElements, generate\r\n'); %New tag
    NumLines = ExtractSection(idSource,Key,idOutput);
    fclose(idSource);

end

if(THICKNESS_EDGES==1)
    %Nodes
    idSource = fopen(strSource,'r');
    Key=sprintf('*Nset, nset=TubeMidExterior\r\n');    %Old tag
    fprintf(idOutput, '*Nset, nset=TubeMidExterior\r\n'); %New tag
    NumLines = ExtractSection(idSource,Key,idOutput);
    fclose(idSource);
    %Elements
    idSource = fopen(strSource,'r');
    %Key=sprintf('*Elset, elset=NoStiffPad\r\n');    %Old tag
    %fprintf(idOutput, '*Elset, elset=NoStiffPad\r\n'); %New tag
    Key=sprintf('*Elset, elset=TubeMidExterior, generate\r\n');    %Old tag
    fprintf(idOutput, '*Elset, elset=TubeMidExterior, generate\r\n'); %New tag
    NumLines = ExtractSection(idSource,Key,idOutput);
    fclose(idSource);

    %Nodes
    idSource = fopen(strSource,'r');
    Key=sprintf('*Nset, nset=TubeMidInterior\r\n');    %Old tag
    fprintf(idOutput, '*Nset, nset=TubeMidInterior\r\n'); %New tag
    NumLines = ExtractSection(idSource,Key,idOutput);
    fclose(idSource);
    %Elements
    idSource = fopen(strSource,'r');
    %Key=sprintf('*Elset, elset=NoStiffPad\r\n');    %Old tag
    %fprintf(idOutput, '*Elset, elset=NoStiffPad\r\n'); %New tag
    Key=sprintf('*Elset, elset=TubeMidInterior, generate\r\n');    %Old tag
    fprintf(idOutput, '*Elset, elset=TubeMidInterior, generate\r\n'); %New tag
    NumLines = ExtractSection(idSource,Key,idOutput);
    fclose(idSource);
end

if(THICKNESS_SETS==1)
    %Nodes
    idSource = fopen(strSource,'r');
    Key=sprintf('*Nset, nset=SetA\r\n');    %Old tag
    fprintf(idOutput, '*Nset, nset=SetA\r\n'); %New tag
    NumLines = ExtractSection(idSource,Key,idOutput);
```

```
    fclose(idSource);

    %Nodes
    idSource = fopen(strSource,'r');
    Key=sprintf('*Nset, nset=SetB\r\n');    %Old tag
    fprintf(idOutput, '*Nset, nset=SetB\r\n'); %New tag
    NumLines = ExtractSection(idSource,Key,idOutput);
    fclose(idSource);

    %Nodes
    idSource = fopen(strSource,'r');
    Key=sprintf('*Nset, nset=SetC\r\n');    %Old tag
    fprintf(idOutput, '*Nset, nset=SetC\r\n'); %New tag
    NumLines = ExtractSection(idSource,Key,idOutput);
    fclose(idSource);

    %Nodes
    idSource = fopen(strSource,'r');
    Key=sprintf('*Nset, nset=SetD\r\n');    %Old tag
    fprintf(idOutput, '*Nset, nset=SetD\r\n'); %New tag
    NumLines = ExtractSection(idSource,Key,idOutput);
    fclose(idSource);

    %Nodes
    idSource = fopen(strSource,'r');
    Key=sprintf('*Nset, nset=SetE\r\n');    %Old tag
    fprintf(idOutput, '*Nset, nset=SetE\r\n'); %New tag
    NumLines = ExtractSection(idSource,Key,idOutput);
    fclose(idSource);
end

%*********************************************
%(10) Rest of the file is pretty static...
%*********************************************
fprintf(idOutput, '*Orientation, name=Ori-1, system=CYLINDRICAL\r\n');
fprintf(idOutput, '          0.,           0.,           0.,           0.,           0.,
1.\r\n');
fprintf(idOutput, '3, 0.\r\n');
if(NO_STIFF_PAD==1)
    fprintf(idOutput, '** Section: %s\r\n',strTubeMaterial);
    fprintf(idOutput,    '*Solid    Section,    elset=TubeElements,    orientation=Ori-1,
material=%s\r\n', strTubeMaterial);
    fprintf(idOutput, ',\r\n');

    fprintf(idOutput, '** Section: NoStiffSect\r\n');
    fprintf(idOutput,    '*Solid    Section,    elset=NoStiffPad,    orientation=Ori-1,
material=NoStiffMat\r\n');
    fprintf(idOutput, ',\r\n');
else
    fprintf(idOutput, '** Section: %s\r\n',strTubeMaterial);
    fprintf(idOutput, '*Solid Section, elset=Tube, orientation=Ori-1, material=%s\r\n',
strTubeMaterial);
    fprintf(idOutput, ',\r\n');
end
fprintf(idOutput, '*End Part\r\n');
fprintf(idOutput, '**  \r\n');
fprintf(idOutput, '**\r\n');

fprintf(idOutput, '************** \r\n');
fprintf(idOutput, '** ASSEMBLY **\r\n');
fprintf(idOutput, '************** \r\n');
```

```
fprintf(idOutput, '**\r\n');
fprintf(idOutput, '*Assembly, name=Assembly\r\n');
fprintf(idOutput, '**  \r\n');
fprintf(idOutput, '*Instance, name=Tube-1, part=Tube\r\n');
fprintf(idOutput, '*End Instance\r\n');
fprintf(idOutput, '**  \r\n');
fprintf(idOutput, '*Instance, name=Seal-Analytical-1, part=Seal-Analytical\r\n');
fprintf(idOutput, '          0.,           0.,          6.25\r\n');
fprintf(idOutput, '          0.,           0.,          6.25,          -1.,           0.,
6.25,          90.\r\n');
fprintf(idOutput, '*Node\r\n');
fprintf(idOutput, '      1,           0.,        -0.25,           0.\r\n');
fprintf(idOutput, '*Nset, nset=Seal-Analytical-1-RefPt_, internal\r\n');
fprintf(idOutput, '1, \r\n');
fprintf(idOutput, '*Nset, nset=SealRef\r\n');
fprintf(idOutput, ' 1,\r\n');
fprintf(idOutput, '*Surface, type=REVOLUTION, name=CP-1-Seal-Analytical-1\r\n');
%fprintf(idOutput, 'START,        1.125,        -0.25\r\n');
%fprintf(idOutput, ' LINE,        1.125,          0.\r\n');
%fprintf(idOutput, ' LINE, 1.19340017982884, 1.95872487417563\r\n');
%fprintf(idOutput,  '  CIRCL,  1.44324788658361,                  2.2,  1.44324788658361,
1.95\r\n');
fprintf(idOutput, 'START,          1.2,        -0.25\r\n');
fprintf(idOutput, ' LINE,          1.2,          0.\r\n');
fprintf(idOutput, ' LINE, 1.24266815198438, 1.95545372125864\r\n');
fprintf(idOutput,  '  CIRCL,  1.49260865875436,                  2.2,  1.49260865875436,
1.95\r\n');

fprintf(idOutput, '*Rigid Body, ref node=Seal-Analytical-1-RefPt_, analytical surface=CP-
1-Seal-Analytical-1\r\n');
fprintf(idOutput, '*End Instance\r\n');
fprintf(idOutput, '**  \r\n');
fprintf(idOutput, '*Instance, name=Die-1, part=Die\r\n');
fprintf(idOutput, '          0.,           0.,           2.\r\n');
fprintf(idOutput, '*Node\r\n');
fprintf(idOutput, '      1,           0.,           0.,           0.\r\n');
fprintf(idOutput, '*Nset, nset=Die-1-RefPt_, internal\r\n');
fprintf(idOutput, '1, \r\n');
fprintf(idOutput, '*Nset, nset=DieRef\r\n');
fprintf(idOutput, ' 1,\r\n');
fprintf(idOutput, '*Surface, type=CYLINDER, name=RigidSurface_, internal\r\n');
%fprintf(idOutput, 'START,         1.25,           0.\r\n');
%fprintf(idOutput, ' LINE,         1.25,        0.875\r\n');
%fprintf(idOutput,  '  CIRCL,  0.875000000000002,               1.25,  0.875000000000002,
0.875\r\n');
%fprintf(idOutput, ' LINE,           0.,         1.25\r\n');
fprintf(idOutput, 'START,         1.25,           0.\r\n');
fprintf(idOutput, 'LINE,         1.25,       0.8125\r\n');
fprintf(idOutput,  'CIRCL,  0.812500000000002,                  1.25,  0.812500000000002,
0.8125\r\n');
fprintf(idOutput, 'LINE,           0.,         1.25\r\n');
fprintf(idOutput,      '*Rigid      Body,      ref      node=Die-1-RefPt_,      analytical
surface=RigidSurface_\r\n');
fprintf(idOutput, '*End Instance\r\n');
fprintf(idOutput, '**  \r\n');
%fprintf(idOutput,    '*Elset,    elset=_CP-1-Tube-1_S2,    internal,    instance=Tube-1,
generate\r\n');
%fprintf(idOutput, '    1,  6400,     1\r\n');
%fprintf(idOutput, '*Surface, type=ELEMENT, name=CP-1-Tube-1\r\n');
%fprintf(idOutput, '_CP-1-Tube-1_S2, S2\r\n');
fprintf(idOutput, '*Surface, type=NODE, name=Tube-1_TubeExterior_CNS_, internal\r\n');
fprintf(idOutput, 'Tube-1.TubeExterior, 1.\r\n');
fprintf(idOutput, '*End Assembly\r\n');
```

```
fprintf(idOutput, '** \r\n');
fprintf(idOutput, '*************** \r\n');
fprintf(idOutput, '** MATERIALS **\r\n');
fprintf(idOutput, '*************** \r\n');
fprintf(idOutput, '** \r\n');

if(NO_STIFF_PAD==1)
    fprintf(idOutput, '** NO STIFFNESS MATERIAL FOR PAD \r\n');
    fprintf(idOutput, '*Material, name=NoStiffMat \r\n');
    fprintf(idOutput, '*Elastic \r\n');
    %fprintf(idOutput, '1., 0.3 \r\n');
    fprintf(idOutput, ' %s \r\n',strElasticMod);
    fprintf(idOutput, '*No Tension \r\n');
    fprintf(idOutput, '** \r\n');
end
fprintf(idOutput, '** Material Data from Ford Automotive Company (Xia) for Al-6061-T4
tubes. \r\n');
fprintf(idOutput, '** Re-extrapolated by Kaplan on 2/28/12. \r\n');
fprintf(idOutput, '*Material, name=FordAl6061T4 \r\n');
fprintf(idOutput, '*Elastic \r\n');
fprintf(idOutput, ' 1.09942e+07, 0.3 \r\n');
fprintf(idOutput, '*Plastic \r\n');
fprintf(idOutput, ' 21988.4,          0. \r\n');
fprintf(idOutput, '  22119.,      0.0001 \r\n');
fprintf(idOutput, ' 22144.3,     0.00012 \r\n');
fprintf(idOutput, ' 22174.4,    0.000144 \r\n');
fprintf(idOutput, ' 22210.1,   0.0001728 \r\n');
fprintf(idOutput, ' 22252.3,  0.00020736 \r\n');
fprintf(idOutput, ' 22302.1, 0.000248832 \r\n');
fprintf(idOutput, ' 22360.6, 0.000298598 \r\n');
fprintf(idOutput, ' 22429.2, 0.000358318 \r\n');
fprintf(idOutput, ' 22509.1, 0.000429982 \r\n');
fprintf(idOutput, ' 22601.9, 0.000515978 \r\n');
fprintf(idOutput, ' 22709.1, 0.000619174 \r\n');
fprintf(idOutput, '  22832., 0.000743008 \r\n');
fprintf(idOutput, ' 22972.3,  0.00089161 \r\n');
fprintf(idOutput, '  23131.,  0.00106993 \r\n');
fprintf(idOutput, ' 23309.4,  0.00128392 \r\n');
fprintf(idOutput, ' 23508.3,   0.0015407 \r\n');
fprintf(idOutput, ' 23728.4,  0.00184884 \r\n');
fprintf(idOutput, ' 23970.5,  0.00221861 \r\n');
fprintf(idOutput, ' 24235.1,  0.00266233 \r\n');
fprintf(idOutput, '  24523.,   0.0031948 \r\n');
fprintf(idOutput, ' 24835.9,  0.00383376 \r\n');
fprintf(idOutput, ' 25176.1,  0.00460051 \r\n');
fprintf(idOutput, ' 25547.6,  0.00552061 \r\n');
fprintf(idOutput, ' 25956.4,  0.00662474 \r\n');
fprintf(idOutput, ' 26441.2,  0.00794968 \r\n');
fprintf(idOutput, ' 26917.4,  0.00953962 \r\n');
fprintf(idOutput, ' 27303.7,    0.010956 \r\n');
fprintf(idOutput, ' 27913.5,   0.0131472 \r\n');
fprintf(idOutput, ' 28641.7,   0.0157766 \r\n');
fprintf(idOutput, ' 29503.9,    0.018932 \r\n');
fprintf(idOutput, ' 30514.5,   0.0227184 \r\n');
fprintf(idOutput, '  31685.,    0.027262 \r\n');
fprintf(idOutput, ' 33022.3,   0.0327144 \r\n');
fprintf(idOutput, ' 34526.5,   0.0392573 \r\n');
fprintf(idOutput, '  36189.,   0.0471088 \r\n');
fprintf(idOutput, '  37991.,   0.0565306 \r\n');
fprintf(idOutput, ' 39903.7,   0.0678367 \r\n');
fprintf(idOutput, ' 41889.2,    0.081404 \r\n');
fprintf(idOutput, ' 43903.1,   0.0976848 \r\n');
fprintf(idOutput, ' 45898.5,    0.117222 \r\n');
```

```
fprintf(idOutput, ' 47830.1,    0.140666 \r\n');
fprintf(idOutput, ' 49658.3,    0.168799 \r\n');
fprintf(idOutput, ' 51352.2,    0.202559 \r\n');
fprintf(idOutput, ' 52890.9,    0.243071 \r\n');
fprintf(idOutput, ' 54263.8,    0.291685 \r\n');
fprintf(idOutput, ' 55469.2,    0.350022 \r\n');
fprintf(idOutput, ' 56512.8,    0.420027 \r\n');
fprintf(idOutput, ' 57405.3,    0.504032 \r\n');
fprintf(idOutput, ' 58160.5,    0.604839 \r\n');
fprintf(idOutput, ' 58794.1,    0.725806 \r\n');
fprintf(idOutput, ' 59321.6,    0.870967 \r\n');
fprintf(idOutput, ' 59758.1,     1.04516 \r\n');
fprintf(idOutput, ' 60117.5,     1.25419 \r\n');
fprintf(idOutput, ' 60412.1,     1.50503 \r\n');
fprintf(idOutput, ' 60652.8,     1.80604 \r\n');
fprintf(idOutput, ' 60848.8,     2.16725 \r\n');

fprintf(idOutput, '** LeeDC7 Data\r\n');
fprintf(idOutput, '*Material, name=Al6061\r\n');
fprintf(idOutput, '*Elastic\r\n');
fprintf(idOutput, ' 9.5e+06, 0.3\r\n');
fprintf(idOutput, '*Plastic\r\n');
fprintf(idOutput, '  36700.,        0.\r\n');
fprintf(idOutput, '  38770.,  4.53e-05\r\n');
fprintf(idOutput, '  40060., 0.0001079\r\n');
fprintf(idOutput, '  41960., 0.0003765\r\n');
fprintf(idOutput, '  43140., 0.0008436\r\n');
fprintf(idOutput, '  44330.,  0.002255\r\n');
fprintf(idOutput, '  45000.,  0.004699\r\n');
fprintf(idOutput, '  45250.,  0.006272\r\n');
fprintf(idOutput, '  45510.,  0.008144\r\n');
fprintf(idOutput, '  45860.,   0.01075\r\n');
fprintf(idOutput, '  45910.,   0.01148\r\n');
fprintf(idOutput, '  46200.,   0.01367\r\n');
fprintf(idOutput, '  46440.,   0.01644\r\n');
fprintf(idOutput, '  46660.,   0.01819\r\n');
fprintf(idOutput, '  46770.,   0.01956\r\n');
fprintf(idOutput, '  47020.,   0.02209\r\n');
fprintf(idOutput, '  47340.,   0.02647\r\n');
fprintf(idOutput, '  47730.,   0.03264\r\n');
fprintf(idOutput, '  47950.,   0.03576\r\n');
fprintf(idOutput, '  48090.,   0.03782\r\n');
fprintf(idOutput, '  48260.,   0.03975\r\n');
fprintf(idOutput, '  48380.,   0.04123\r\n');
fprintf(idOutput, '  48490.,   0.04262\r\n');
fprintf(idOutput, '  48560.,   0.04361\r\n');
fprintf(idOutput, '  48650.,   0.04491\r\n');
fprintf(idOutput, '  48830.,   0.04722\r\n');
fprintf(idOutput, '  48890.,    0.0485\r\n');
fprintf(idOutput, '  49000.,   0.05008\r\n');
fprintf(idOutput, '  49100.,    0.0517\r\n');
fprintf(idOutput, ' 49180.7,   0.05293\r\n');
fprintf(idOutput, ' 49284.4,   0.05451\r\n');
fprintf(idOutput, ' 49387.4,   0.05608\r\n');
fprintf(idOutput, ' 49523.3,   0.05815\r\n');
fprintf(idOutput, ' 49587.6,   0.05913\r\n');
fprintf(idOutput, ' 49915.7,   0.06413\r\n');
fprintf(idOutput, ' 50243.8,   0.06913\r\n');
fprintf(idOutput, '  50572.,   0.07413\r\n');
fprintf(idOutput, ' 50900.1,   0.07913\r\n');
fprintf(idOutput, ' 51228.2,   0.08413\r\n');
fprintf(idOutput, ' 51556.3,   0.08913\r\n');
fprintf(idOutput, ' 51884.5,   0.09413\r\n');
```

```
fprintf(idOutput, ' 52212.6,   0.09913\r\n');
fprintf(idOutput, ' 52540.7,   0.10413\r\n');
fprintf(idOutput, ' 52868.8,   0.10913\r\n');
fprintf(idOutput, '  53197.,   0.11413\r\n');
fprintf(idOutput, ' 53525.1,   0.11913\r\n');
fprintf(idOutput, ' 53853.2,   0.12413\r\n');
fprintf(idOutput, ' 54181.3,   0.12913\r\n');
fprintf(idOutput, ' 54509.5,   0.13413\r\n');
fprintf(idOutput, ' 54837.6,   0.13913\r\n');
fprintf(idOutput, ' 55165.7,   0.14413\r\n');
fprintf(idOutput, ' 55493.8,   0.14913\r\n');
fprintf(idOutput, '  55822.,   0.15413\r\n');
fprintf(idOutput, ' 56150.1,   0.15913\r\n');
fprintf(idOutput, ' 56478.2,   0.16413\r\n');
fprintf(idOutput, ' 56806.3,   0.16913\r\n');
fprintf(idOutput, '  59300.,      0.21\r\n');
fprintf(idOutput, '  63800.,       0.3\r\n');
fprintf(idOutput, '  70500.,       0.5\r\n');
fprintf(idOutput, '  79000.,        1.\r\n');
fprintf(idOutput, '  85000.,        2.\r\n');

fprintf(idOutput, '*Material, name=Steel1018\r\n');
fprintf(idOutput, '*Elastic\r\n');
fprintf(idOutput, ' 2.9e+07, 0.3\r\n');
fprintf(idOutput, '*Plastic\r\n');
fprintf(idOutput, '15800.,     0.\r\n');
fprintf(idOutput, '16000., 0.0001\r\n');
fprintf(idOutput, '16200., 0.0002\r\n');
fprintf(idOutput, '16500., 0.0003\r\n');
fprintf(idOutput, '16800., 0.0004\r\n');
fprintf(idOutput, '17000., 0.0005\r\n');
fprintf(idOutput, '17300., 0.0006\r\n');
fprintf(idOutput, '17600., 0.0007\r\n');
fprintf(idOutput, '17900., 0.0008\r\n');
fprintf(idOutput, '18200., 0.0009\r\n');
fprintf(idOutput, '18500.,  0.001\r\n');
fprintf(idOutput, '18800., 0.0011\r\n');
fprintf(idOutput, '19000., 0.0012\r\n');
fprintf(idOutput, '19300., 0.0013\r\n');
fprintf(idOutput, '19500., 0.0014\r\n');
fprintf(idOutput, '19700., 0.0015\r\n');
fprintf(idOutput, '19800., 0.0016\r\n');
fprintf(idOutput, '20000., 0.0017\r\n');
fprintf(idOutput, '20100., 0.0018\r\n');
fprintf(idOutput, '20100., 0.0019\r\n');
fprintf(idOutput, '20200.,  0.002\r\n');
fprintf(idOutput, '21000.,  0.003\r\n');
fprintf(idOutput, '21700.,  0.004\r\n');
fprintf(idOutput, '22400.,  0.005\r\n');
fprintf(idOutput, '23000.,  0.006\r\n');
fprintf(idOutput, '23600.,  0.007\r\n');
fprintf(idOutput, '24200.,  0.008\r\n');
fprintf(idOutput, '24700.,  0.009\r\n');
fprintf(idOutput, '25200.,   0.01\r\n');
fprintf(idOutput, '25700.,  0.011\r\n');
fprintf(idOutput, '26200.,  0.012\r\n');
fprintf(idOutput, '26600.,  0.013\r\n');
fprintf(idOutput, '27100.,  0.014\r\n');
fprintf(idOutput, '27500.,  0.015\r\n');
fprintf(idOutput, '27900.,  0.016\r\n');
fprintf(idOutput, '28400.,  0.017\r\n');
fprintf(idOutput, '28800.,  0.018\r\n');
fprintf(idOutput, '29100.,  0.019\r\n');
```

```
fprintf(idOutput, '29500.,   0.02\r\n');
fprintf(idOutput, '29900.,  0.021\r\n');
fprintf(idOutput, '30300.,  0.022\r\n');
fprintf(idOutput, '30600.,  0.023\r\n');
fprintf(idOutput, '31000.,  0.024\r\n');
fprintf(idOutput, '31300.,  0.025\r\n');
fprintf(idOutput, '31600.,  0.026\r\n');
fprintf(idOutput, '32000.,  0.027\r\n');
fprintf(idOutput, '32300.,  0.028\r\n');
fprintf(idOutput, '32600.,  0.029\r\n');
fprintf(idOutput, '32900.,   0.03\r\n');
fprintf(idOutput, '33200.,  0.031\r\n');
fprintf(idOutput, '33500.,  0.032\r\n');
fprintf(idOutput, '33800.,  0.033\r\n');
fprintf(idOutput, '34100.,  0.034\r\n');
fprintf(idOutput, '34400.,  0.035\r\n');
fprintf(idOutput, '34600.,  0.036\r\n');
fprintf(idOutput, '34900.,  0.037\r\n');
fprintf(idOutput, '35200.,  0.038\r\n');
fprintf(idOutput, '35400.,  0.039\r\n');
fprintf(idOutput, '35700.,   0.04\r\n');
fprintf(idOutput, '36000.,  0.041\r\n');
fprintf(idOutput, '36200.,  0.042\r\n');
fprintf(idOutput, '36400.,  0.043\r\n');
fprintf(idOutput, '36700.,  0.044\r\n');
fprintf(idOutput, '36900.,  0.045\r\n');
fprintf(idOutput, '37200.,  0.046\r\n');
fprintf(idOutput, '37400.,  0.047\r\n');
fprintf(idOutput, '37600.,  0.048\r\n');
fprintf(idOutput, '37900.,  0.049\r\n');
fprintf(idOutput, '38100.,   0.05\r\n');
fprintf(idOutput, '38300.,  0.051\r\n');
fprintf(idOutput, '38500.,  0.052\r\n');
fprintf(idOutput, '38700.,  0.053\r\n');
fprintf(idOutput, '39000.,  0.054\r\n');
fprintf(idOutput, '39200.,  0.055\r\n');
fprintf(idOutput, '39400.,  0.056\r\n');
fprintf(idOutput, '39600.,  0.057\r\n');
fprintf(idOutput, '39800.,  0.058\r\n');
fprintf(idOutput, '40000.,  0.059\r\n');
fprintf(idOutput, '40200.,   0.06\r\n');
fprintf(idOutput, '40400.,  0.061\r\n');
fprintf(idOutput, '40600.,  0.062\r\n');
fprintf(idOutput, '40700.,  0.063\r\n');
fprintf(idOutput, '40900.,  0.064\r\n');
fprintf(idOutput, '41100.,  0.065\r\n');
fprintf(idOutput, '41300.,  0.066\r\n');
fprintf(idOutput, '41500.,  0.067\r\n');
fprintf(idOutput, '41700.,  0.068\r\n');
fprintf(idOutput, '41800.,  0.069\r\n');
fprintf(idOutput, '42000.,   0.07\r\n');
fprintf(idOutput, '42200.,  0.071\r\n');
fprintf(idOutput, '42400.,  0.072\r\n');
fprintf(idOutput, '42500.,  0.073\r\n');
fprintf(idOutput, '42700.,  0.074\r\n');
fprintf(idOutput, '42900.,  0.075\r\n');
fprintf(idOutput, '43000.,  0.076\r\n');
fprintf(idOutput, '43200.,  0.077\r\n');
fprintf(idOutput, '43400.,  0.078\r\n');
fprintf(idOutput, '43500.,  0.079\r\n');
fprintf(idOutput, '43700.,   0.08\r\n');
fprintf(idOutput, '43800.,  0.081\r\n');
fprintf(idOutput, '44000.,  0.082\r\n');
```

```
fprintf(idOutput, '44100.,  0.083\r\n');
fprintf(idOutput, '44300.,  0.084\r\n');
fprintf(idOutput, '44400.,  0.085\r\n');
fprintf(idOutput, '44600.,  0.086\r\n');
fprintf(idOutput, '44700.,  0.087\r\n');
fprintf(idOutput, '44900.,  0.088\r\n');
fprintf(idOutput, '45000.,  0.089\r\n');
fprintf(idOutput, '45200.,   0.09\r\n');
fprintf(idOutput, '45300.,  0.091\r\n');
fprintf(idOutput, '45400.,  0.092\r\n');
fprintf(idOutput, '45600.,  0.093\r\n');
fprintf(idOutput, '45700.,  0.094\r\n');
fprintf(idOutput, '45900.,  0.095\r\n');
fprintf(idOutput, '46000.,  0.096\r\n');
fprintf(idOutput, '46100.,  0.097\r\n');
fprintf(idOutput, '46300.,  0.098\r\n');
fprintf(idOutput, '46400.,  0.099\r\n');
fprintf(idOutput, '46500.,    0.1\r\n');
fprintf(idOutput, '47800.,   0.11\r\n');
fprintf(idOutput, '48900.,   0.12\r\n');
fprintf(idOutput, '50000.,   0.13\r\n');
fprintf(idOutput, '51000.,   0.14\r\n');
fprintf(idOutput, '51900.,   0.15\r\n');
fprintf(idOutput, '52800.,   0.16\r\n');
fprintf(idOutput, '53600.,   0.17\r\n');
fprintf(idOutput, '54300.,   0.18\r\n');
fprintf(idOutput, '55100.,   0.19\r\n');
fprintf(idOutput, '55700.,    0.2\r\n');
fprintf(idOutput, '56400.,   0.21\r\n');
fprintf(idOutput, '57000.,   0.22\r\n');
fprintf(idOutput, '57600.,   0.23\r\n');
fprintf(idOutput, '58100.,   0.24\r\n');
fprintf(idOutput, '58600.,   0.25\r\n');
fprintf(idOutput, '59100.,   0.26\r\n');
fprintf(idOutput, '59600.,   0.27\r\n');
fprintf(idOutput, '60100.,   0.28\r\n');
fprintf(idOutput, '60500.,   0.29\r\n');
fprintf(idOutput, '61000.,    0.3\r\n');
fprintf(idOutput, '61400.,   0.31\r\n');
fprintf(idOutput, '61700.,   0.32\r\n');
fprintf(idOutput, '62100.,   0.33\r\n');
fprintf(idOutput, '62500.,   0.34\r\n');
fprintf(idOutput, '62800.,   0.35\r\n');
fprintf(idOutput, '63200.,   0.36\r\n');
fprintf(idOutput, '63500.,   0.37\r\n');
fprintf(idOutput, '63800.,   0.38\r\n');
fprintf(idOutput, '64100.,   0.39\r\n');
fprintf(idOutput, '64400.,    0.4\r\n');
fprintf(idOutput, '64700.,   0.41\r\n');
fprintf(idOutput, '65000.,   0.42\r\n');
fprintf(idOutput, '65200.,   0.43\r\n');
fprintf(idOutput, '65500.,   0.44\r\n');
fprintf(idOutput, '65800.,   0.45\r\n');
fprintf(idOutput, '66000.,   0.46\r\n');
fprintf(idOutput, '66200.,   0.47\r\n');
fprintf(idOutput, '66500.,   0.48\r\n');
fprintf(idOutput, '66700.,   0.49\r\n');
fprintf(idOutput, '66900.,    0.5\r\n');
fprintf(idOutput, '67100.,   0.51\r\n');
fprintf(idOutput, '67300.,   0.52\r\n');
fprintf(idOutput, '67500.,   0.53\r\n');
fprintf(idOutput, '67700.,   0.54\r\n');
fprintf(idOutput, '67900.,   0.55\r\n');
```

```
fprintf(idOutput, '68100.,   0.56\r\n');
fprintf(idOutput, '68300.,   0.57\r\n');
fprintf(idOutput, '68500.,   0.58\r\n');
fprintf(idOutput, '68600.,   0.59\r\n');
fprintf(idOutput, '68800.,    0.6\r\n');
fprintf(idOutput, '69000.,   0.61\r\n');
fprintf(idOutput, '69100.,   0.62\r\n');
fprintf(idOutput, '69300.,   0.63\r\n');
fprintf(idOutput, '69500.,   0.64\r\n');
fprintf(idOutput, '69600.,   0.65\r\n');
fprintf(idOutput, '69800.,   0.66\r\n');
fprintf(idOutput, '69900.,   0.67\r\n');
fprintf(idOutput, '70100.,   0.68\r\n');
fprintf(idOutput, '70200.,   0.69\r\n');
fprintf(idOutput, '70300.,    0.7\r\n');
fprintf(idOutput, '70500.,   0.71\r\n');
fprintf(idOutput, '70600.,   0.72\r\n');
fprintf(idOutput, '70700.,   0.73\r\n');
fprintf(idOutput, '70800.,   0.74\r\n');
fprintf(idOutput, '71000.,   0.75\r\n');
fprintf(idOutput, '71100.,   0.76\r\n');
fprintf(idOutput, '71200.,   0.77\r\n');
fprintf(idOutput, '71300.,   0.78\r\n');
fprintf(idOutput, '71400.,   0.79\r\n');
fprintf(idOutput, '71600.,    0.8\r\n');
fprintf(idOutput, '71700.,   0.81\r\n');
fprintf(idOutput, '71800.,   0.82\r\n');
fprintf(idOutput, '71900.,   0.83\r\n');
fprintf(idOutput, '72000.,   0.84\r\n');
fprintf(idOutput, '72100.,   0.85\r\n');
fprintf(idOutput, '72200.,   0.86\r\n');
fprintf(idOutput, '72300.,   0.87\r\n');
fprintf(idOutput, '72400.,   0.88\r\n');
fprintf(idOutput, '72500.,   0.89\r\n');
fprintf(idOutput, '72600.,    0.9\r\n');
fprintf(idOutput, '72700.,   0.91\r\n');
fprintf(idOutput, '72800.,   0.92\r\n');
fprintf(idOutput, '72900.,   0.93\r\n');
fprintf(idOutput, '72900.,   0.94\r\n');
fprintf(idOutput, '73000.,   0.95\r\n');
fprintf(idOutput, '73100.,   0.96\r\n');
fprintf(idOutput, '73200.,   0.97\r\n');
fprintf(idOutput, '73300.,   0.98\r\n');
fprintf(idOutput, '73400.,   0.99\r\n');
fprintf(idOutput, '73500.,     1.\r\n');
fprintf(idOutput, '73500.,   1.01\r\n');
fprintf(idOutput, '73600.,   1.02\r\n');
fprintf(idOutput, '73700.,   1.03\r\n');
fprintf(idOutput, '73800.,   1.04\r\n');
fprintf(idOutput, '73800.,   1.05\r\n');
fprintf(idOutput, '73900.,   1.06\r\n');
fprintf(idOutput, '74000.,   1.07\r\n');
fprintf(idOutput, '74100.,   1.08\r\n');
fprintf(idOutput, '74100.,   1.09\r\n');
fprintf(idOutput, '74200.,    1.1\r\n');
fprintf(idOutput, '74300.,   1.11\r\n');
fprintf(idOutput, '74300.,   1.12\r\n');
fprintf(idOutput, '74400.,   1.13\r\n');
fprintf(idOutput, '74500.,   1.14\r\n');
fprintf(idOutput, '74500.,   1.15\r\n');
fprintf(idOutput, '74600.,   1.16\r\n');
fprintf(idOutput, '74700.,   1.17\r\n');
fprintf(idOutput, '74700.,   1.18\r\n');
```

```
fprintf(idOutput, '74800.,   1.19\r\n');
fprintf(idOutput, '74900.,    1.2\r\n');
fprintf(idOutput, '74900.,   1.21\r\n');
fprintf(idOutput, '75000.,   1.22\r\n');
fprintf(idOutput, '75000.,   1.23\r\n');
fprintf(idOutput, '75100.,   1.24\r\n');
fprintf(idOutput, '75100.,   1.25\r\n');
fprintf(idOutput, '75200.,   1.26\r\n');
fprintf(idOutput, '75300.,   1.27\r\n');
fprintf(idOutput, '75300.,   1.28\r\n');
fprintf(idOutput, '75400.,   1.29\r\n');
fprintf(idOutput, '75400.,    1.3\r\n');
fprintf(idOutput, '75500.,   1.31\r\n');
fprintf(idOutput, '75500.,   1.32\r\n');
fprintf(idOutput, '75600.,   1.33\r\n');
fprintf(idOutput, '75600.,   1.34\r\n');
fprintf(idOutput, '75700.,   1.35\r\n');
fprintf(idOutput, '75700.,   1.36\r\n');
fprintf(idOutput, '75800.,   1.37\r\n');
fprintf(idOutput, '75800.,   1.38\r\n');
fprintf(idOutput, '75900.,   1.39\r\n');
fprintf(idOutput, '75900.,    1.4\r\n');
fprintf(idOutput, '76000.,   1.41\r\n');
fprintf(idOutput, '76000.,   1.42\r\n');
fprintf(idOutput, '76100.,   1.43\r\n');
fprintf(idOutput, '76100.,   1.44\r\n');
fprintf(idOutput, '76200.,   1.45\r\n');
fprintf(idOutput, '76200.,   1.46\r\n');
fprintf(idOutput, '76300.,   1.47\r\n');
fprintf(idOutput, '76300.,   1.48\r\n');
fprintf(idOutput, '76300.,   1.49\r\n');
fprintf(idOutput, '76400.,    1.5\r\n');
fprintf(idOutput, '76800.,    1.6\r\n');
fprintf(idOutput, '77200.,    1.7\r\n');
fprintf(idOutput, '77500.,    1.8\r\n');
fprintf(idOutput, '77800.,    1.9\r\n');
fprintf(idOutput, '78100.,     2.\r\n');

fprintf(idOutput, '** Isothermal @ 25C\r\n');
fprintf(idOutput, '*Material, name=SS304\r\n');
fprintf(idOutput, '*Elastic\r\n');
fprintf(idOutput, ' 2.71221e+07, 0.3\r\n');
fprintf(idOutput, '*Plastic\r\n');
fprintf(idOutput, ' 30631.5,          0.\r\n');
fprintf(idOutput, ' 32471.1, 1.62659e-05\r\n');
fprintf(idOutput, ' 34257.7,   4.081e-05\r\n');
fprintf(idOutput, ' 36449.7, 0.000277907\r\n');
fprintf(idOutput, ' 37419.8, 0.000401373\r\n');
fprintf(idOutput, '  39168., 0.000625935\r\n');
fprintf(idOutput, ' 40793.6, 0.000877844\r\n');
fprintf(idOutput, ' 41556.3,  0.00100066\r\n');
fprintf(idOutput, ' 43440.9,  0.00132213\r\n');
fprintf(idOutput, ' 44428.7,  0.00175335\r\n');
fprintf(idOutput, ' 45220.7,  0.00225318\r\n');
fprintf(idOutput, ' 45937.3,  0.00279403\r\n');
fprintf(idOutput, ' 46557.2,   0.0032623\r\n');
fprintf(idOutput, ' 47025.9,  0.00381829\r\n');
fprintf(idOutput, ' 47511.6,  0.00444961\r\n');
fprintf(idOutput, ' 47906.2,  0.00501072\r\n');
fprintf(idOutput, ' 50669.8,   0.0103673\r\n');
fprintf(idOutput, ' 52808.1,   0.0156498\r\n');
fprintf(idOutput, ' 54510.4,   0.0201893\r\n');
fprintf(idOutput, ' 56289.3,   0.0254975\r\n');
```

```
fprintf(idOutput, ' 57991.6,   0.0306104\r\n');
fprintf(idOutput, ' 59434.1,   0.0350649\r\n');
fprintf(idOutput, ' 61329.3,   0.0410754\r\n');
fprintf(idOutput, ' 62649.9,   0.0452903\r\n');
fprintf(idOutput, ' 64261.4,   0.0505191\r\n');
fprintf(idOutput, '  67135.,   0.0601545\r\n');
fprintf(idOutput, ' 70137.8,   0.0704145\r\n');
fprintf(idOutput, ' 72916.8,   0.0801878\r\n');
fprintf(idOutput, ' 75723.1,   0.0901073\r\n');
fprintf(idOutput, ' 78502.3,    0.100243\r\n');
fprintf(idOutput, ' 81203.9,    0.110129\r\n');
fprintf(idOutput, ' 83854.7,    0.120348\r\n');
fprintf(idOutput, ' 86286.6,    0.130228\r\n');
fprintf(idOutput, ' 88694.7,     0.14015\r\n');
fprintf(idOutput, ' 91148.5,    0.150269\r\n');
fprintf(idOutput, ' 93586.8,    0.160409\r\n');
fprintf(idOutput, '  95898.,    0.170081\r\n');
fprintf(idOutput, ' 98277.1,    0.180055\r\n');
fprintf(idOutput, ' 100755.,    0.190487\r\n');
fprintf(idOutput, ' 103044.,     0.20022\r\n');
fprintf(idOutput, ' 105337.,    0.210007\r\n');
fprintf(idOutput, ' 107702.,    0.220122\r\n');
fprintf(idOutput, ' 110054.,    0.230248\r\n');
fprintf(idOutput, ' 112369.,    0.240237\r\n');
fprintf(idOutput, ' 114633.,     0.25006\r\n');
fprintf(idOutput, ' 116984.,    0.260318\r\n');
fprintf(idOutput, ' 119241.,    0.270248\r\n');
fprintf(idOutput, ' 121512.,    0.280195\r\n');
fprintf(idOutput, ' 123969.,    0.290734\r\n');
fprintf(idOutput, ' 126226.,    0.300016\r\n');
fprintf(idOutput, ' 128767.,    0.310192\r\n');
fprintf(idOutput, ' 131266.,    0.320052\r\n');
fprintf(idOutput, ' 133821.,    0.330076\r\n');
fprintf(idOutput, ' 136452.,     0.34032\r\n');
fprintf(idOutput, ' 138969.,    0.350099\r\n');
fprintf(idOutput, ' 141556.,     0.36015\r\n');
fprintf(idOutput, ' 144123.,    0.370134\r\n');
fprintf(idOutput, ' 146685.,    0.380098\r\n');
fprintf(idOutput, ' 149258.,    0.390111\r\n');
fprintf(idOutput, ' 151809.,    0.400039\r\n');
fprintf(idOutput, ' 154423.,    0.410216\r\n');
fprintf(idOutput, ' 156978.,    0.420178\r\n');
fprintf(idOutput, ' 159504.,    0.430121\r\n');
fprintf(idOutput, ' 162006.,    0.440101\r\n');
fprintf(idOutput, ' 164484.,    0.450151\r\n');
fprintf(idOutput, ' 166981.,    0.460296\r\n');
fprintf(idOutput, ' 169370.,    0.470068\r\n');
fprintf(idOutput, ' 171842.,    0.480234\r\n');
fprintf(idOutput, ' 174236.,    0.490308\r\n');
fprintf(idOutput, ' 176540.,    0.500136\r\n');
fprintf(idOutput, ' 178800.,     0.51025\r\n');
fprintf(idOutput, ' 180889.,    0.520196\r\n');
fprintf(idOutput, ' 182964.,    0.530198\r\n');
fprintf(idOutput, ' 184993.,    0.540145\r\n');
fprintf(idOutput, ' 186973.,    0.550058\r\n');
fprintf(idOutput, ' 188853.,    0.560315\r\n');
fprintf(idOutput, ' 191451.,    0.574845\r\n');
fprintf(idOutput, ' 200321.,    0.624845\r\n');
fprintf(idOutput, ' 206585.,    0.674845\r\n');
fprintf(idOutput, ' 212576.,    0.724845\r\n');
fprintf(idOutput, ' 218325.,    0.774845\r\n');
fprintf(idOutput, ' 223854.,    0.824845\r\n');
fprintf(idOutput, ' 229186.,    0.874845\r\n');
```

```
fprintf(idOutput, ' 234339.,    0.924845\r\n');
fprintf(idOutput, ' 239326.,    0.974845\r\n');
fprintf(idOutput, ' 244163.,     1.02484\r\n');
fprintf(idOutput, ' 248860.,     1.07484\r\n');
fprintf(idOutput, ' 253427.,     1.12484\r\n');
fprintf(idOutput, ' 257875.,     1.17484\r\n');
fprintf(idOutput, ' 262210.,     1.22484\r\n');
fprintf(idOutput, ' 266440.,     1.27484\r\n');
fprintf(idOutput, ' 270572.,     1.32484\r\n');
fprintf(idOutput, ' 274611.,     1.37484\r\n');
fprintf(idOutput, ' 278563.,     1.42484\r\n');
fprintf(idOutput, ' 282433.,     1.47484\r\n');
fprintf(idOutput, ' 286225.,     1.52484\r\n');
fprintf(idOutput, ' 289942.,     1.57484\r\n');
fprintf(idOutput, ' 293590.,     1.62484\r\n');
fprintf(idOutput, ' 297171.,     1.67484\r\n');
fprintf(idOutput, ' 300688.,     1.72484\r\n');
fprintf(idOutput, ' 304145.,     1.77484\r\n');
fprintf(idOutput, ' 307544.,     1.82484\r\n');
fprintf(idOutput, ' 310887.,     1.87484\r\n');
fprintf(idOutput, ' 314177.,     1.92484\r\n');
fprintf(idOutput, ' 317417.,     1.97484\r\n');
fprintf(idOutput, ' 320607.,     2.02484\r\n');
fprintf(idOutput, '** \r\n');

fprintf(idOutput, '**************************** \r\n');
fprintf(idOutput, '** INTERACTION PROPERTIES **\r\n');
fprintf(idOutput, '**************************** \r\n');
fprintf(idOutput, '** \r\n');
fprintf(idOutput, '*Surface Interaction, name=DieTube\r\n');
fprintf(idOutput, '1.,\r\n');
fprintf(idOutput, '*Friction, slip tolerance=0.005\r\n');
fprintf(idOutput, ' 0.2,\r\n');
fprintf(idOutput, '*Surface Behavior, no separation, pressure-overclosure=HARD\r\n');
fprintf(idOutput, '*Surface Interaction, name=SealTube\r\n');
fprintf(idOutput, '1.,\r\n');
fprintf(idOutput, '*Friction, slip tolerance=0.005\r\n');
fprintf(idOutput, ' 0.2,\r\n');
fprintf(idOutput, '*Surface Behavior, no separation, pressure-overclosure=HARD\r\n');
fprintf(idOutput, '** \r\n');
fprintf(idOutput, '************************ \r\n');
fprintf(idOutput, '** BOUNDARY CONDITIONS **\r\n');
fprintf(idOutput, '************************ \r\n');
fprintf(idOutput, '** \r\n');
fprintf(idOutput, '** Name: DieFixed Type: Symmetry/Antisymmetry/Encastre\r\n');
fprintf(idOutput, '*Boundary\r\n');
fprintf(idOutput, 'Die-1.DieRef, ENCASTRE\r\n');
fprintf(idOutput, '** Name: SealFixed Type: Symmetry/Antisymmetry/Encastre\r\n');
fprintf(idOutput, '*Boundary\r\n');
fprintf(idOutput, 'Seal-Analytical-1.SealRef, ENCASTRE\r\n');
fprintf(idOutput, '** Name: TubeSymAxial Type: Symmetry/Antisymmetry/Encastre\r\n');
fprintf(idOutput, '*Boundary\r\n');
fprintf(idOutput, 'Tube-1.ZSYMSET, ZSYMM\r\n');
fprintf(idOutput, '** Name: TubeSymX Type: Symmetry/Antisymmetry/Encastre\r\n');
fprintf(idOutput, '*Boundary\r\n');
fprintf(idOutput, 'Tube-1.XSYMSET, XSYMM\r\n');
fprintf(idOutput, '** Name: TubeSymY Type: Symmetry/Antisymmetry/Encastre\r\n');
fprintf(idOutput, '*Boundary\r\n');
fprintf(idOutput, 'Tube-1.YSYMSET, YSYMM\r\n');
if(V_CONTROL==1)
    fprintf(idOutput,          '**          Name:          RigidCavityEnd          Type:
Symmetry/Antisymmetry/Encastre\r\n');
    fprintf(idOutput, '*Boundary\r\n');
```

```
    fprintf(idOutput, 'Tube-1.RigidCavityEnd, ENCASTRE\r\n');
end

fprintf(idOutput, '** \r\n');
fprintf(idOutput, '****************** \r\n');
fprintf(idOutput, '** INTERACTIONS **\r\n');
fprintf(idOutput, '****************** \r\n');
fprintf(idOutput, '** \r\n');
fprintf(idOutput, '** Interaction: DieTubeContact\r\n');
fprintf(idOutput, '*Contact Pair, interaction=DieTube, tracking=STATE\r\n');
fprintf(idOutput, 'Tube-1_TubeExterior_CNS_, Die-1.RigidSurface_\r\n');
fprintf(idOutput, '** Interaction: TubeSealContact\r\n');
fprintf(idOutput, '*Contact Pair, interaction=SealTube, tracking=STATE\r\n');
fprintf(idOutput,   'Tube-1_TubeExterior_CNS_,   Seal-Analytical-1.CP-1-Seal-Analytical-
1\r\n');
fprintf(idOutput,  '**  ----------------------------------------------------------------
\r\n');
fprintf(idOutput, '** \r\n');
fprintf(idOutput, '************************** \r\n');
fprintf(idOutput, '** STEP: Pressurization **\r\n');
fprintf(idOutput, '************************** \r\n');
fprintf(idOutput, '** \r\n');
%fprintf(idOutput, '*Step, name=Pressurization, nlgeom=YES\r\n');
%modified Jan 30 '12, needed more than 100 increments
fprintf(idOutput, '*Step, name=Pressurization, nlgeom=YES, inc=200\r\n');
fprintf(idOutput, '*Static\r\n');
%modified Jan 28 '12, works better with smaller initial step.
fprintf(idOutput, '0.0025, 1., 1e-08, 0.1\r\n');
if(THICKNESS_SETS==1)
    fprintf(idOutput, '*NODE PRINT, SUMMARY=NO, nset=Tube-1.SetA\r\n');
    fprintf(idOutput, 'COOR1, COOR2\r\n');
end

fprintf(idOutput, '** \r\n');
fprintf(idOutput, '************************** \r\n');
fprintf(idOutput, '** LOADS (V or P control **\r\n');
fprintf(idOutput, '************************** \r\n');

if (V_CONTROL==1)
    fprintf(idOutput, '** Volume Control \r\n');
    fprintf(idOutput, '***** Fluid Density is 0.036 lb/in^3, \r\n');
    fprintf(idOutput, '***** which is correct since this assembly \r\n');
    fprintf(idOutput, '***** is in inches. Controlled by CavityRef.\r\n');
    fprintf(idOutput, '*fluid flux\r\n');
    fprintf(idOutput, 'Tube-1.CavityRef, 0.1\r\n');
    fprintf(idOutput, '** \r\n');
else
    fprintf(idOutput, '** Pressure Control \r\n');
    fprintf(idOutput, '*Dsload\r\n');
    fprintf(idOutput, 'Tube-1.TubeInterior, P, 10000.\r\n');
    fprintf(idOutput, '** \r\n');
end
fprintf(idOutput, '** \r\n');
fprintf(idOutput, '********************** \r\n');
fprintf(idOutput, '** OUTPUT REQUESTS **\r\n');
fprintf(idOutput, '********************** \r\n');
fprintf(idOutput, '** \r\n');
fprintf(idOutput, '*Restart, write, frequency=0\r\n');
fprintf(idOutput, '** \r\n');
fprintf(idOutput, '** FIELD OUTPUT: F-Output-1\r\n');
fprintf(idOutput, '** \r\n');
fprintf(idOutput, '*Output, field\r\n');
```

```
fprintf(idOutput, '*Node Output\r\n');
fprintf(idOutput, 'CF, RF, U, COORD\r\n');
fprintf(idOutput, '*Element Output, directions=YES\r\n');
fprintf(idOutput, 'LE, NE, P, PE, PEEQ, PEMAG, S\r\n');
fprintf(idOutput, '** \r\n');
fprintf(idOutput, '****************************** \r\n');
fprintf(idOutput, '** HISTORY OUTPUT: H-Output-1 **\r\n');
fprintf(idOutput, '****************************** \r\n');
fprintf(idOutput, '*Contact Output\r\n');
fprintf(idOutput, 'CDISP, CSTRESS\r\n');
fprintf(idOutput, '*Output, history, variable=PRESELECT\r\n');
fprintf(idOutput, '*node output, nset=Tube-1.CavityRef\r\n');
fprintf(idOutput, ' pcav, cvol\r\n');
fprintf(idOutput, '**\r\n');

if(THICKNESS_SETS==1)
    fprintf(idOutput, '** HISTORY OUTPUT: ThickA\r\n');
    fprintf(idOutput, '** \r\n');
    %fprintf(idOutput, '*Node Output, nset=Tube-1.SetA\r\n');
    fprintf(idOutput, '*Node Output, global=NO, nset=Tube-1.SetA\r\n');
    fprintf(idOutput, 'COOR1, COOR2,\r\n');
    fprintf(idOutput, '** \r\n');
    fprintf(idOutput, '** HISTORY OUTPUT: ThickB\r\n');
    fprintf(idOutput, '** \r\n');
    fprintf(idOutput, '*Node Output, global=NO, nset=Tube-1.SetB\r\n');
    fprintf(idOutput, 'COOR1, COOR2,\r\n');
    fprintf(idOutput, '** \r\n');
    fprintf(idOutput, '** HISTORY OUTPUT: ThickC\r\n');
    fprintf(idOutput, '** \r\n');
    fprintf(idOutput, '*Node Output, global=NO, nset=Tube-1.SetC\r\n');
    fprintf(idOutput, 'COOR1, COOR2,\r\n');
    fprintf(idOutput, '** HISTORY OUTPUT: ThickD\r\n');
    fprintf(idOutput, '** \r\n');
    fprintf(idOutput, '*Node Output, global=NO, nset=Tube-1.SetD\r\n');
    fprintf(idOutput, 'COOR1, COOR2,\r\n');
    fprintf(idOutput, '** \r\n');
    fprintf(idOutput, '** HISTORY OUTPUT: ThickE\r\n');
    fprintf(idOutput, '** \r\n');
    fprintf(idOutput, '*Node Output, global=NO, nset=Tube-1.SetE\r\n');
    fprintf(idOutput, 'COOR1, COOR2,\r\n');
end

fprintf(idOutput, '*End Step\r\n');


fprintf('** COMPLETE! **\n');
fclose(idOutput);

return;
```